UNIVERSITÀ DI PARMA

UNIVERSITA' DEGLI STUDI DI PARMA

DOTTORATO DI RICERCA IN
"*Ingegneria delle infrastrutture e del territorio*"

CICLO XXXIII°

Three-dimensional monitoring of the tunnel face: development of an innovative tool for preconvergence monitoring

Coordinatore:
Chiar.mo Prof. Sandro Longo

Tutore:
Chiar.mo Prof. Andrea Segalini

Dottorando: Edoardo Cavalca

Anni Accademici 2017/2018 – 2019/2020

Table of contents

List of figures 6

List of tables 14

List of equations 15

Introduction 17

1. Tunnel design and monitoring role in underground constructions 19

2. Rock mass and ground characterization and tunnelling approaches 25

2.1. Rock mass and ground characterization 25

2.2. ADECO – RS Approach 28

3. Tunnel monitoring 34

3.1. Stresses measures 34

3.1.1. Load cells 34

3.2. Measure of water level and pore pressure 35

3.2.1. Open circuit piezometer 35

3.2.2. Casagrande piezometer 36

3.3. Measure of deformations 36

3.3.1. Inclinometers 36

3.3.2. Magnetic extensometer 37

3.3.3. Single and multipoint extensometers 37

3.3.4. Tilt meter 38

3.3.5. Convergence measurements 38

3.3.6. Extrusion measurements 39

3.3.7. Preconvergence measurements 39

4. Pre-Conv Array 42

4.1. Introduction 42

4.1.1. Conventional tunnel excavation (preconfinement not required) 46

4.1.2. Conventional tunnel excavation with preconfinement intervention 49
4.1.3. Shielded TBM 50
4.1.4. TBM from vertical shafts 51
4.2. Pre-Conv Links and calibration procedures 52
4.2.1. Accelerometers calibration 53
4.2.2. Thermometers calibration 56
4.3. Calculation principles 57
4.3.1. Segment of relevance and calculation point definition 57
4.3.2. Self-check controls 61
4.4. Laboratory tests 66
4.4.1. Pre-Conv Array horizontally installed 68
4.4.2. Pre-Conv Array tilted installed 70
4.5. Differences to other preconvergence monitoring system 72
5. Introduction to the case studies 73
5.1. Pressure test 75
5.2. Thermal test 78
5.3. Thermal filter 81
6. Case Study 1 – Tunnel in the North of Italy 92
6.1. Introduction: geological and geotechnical framework 92
6.2. Tunnel excavation and evaluation of expected displacements 94
6.3. Pre-Conv Array installation and excavation works 97
6.4. Monitoring results 99
6.5. Monitoring data validation 114
6.6. Conclusion 120
7. Case Study 2 – Tunnel SS30 in the Principality of Monaco 123
7.1. Introduction: geological and geotechnical framework 123
7.2. Tunnel excavation and evaluation of expected displacements 125
7.3. Pre-Conv Array installation and excavation works 127

7.4. Monitoring results 129
7.5. Monitoring data validation 142
7.6. Conclusion 156
8. Conclusion 158
References 162
Ringraziamenti 169

List of figures

Figure 1.1 Longitudinal deformations profile. Source (E. Hoek et al., 2008) 20
Figure 1.2 Fictitious pressure near the working face. Source (AFTES, 1978) 21
Figure 1.3 Interaction between GRC-SCC-LDP. Source:(Carranza-Torres & Fairhurst, 2000) 22
Figure 1.4 Observational method flow chart 23
Figure 1.5 Back analysis and forward analysis. Source: (Sakurai et al., 2003) 24
Figure 2.1 Tunnel deformation response during the excavation.(Lunardi, 1994) 28
Figure 2.2 Rock mass behaviour categories. Source: (Lunardi, 1994) 29
Figure 2.3 Left: Cavity preconfinement used in ADECO – RS approach. Right: Cavity confinement action (Lunardi, 1994) 30
Figure 2.4 Radial displacement of a point A in a deformable or rigid advance core. (Lunardi, 2008) 31
Figure 2.5 Principal preconfinement method applied in ADECO – RS approach (Lunardi, 2008) 32
Figure 2.6 ADECO – RS framework used for all types of ground or rock mass (Lunardi, 2008) 33
Figure 3.1 Example of an electric load cell (source: Earth System S.r.l.) 34
Figure 3.2 Example of a hydraulic pressure cell (source: Earth system S.r.l.) 35
Figure 3.3 Example of an open standpipe piezometer (source: Geotech AB) 35
Figure 3.4 Example of a Casagrande piezometer (source: Earth System S.r.l.) 36
Figure 3.5 Example of a manual inclinometer and ABS or aluminium casing. (source: Slope Indicator) 36
Figure 3.6 Example of a magnetic extensometer probe (source: Soil Instruments) 37
Figure 3.7 Typical extensometer monitoring (Lunardi, 1994) 37
Figure 3.8 Example of a tilt meters (source: Earth System S.r.l.) 38
Figure 3.9 Example of a geodetic survey in tunnels (source: Monteith & Sutherland survey) 38
Figure 3.10 Example of a extrusion monitoring . Source: (Lunardi, 2000) 39
Figure 3.11 Relationship between extrusion and preconvergence. Source: (Lunardi, 2008) 40
Figure 3.12 Tunnel monitoring typical layout, showing both surface and deep deformations monitoring. Source: (Lunardi, 1994) 41
Figure 4.1 3D monitoring of a tunnel face. Adapted from (Segalini et al., 2018b) 43
Figure 4.2 Pre-Conv Link axis definition 44
Figure 4.3 Principle of the monitoring system. Adapted from (Segalini et al., 2019) 44

Figure 4.4 Phase 1: Tunnel excavation until the monitored section; Phase 2: sub-horizontal borehole excavation; Phase 3: Pre-Conv installation; Phase 4: Tunnel advance and monitoring of induced deformations. Figure adapted from (Savi et al., 2019) 46
Figure 4.5 Phase 1: Tunnel excavation until the monitored section and pilot tunnel realization; Phase 2: Horizontal borehole; Phase 3: Pre-Conv Array installation; Phase 4: Tunnel advance and monitoring of induced deformations. Figure adapted from (Savi et al., 2019)..... 47
Figure 4.6 Phase 1: Tunnel excavation until the monitored section; Phase 2: Curved borehole realization; Phase 3: Pre-Conv Array installation; Phase 4: Tunnel advance and monitoring of induced deformations. Figure adapted from (Savi et al., 2019) 48
Figure 4.7 Phase 1: Tunnel excavation until the monitored section; Phase 2: Umbrella of jet-grouting realization; Phase 3: Pre-Conv Array installation inside the jet-grouting pipe; Phase 4: Tunnel advance and monitoring of induced deformations. Figure adapted from (Savi et al., 2019)..... 49
Figure 4.8 Phase 1: Tunnel excavation by shielded TBM until the monitored section; Phase 2: Borehole realization starting from the TBM shield; Phase 3: Pre-Conv Array installation; Phase 4: Tunnel advance and monitoring of induced deformations. Figure adapted from (Savi et al., 2019) 50
Figure 4.9 Phase 1: The TBM excavation is preceded by two vertical shafts excavation for TBM positioning and retrieval; Phase 2: Two horizontal boreholes above tunnel crown are realized to insert the Pre-Conv Array; Phase 3: TBM excavation and monitoring of vertical displacements; Phase 4: Monitoring of vertical displacements during tunnel operational phase. Figure adapted from (Savi et al., 2019) 51
Figure 4.10 Pre-Conv Link equipped with 3D MEMS sensor and axis definition. Adapted from (Carri, 2019) 52
Figure 4.11 Dodecahedron designed for MEMS accelerometers calibration (Source: ASE S.r.l. manual)..... 54
Figure 4.12 Segment of relevance and calculation point of Pre-Conv Array. Adapted from (Carri, 2019) 58
Figure 4.13 Calculation scheme of Pre-Conv Array..... 58
Figure 4.14 Displacement evaluation elaborated without running average (blue), and calculated with a centred running average of 3 (orange), 5 (grey) or 11 (yellow) data. (Carri, 2019) 64
Figure 4.15 Definition of instrumental noise and displacements. Adapted from (Carri, 2019) 65
Figure 4.16 Representation of non-working sensor on web platform (ASE S.r.l. web platform) 65
Figure 4.17 Detail of the mechanical structure developed to connect the Pre-Conv Array to the threaded metal rod, the locking system and the topographic target placed at the calculation point. Source: (Savi et al., 2019)..... 66

Figure 4.18 Physical apparatus developed to test the Pre-Conv Array prototype (Rods R1-R7; Nodes N1-N6; Fixed points P_0-P_3) (Savi et al., 2019) 67
Figure 4.19 Displacement recorded by Pre-Conv Array (dotted line) and topographic survey, starting from a horizontal configuration. (Savi et al., 2019) 68
Figure 4.20 Displacement recorded by Pre-Conv Array (dotted line) and topographic survey, starting from a 4-degress tilted configuration. (Savi et al., 2019) 70
Figure 5.1 Displacement and temperature recorded by Calculation Point n°9 74
Figure 5.2 X raw acceleration and temperature recorded by Calculation Point n°9 74
Figure 5.3 Displacements recorded along x-axis and applied pressure 76
Figure 5.4 Displacements recorded along y-axis and applied pressure 76
Figure 5.5 Autoclave loading scheme 77
Figure 5.6 Possible deformations induced on MEMS sensor by pressure variations 78
Figure 5.7 Sensor immersed in the concrete mortar inside a PVC casing 79
Figure 5.8 Sensor placed inside plastic box and surrounded by ground 79
Figure 5.9 Pre-Conv Link 1 cemented with compensated shrinkage mortar. Displacements along x-axis and recorded temperature 80
Figure 5.10 Pre-Conv Link 2 without compensated shrinkage mortar. Displacements along x-axis and recorded temperature 80
Figure 5.11 Example of linear and second-degree interpolation of Pre-Conv Links. Left: Pre-Conv Link 18, right: Pre-Conv Link 12 82
Figure 5.12 Comparison of displacement using a linear interpolation (black line) or a second-degree equation (blue line) for Pre-Conv Link 18. The red line represents the measured temperature 83
Figure 5.13 Comparison of displacement using a linear interpolation (black line) or a second-degree equation (blue line) for Pre-Conv Link 12. The red line represents the measured temperature 83
Figure 5.14 Displacements comparison using a linear interpolation (black line) or the broken curve parameters (blue line) for Pre-Conv Link 12. The red line indicates the recorded temperature 85
Figure 5.15 Displacement comparison using a linear interpolation (black line) or the broken curve parameters (blue line) for Pre-Conv Link 18. The red line indicates the recorded temperature 86
Figure 5.16 Example of data normalization for Pre-Conv Link 18 88
Figure 5.17 Daily temperature and displacements slope (on the left), and relates delta (on the right). Pre-Conv Link 18 88
Figure 5.18 Example of range used to evaluate a and b parameters for the pilot site installation in the north of Italy 91
Figure 6.1 Aerial photography of the construction site 92

Figure 6.2 Geomechanical section of the tunnel 93
Figure 6.3 Typical excavation section 94
Figure 6.4 Advance method and confinement and preconfinement support systems 94
Figure 6.5 Verification sections (blue line) 95
Figure 6.6 Geodetic monitoring during the tunnel construction 96
Figure 6.7 Left: Pre-Conv Array installation. Right: Pre-Conv Array preparation 97
Figure 6.8 Example of the monitored section 97
Figure 6.9 Local displacement calculated for C.P. 1 by applying different delta slope 100
Figure 6.10 Local displacement calculated for C.P. 11 by applying different delta slope 101
Figure 6.11 Local displacements occurred during the first excavation stage. The black dotted line indicates the tunnel face position referred to the Pre-Conv Array Calculation Points. 102
Figure 6.12 Left: Vertical local displacements evaluated from zero reference. Right: cumulated displacements evaluated from the referring date. The black dotted line indicates the front position 102
Figure 6.13 Local displacements occurred during the tunnel face advance of 2.50 m. The black dotted line indicates the tunnel face position referred to the Pre-Conv Array calculation Points. 103
Figure 6.14 Left: Vertical local displacements evaluated from zero reference. Right: cumulated displacements evaluated from the referring date. The black dotted line indicates the front position 103
Figure 6.15 Local displacements occurred during the tunnel face advance of 3.75 m. The black dotted line indicates the tunnel face position referred to the Pre-Conv Array calculation Points. 104
Figure 6.16 Left: Vertical local displacements evaluated from zero reference. Right: cumulated displacements evaluated from the referring date. The black dotted line indicates the front position 104
Figure 6.17 Local displacements occurred during the tunnel face advance of 5.00 m. The black dotted line indicates the tunnel face position referred to the Pre-Conv Array calculation Points. 105
Figure 6.18 Left: Vertical local displacements evaluated from zero reference. Right: cumulated displacements evaluated from the referring date. The black dotted line indicates the front position 105
Figure 6.19 Local displacements occurred during the tunnel face advance of 8.75 m. The black dotted line indicates the tunnel face position referred to the Pre-Conv Array calculation Points. 106
Figure 6.20 Left: Vertical local displacements evaluated from zero reference. Right: cumulated displacements evaluated from the referring date. The black dotted line indicates the front position 106

Figure 6.21 Local displacements occurred during the tunnel face advance of 10.00 m. The black dotted line indicates the tunnel face position referred to the Pre-Conv Array calculation Points ... 107
Figure 6.22 Left: Vertical local displacements evaluated from zero reference. Right: cumulated displacements evaluated from the referring date. The black dotted line indicates the front position ... 107
Figure 6.23 Local displacements occurred during the tunnel face advance of 11.25 m. The black dotted line indicates the tunnel face position referred to the Pre-Conv Array calculation Points ... 108
Figure 6.24 Left: Vertical local displacements evaluated from zero reference. Right: cumulated displacements evaluated from the referring date. The black dotted line indicates the front position ... 108
Figure 6.25 Local displacements occurred during the tunnel face advance of 12.50 m. The black dotted line indicates the tunnel face position referred to the Pre-Conv Array calculation Points ... 109
Figure 6.26 Left: Vertical local displacements evaluated from zero reference. Right: cumulated displacements evaluated from the referring date. The black dotted line indicates the front position ... 109
Figure 6.27 Local displacements occurred during the tunnel face advance of 13.75 m. The black dotted line indicates the tunnel face position referred to the Pre-Conv Array calculation Points ... 110
Figure 6.28 Left: Vertical local displacements evaluated from zero reference. Right: cumulated displacements evaluated from the referring date. The black dotted line indicates the front position ... 110
Figure 6.29 Local displacements occurred during the tunnel face advance of 15.00 m. The black dotted line indicates the tunnel face position referred to the Pre-Conv Array calculation Points ... 111
Figure 6.30 Left: Vertical local displacements evaluated from zero reference. Right: cumulated displacements evaluated from the referring date. The black dotted line indicates the front position ... 111
Figure 6.31 Left: Vertical local displacements during fore poles installation. Right: Vertical local displacements during fore poles injection ... 112
Figure 6.32 Local displacements occurred during the tunnel face advance of 16.25 m. The black dotted line indicates the tunnel face position referred to the Pre-Conv Array calculation Points ... 112
Figure 6.33 Left: Vertical local displacements evaluated from zero reference. Right: cumulated displacements evaluated from the referring date. Black dotted line indicates the front position ... 113
Figure 6.34 Local displacements occurred during the tunnel face advance of 17.50 m. The black dotted line indicates the tunnel face position referred to the Pre-Conv Array calculation Points ... 113

Figure 6.35 Left: Vertical local displacements evaluated from zero reference. Right: cumulated displacements evaluated from the referring date. The black dotted line indicates the front position 114
Figure 6.36 Deformation profiles derived from: elastic models (Panet, 1995); measurements in a tunnel (Chern et al., 1998) and best fit to the measurements from Hoek. Source: (Carranza-Torres & Fairhurst, 2000) 115
Figure 6.37 Comparison between instrumental data and theoretical curves. Pre-Conv Link from 1 to 6 116
Figure 6.38 Comparison between instrumental data and theoretical curves. Pre-Conv Link from 7 to 12 117
Figure 6.39 Comparison between instrumental data and theoretical curves. Pre-Conv Link from 13 to 18 118
Figure 6.40 Comparison between Pre-Conv Link 11 and topographic survey 119
Figure 6.41 Example of GRC and evaluated LDP during the excavation advance of +15.00 m 121
Figure 6.42 GRC, LDP and SCC 121
Figure 7.1 EVOS project 123
Figure 7.2 Tunnel SS30 floor plan 123
Figure 7.3 Geomechanical section of the tunnel SS30 124
Figure 7.4 Tunnel entrance section and Pre-Conv array position (red dot) 125
Figure 7.5 Vertical settlement defined in the numerical model 126
Figure 7.6 Geodetic survey on the tunnel entrance 126
Figure 7.7 Pre-Conv Array installation procedure 127
Figure 7.8 Pre-Conv Links position on the monitored section 127
Figure 7.9 Range used for evaluating a and b parameters for the second pilot site installation 129
Figure 7.10 Evaluated local displacement for calculation point n°14 with different delta slope 131
Figure 7.11 Evaluated local displacement for calculation point n°5 with different delta slope 131
Figure 7.12 Local displacements occurred during the tunnel face advance of 0.35 m. The black dotted line indicates the tunnel face position referred to the Pre-Conv Array calculation Points 132
Figure 7.13 Left: Vertical local displacements evaluated from zero reference. Right: cumulated displacements evaluated from the referring date. The black dotted line indicates the front position 132
Figure 7.14 Local displacements occurred during the tunnel face advance of 1.35 m. The black dotted line indicates the tunnel face position referred to the Pre-Conv Array calculation Points 133

Figure 7.15 Left: Vertical local displacements evaluated from zero reference. Right: cumulated displacements evaluated from the referring date. The black dotted line indicates the front position 133
Figure 7.16 Local displacements occurred during the tunnel face advance of 2.35 m. The black dotted line indicates the tunnel face position referred to the Pre-Conv Array calculation Points 134
Figure 7.17 Left: Vertical local displacements evaluated from zero reference. Right: cumulated displacements evaluated from the referring date. The black dotted line indicates the front position 134
Figure 7.18 Local displacements occurred during the tunnel face advance of 3.35 m. The black dotted line indicates the tunnel face position referred to the Pre-Conv Array calculation Points 135
Figure 7.19 Left: Vertical local displacements evaluated from zero reference. Right: cumulated displacements evaluated from the referring date. The black dotted line indicates the front position 135
Figure 7.20 Local displacements occurred during the tunnel face advance of 5.35 m. The black dotted line indicates the tunnel face position referred to the Pre-Conv Array calculation Points 136
Figure 7.21 Left: Vertical local displacements evaluated from zero reference. Right: cumulated displacements evaluated from the referring date. The black dotted line indicates the front position 136
Figure 7.22 Local displacements occurred during the tunnel face advance of 7.35 m. The black dotted line indicates the tunnel face position referred to the Pre-Conv Array calculation Points 137
Figure 7.23 Left: Vertical local displacements evaluated from zero reference. Right: cumulated displacements evaluated from the referring date. The black dotted line indicates the front position 137
Figure 7.24 Local displacements occurred during the tunnel face advance of 9.35 m. The black dotted line indicates the tunnel face position referred to the Pre-Conv Array calculation Points 138
Figure 7.25 Left: Vertical local displacements evaluated from zero reference. Right: cumulated displacements evaluated from the referring date. The black dotted line indicates the front position 138
Figure 7.26 Local displacements occurred during the tunnel face advance of 11.35 m. The black dotted line indicates the tunnel face position referred to the Pre-Conv Array calculation Points ... 139
Figure 7.27 Left: Vertical local displacements evaluated from zero reference. Right: cumulated displacements evaluated from the referring date. The black dotted line indicates the front position 139

Figure 7.28 Local displacements occurred during the tunnel face advance of 13.35 m. The black dotted line indicates the tunnel face position referred to the Pre-Conv Array calculation Points ... 140
Figure 7.29 Left: Vertical local displacements evaluated from zero reference. Right: cumulated displacements evaluated from the referring date. The black dotted line indicates the front position ... 140
Figure 7.30 Local displacements occurred during the tunnel face advance of 14.35 m. The black dotted line indicates the tunnel face position referred to the Pre-Conv Array calculation Points ... 141
Figure 7.31 Left: Vertical local displacements evaluated from zero reference. Right: cumulated displacements evaluated from the referring date. The black dotted line indicates the front position ... 141
Figure 7.32 Topographic stations installed ... 142
Figure 7.33 Comparison between C.P. 15 and topographic survey at +0.40 m ... 143
Figure 7.34 Comparison between C.P. 11 and topographic survey at +4.40 m ... 144
Figure 7.35 Comparison between C.P. 6 and topographic survey at +9.40 m ... 144
Figure 7.36 Comparison between C.P. 1 and topographic survey at +14.40 m ... 145
Figure 7.37 Axisymmetric model in RS2® ... 146
Figure 7.38 Longitudinal displacement profile on the tunnel crown for the unsupported tunnel ... 147
Figure 7.39 Left: 2D plane stress model. Right: zoom of the supported excavation face ... 151
Figure 7.40 LDP of the supported tunnel obtained from the plane stress model ... 151
Figure 7.41 Comparison between instrumental data and LDP obtained through the numerical model. Pre-Conv Link from 1 to 6 ... 153
Figure 7.42 Comparison between instrumental data and LDP obtained through the numerical model. Pre-Conv Link from 7 to 12 ... 154
Figure 7.43 Comparison between instrumental data and LDP obtained through the numerical model. Pre-Conv Link from 13 to 15 ... 155
Figure 7.44 Vertical displacement of the topographic target I14 ... 156
Figure 7.45 Left: Vertical local displacements evaluated from zero reference. Right: cumulated displacements evaluated from the referring date considering the vertical settlement of the anchor. Black dotted line indicates the front position ... 157

List of tables

Table 2.1 Rock mass classification systems 27
Table 4.1 Possible installation procedures 45
Table 4.2 Main features of 3D MEMS 52
Table 4.3 Preconvergence reference values derived from extrusion monitored data (Savi et al., 2019) 67
Table 4.4 Displacement comparison between topographic and monitoring tool measurements – horizontal starting configuration. (Savi et al., 2019) 68
Table 4.5 Difference between displacements recorded by theodolite and Pre-Conv Array, and corresponding percentage error - horizontal starting configuration. (Savi et al., 2019) 69
Table 4.6 Displacements recorded by theodolite and Pre-Conv Array, and corresponding percentage errors - 4-degrees tilted starting configuration. (Savi et al., 2019) 70
Table 4.7 Difference between displacements recorded by theodolite and Pre-Conv Array, and corresponding percentage error - 4-degrees tilted starting configuration. (Savi et al., 2019) 71
Table 5.1 Pressure stages applied on Pre-Conv Link 75
Table 5.2 Calibration parameters of Pre-Conv Link 12 obtained from the broken curve method 84
Table 5.3 Example of a and b parameters obtained for the pilot site installation in the north of Italy 91
Table 6.1 Geotechnical parameters of glacial deposits 93
Table 6.2 Expected displacements obtained by the numerical model 96
Table 6.3 Absolute coordinates x and y for each calculation points 98
Table 6.4 Excavation advance 98
Table 7.1 Geotechnical parameters of the involved ground 125
Table 7.2 Calculation points absolute coordinates x and y 128
Table 7.3 Excavation advance as declared by the construction company 128
Table 7.4 a and b parameters obtained for the second pilot site installation 130
Table 7.5 Mechanical and deformative parameters of the cover soil 146
Table 7.6 Shotcrete mechanical properties 149
Table 7.7 HEB 100 Steel ribs mechanical properties 149
Table 7.8 Elastic modulus for each modelled stage obtained from the axisymmetric models 150
Table 7.9 Homogeneous elastic modulus and thickness 150

List of equations

[1.1] 20
[4.1] 54
[4.2] 55
[4.3] 55
[4.4] 55
[4.5] 56
[4.6] 56
[4.7] 59
[4.8] 59
[4.9] 59
[4.10] 59
[4.11] 59
[4.12] 60
[4.13] 60
[4.14] 60
[4.15] 60
[4.16] 60
[4.17] 60
[4.18] 60
[4.19] 60
[4.20] 60
[4.21] 61
[4.22] 61
[4.23] 61
[4.24] 61
[4.25] 62
[4.26] 62
[4.27] 62
[4.28] 62
[4.29] 63
[4.30] 63
[4.31] 63

[4.32] 67
[5.1] 77
[5.2] 81
[5.3] 81
[5.4] 87
[5.5] 87
[5.6] 89
[5.7] 89
[5.8] 90
[5.9] 90
[6.1] 114
[6.2] 115
[7.1] 148
[7.2] 148
[7.3] 148

Introduction

In the traditional design of tunnels excavation, various hypotheses are used for schematizing the mechanical and deformative behaviour of the surrounding rock mass. Due to a large number of uncertainties and to the anisotropic nature of the rock masses, the design assumptions should be validated during the construction phase. This validation is usually carried out employing regular monitoring of the rock mass deformation around the tunnel face. Various studies highlighted the relationship between tunnel convergence, preconvergence, and front extrusion, which are recognized as key parameters to understand the rock mass mechanical behaviour. Often, tunnels are built in critical conditions, such as soft soils and low ground cover, with the risk of interfering with pre-existing buildings or the nearby infrastructures. To better characterize the rock mass mechanical features, solutions and design improvements can be planned by measuring the deformations in a three-dimensional manner, both convergence and preconvergence, caused by the excavation. This approach, in agreement with the "Analisi delle Deformazioni Controllate nelle Rocce e nei Suoli" (ADECO – RS) philosophy, consists of the analysis of the deformation response of the advance core ahead of the tunnel face. In this perspective, the monitoring phase assumes an important role during the tunnel excavation but also during the project design, where continuous monitoring of the rock mass response can help the project manager to take decisions and to modify the project as in the "learn as you go" philosophy. Moreover, such approach allows to contain excavation cost and realization times.

The work presented in this thesis focuses on the development of an innovative and automatic tool for the monitoring of the preconvergence deformations, called Pre-Conv Array, developed at the University of Parma. First of all, the general characteristic of the proposed tool are presented, together with the ones of the on-board sensors, and their calibration procedure. Afterwards, the calculation process that defines the recorded displacements is explained, as well as the statistical approach adopted to elaborate the large amount of data obtained during the entire monitoring period.

Secondly, we discuss the external factors that influence the sensor's response, such as the mortar concrete maturation or the day and night thermal cycles, along with laboratory tests conducted to define the magnitude of such influence. Moreover, we present a method developed to compensate thermal effects on data, based on the daily trend of both displacements and temperature.

Finally, we present two different case studies where the Pre-Conv Array has been successfully installed. The displacements recorded during the entire monitoring phase are presented. To validate

the proposed technology, we compared Pre-Conv Array data with the ones obtained through traditional instruments and numerical models.

Taken together, the research presented here highlights that the Pre-Conv Array turned out to be a fundamental instrument to monitor the stability of the advance core, and to help the project designer in defining the best project solutions.

1. Tunnel design and monitoring role in underground constructions

Underground works are anthropic construction that consists of a cavity opening inside the ground. The realization of tunnels could be very hard both to design and to realize due to external factors as the surrounding ground mechanical and deformative parameters, and time-costs analysis that can ultimately compromise the entire project development. When underground works are planned there are several related problems. For instance, the medium in which the construction will be excavated cannot be completely indagated to know exactly the mechanical and deformative parameters of the rock mass or the surrounding ground. For these reasons, a series of hypothesis must be applied to forecast surface and depth displacements induced by the excavation itself. Indeed, an inadequate survey phase can induce an increase in costs and realization time as well as the related construction risks.

Starting from a survey phase, where the mechanical and deformative rock mass parameters are estimated, a tunnel designer must analyse the influence of the excavation both inside the medium and on the surface. Indeed, tunnel excavation induces changes in the original stress field and deformations in rock masses (AFTES, 1978). It is important to predict deformations caused by tunnels excavation to assess the potential effects on the existing buildings and on the designed support systems.

Deformations can be evaluated by using different approaches, among others, there is the Convergence-Confinement method (C.C), developed between the 60's and '70s, which is based on observations and studies conducted by Fenner (Fenner, 1938). The C.C. method reduces the tunnel excavation in a plane problem on the assumption of a circular face excavated in an isotropic and homogeneous material in which the initial stress is considered isotropic. These hypotheses are valid for a deep tunnel, where the cover is of the order of 3-4 diameters. This method allows to estimate the pressure acting on a support system near the tunnel face. The C.C. method is composed of three basic components (Carranza-Torres & Fairhurst, 2000):

- Longitudinal Deformation Profile (LDP);
- Support Characteristic Curve (SCC);
- Ground Reaction Curve (GRC).

The LDP represents radial displacements that occurred on an unsupported cylindrical excavation ahead and behind the tunnel face (Figure 1.1) for a fixed section. The represented profile shows a slight increase of radial displacement ahead of the tunnel face. In the proximity of the excavation face, the displacement increases until a value u, which represents the maximum convergence occurred

far from the face. The LDP is useful to define the distance from the face to the support installation and to define the displacement occurred before the support application in a quite straightforward manner.

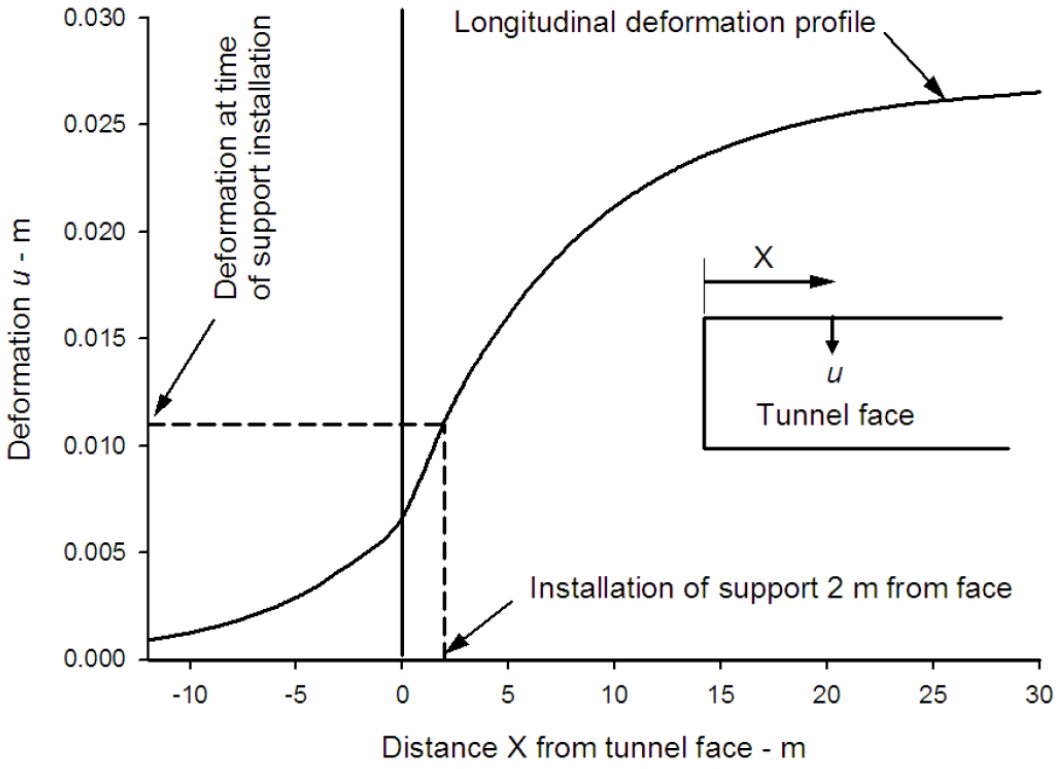

Figure 1.1 Longitudinal deformations profile. Source (E. Hoek et al., 2008)

SCC defines the relationship between the increasing pressure p_s acting on a support and the increasing of the radial displacement u_r of the support. The relationship is determined as a function of:

- the geometrical and mechanical characteristic of the support;
- Young's Modulus;
- Poisson's ratio;
- the thickness of support;
- the compressive and tensile strength of the material.

The GRC represents the relationship between the confinement pressure acting on the tunnel face and the related convergence displacement. Tunnel heading is represented by a progressive reduction of a fictitious pressure p applied on the face, simulating the rock mass deconfinement due to the tunnel advance (Figure 1.2). The deconfinement pressure can be evaluated by the Equation [1.1]:

$$\sigma_r = (1 - \lambda)\sigma_0 \qquad [1.1]$$

Where:

- σ_r is the stress acting on the tunnel face;
- σ_0 represents the initial stress state (considered as isotropic);
- λ is the deconfinement rate.

Far ahead from tunnel face, the stress state is equal to the initial isotropic field stress σ_0. While the tunnel face reaches the reference section, the acting pressure on the tunnel face decreases until a value equal to 0 (for unsupported tunnels) far behind tunnel face.

Deconfinement rate λ is a fundamental factor that permits to reproduce the three-dimensional tunnel excavation in a two-dimensional approach. It can be derived by several empirical equations as in (Panet & Guenot, 1982) or in (Labasse, 1949) or by numerical models as in (E. Hoek et al., 2008).

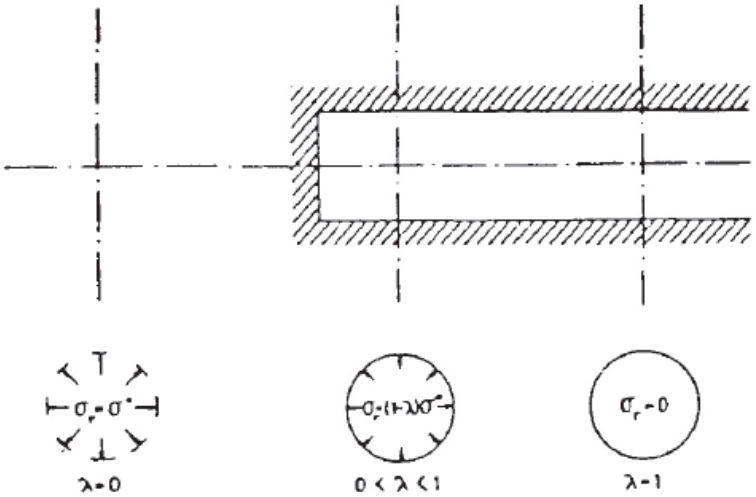

Figure 1.2 Fictitious pressure near the working face. Source (AFTES, 1978)

Figure 1.3 shows an example of the interaction between GRC-SCC-LDP. The GRC is divided in convergence of side wall, roof and floor since the difference of gravitational loading (Daemen, 1975).

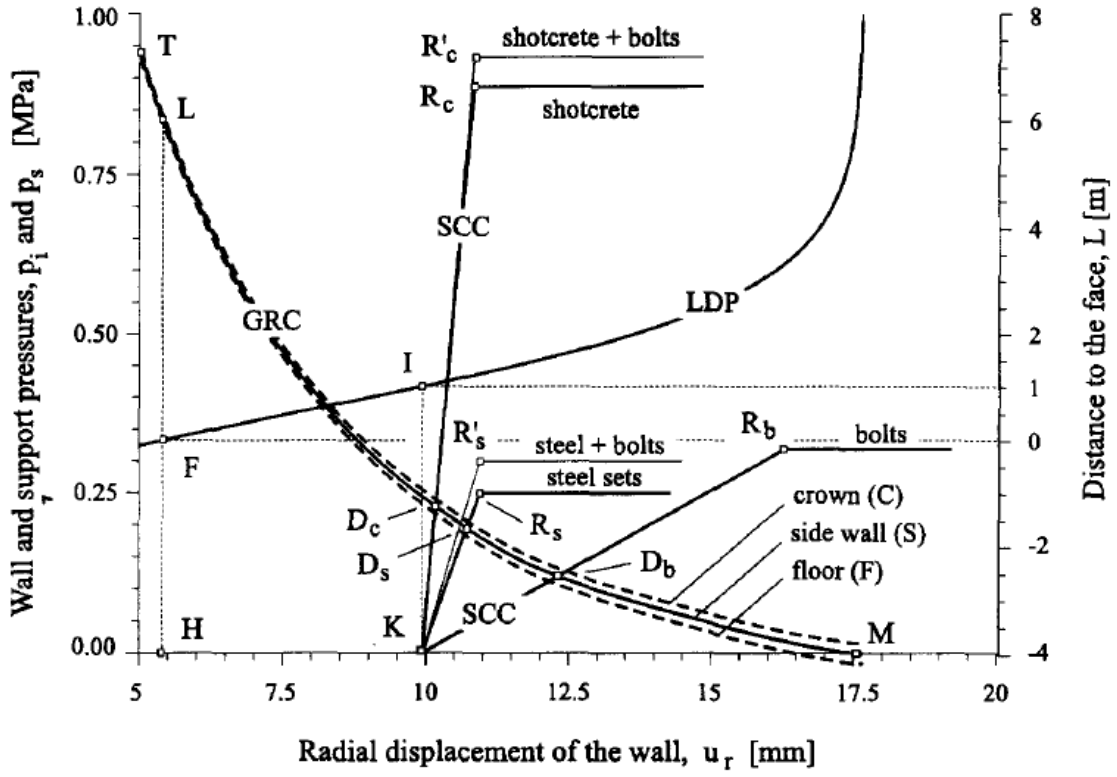

Figure 1.3 Interaction between GRC-SCC-LDP. Source:(Carranza-Torres & Fairhurst, 2000)

Considering the support installation at 1 meter behind the tunnel face, the LDP permits to define a point K (Figure 1.3) which represents the starting point for the SCC. Point K exactly indicates the radial displacement occurred before tunnel advance (tunnel preconvergence) and the related pressure which will be applied on the support system. Knowing the real trend of LDP, is it possible to design the appropriate support system and to verify the installation distance from the face. Moreover, displacement monitoring ahead of tunnel face permits to evaluate the appropriate preconfinement system to apply in the advance core for a safety excavation, with the additional advantage of money-saving(M. J. Kavvadas, 2003; Lunardi, 1991, 1999).

The LDP curve is generally estimated without on-site measurements because preconvergence is hardly taken or evaluated by manual or traditional systems, such as horizontal inclinometer, or multi-base rod extensometer on the surface. Indeed, these monitoring systems cannot provide data during the excavation phase and the sampling frequency is also quite limited. These limitations could cause a lower accuracy and could not help in defining relationships between the measured quantities. Instead, extensive and continuous monitoring ahead of the face can help the project manager to decide the appropriate support system and advance method, reducing costs and saving time.

The observational method (Peck, 1969) represents one of the most fundamental tools to reduce costs, improve on-site safety, and mitigate construction risks safeguarding the operativity of constructions. This method applies the "learn as you go" philosophy to improve the available information on monitored sites. After the geological and geotechnical characterization of the rock mass, a preliminary project is designed, also identifying the possible risks and the related threshold values. During tunnel excavation, some differences in terms of geological and geotechnical parameters could be highlighted. Without a continuous monitoring system, two options are available: i) adopt a higher safety factor, or ii) taking decisions experience-based. The first method generally involves higher costs because, for example, support systems could be over-dimensioned. The second method could be very dangerous in terms of safety and risk management. Only a continuous monitoring system permits to design and advance in project construction by limiting risks.

During the design phase, it is also necessary to project the most appropriate monitoring system, able to measure the principal physical quantities involved in the project, such as deformation, settlement, tension, pressure, or forces. The monitoring system has to work during the entire project development, validating the project hypothesis, and helping to define new project solutions to be adopted (NTC, 2018). The geotechnical report should explain the monitoring plan, by evaluating the needed instruments, data acquisition, sampling frequency, and data storage.

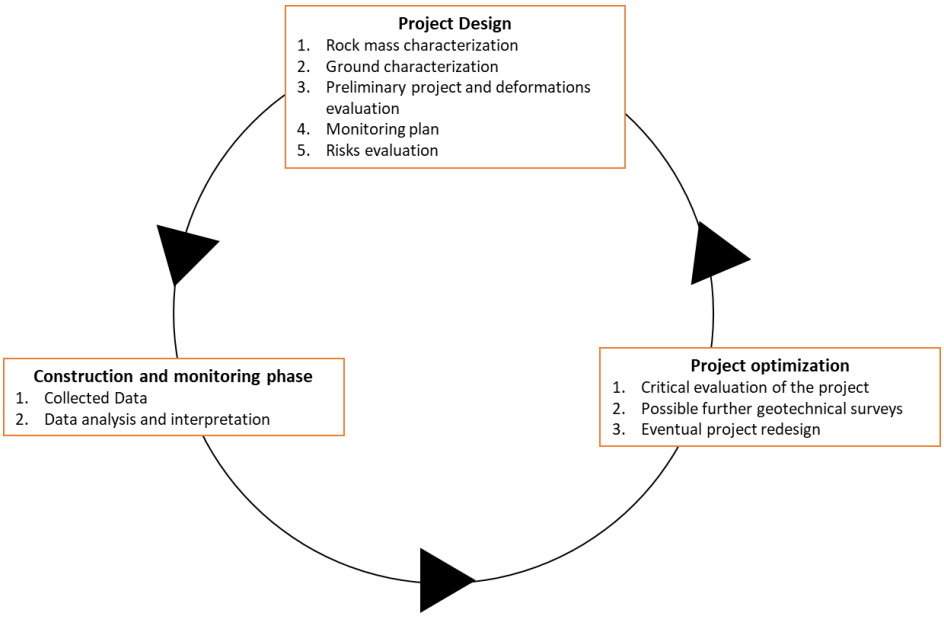

Figure 1.4 Observational method flow chart

Collected monitoring data are then used as input for geotechnical numerical models, applying the back-analysis methods (Figure 1.4). Once the numerical model is accurate and reliable, it can be used

to apply forward analyses to simulate different working stages and to design an appropriate support, confinement, and preconfinement systems (Figure 1.5).

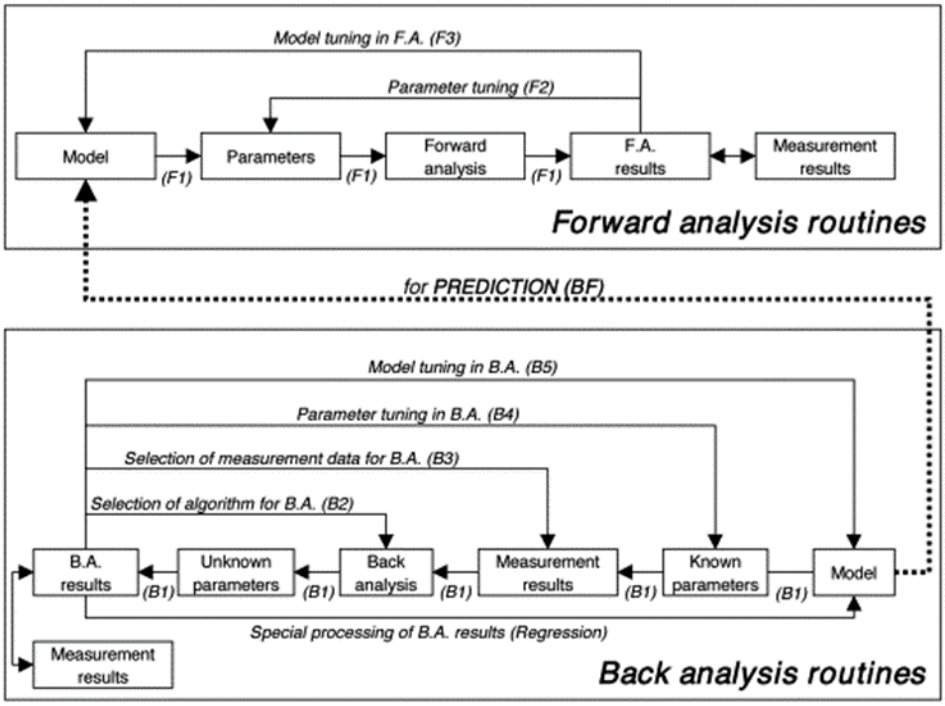

Figure 1.5 Back analysis and forward analysis. Source: (Sakurai et al., 2003)

In the following chapter, I will define the principal deformations phenomena acting on a tunnel. Moreover, I will present and discuss a new and innovative tool for the preconvergence monitoring.

2. Rock mass and ground characterization and tunnelling approaches

2.1. Rock mass and ground characterization

Rock mass and ground characterization in underground works is a key aspect to consider during the initial phase of the project. A good characterization could help the project designer to understand the rock mass or ground behaviour, to predict the expected deformations, to determine the best excavation method, and, finally, to realize the support project (Cai, 2011).

The Ministerial Decree 17/01/2018 (NTC, 2018) prescribes geological and geotechnical surveys as a function of the type of construction or works to realize. The geological surveys give a characterization of soil or rock mass, a description of the active morphological processes, and a reconstruction of the ground lithostratigraphy. According to Carter (Carter, 1992) and the U.S. National Tunnel Committee (Subcommittee on Geotechnical Site Investigations 1984), a good knowledge of the geological aspects allows containing the project costs. The geological differences that an underground work could highlight during the excavation phases represent the higher increase in costs. If a low budget survey is applied, a higher difference in terms of estimated costs could be identified at the end of the project. Generally, low differences in terms of estimated and effective construction costs could be found when the survey budget is equal to approximately 1% of the total tunnel costs (Tanzini, 2015).

Dodds (Dodds, 1982) has defined a geological and geotechnical guideline to follow in order to choose the velocity advance, the best excavation method, to contain costs, and to ensure security during and after the construction works. Dodds's guideline could be summarized as follows:

- Bibliographic research on the investigated site;
- Aerial photogrammetry of the investigated site. Aerial pictures help in having an overall view of all the geological aspects as topography, presence of rivers, drainage basin, or slope steepness;
- Surface geological surveys (discontinuities survey);
- Geophysics surveys: this non-destructive and cost-effective approach helps to reach higher investigated depth, to define differences in the lithological units and eventually the fractured rock and the bedrock could be highlighted;
- Boreholes: this is the most common survey used in rock and soils mechanics which gives the punctual geological information at different depth;
- Pilot tunnel: these underground works permit to have direct access to the rock mass portion where the tunnel will be constructed. The pilot tunnel has a smaller section than the projected

tunnel, but it is possible to directly observe the rock mass, evaluating the best excavation method or the physical properties. It also permits directly measurements on-site as the stress state of the rock mass or loading tests;

- Laboratory tests: evaluation of the rock mass mechanical and deformative parameters as the cohesion, the friction angle, the Young modulus, the uniaxial compressive strength, the tensile strength, the joints mechanical and deformative parameters, and more other parameters to taking into account;
- Physical model;
- Monitoring phase: this represents the key aspect during both the construction and the operating phase. The underground monitoring phase will be widely discussed in this thesis in the following chapters, due to the introduction of a new tool for directly monitoring the preconvergence deformations. The underground constructions are a very complex problem because, instead of the traditional civil construction, the medium, the action, and the reaction of the rock mass cannot be exactly predicted as in a steel or concrete building. A monitoring phase during the entire project development can verify the appropriateness of the design hypothesis, the stress and deformation state of the rock mass, and controlling the structure operativity as well as the rheological and hydrogeological conditions surrounding the tunnel in specific sections (Lunardi, 1994).

After the preliminary surveys, the rock mass can be classified in different rock mass classification systems (Pantelidis, 2009). The rock mass classification is the process of placing a rock mass into groups or classes on a defined relationship and assigning a unique description (or number) to it on the basis of similar properties/characteristics, such that the behaviour of the rock mass can be predicted. The rock mass classification systems were designed to act as an engineering design aid and were not intended to substitute field observation, analytical considerations, measurements, and engineering judgement (Bieniawski, 1993). Typical rock mass classification systems are given in Table 2.1.

Table 2.1 Rock mass classification systems

Rock mass classification system	Originator	Country of origin	Application areas
Rock Load	Terzaghi, 1946	USA	Tunnels with steel support
Stand-up time	Lauffer, 1958	Australia	Tunnelling
Rock Quality Designation (RQD)	Deere et al., 1967	USA	Core logging, tunnelling
Rock Structure Rating (RSR)	Wickham et al., 1972	USA	Tunnelling
Rock Mass Rating (RMR)	Bieniawski, 1979 (1989)	South Africa	Tunnels, mines, slopes, foundations
Modified Rock Mass Rating (M-RMR)	Unal and Ozkan, 1990	Turkey	Mining
Rock Mass Quality (Q)	Barton et al., 1974 (2002)	Norway	Tunnels, mines, foundations
Strength-Block Size	Franklin, 1975	Canada	Tunnelling
Basic Geotechnical Classification	ISRM, 1981	International	General
Rock Mass Strength (RMS)	Stille et al., 1982	Sweden	Metal mining
Unified Rock Mass Classification System (URCS)	Williamson, 1984	USA	General
Communication Weakening Coefficient System (WCS)	Singh, 1986	India	Coal mining
Rock Mass Index (RMi)	Palmstrom, 1996	Sweden	Tunnelling
Geotechnical Strength Index (GSI)	Hoek and Brown, 1997	Canada	Underground excavations

2.2. ADECO – RS Approach

The Analysis of Controlled Deformation in Rock and Soils (ADECO – RS) approach was conceived by Eng. Pietro Lunardi during his profession and long-time experience in the tunnelling field. This tunnelling approach was born after three research stages (Lunardi, 1994, 2008) where numerous tunnels were studied in order to characterize the rock mass or soil deformative behaviour during the excavation phases. This approach is focused on the rock mass deformations ahead of the tunnel face and on reinforcement systems applied to control the ground deformative response. The most important portion of the tunnel to be studied is the advance core. Advance core is the volume of rock mass ahead of the excavated face. Both height and length of the advance core are of the same size as the tunnel diameter. According to ADECO – RS approach, three different ground deformations can be defined (Figure 2.1):

- **Extrusion**: the primary deformation response of the tunnel. It is dependent on the rock mass mechanical behaviour. Extrusion represents a tunnel face longitudinal swelling;
- **Preconvergence of the cavity**: convergence of the tunnel profile ahead of the excavated face. It mainly depends on the deformative behaviour of the rock mass in addition to the original in situ stress state;
- **Convergence of the cavity**: the decrease of the theoretical cross-section of the excavated portion behind the tunnel face.

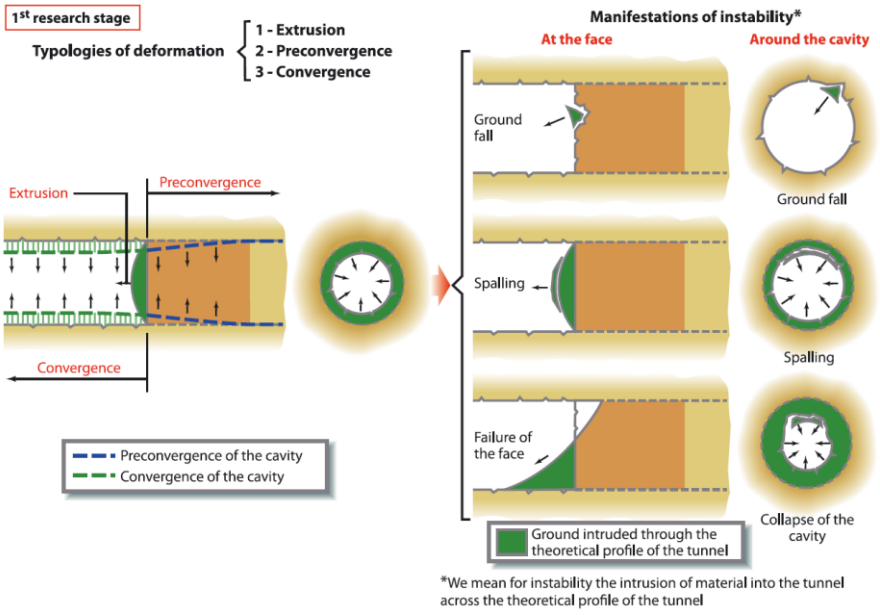

Figure 2.1 Tunnel deformation response during the excavation.(Lunardi, 1994)

Field observations and deformations monitoring show that there is a clear connection between extrusion, preconvergence, and convergence (Lunardi, 2000). These deformations are recognized as the key aspect of all the rock mass response processes.

The observation of the deformative response of rock mass allows defining its behaviour categories. Three fundamental behaviour categories could be identified (Lunardi, 1994) (Figure 2.2):

- Category A: Stable core-face. The stress state around the cavity is lower than the strength properties of the surrounding ground, so the deformations are in the elastic range. Tunnel face is stable, only local instability may occur caused by unfavourable configurations of the discontinuities;
- Category B: Stable core-face in the short term. The stress state around the cavity is a bit higher than the rock mass strength parameters. Instability may occur but usually, a support system is required;
- Category C: Unstable core-face. The stress state around the cavity is considerably higher than the rock mass strength characteristic. Without any intervention, the tunnel face will collapse caused by high radial deformations.

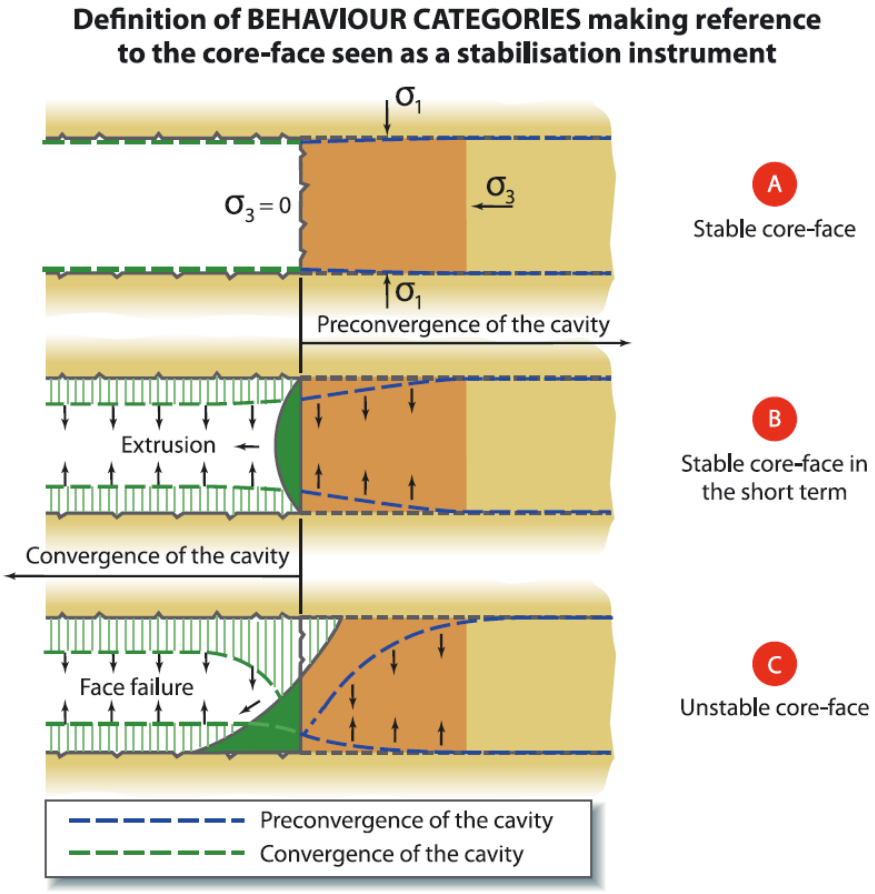

Figure 2.2 Rock mass behaviour categories. Source: (Lunardi, 1994)

Acting directly on the advance core stiffness by different preconfinement systems can reduce the ground deformations response (Lunardi, 1999) as schematized in Figure 2.3.

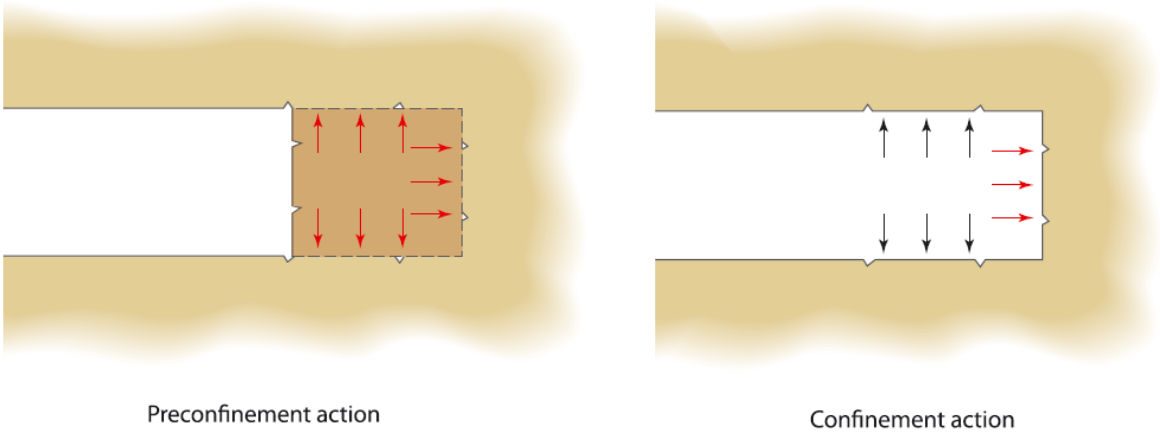

Figure 2.3 Left: Cavity preconfinement used in ADECO – RS approach. Right: Cavity confinement action (Lunardi, 1994)

Cavity preconfinement reduces the cavity radial displacement. In fact, consider point A located on the tunnel crown (Figure 2.4). When the distance between A and the tunnel face is higher than the advance core length, the stress condition is equal to radial confinement pressure p_0, corresponding to the original pressure. During the excavation advance, the radial pressure p_1 decreases so point A starts to radially move downward. Finally, when the tunnel face is passed, the displacements of the point A, where p_2 is equal to zero, continue in an elastic or elastic-plastic range. The mechanical behaviour depends on the original stress-state, the ground mechanical characteristics around the face and the supports radial confinement pressure. The following figure shows the difference between a deformable advance core (curve I) and a rigid, or reinforced, advance core (curve II). The radial deformation of point A are lower for a reinforced core, where the elastic modulus is higher than the original elastic modulus of the ground.

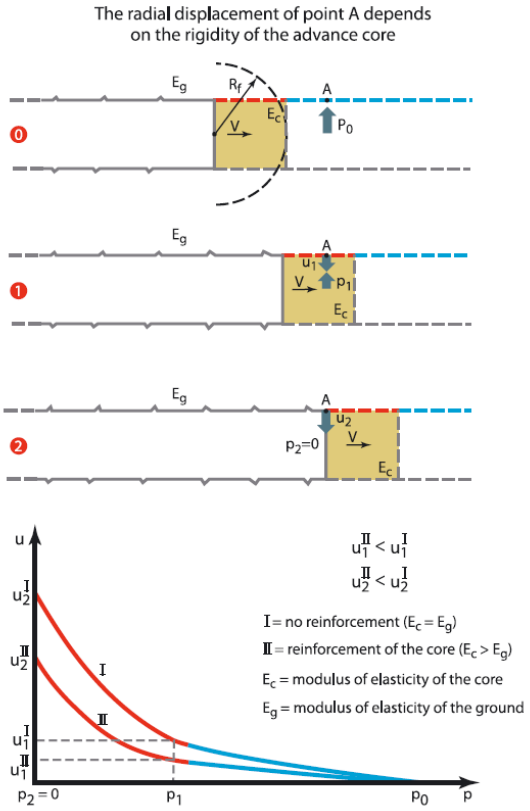

Figure 2.4 Radial displacement of a point A in a deformable or rigid advance core. (Lunardi, 2008)

Various types of preconfinement systems can be applied as a function of the stress state and the mechanical characteristic of the surrounding rock mass (Peila, 1994). If the stress state is lower related to the medium characteristic, only radial action can be used without any longitudinal pre-reinforcement inside the advance core. Instead, if the stress state has a high value it is necessary to apply a reinforcement system both longitudinally and radially.

The advance core preconfinement is obtained through four principal methods (Lunardi & Bindi, 2004):

- Fibreglass reinforcement (FGT);
- Fibreglass reinforcement and mechanical pre-cutting (FGT + PT): mechanical pre-cutting is applied by a cutting drill at the tunnel crown. The excavation is finally quickly filled with shotcrete;
- Fibreglass reinforcement and sub-horizontal jet-grouting (FGT + HGJ): this method mechanically improves the surrounding rock mass, creating an arch effect on the tunnel crown;
- FGT + FGT: fibreglass reinforcement of the core, placed in advance and injected with grout.

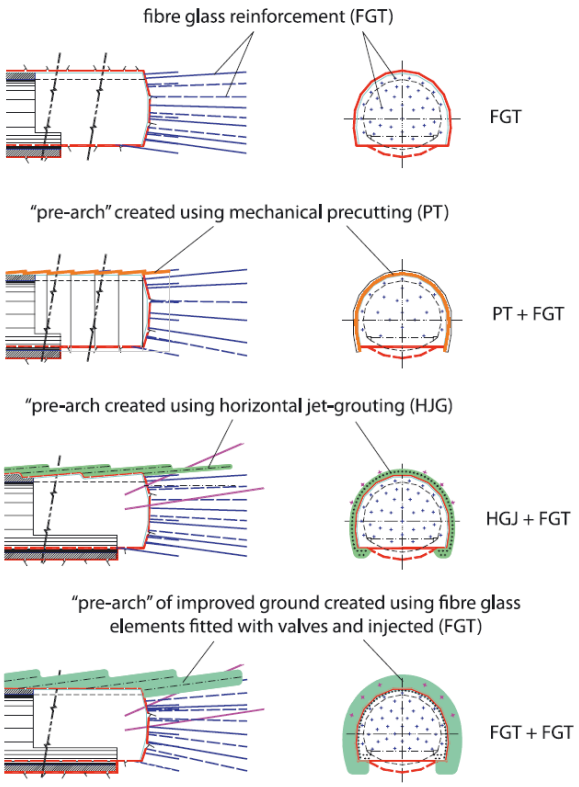

Figure 2.5 Principal preconfinement method applied in ADECO – RS approach (Lunardi, 2008)

ADECO – RS approach suggests a basic framework (Figure 2.8) to follow and apply during the design and the constructions of underground works. Design phases consist of a survey plan for determining the medium characteristic, a diagnosis phase where the tunnel is divided in various section as a function of the mechanical strength and expected deformations, and a therapy phase in which the designer evaluates the best preconfinement or simple confinement system to apply in order to reduce deformations. Finally, the construction phase is divided into an operational phase, where the works are carried out based on the project hypothesis, and in a monitoring phase. While the tunnel is excavated, deformations are measured and interpreted to verify the project assumption. According to the developed approach, the monitoring of the advance core represents a key aspect of tunnelling. Tunnel preconvergence represents the first deformative response of the advance core, so a preconfinement intervention could improve face stability. However, a preconfinement intervention must be controlled and monitored for all the construction phase to validate the support efficiency and the applied advance method (Lunardi & Cassani, 2006).

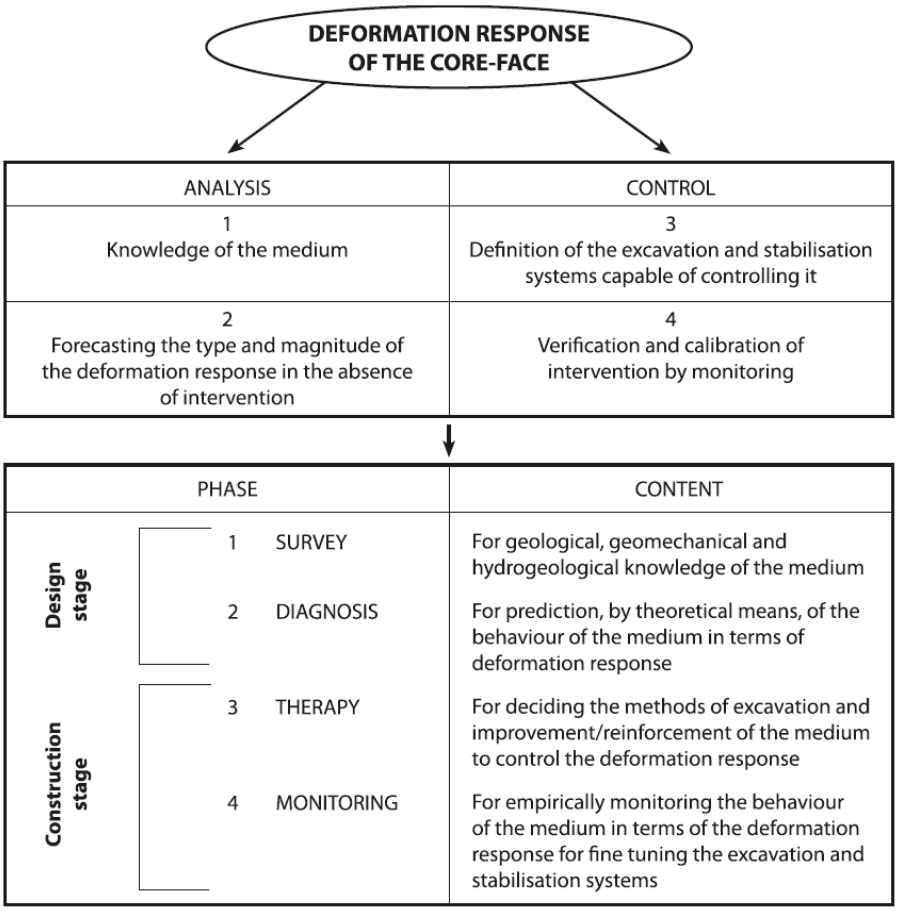

Figure 2.6 ADECO – RS framework used for all types of ground or rock mass (Lunardi, 2008)

The ADECO – RS approach was successfully applied in several tunnel projects (Lunardi, 2001; Lunardi et al., 1992, 2007, 2014), even when other tunnelling approaches failed as for Tartaguille tunnel (Lunardi, 1991). Tartaguille tunnel was initially built with another tunnelling approach, called "New Austrian Tunnelling Method" (NATM). The measured convergence phenomena were too high to keep the cavity open. Only after a preconfinement intervention, deformations were controlled and monitored, and finally, the project was completed in advance and relative costs were lower than budgeted.

3. Tunnel monitoring

Tunnels are complex constructions generally built in difficult geological contexts. Monitoring systems must detect the interaction between the excavation phases and the surrounding ground as well as the relationship with surface buildings due to settlements that can be induced by works (Kavvadas, 2003). The activation of the monitoring system should be performed in advance of the beginnings of the construction works to monitoring the induced changes that may occur. Acquired monitoring data should be rapidly elaborated and sent to the technicians responsible of the project. Nowadays digital sensors can easily connect to data logger and the monitoring data could be rapidly sent to an elaboration centre where the data are finally elaborated and interpreted to verify the geotechnical conditions on site (Segalini et al., 2017).

Generally, a tunnel project provides critical cross-sections to be monitored. The cross-sections position depends on the geological criticality as the change of excavated medium, presence of soft soils, or high presence of discontinuities or faults.

This chapter will briefly introduce the available monitoring instruments for underground works, divided into the physical quantities to measure.

3.1. Stresses measures

3.1.1. Load cells

Load cells (Figure 3.1) are instruments for the measure of the forces applied on a structure as steel ribs or tie rods. The electric load cell generates an electrical signal proportional to the applied forces. The signal is converted into physical units by applying the calibration coefficients. Generally, load cells in underground constructions are used to monitor the forces on the linings.

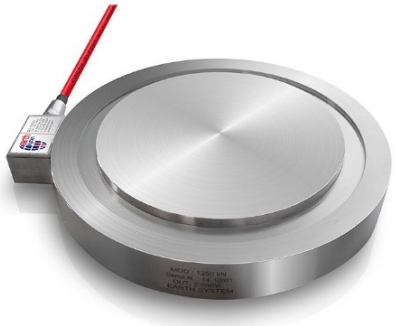

Figure 3.1 Example of an electric load cell (source: Earth System S.r.l.)

3.1.2. Pressure cells

Pressure cell (Figure 3.2) measures the distribution of radial or tangential pressure on tunnel linings. Pressure cells can be hydraulic or a membrane cell. Hydraulic pressure cell consists of two rectangular or square steel plates welded together and separated inside by a small cavity filled with a not aerated oil connected to an electrical transducer that converts every pressure change into an electrical signal variation.

Figure 3.2 Example of a hydraulic pressure cell (source: Earth system S.r.l.)

3.2. Measure of water level and pore pressure

3.2.1. Open circuit piezometer

Piezometers (Figure 3.3) are instruments for the water level measure. Open circuit piezometers are composed of a filter cell inserted in a blind pipe. The borehole is filled with sand, so the water can enter inside the standpipe reaching a pressure equilibrium corresponding to the surrounding water level.

Figure 3.3 Example of an open standpipe piezometer (source: Geotech AB)

3.2.2. Casagrande piezometer

The Casagrande piezometer (Figure 3.4) monitors the water pressure in permeable soils. It consists of an isolated filter cell inside a borehole sealed by bentonite, concrete, or clay to prevent the contamination of the water level with other aquifers.

Figure 3.4 Example of a Casagrande piezometer (source: Earth System S.r.l.)

3.3. Measure of deformations

3.3.1. Inclinometers

Inclinometers (Figure 3.5) are instruments for monitoring differential deformations in soils or geotechnical structures. In underground works, they are used for monitoring the displacement related to tunnel construction and usually are placed beside and up to the crown of tunnels. The inclinometer system consists of a pipe inserted in a borehole and in an inclinometer probe. The probe has two couples of wheels that ensure the azimuthal direction. The measures are carried out by an operator who inserts the probe in the grooves of the ABS or aluminium case and reads the deviation value along the entire pipe depth, generally every 50 cm. The readings are evaluated and stored by a control unit.

There are also in place inclinometers that work following the same procedure, but the inclinometer sensors are at fixed depth inside the pipe. The readings are carried out by an automatic data acquisition system.

Figure 3.5 Example of a manual inclinometer and ABS or aluminium casing. (source: Slope Indicator)

Nowadays inclinometers are often automated and based on new electronics technologies. There are several types of inclinometers in the marketplace as Mems Underground Monitoring System,

MUMS®, (Segalini et al., 2014), Automated Inclinometer System (AIS) (Lollino, 1992) or Differential Monitoring of Stability (DMS®) produced since 2001 by CSG S.r.l.

3.3.2. Magnetic extensometer

The magnetic extensometer (Figure 3.6) monitors settlements and subsidence during and after tunnels excavation. The system consists of a PVC casing encased in a corrugated pipe. Magnetic rings are fixed at a predetermined distance along the pipe that is anchored to the ground. The probe detects the variation of magnetic field compared to the first reading to evaluate ground settlements.

Figure 3.6 Example of a magnetic extensometer probe (source: Soil Instruments)

3.3.3. Single and multipoint extensometers

Single and multipoint extensometers (Figure 3.7) evaluate the ground radial deformation around the cavity. Single extensometer has a single measurement point instead of multiple extensometers that can have a maximum of seven measure points. Extensometer rods are inserted and free to slide in a drill hole around the cavity. The movements are transferred to the head of the instrument and measured with a digital comparator or an electric displacement transducer.

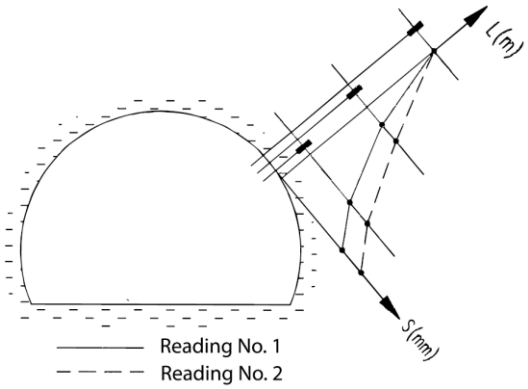

Figure 3.7 Typical extensometer monitoring (Lunardi, 1994)

3.3.4. Tilt meter

Tilt meters (Figure 3.8) measure rotations in a single point by 1D/2D Micro Electro-Mechanical Systems (MEMS). Generally, in underground works tilt meters monitor rotations of surface buildings to evaluate the excavation influence.

Figure 3.8 Example of a tilt meters (source: Earth System S.r.l.)

3.3.5. Convergence measurements

Convergence measurements are carried out for defining the reduction of the tunnel section area due to the stress redistribution around the free surface (Riaz, 2015). Convergence can be measured with a tape extensometer, that measures distances between reference points fixed on tunnel walls or with an extensometer radially installed around the cavity. In most tunnel monitoring applications, convergence is measured in three-dimension by geodetic surveys using a total station (Kontogianni & Stiros, 2005) (Figure 3.9). The total station is placed at a predetermined position inside or at the entrance of the tunnel, measuring optical reflectors placed along the tunnel face creating the convergence star.

Figure 3.9 Example of a geodetic survey in tunnels (source: Monteith & Sutherland survey)

Another convergence monitoring tool has been developed using the MUMS approach. This tool, called Cir Array, automatically measures convergence along a critical section using MEMS accelerometers. Cir Arrays were successfully installed in different tunnelling projects (Cavalca et al., 2018), (Savi et al., 2019). Monitoring results are represented by local and cumulate displacements

along the monitored section. Moreover, a convergence star is estimated and represented as in the topographic traditional monitoring.

3.3.6. Extrusion measurements

Extrusion measurements (Figure 3.10) evaluate the longitudinal deformation of the de-stressed zone ahead of the tunnel. Extensometers station is usually installed in the centre of the tunnel face for 2-3 tunnel diameters length. The monitoring station consists of an incremental extensometer and metal rings inserted in a pipe at regular interval, typically 1 meter (Tonon, 2011). The distance between metal rings could be measured by inserting a probe that evaluates distances variation from the generated electrical signal of measuring rings. Generally this method provides an accuracy of ±0.003 m/m (Lunardi, 2000).

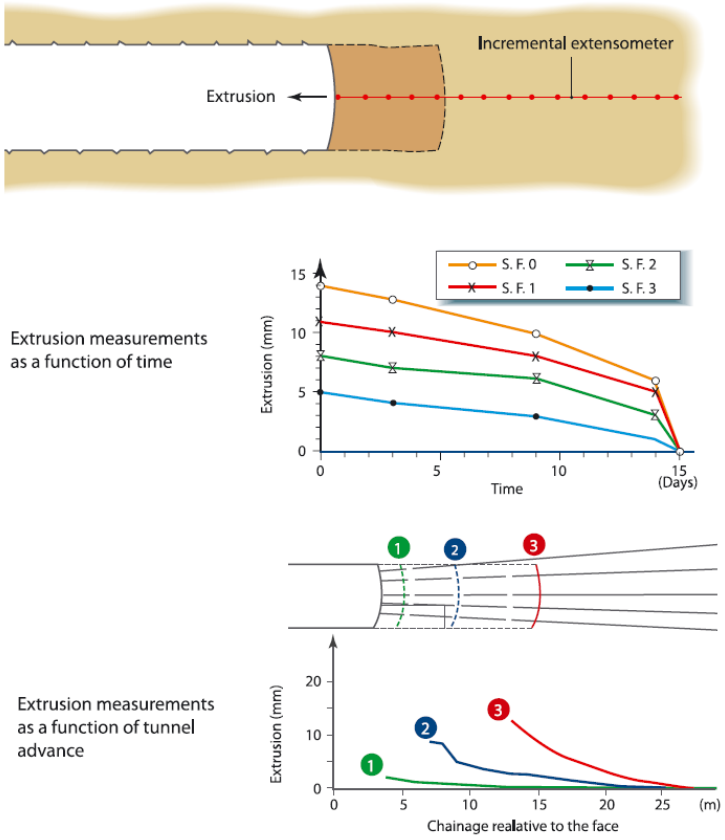

Figure 3.10 Example of a extrusion monitoring . Source: (Lunardi, 2000)

3.3.7. Preconvergence measurements

The first preconvergence measurements were carried out by multi-point extensometers installed vertically above the tunnel cavity (Lunardi, 1994). These measurements can be executed only for shallow tunnels or when the overburden is limited. The study of the deformation response evaluated by preconvergence monitoring together with extrusion measurements, permitted to define a

relationship between these two quantities, depending on the extrusion type occurred on the tunnel face (Figure 3.11). Indeed, extrusion can be cylindrical, spherical dome, and combined cylindrical dome-like (Lunardi, 2008).

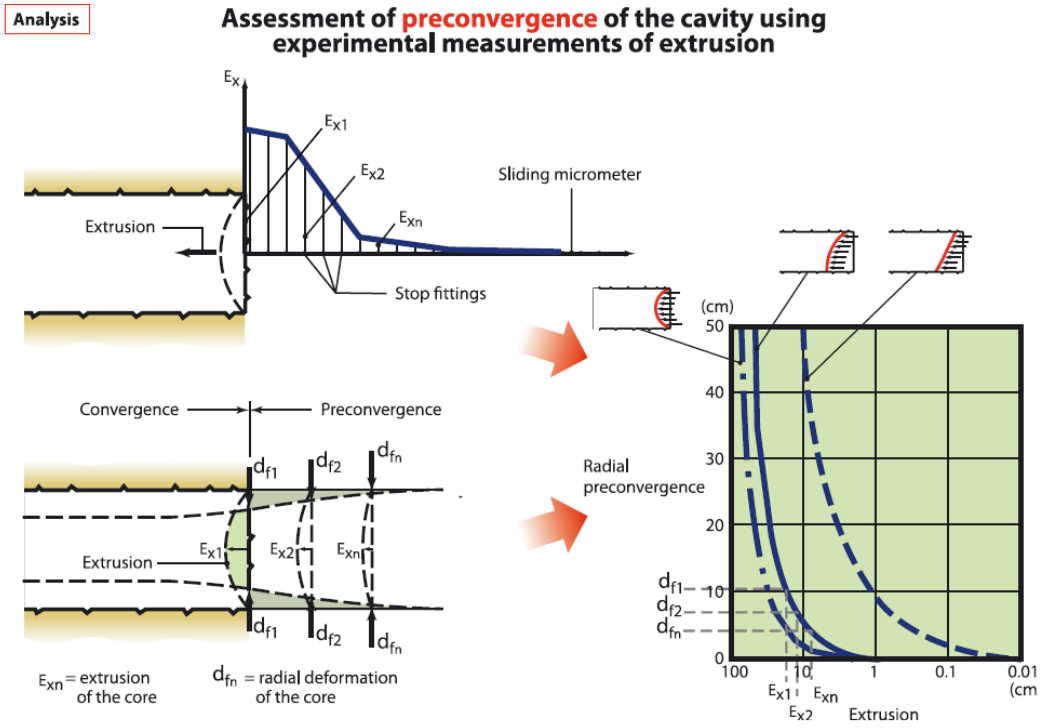

Figure 3.11 Relationship between extrusion and preconvergence. Source: (Lunardi, 2008)

By the presented table in Figure 3.11 is possible to estimate the preconvergence deformations acting on the advance core as a function of the measured extrusion on the tunnel face.

Nowadays other preconvergence measurements are executed, principally by horizontal inclinometer(Chung et al., 2010; Jeon et al., 2005; C.-H. Kim et al., 2008; C. Kim, 2013) or by in-place horizontal inclinometer installed at the tunnel entrance or parallel to the pipe roof (Volkmann & Schubert, 2005). The main differences between the proposed preconvergence monitoring system and horizontal inclinometers will be discussed in the following chapter.

To summarize the tunnel monitoring tools, a possible monitoring plan layout is shown in Figure 3.12. The figure shows a typical monitoring plan both for shallow and deep tunnels, considering also the monitoring of the nearby buildings in terms of vibrations induced by excavation works, and rotation due to ground settlements.

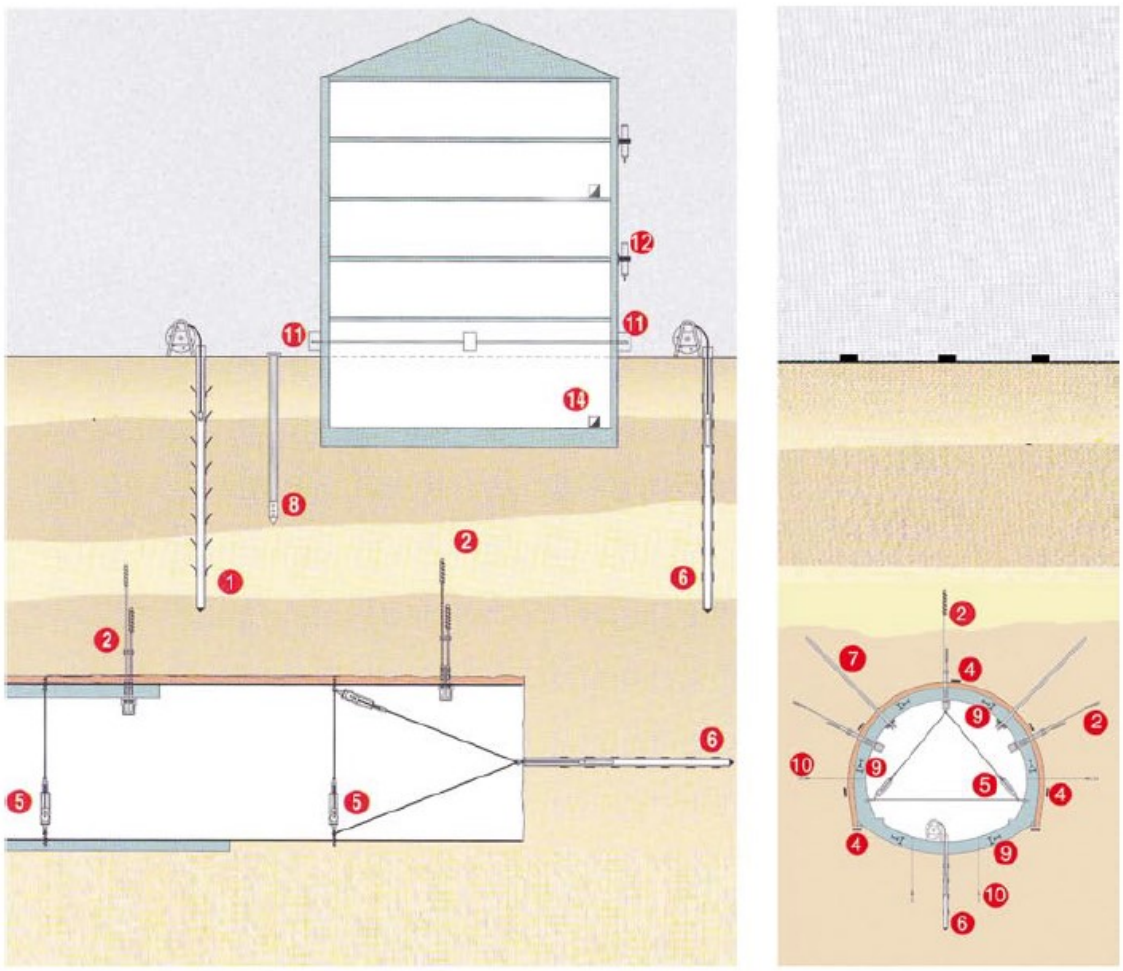

1 **Magnetic settlement meters**
Ground settlement

2 **Multipoint extensometers**
Deformation / plasticitation of the ground

3 **Smach accelerograph**
Vibrations during excavation

4 **Pressure cells**
Pressure on the ground-lining interface

5 **Tape distometers**
Convergence in the tunnel

6 **Incremental extensometers, inclinometers**
Ground extrusion and deformation

7 **Anchor load cells**
Rock bolts and anchors pull

8 **Piezometric-settlement column**
Piezometry and settlement

9 **Strain gauges**
Lining stress and strain

10 **Electrical piezometers**
To control neutral pressures

11 **DSM level measurement system**
Differential settlements

12 **Surface clinometers**
Vertical inclination of buildings

Figure 3.12 Tunnel monitoring typical layout, showing both surface and deep deformations monitoring. Source: (Lunardi, 1994)

4. Pre-Conv Array

4.1. Introduction

Pre-Conv Array is an innovative instrument to measure the preconvergence during tunnels excavation. Pre-Conv Array has been developed after several years of landslide and tunnel monitoring and risk management researches by ASE S.r.l., a spin-off of the University of Parma(Segalini et al., 2014, 2017). This innovative monitoring idea was born in 2011 when an automated inclinometer tool was designed to replace manual measurement procedures (Segalini et al., 2011). The proposed automated monitoring system presents clear advantages compared to traditional instruments(Carri, 2019):

- It reduces the uncertainties due to manual measurements;
- It permits to collect data, even if the construction site is not accessible or in case of bad weather;
- It presents a higher reading frequency than traditional systems, so collected data are subjected to statistical approaches to validate the results and to apply Early Warning System, if required.

Since 2011 several other monitoring systems have been designed, such as an automated inclinometer or underground monitoring instruments. Underground monitoring systems developed comprise Cir Array, for the tunnel convergence monitoring (Segalini et al., 2018b), and Rad Array for radial displacements monitoring around the tunnel face (Segalini et al., 2018a). Both Cir Arrays and Rad Arrays measure deformations along the tunnel face or in critical sections already excavated. However, these systems do not provide information on deformations ahead of the advance core, therefore, it is not possible to gain extensive three-dimensional monitoring ahead and behind tunnel face. The main advantage of such three-dimensional deformative state monitoring is to improve the knowledge of the surrounding rock mass and, most importantly, it permits to define the appropriate support system to apply and the appropriate advance method. Preconvergence measurements, together with convergence and radial monitoring show the advantage to define the complete three-dimensional radial displacements acting on the tunnel face, to validate numerical models of the tunnel, and, finally, to define the effective displacements recorded before the support installation (Figure 4.1).

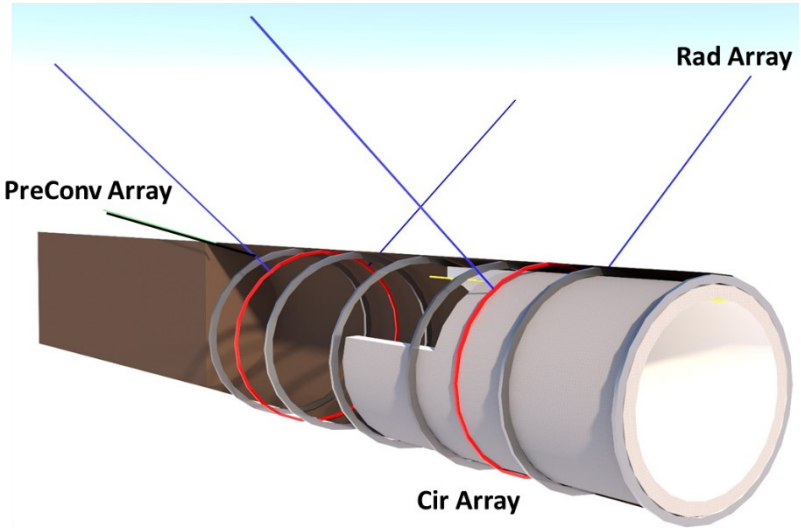

Figure 4.1 3D monitoring of a tunnel face. Adapted from (Segalini et al., 2018b)

Once the excavation phase passes the monitored section or one of the embedded sensors, the instrumented chain can be used for the convergence evaluation. The Pre-Conv Array returns deformations ahead and behind the tunnel face, so after the tunnel construction. These data can be used for convergence evaluation on the tunnel crown, allowing to monitor also the operativity phase of tunnels.

Pre-Conv Array consists of a chain of synthetic resin sensors (Pre-Conv Links) (Figure 4.2), located at predefined distances. The sensors measure the ground differential vertical settlements due to excavation phases. Each sensor is linked by a quadrupole electrical cable and a fiberglass rod to preserve the correct alignment and distance between each sensor. The sensors are 5.4 cm wide and 3.9 cm height, with a bottom plate, realized to prevent sensor rotation during the installation phase.

Figure 4.2 shows an example of the realized Pre-Conv Link, defining the reference system for each node. The *X* axis is longitudinally directed in the excavation direction, giving the vertical settlements, while the *Y* axis is orthogonally directed with respect to the previous one, giving roll information. Finally, the *Z* axis is directed downward, parallel to the gravity vector.

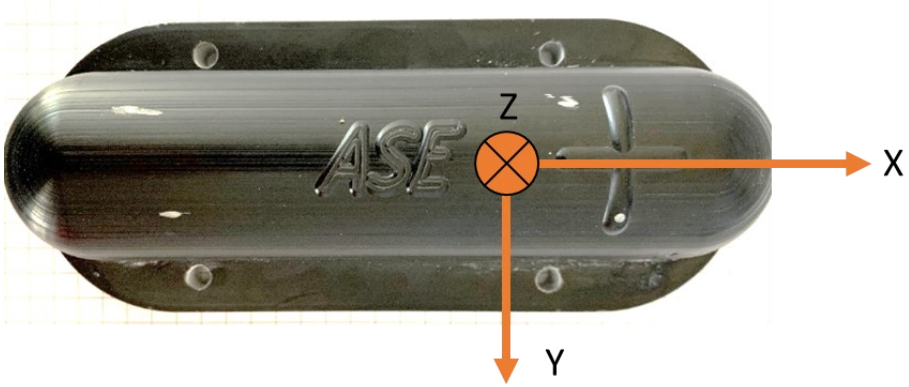

Figure 4.2 Pre-Conv Link axis definition

The principle of the monitoring system is schematized in Figure 4.3.

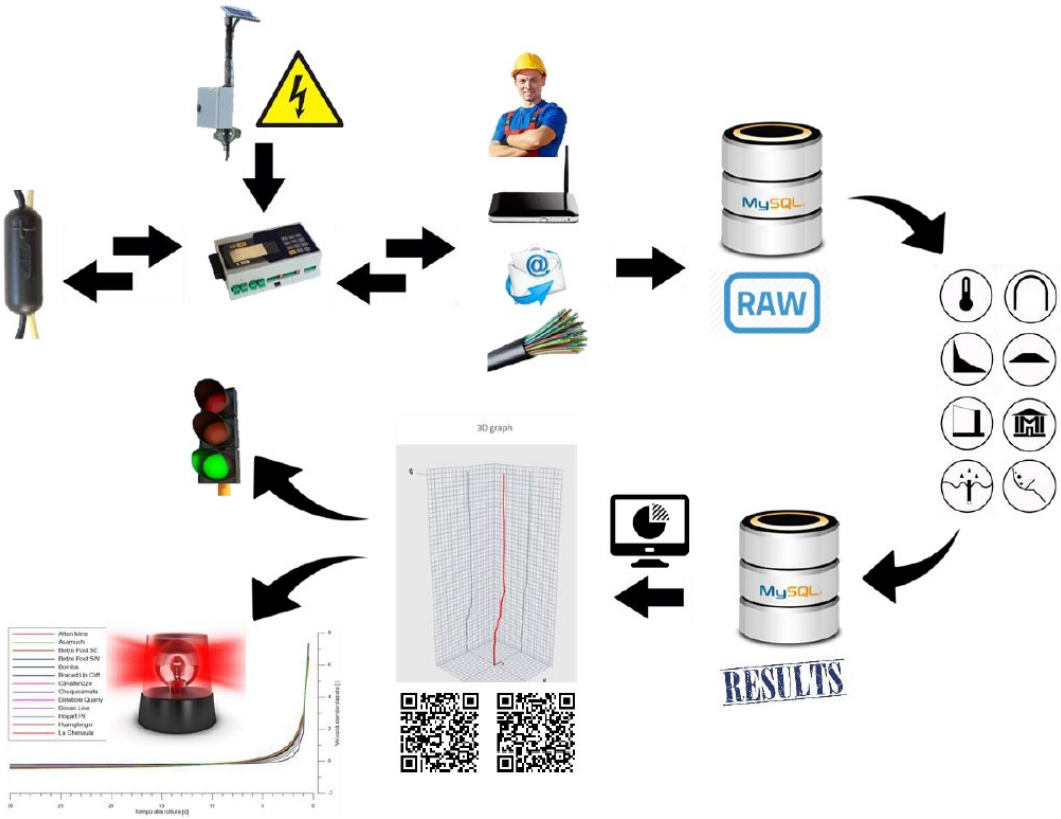

Figure 4.3 Principle of the monitoring system. Adapted from (Segalini et al., 2019)

The array is fully automated and monitoring data are collected by a controlled data logger with an RS485 communication protocol. Pre-Conv Links are queried by a control unit ASE801 at predefined sample time, which is a function of the monitoring requirements and work phases. Control units query each sensor 64 times in about 1 second, the resulting mean value is saved in an external SD card. This process represents the first filter to raw data, removing uncertainties or spike values due, for example,

to vibrations induced by excavation works. Generally, the control unit is powered by an electrical line, which is usually available in the construction site but can be also powered by a solar panel and a 12 V 7 Ah battery in hardly accessible sites. Then, the collected data are automatically sent by a UMTS router to a local elaboration centre. However, during the monitoring phase, the data can also be manually sent by an operator. This possibility is especially important during the first days of monitoring when the excavation works do not guarantee a safe installation of the collecting system inside or near the tunnel. Raw data are sent and stored in a database that implements multiple daily backups. Moreover, raw data are automatically elaborated by a specific algorithm that converts electrical signals into physical quantities, removing spike noises or accidental errors, therefore providing a second filtering step. The algorithm processing will be described in section 4.3. Elaborated data are then loaded in a dynamic Web platform, which can be accessed through security credentials. The authentication procedure is fundamental to deal with monitoring data. A huge number of monitored sites requires accurate security management and an easy interpretation of the results through several available graphs. Finally, by providing alarm or attention thresholds, alert, or alarm messages can be activated and sent to the authority responsible for the monitoring.

Pre-Conv Array can be installed in several configurations. The installation differences depend on the geomechanical parameters of the surrounding rock mass. Table 4.1 schematizes four possible application field categories depending on the excavation method.

Table 4.1 Possible installation procedures

Tunnel excavation method	Possible installation
Conventional tunnel excavation (preconfinement intervention not required)	Sub-horizontal borehole above tunnel crown
	Sub-horizontal drilling after a pilot tunnel realization
	Guided perforation above tunnel crown
Conventional tunnel excavation (preconfinement intervention required as umbrellas)	Instrument installation inside pipe used for jet-grouting preconfinement
Tunnel Boring Machine (TBM)	Sub-horizontal borehole above tunnel crown
TBM from vertical shafts	Horizontal borehole above tunnel crown

4.1.1. Conventional tunnel excavation (preconfinement not required)

Tunnels are excavated in a rock mass with high strength parameters, so a preconfinement intervention is not required. In this case, the installation could be executed by three methods.

4.1.1.1. Sub-horizontal borehole above tunnel crown

The first method consists of a sub-horizontal borehole (4÷6°) realized above the tunnel crown, with a minimum 80 mm diameter. The borehole could be coated by a PVC pipe in which the instruments could be installed and finally cemented (Figure 4.4).

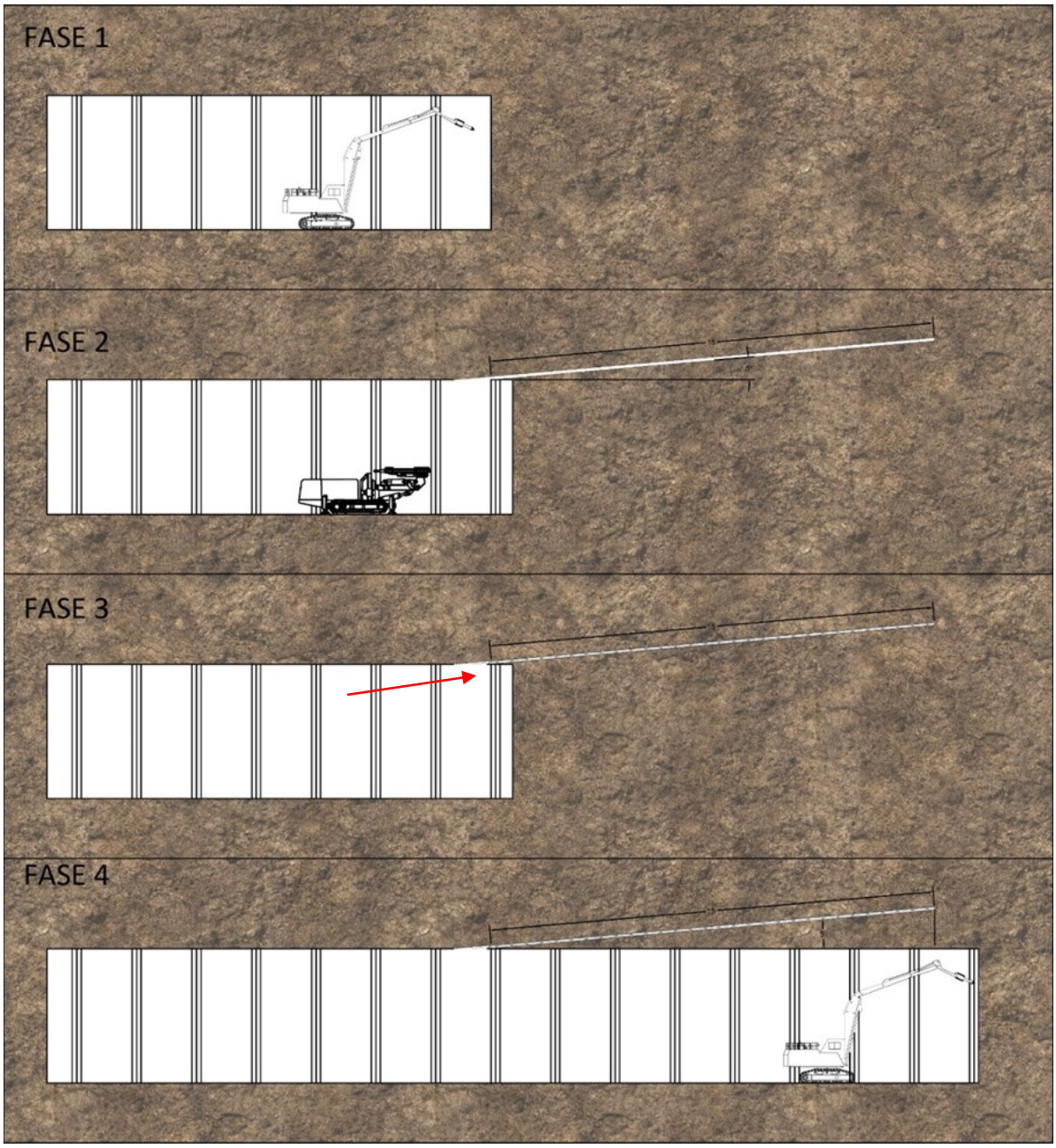

Figure 4.4 Phase 1: Tunnel excavation until the monitored section; Phase 2: sub-horizontal borehole excavation; Phase 3: Pre-Conv installation; Phase 4: Tunnel advance and monitoring of induced deformations. Figure adapted from (Savi et al., 2019)

4.1.1.2. Sub-horizontal drilling after a pilot tunnel realization

The second possible installation method without preconfinement, consists of a small pilot tunnel excavation, realized to install horizontally the Pre-Conv Array (Figure 4.5).

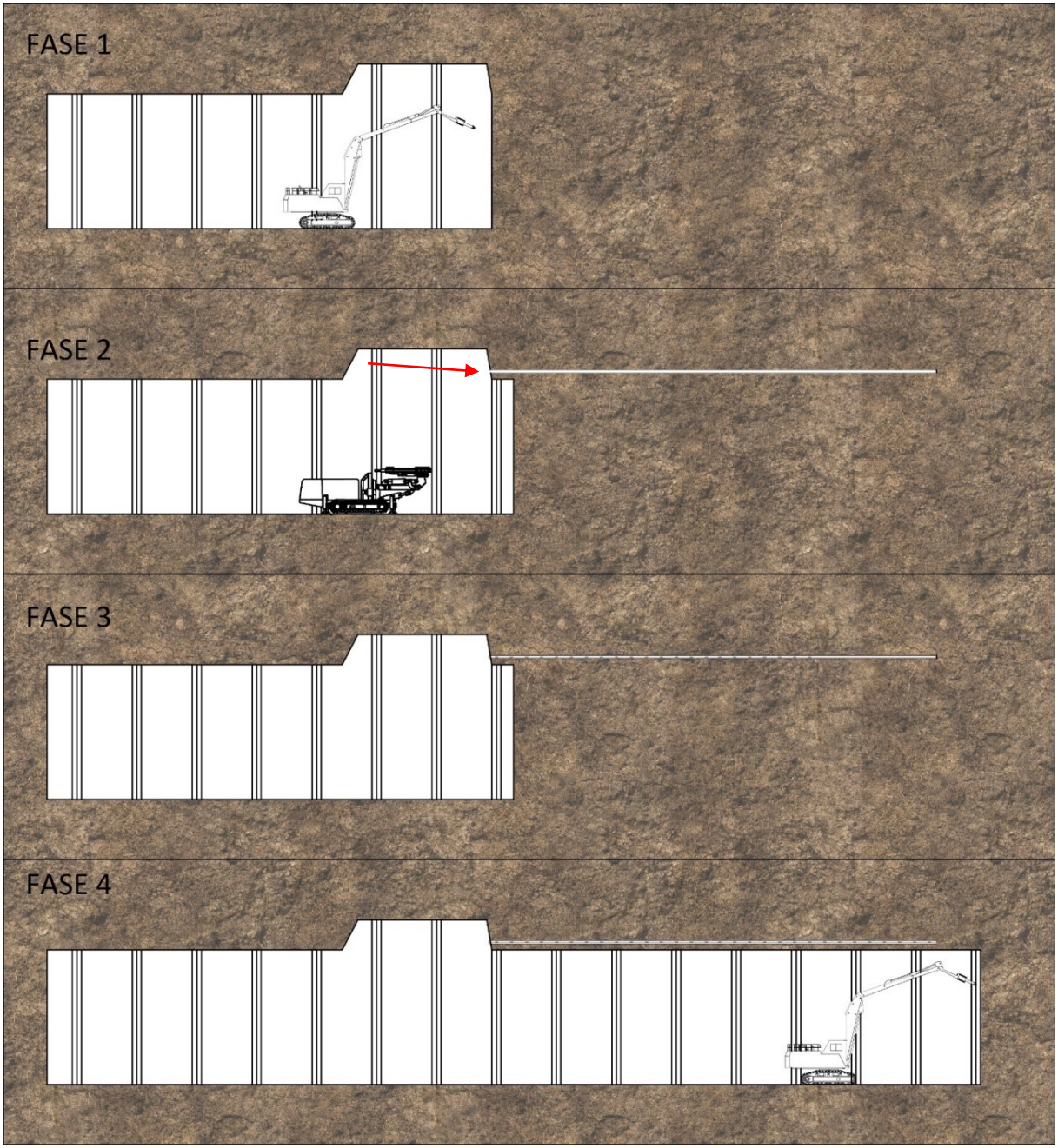

Figure 4.5 Phase 1: Tunnel excavation until the monitored section and pilot tunnel realization; Phase 2: Horizontal borehole; Phase 3: Pre-Conv Array installation; Phase 4: Tunnel advance and monitoring of induced deformations. Figure adapted from (Savi et al., 2019)

4.1.1.3. Guided perforation above tunnel crown

The third installation method consists of a guided installation above the tunnel crown, where the initial portion of the borehole is curved. The remaining Pre-Conv Links are installed horizontally (Figure 4.6).

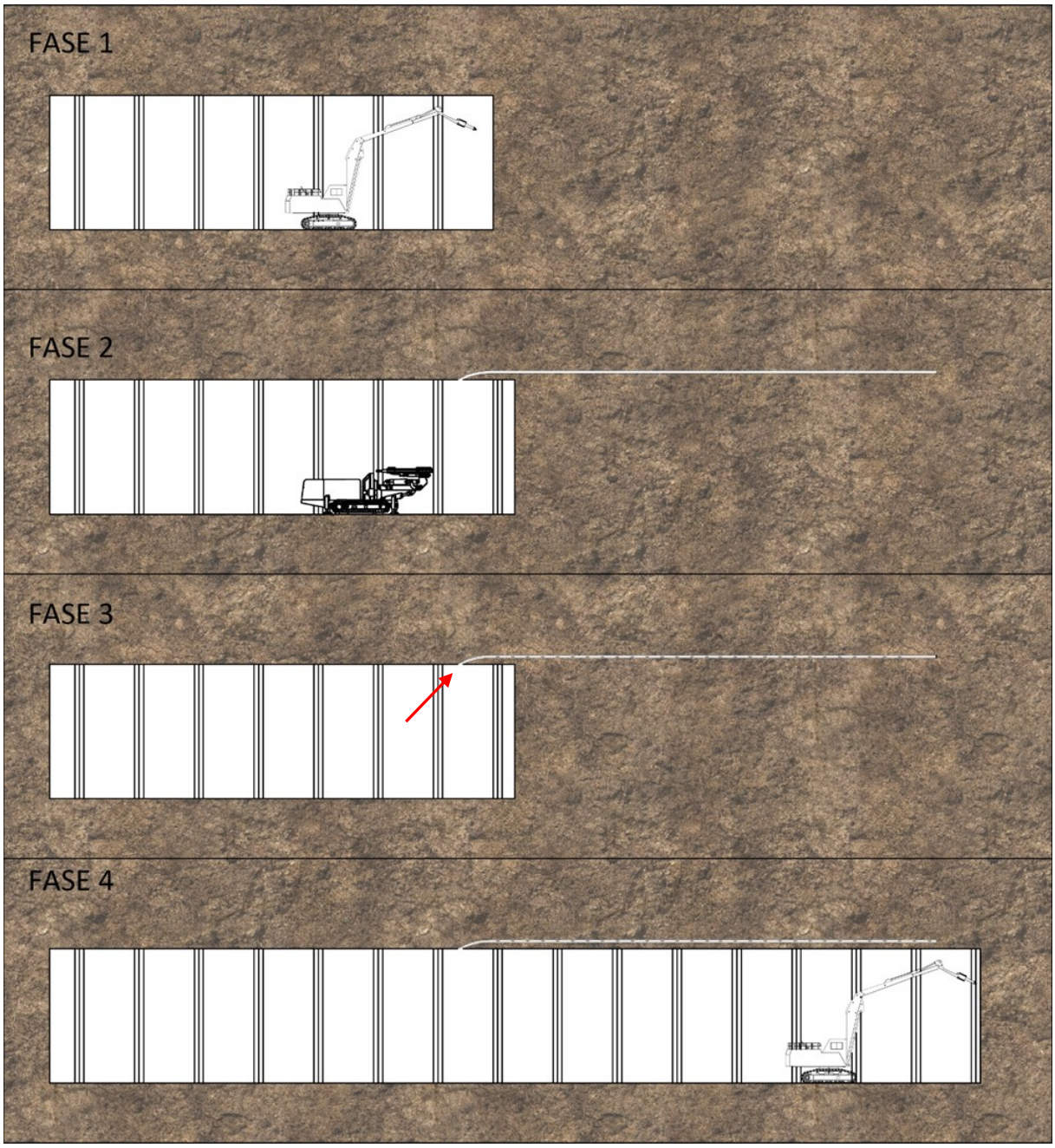

Figure 4.6 Phase 1: Tunnel excavation until the monitored section; Phase 2: Curved borehole realization; Phase 3: Pre-Conv Array installation; Phase 4: Tunnel advance and monitoring of induced deformations. Figure adapted from (Savi et al., 2019)

4.1.2. Conventional tunnel excavation with preconfinement intervention

In case the realized tunnel requires a preconfinement intervention, as 'umbrellas' of sub-horizontal jet-grouting columns of improved ground, Pre-Conv Array could be directly installed and cemented inside the borehole, to evaluate the support efficiency and stability in time (Figure 4.7).

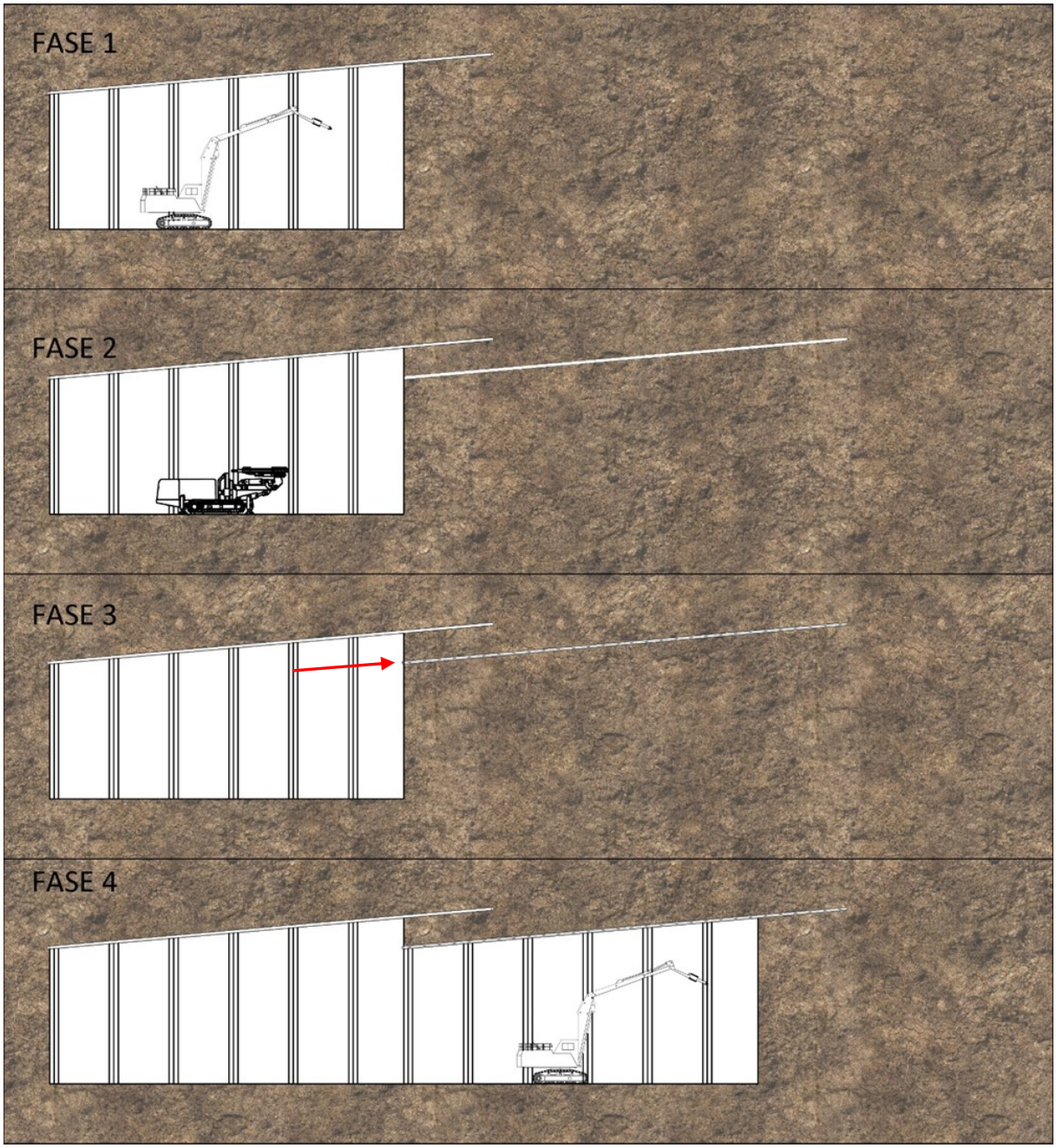

Figure 4.7 Phase 1: Tunnel excavation until the monitored section; Phase 2: Umbrella of jet-grouting realization; Phase 3: Pre-Conv Array installation inside the jet-grouting pipe; Phase 4: Tunnel advance and monitoring of induced deformations. Figure adapted from (Savi et al., 2019)

4.1.3. Shielded TBM

The following installation method can be used in case the tunnel is excavated by shielded TBM. The Pre-Conv Array is installed inside a borehole realized throughout the TBM shield during the excavation phase. In shallow tunnels, the preconvergence monitoring is useful to define the TBM head pressure, therefore avoiding surface settlements (Tanzini, 2015) (Figure 4.8).

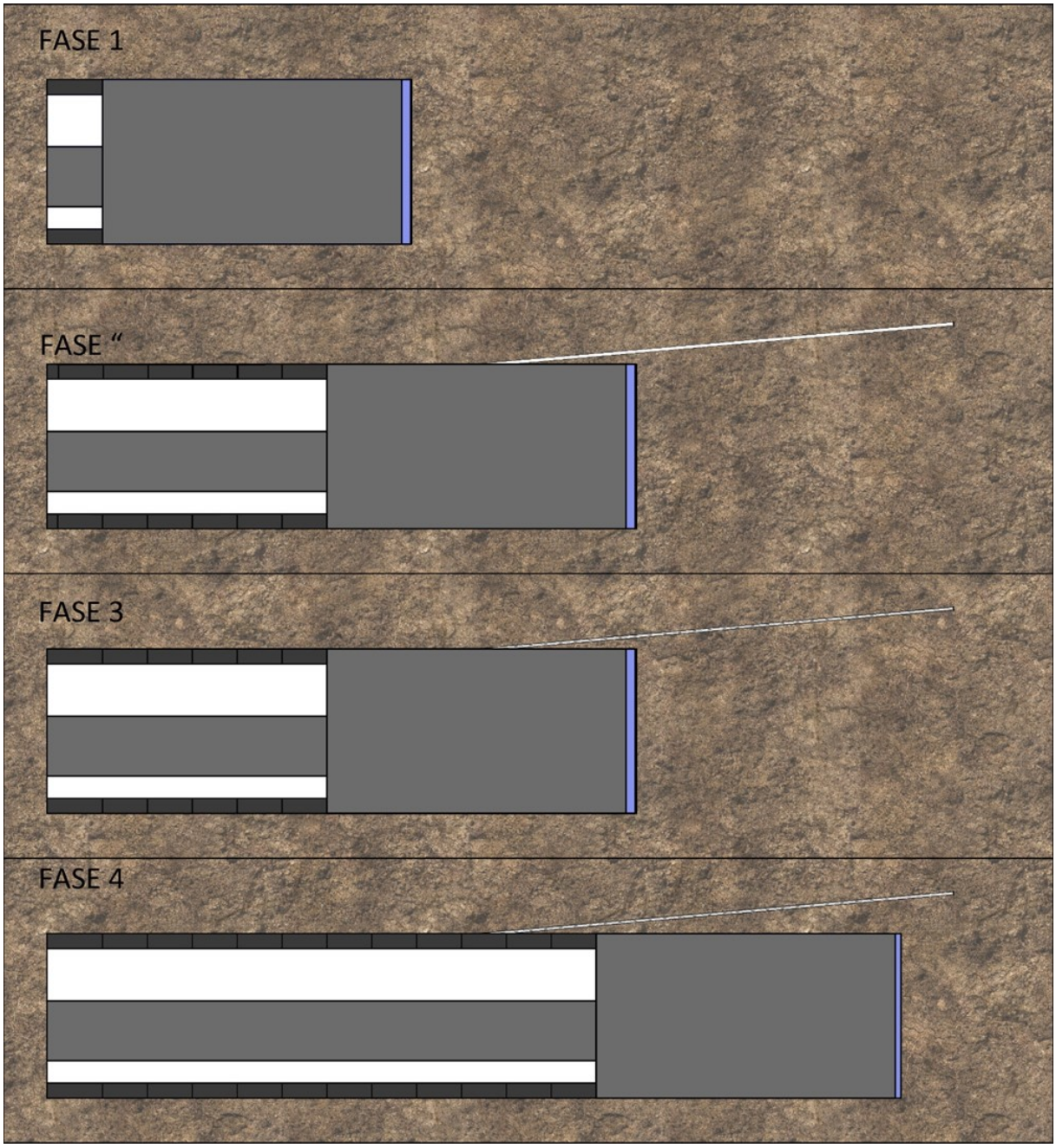

Figure 4.8 Phase 1: Tunnel excavation by shielded TBM until the monitored section; Phase 2: Borehole realization starting from the TBM shield; Phase 3: Pre-Conv Array installation; Phase 4: Tunnel advance and monitoring of induced deformations. Figure adapted from (Savi et al., 2019)

4.1.4. TBM from vertical shafts

Pre-Conv Array can also be installed in shallow tunnels to control and evaluate settlements during excavation in critical sections, as under buildings or strategic infrastructures. In this case two vertical shafts may be realized for the TBM positioning, then two horizontal boreholes are excavated to install the monitoring instrumentation (Figure 4.9).

Figure 4.9 Phase 1: The TBM excavation is preceded by two vertical shafts excavation for TBM positioning and retrieval; Phase 2: Two horizontal boreholes above tunnel crown are realized to insert the Pre-Conv Array; Phase 3: TBM excavation and monitoring of vertical displacements; Phase 4: Monitoring of vertical displacements during tunnel operational phase. Figure adapted from (Savi et al., 2019)

4.2. Pre-Conv Links and calibration procedures

Pre-Conv Links are equipped with 3D Micro Electro-Mechanical System (MEMS) and a temperature sensor (Figure 4.10). Pre-Conv Links are designed to monitor differential vertical settlements above tunnel crown during tunnel advance according to the ADECO – RS approach, where the advance core monitoring is defined as a key aspect in tunnelling (Lunardi, 1991).

Pre-Conv Link cannot detect rigid settlements, as well as the other gravity-based sensors. The main features of the used MEMS will be described in the following sections (Table 4.2).

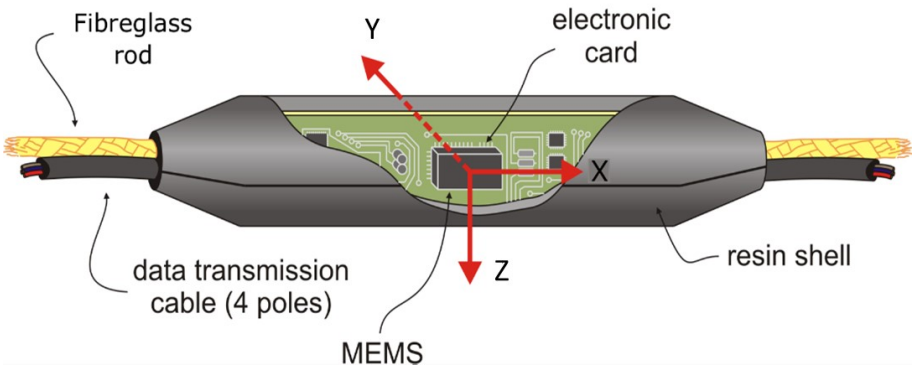

Figure 4.10 Pre-Conv Link equipped with 3D MEMS sensor and axis definition. Adapted from (Carri, 2019)

Table 4.2 Main features of 3D MEMS

MEMS features	
Linear acceleration measurement range	± 2 g
Linear acceleration sensitivity	0.244 mg/ADC
Linear acceleration sensitivity change vs. temperature	±0.008 %/°C
Zero-g level offset accuracy	± 20 mg
Zero-g level change versus temperature	± 0.15 mg/°C
Acceleration noise density	126 μg/$\sqrt{Hz}$
Temperature sensor change vs. temperature	0.96 °C/ADC
Operative temperature range	-40 ÷ +85 °C

4.2.1. Accelerometers calibration

The procedure of calibration of the accelerometers reconstructs a matrix of 11 parameters for each node, which are:

- g_{x_j}: acceleration gain of *x* instrumental axes for node *j*;
- g_{xT_j}: gain of the accelerometer thermal correction along the *x*-axis of node *j*;
- o_{xT_j}: thermal offset along the *x*-axis of node *j*;
- g_{y_j}: acceleration gain of *y* instrumental axes for node *j*;
- g_{yT_j}: gain of the accelerometer thermal correction along the *y*-axis of node *j*;
- o_{yT_j}: thermal offset along the *y*-axis of node *j*;
- g_{z_j}: acceleration gain of *z* instrumental axes for node *j*;
- g_{zT_j}: gain of the accelerometer thermal correction along the *z*-axis of node *j*;
- o_{zT_j}: thermal offset along the *z*-axis of node *j*;
- m_j: temperature gain for node *j*;
- q_j: temperature offset for node *j*.

Accelerometers of Pre-Conv Link sensors are calibrated through a thermal chamber controlled by a PLC processor. The thermal chamber is designed to host 70 nodes inside a dodecahedron. Calibrating nodes are inserted without resin shell. Indeed, nodes cannot be placed into thermal chamber with fiberglass rod installed inside the resin shell (Figure 4.11).

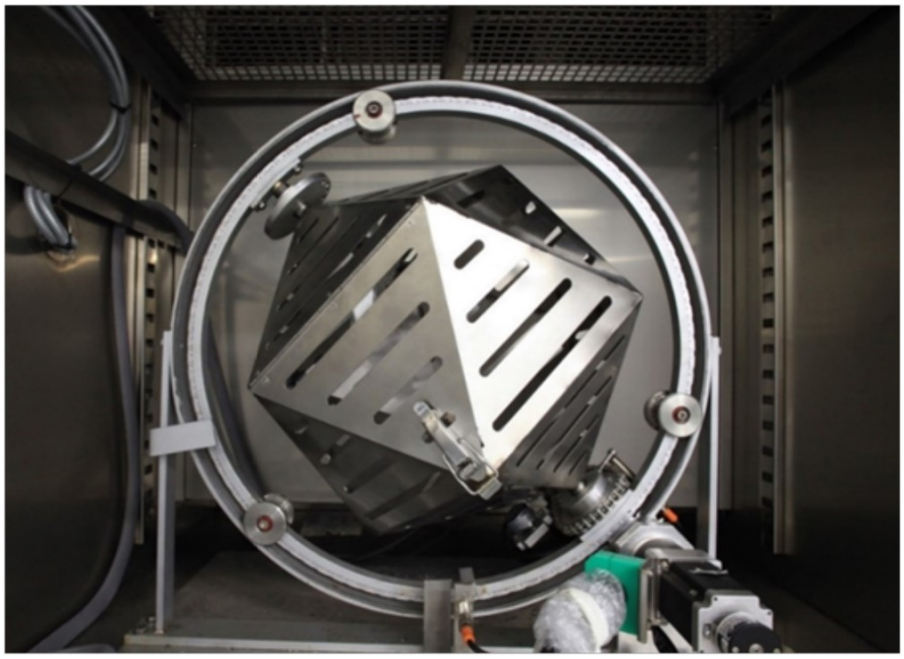

Figure 4.11 Dodecahedron designed for MEMS accelerometers calibration (Source: ASE S.r.l. manual)

The PLC processor reads each sensor at 24 positions for 10 different temperatures. The calibration parameters can be estimated using a linear regression (Skog & Händel, 2006). Since the gravity acceleration is known, the norm of the three instrumental axis measures must provide that exact value. The first 6 calibration parameters $g_{x_{j,t}}$, $i_{x_{j,t}}$, $g_{y_{j,t}}$, $i_{y_{j,t}}$, $g_{z_{j,t}}$, $i_{z_{j,t}}$ can be estimated by minimizing the $\varepsilon_{j,t}$ value as in Equation [4.1].

$$\varepsilon_{j,t} = \sum_{1}^{24} \left[G - \sqrt{\left(g_{x_{j,t}} a'_{x_j} + i_{x_{j,t}}\right)^2 + \left(g_{y_{j,t}} a'_{y_j} + i_{y_{j,t}}\right)^2 + \left(g_{z_{j,t}} a'_{z_j} + i_{z_{j,t}}\right)^2} \right] \quad [4.1]$$

Where:

- G represents the gravity acceleration (known variable), expressed in g (1 g = 9.80665 m/s^2);
- $g_{x_{j,t}}$ indicates the acceleration gain of x axes for node j, at temperature t;
- a'_{x_j} is the electrical value, expressed in ADC points of gravity acceleration along x axis for node j;
- i_{x_j} is the intercept gain of x axes for node j at temperature t;
- $\varepsilon_{j,t}$ is the sum of residuals for node j at temperature t. This value must be minimized using the linear regression method.

Once the six parameters are obtained for each node and temperature, the gains of the instrumental axis are calculated by the following equations.

The Equation [4.2] evaluates the maximum offset $g_{x_{j,t_M}}$ of the acceleration gain dataset for each instrumental axis. This value is finally removed from the dataset.

$$g_{x_{j,t_M}} = max\begin{bmatrix} g_{x_{j,t_1}} - \frac{\sum_{i=1}^{10} g_{x_{j,t_i}}}{10} \\ \vdots \\ g_{x_{j,t_{10}}} - \frac{\sum_{i=1}^{10} g_{x_{j,t_i}}}{10} \end{bmatrix} \quad [4.2]$$

Where:

- $g_{x_{j,t_M}}$ is the maximum offset of the acceleration gain dataset made by ten temperatures, related to *x* instrumental axes for node *j*;
- $g_{x_{j,t_i}}$ is the acceleration gain of *x* instrumental axes for node *j* at temperature t_i.

The second step removes the secondary maximum applying the Equation [4.2] to the remaining dataset. Then, it is possible to apply Equation [4.3] to the matrix including the eight gain parameters for each axis and node, obtaining the acceleration gain parameter for one of the three instrumental axis of node *j*.

$$g_{x_j} = \frac{\left(\sum_{i=1}^{8} g_{x_{j,t_i}}\right)}{8} \quad [4.3]$$

Where:

- $g_{x_{j,t_i}}$ is the acceleration gain of *x* axis for node *j* at temperature t_i;
- g_{x_j} is the acceleration gain of *x* axis for node *j*;

The complete thermal correction of sensors is evaluated calculating different linear regression to the entire dataset represented by $i_{x_{j,t}}$, $i_{y_{j,t}}$ and $i_{z_{j,t}}$ parameters. Finally, the conversion equation from ADC data to physical units is:

$$a_{x_j} = g_{x_j} a'_{x_j} + g_{xT_j} T'_j \quad [4.4]$$

Where:

- a_{x_j} represents gravity acceleration expressed in physical units (referred to acceleration vector *g*), on the *x*-axis (instrumental reference system) of node *j*;
- g_{x_j} is the acceleration gain of axis *x* for node *j*;
- a'_{x_j} is gravity acceleration value, expressed in electrical units, on the *x*-axis (instrumental reference system) of node *j*;

- g_{xT_j} is the gain of the thermal correction along the *x*-axis of node *j*;
- T'_j indicates temperature value, expressed in electrical units, of node *j*;

The calibration procedure cannot provide the absolute position of each sensors, but it is useful defining differential values, starting from a zero reference.

4.2.2. Thermometers calibration

Thermometers calibration is executed inside the thermal chamber together with accelerometers. The nodes are read 24 times for 10 different temperatures, estimating gain, and offset to apply to convert raw data in thermal value (Aydemir & Saranli, 2012). First, the mean temperature is calculated from the 24 recorder temperatures as in the Equation [4.5]:

$$T'_j = \frac{\sum_{i=1}^{24} T'_{ij}}{24} \qquad [4.5]$$

Where:

- T'_{ij} is the ADC temperature recorded at position *i*, of node *j*;
- T'_j represents the raw value of temperature of node *j*.

The calibration parameters to obtain are the gain m_j and the offset q_j as expressed in Equation [4.6]:

$$T_j = m_j T'_j + q_j \qquad [4.6]$$

In which:

- T_j represents the temperature of node *j*, expressed in Celsius degrees;
- T'_j is the ADC value of temperature of node *j*;
- m_j represents the gain of temperature for node *j*;
- q_j is the offset of temperature for node *j*.

Once obtained thermal and accelerometers calibration coefficients, the Array is almost ready to be installed and to starting the monitoring activity.

A last verification is conducted on all the realized Arrays. Every instrument must be placed inside an autoclave where the pressure is constantly applied and controlled. Monitoring tools remain inside the autoclave for approximately 24 hours, constantly queried by the ASE801 Data Logger. If no water infiltration or node error are detected the Array is ready to be shipped and then installed.

4.3. Calculation principles

Pre-Conv Links elaboration is based on data acquired by accelerometers installed inside each node. In particular, the elaboration considers principally the variation of acceleration acquired by *x*-axis (Figure 4.10), because the studied deformations take place mainly along the vertical direction. Differently from other applications, as MUMS (Segalini et al., 2011) or Cir Array (Savi et al., 2019), Pre-Conv Array has a predominantly mono-dimensional elaboration approach, where the acceleration acquired by the other axis is mostly used for calculating the coherence of gravity acceleration vector. This results in a series of displacement, local and cumulated, acting along the *Y-Z* plane.

The data elaboration is based on the following assumptions:

- The alignment between *x*-axis of each node is preserved using fibreglass connection. This assumption is mainly applied in other underground application, as the convergence monitoring. In Pre-Conv Array the deformations are elaborated along the *x*-axis, so a sensor roll should not induce any variation in results;
- The distance between each node is considered rigid. This assumption implies that the displacement defined by a variation of acceleration of a node, is considered for the entire length of the segment of relevance, generally fixed at 1 meter in underground monitoring;
- The data elaboration requires a fixed point from which the calculation starts. This point is called anchor. The Pre-Conv anchor is defined as the start of the first segment of relevance for the first node inside tunnel advance core. During the first excavation phases, this point cannot be stationary, but it is inserted in the first excavated and supported portion of monitored tunnel. This implies that after a couple of days (depending on advance velocity) the support should stabilize all the deformation effect of the anchor point.

4.3.1. Segment of relevance and calculation point definition

The distance between each node is fixed thanks to the presence of fibreglass rod and the alignment between nodes is preserved. Each node has its segment of relevance and calculation point (Figure 4.12) starting from the middle point between the considered node and the previous one, terminating in the middle point between the considered node and the following one.

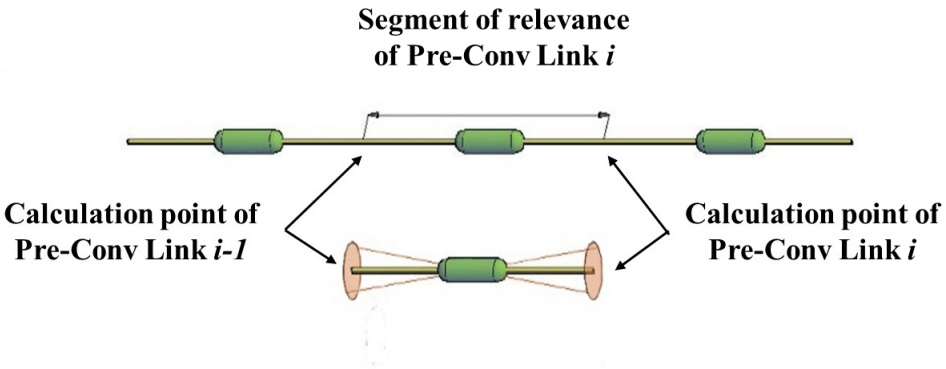

Figure 4.12 Segment of relevance and calculation point of Pre-Conv Array. Adapted from (Carri, 2019)

The displacement elaboration starts from the anchor until the last calculation point, so a calculation direction is defined. This means that if a displacement occurs after a calculation point, this will be recognized as vertical settlement directed downwards. Instead, if a displacement occurred ahead of a calculation point, it will be defined as a vertical displacement directed upwards (Figure 4.13).

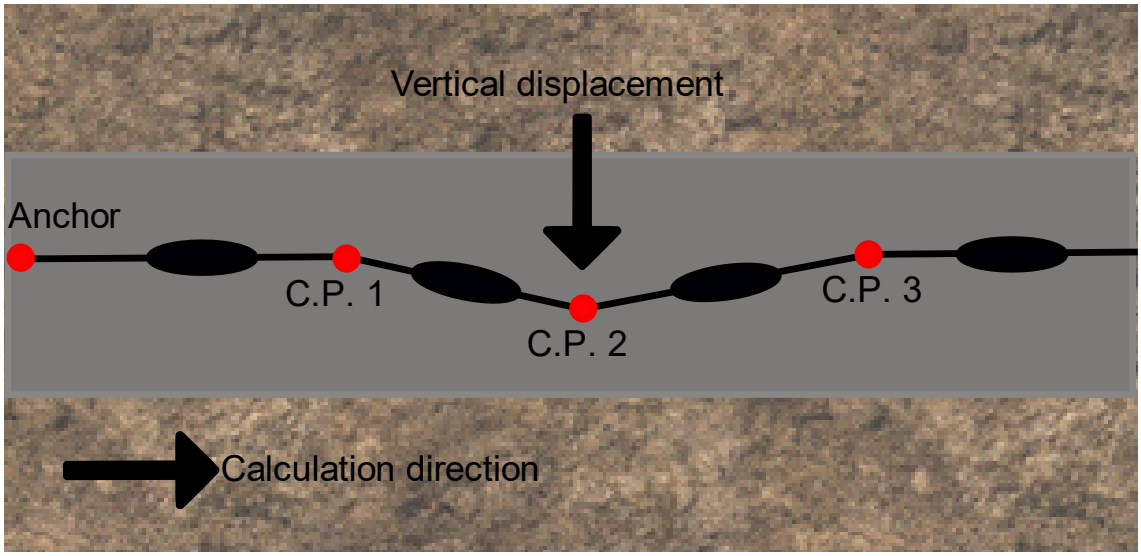

Figure 4.13 Calculation scheme of Pre-Conv Array

Figure 4.13 shows a possible displacement configuration. As mentioned above, the absolute position of each sensor cannot be defined. For this reason, the displacement evaluated from accelerometers can consider only relative tilt change. Indeed, the Calculation Point 2 shows a downwards vertical displacement because Pre-Conv Link n°2 is rotating clockwise, instead the calculation point 3 shows exactly the opposite, a vertical displacement directed upwards.

The anchor has a segment of relevance assigned by default as 0. The segment of the first node is calculated as:

$$SoR_1 = \frac{L_{anchor} + L_1}{2} \quad [4.7]$$

Where:

- SoR_i represents the segment of relevance for *i*-node;
- L_{anchor} is equal to 0;
- L_1 is the distance (or length) between the anchor and the first node.

The remaining segments of relevance, until the second last node, are calculated with the following equation:

$$SoR_i = \frac{l_i + l_{i+1}}{2} - \frac{l_i + l_{i-1}}{2} \quad [4.8]$$

The SoR of the last node is evaluated with equation [4.9]:

$$SoR_n = \left(l_{last} - \frac{l_{last-1} + l_{last}}{2}\right) \cdot 2 \quad [4.9]$$

The calculation points are placed at the end of each SoR (Figure 4.12). The calculation point of the anchor is considered at the same distance of the anchor, which is the referring point equal to 0. The remaining calculation points are calculated with equation [4.10]:

$$CP_i = CP_{i-1} + SoR_i \quad [4.10]$$

Where:

- CP_i is the calculation point of the *i*-node;
- CP_{i-1} is the calculation point of the precious considered node. For anchor this value is equal to 0;

Once the raw data reach the database, an automated algorithm called Ase Tunnel Displacements (ATD) starts converting raw value into physical quantities. The conversion links each node to its parameters defined during instrumental calibration.

The complete conversion equation for each axis is obtained combining Equation [4.4] and [4.6]. The following represented equation is valid for *x*-axis:

$$a_{x_j} = g_{x_j} a'_{x_j} + m_j T'_j + q_j \quad [4.11]$$

The acceleration is evaluated for each axis, determining a_{x_j}, a_{y_j}, a_{z_j} for the *j*-node. From these values the resultant can be calculated with equation [4.12]:

$$Res_j = \sqrt{{a_{x_j}}^2 + {a_{y_j}}^2 + {a_{z_j}}^2} \quad [4.12]$$

Where Res_j represents the resultant of the calculated acceleration of *j*-node.

Once the acceleration measured for each instrumental axis are determined, the displacements are calculated along Y-Z plane (referring to Figure 4.9) using the following equations:

$$Y_{ij} = SoR_i \cdot \sqrt{1 - {a_{x_{ij}}}^2} = SoR_i \cdot \cos \beta_i \quad [4.13]$$

$$Z_{ij} = -1 \cdot SoR_i \cdot a_{x_{ij}} = -1 \cdot SoR_i \cdot \sin \beta_i \quad [4.14]$$

$$\alpha_{x_{ij}} = \sin^{-1} a_{y_{ij}} \quad [4.15]$$

$$\alpha_{y_{ij}} = -1 \cdot \sin^{-1} a_{x_{ij}} \quad [4.16]$$

Where:

- Y_{ij} represents the local Y coordinate increasing of *i*-node compared to *i-1* node at time *j*;
- Z_{ij} represents the local Z coordinate increasing of *i*-node compared to *i-1* node at time *j*;
- $a_{x_{ij}}$ is the calculated acceleration along *x*-axis of *i*-node at time *j*;
- $a_{y_{ij}}$ is the calculated acceleration along y-axis of *i*-node at time *j*;
- β_i is the inclination angle measured along *x*-axis on the horizontal level;
- $\alpha_{x_{ij}}$ is the inclination angle measured along *x*-axis measured by *i*-node at time *j*;
- $\alpha_{y_{ij}}$ is the roll angle measured along y-axis measured by *i*-node at time *j*.

Once the coordinates increasing is evaluated, the absolute position of each node is estimated starting from the absolute coordinated defined during the monitoring project. For the first sensor the absolute coordinates are:

$$Y_{abs,ij} = Y_{ij} \quad [4.17]$$

$$Z_{abs,ij} = Z_{ij} \quad [4.18]$$

Absolute coordinates for subsequent nodes are finally calculated as:

$$Y_{abs,ij} = Y_{ij} + Y_{i-1,j} \quad [4.19]$$

$$Z_{abs,ij} = Z_{ij} + Z_{i-1,j} \quad [4.20]$$

The cumulated displacements are finally evaluated by summing the local contribution, Y_{ij} and Z_{ij}.

4.3.2. Self-check controls

Automated monitoring, as well as other automatized tool, needs to apply self-check data control to individuate spike noises, wrong measurements, malfunctions, and generally every external factor that can affect data elaboration. The ATD software provides a series of different controls that automatically start during data elaboration. The applied self-check controls are:

- Identification of spike noises;
- The coherence of gravity acceleration;
- Variability of gravity acceleration;
- The coherence of measured temperature;
- Running average;
- Definition of instrumental noise;
- Recognition of not-operating sensors.

4.3.2.1. Identification of spike noises

Spike noises represent an electrical disturbance related to external factors, such as vibration caused by tunnel excavation. Spike noises are evaluated using statistical tools, such as Scaled Median Absolute Deviation (MAD). MAD (Hoaglin et al., 1983) represents the median of absolute deviations from data's median, Equation [4.21], [4.22], [4.23], [4.24].

$$MAD = c * median(|X_i - median(X)|) \quad [4.21]$$

$$c = \frac{-1}{\sqrt{2} * erfc^{-1}\left(\frac{3}{2}\right)} \quad [4.22]$$

$$erfc(x) = \frac{2}{\sqrt{\pi}\int_x^{\infty} e^{-t^2} dt} = 1 - erf(x) \quad [4.23]$$

$$erf(x) = \frac{2}{\sqrt{\pi}}\int_0^x e^{-t^2} dt \quad [4.24]$$

Where:

- X_i is the datum to be determined;
- $erfc(x)$ is the complementary error function;
- $erf(x)$ is the function error (Glaisher, 1871).

Vibrations or earthquakes may induce a quick variation in acceleration measures that may activate an alarm or a threshold overcoming. The recognition of spike noises perfectly works when the considered dataset is centred, so last reached data could be evaluated after some hours, depending on the sample acquisition frequency and data transmission frequency.

$$out_i = f(t_{sp}, t_{ft}, d_w) \quad [4.25]$$

Where:

- out_i is the function for identifying outliers;
- t_{sp} represents the sample period;
- t_{ft} is the frequency of data transmission;
- d_w is the number of data considered in dataset window.

Parameters in equation [4.25] must be defined depending on monitoring needs. If rapid displacements are expected, a higher sample period should be used to validate position variation in a short time.

$$t_{sp} = f(v, d_w, e_p) \quad [4.26]$$

Where:

- v is the displacement rate;
- e_p is the electrical power.

For what concern t_{ft}, two more features should be considered. First, data transmission frequency influences data elaboration, so for near-real time applications this value should be higher, and possibly equal to t_{sp}. Second, So many data transmission requires also more electrical power, to be considered during the monitoring plan project.

$$t_{ft} = f(e_p, v, d_w, t_r) \quad [4.27]$$

Where t_r is the expected time for providing monitoring results.

Data considered inside the dataset windows depend on the geotechnical phenomena to monitor. It is important to highlight that a small window reduces calculation time but could be not statistically based. A higher amount of data considered could cause long validation time improving the statistical process of spike noises. Therefore, it could be not found small outliers that are near to data trend.

4.3.2.2. Coherence of gravity accelerations

Once data reach raw database, due to the 3D MEMS nature, the value of gravity acceleration vector at each elaboration step are compared. The normalized vector obtained from the acquired acceleration of three instrumental axis should verify Equation [4.28].

$$\frac{\sqrt{a_x^2 + a_y^2 + a_z^2}}{g} = 1 \quad [4.28]$$

External factors or instrumental noises could influence the value of acceleration, so an admitted variation from g is considered.

$$\left|1 - \frac{\sqrt{a_x^2 + a_y^2 + a_z^2}}{g}\right| \geq \Delta_g \quad [4.29]$$

Where Δ_g represents a tolerance value of gravity vector calculated from the instrumental axis acceleration. In underground applications this tolerance is generally considered as 0.05 g.

4.3.2.3. Variability of gravity acceleration vector

The acceleration recorded by instrumental axis is subjected, as well as other electronical devices, to instrumental noise. In addition to the previous filter, Equation [4.30], an automatic filter controls instrumental gravity variation between two consecutive measures.

$$\left|\frac{\sqrt{a_{x_t}^2 + a_{y_t}^2 + a_{z_t}^2}}{g} - \frac{\sqrt{a_{x_{t-1}}^2 + a_{y_{t-1}}^2 + a_{z_{t-1}}^2}}{g}\right| > \varepsilon_g \quad [4.30]$$

Where ε_g is generally considered equal to 0.0025 g.

4.3.2.4. Coherence of measured temperature

Recorded node temperature should not exceed defined extreme values, where the sensor is out operative measurement range. In case a sensor measures temperature, T_{meas}, which is higher (T_{high}) or lower (T_{low}) certain values, data are not considered in the final elaboration. The extreme values are 70 °C for T_{high} and -20 °C for T_{low}.

$$T_{meas} < T_{low} \text{ V } T_{meas} > T_{high} \quad [4.31]$$

4.3.2.5. Running average

The centred running average is applied together with the spike noises recognition filter, identifying, and reducing instrumental noise. The definition of the number of data to consider using the running average is a complex problem. The dataset window should not be too narrow or too wide. A fast displacement can be reduced, anticipating the activation time, and postponing the conclusion time. Figure 4.14 shows a rapid movement elaborated without running average (blue line) and finally elaborated with running average built on three different windows composed of 3, 5, and 11 measures, respectively. The elaboration without running average shows a fast displacement followed by instrumental noise of 1.7 mm. Elaborating the same data with a running average built on different windows allows to highlight that the displacement seems to starts earlier, finishing after some

timepoints, depending on the size of the chosen window. Indeed, with a running average of 11 measures (yellow line) the displacement is anticipated and delayed of 5 data, reducing the instrumental noise to 0.9 mm. In conclusion, to detect small deformations, a large dataset is required, instead, if deformations of higher amplitude are expected, a very narrow window should be used.

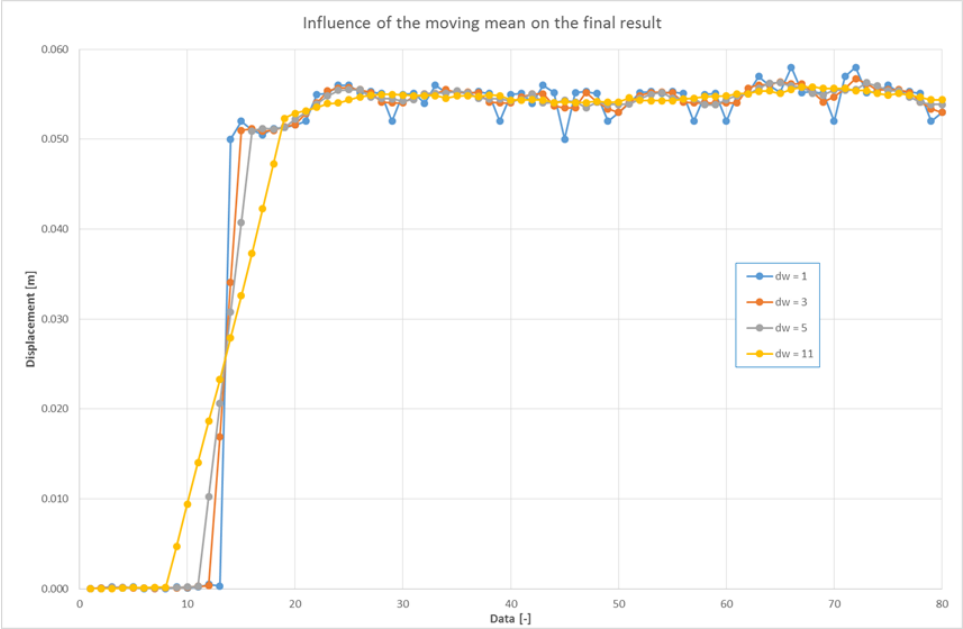

Figure 4.14 Displacement evaluation elaborated without running average (blue), and calculated with a centred running average of 3 (orange), 5 (grey) or 11 (yellow) data. (Carri, 2019)

4.3.2.6. Definition of instrumental noise

Every electronic sensor or device is influenced by its instrumental noise. This value must be detected and quantified. The real instrumental noise is generally different from the same value indicated in data sheet or defined by laboratory tests, so a real value could be identified from monitoring data on-site. Defining instrumental noise is possible to accurately evaluate small displacement may occurred during monitoring phase. Figure 4.15 shows a displacement recorder by three different Pre-Conv Links during the monitoring of tunnel excavation. Each dataset is influenced by a data oscillation, but the grey and blue line indicate a rapid acceleration change. This fast variation is recognized as a real displacement. For example, the orange line provides only data oscillation without any displacement detection.

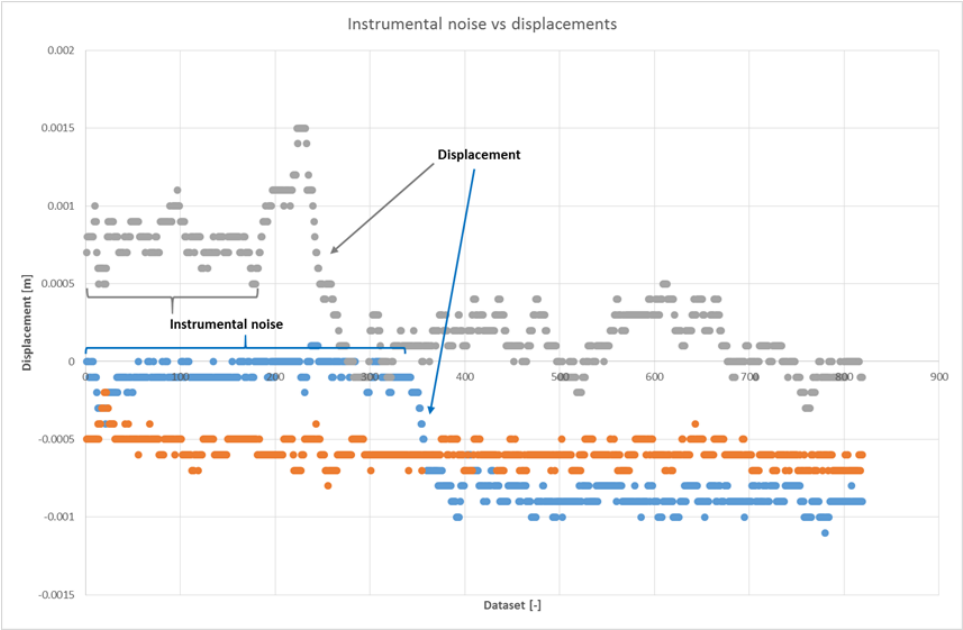

Figure 4.15 Definition of instrumental noise and displacements. Adapted from (Carri, 2019)

4.3.2.7. Not operating sensors

Previous filters considered external factors that may induce a wrong sensor response. It might happen that a node could be compromised for some reasons and does not answer to datalogger. In this case datalogger queries the sensor twice and if it still does not work, acquisition system bypasses the reading of that node switching to the following one. If this happens, the acquisition system reports a code error and ATD software automatically recognizes this malfunction highlighting the non-working sensor with a red exclamation mark on web platform, as reported in Figure 4.16. Therefore, the responsible of monitoring can easily identify this malfunction avoiding to consider the related data.

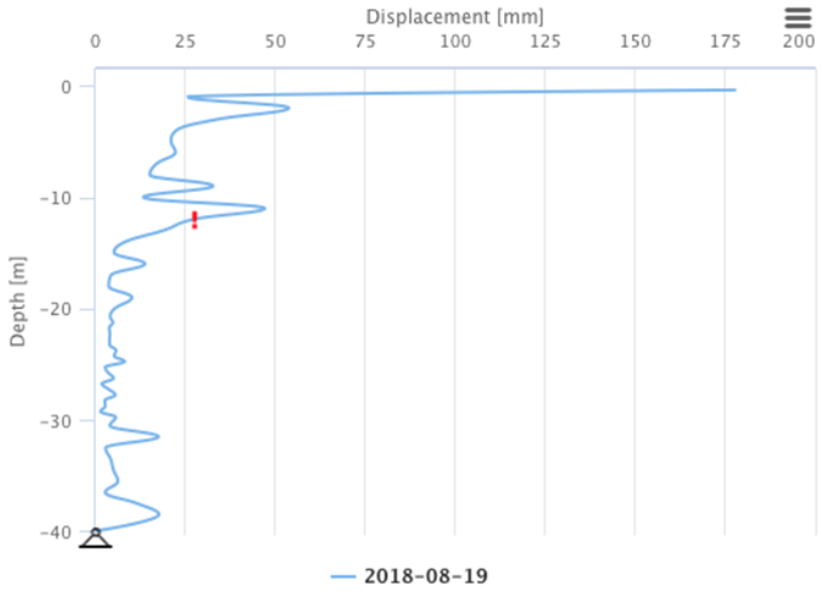

Figure 4.16 Representation of non-working sensor on web platform (ASE S.r.l. web platform)

4.4. Laboratory tests

The Pre-Conv Array is a monitoring instrument derived from several years of underground monitoring research applying the MUMS technology (Cavalca et al., 2018; Segalini et al., 2018a), where onboard sensors and the automatic algorithm was widely tested and validated.

The proposed monitoring tool was initially tested in laboratory to verifying the ability in defining preconvergence deformations (Savi et al., 2019). Due to lack of measured preconvergence data, the test was initially derived on deformations obtained through extrusion measurements on the advance core (Lunardi, 2000) as defined in Figure 3.11, assuming a spherical dome-like extrusion shape.

The test was realized using six Pre-Conv Links with a segment of relevance equal to 1 meter anchored to metal rods at 0.5 meters from each links, corresponding to the calculation point of each node. The metal rods were fixed to the wall and predefined vertical displacements were applied to an L-shape connector sliding along the vertical direction (Figure 4.17). Besides, a topographic target was placed on the calculation point of each sensor to measures the imposed deformation multiple times, and, finally, validate the instrument.

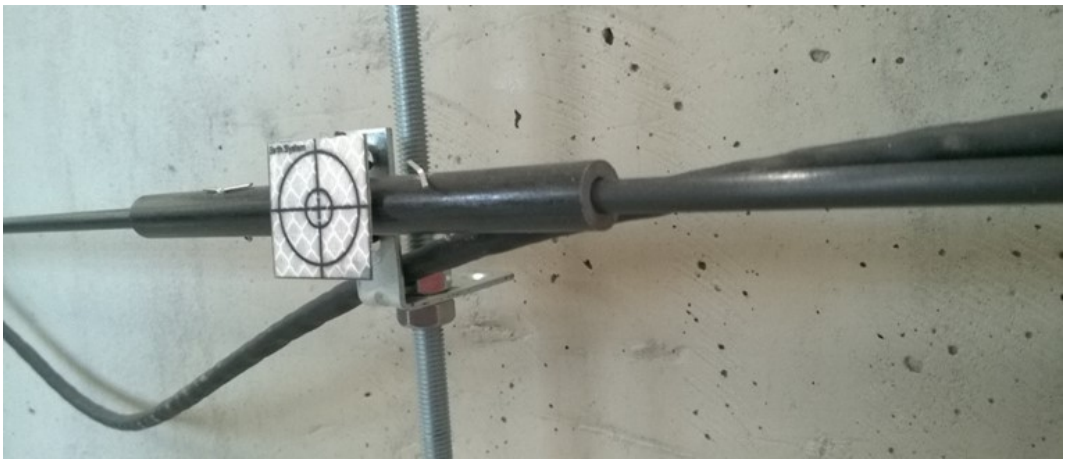

Figure 4.17 Detail of the mechanical structure developed to connect the Pre-Conv Array to the threaded metal rod, the locking system and the topographic target placed at the calculation point. Source: (Savi et al., 2019)

The Preconvergence values were derived from a full-scale experiment performed by (Lunardi, 1994). The experiment consists of an extrusion and preconvergence monitoring by placing multi-base rod extensometers over the tunnel crown during the excavation advance, and by horizontal extensometer for 2-3 tunnel diameters.

Imposed vertical settlements on Pre-Conv array were gradually applied in three-step deformations, simulating the excavation advance. For each step, five measurements were taken to apply a statistical approach, using the recorded mean value of each assigned deformation (Table 4.3).

Table 4.3 Preconvergence reference values derived from extrusion monitored data (Savi et al., 2019)

Distance ahead of excavation face [m]	0	1	2	3	4	5	6
Zero reference	0	0	0	0	0	0	0
Step 1 [cm]	-2.38	-2.01	-1.55	0	0	0	0
Step 2 [cm]	-4.75	-4.03	-3.10	-1.35	-0.85	0	0
Step 3 [cm]	-7.20	-6.10	-4.70	-2.70	-1.70	-0.90	0

The test was repeated for two initial conditions: the first test was performed starting from a horizontal configuration, while in the second case the Pre-Conv Array was tilted of 4 degrees. Indeed, as explained in the previous paragraph, the instrument could be installed horizontally above the tunnel crown or inserted in advance preconfinement supports, generally tilted of 4÷6 °. At each deformation step, a percentage error was calculated to define the difference between the testing tool measurements, x_{PC}, and topographic measures recorded by theodolite, x_t using Equation 4.32:

$$E\ [\%] = \left(1 - \frac{x_{PC}}{x_t}\right) \cdot 100 \qquad [4.32]$$

The topographic survey was carried out using a Topcon DS200 total station, with a focal length of 165 mm and a focal lens of 45 mm. The sensibility in the distance measuring is ±2 mm while the accuracy on the angle is 0.3 mgon (Topcon Manual). The zero for the azimuth was assessed using a referral point P0, while the roto-translation of the theodolite reference system to the Pre-Conv Array reference system was performed using known points P1, P3, and R7. The physical apparatus and topographic marker positions are represented in Figure 4.18.

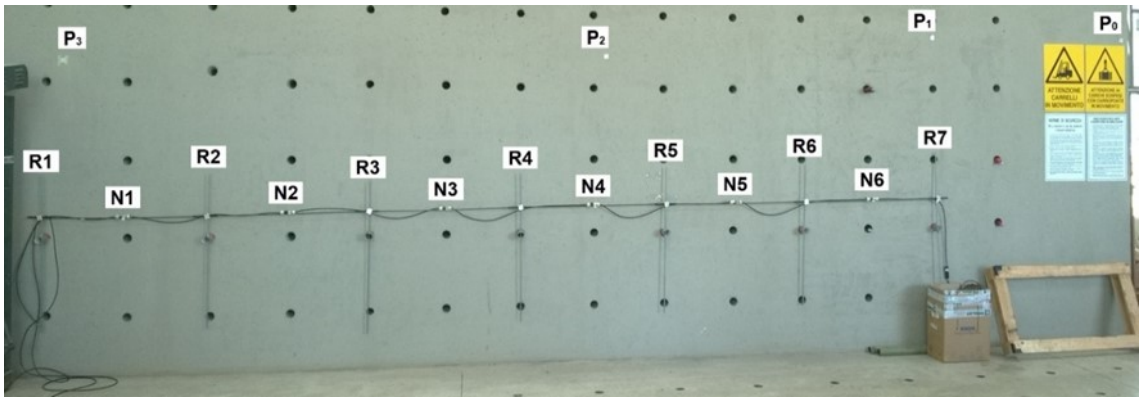

Figure 4.18 Physical apparatus developed to test the Pre-Conv Array prototype (Rods R1-R7; Nodes N1-N6; Fixed points P_0-P_3) (Savi et al., 2019)

4.4.1. Pre-Conv Array horizontally installed

This first test was performed using a horizontal configuration, by imposing the same height between N1 and N6 (Figure 4.18). Figure 4.19 and Table 4.4 show the values of the displacements recorded by the Pre-Conv Array and by the theodolite. Table 4.5 shows the difference between the displacements recorded by the theodolite and the Pre-Conv Array.

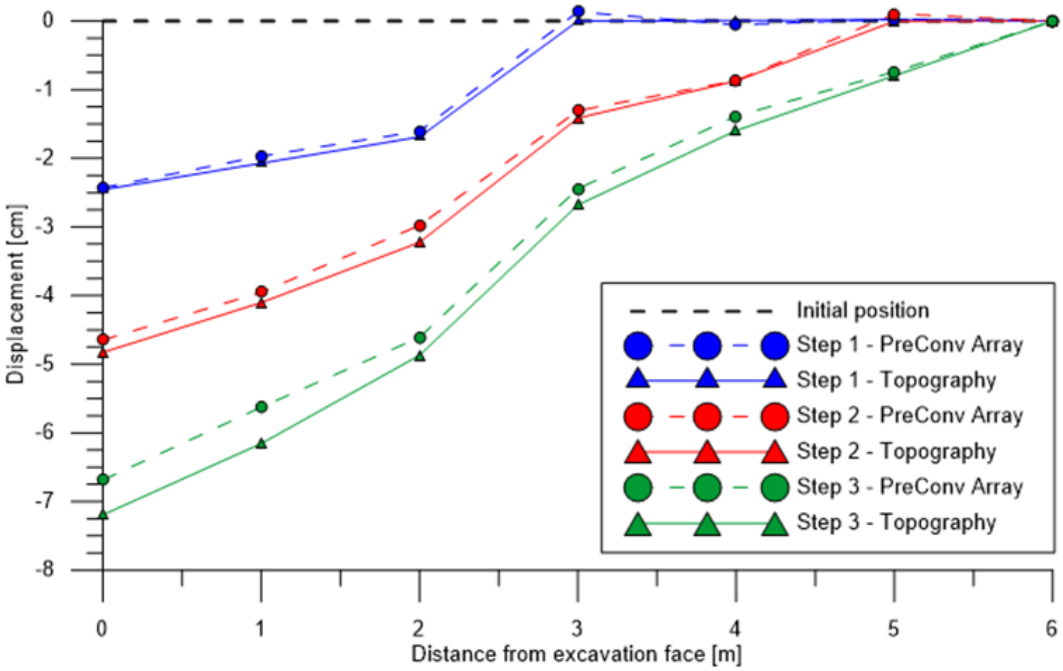

Figure 4.19 Displacement recorded by Pre-Conv Array (dotted line) and topographic survey, starting from a horizontal configuration. (Savi et al., 2019)

Table 4.4 Displacement comparison between topographic and monitoring tool measurements – horizontal starting configuration. (Savi et al., 2019)

Distance from excavation face [m]	Topographic survey [cm]			Pre-Conv Array [cm]		
	Step 1	Step 2	Step 3	Step 1	Step 2	Step 3
0	-2.45	-4.83	-7.19	-2.43	-4.65	-6.68
1	-2.07	-4.10	-6.15	-1.97	-3.95	-5.62
2	-1.69	-3.22	-4.87	-1.61	-2.97	-4.61
3	0.00	-1.42	-2.68	0.13	-1.31	-2.45
4	0.01	-0.86	-1.59	-0.05	-0.87	-1.38
5	0.02	0.00	-0.80	0.03	0.11	-0.74
6	0.00	0.00	0.00	0.00	0.00	0.00

Table 4.5 Difference between displacements recorded by theodolite and Pre-Conv Array, and corresponding percentage error - horizontal starting configuration. (Savi et al., 2019)

Distance from excavation face [m]	Measure difference [cm]			Error [%]		
	Step 1	Step 2	Step 3	Step 1	Step 2	Step 3
0	0.02	0.18	0.51	1%	4%	7%
1	0.10	0.15	0.53	5%	4%	9%
2	0.08	0.25	0.26	5%	8%	5%
3	0.13	0.11	0.23	-	8%	9%
4	-0.06	0.01	0.21	-	1%	13%
5	0.01	0.11	0.06	-	-	7%
6	0	0	0	-	-	-

Data presented in Table 4.4 and Table 4.5 show that Pre-Conv Array slightly underestimates vertical displacement far from the simulated tunnel face. This behaviour is probably due to the cumulated nature of displacements presented in the chart, where the presence of a minor difference in a specific node can propagate through the following calculation points by multiplying the local acceleration variation for the segment of relevance. In the case here exposed, this difference reaches a maximum value of 0.53 cm, corresponding to a 9% error. Of note, the presented results refer to undisturbed laboratory conditions. For this reason, a high sampling frequency is suggested to obtain similar results in an on-site application, where several external actions are usually present.

4.4.2. Pre-Conv Array tilted installed

The second test was executed simulating a tilted configuration, as in sub-horizontal jet-grouting preconfinement intervention. Pre-Conv Array was tilted of 4°, considering R7 as a fixed point taken as a zero-vertical reference (Figure 4.20). The comparison between Pre-Conv and topographic measurements is shown in Table 4.6, while the difference between displacements recorded by theodolite and Pre-Conv Array is shown in Table 4.7.

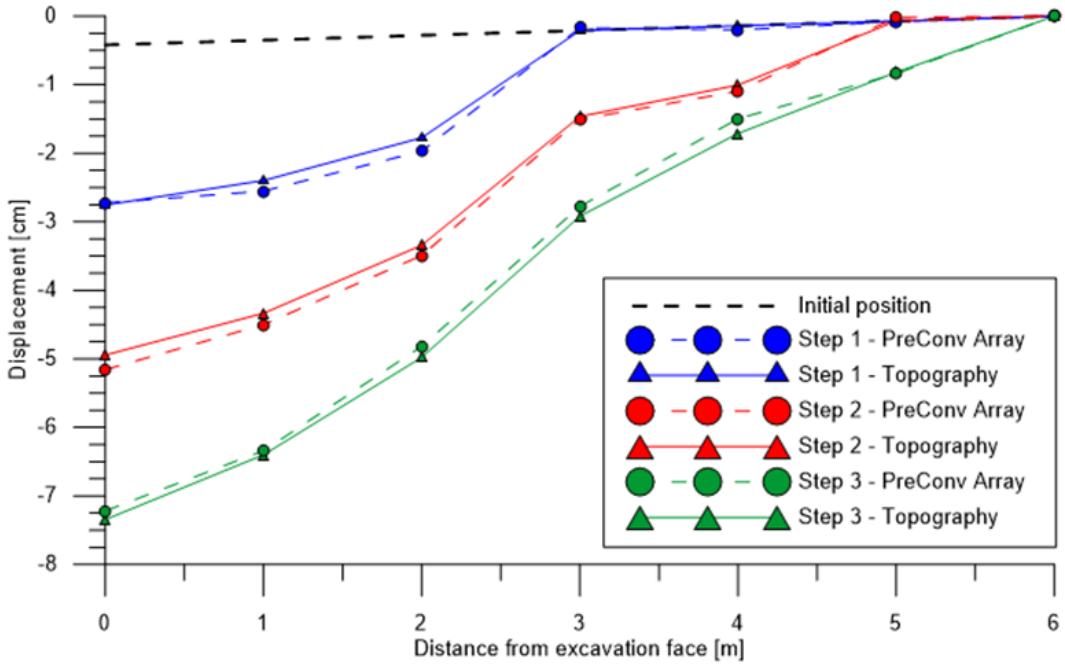

Figure 4.20 Displacement recorded by Pre-Conv Array (dotted line) and topographic survey, starting from a 4-degress tilted configuration. (Savi et al., 2019)

Table 4.6 Displacements recorded by theodolite and Pre-Conv Array, and corresponding percentage errors - 4-degrees tilted starting configuration. (Savi et al., 2019)

Distance from excavation face [m]	Topographic survey [cm]			Pre-Conv Array [cm]		
	Step 1	Step 2	Step 3	Step 1	Step 2	Step 3
0	-2.75	-4.95	-7.34	-2.72	-5.16	-7.22
1	-2.39	-4.34	-6.40	-2.56	-4.50	-6.34
2	-1.78	-3.34	-4.98	-1.97	-3.49	-4.82
3	-0.21	-1.47	-2.92	-0.18	-1.51	-2.78
4	-0.14	-1.00	-1.71	-0.20	-1.09	-1.50
5	-0.07	-0.07	-0.82	-0.08	-0.02	-0.84
6	0.00	0.00	0.00	0.00	0.00	0.00

Tilted configuration does not show the slight underestimation highlighted in the previous test. Indeed, the first two steps show opposite behaviour, slightly overestimating the imposed vertical displacement. Instead, the third step presents a similar trend to the horizontal configuration. The error

values reported in Table 4.7 confirm this statement, underlighting the good correspondence between data recorded by the Pre-Conv Array and the topographic survey. In this specific experiment, 10 out of 14 measurements show a difference equal or less than 5%, with a maximum difference of 0.21 cm.

Sensibility analysis performed during both tests returned a value of 0.15 mm/meter, due to the mono-dimensional approach of the Pre-Conv Array data elaboration.

Table 4.7 Difference between displacements recorded by theodolite and Pre-Conv Array, and corresponding percentage error - 4-degrees tilted starting configuration. (Savi et al., 2019)

Distance from	**Measure difference [cm]**			**Error [%]**		
excavation face [m]	**Step 1**	**Step 2**	**Step 3**	**Step 1**	**Step 2**	**Step 3**
0	0.03	-0.21	0.12	1%	5%	2%
1	-0.15	-0.16	0.06	8%	4%	1%
2	-0.19	-0.15	0.16	13%	5%	3%
3	0.03	-0.04	0.14	-	3%	5%
4	-0.06	-0.09	0.21	-	10%	14%
5	-0.01	0.05	-0.02	-	-	3%
6	0	0	0	-	-	-

4.5. Differences to other preconvergence monitoring system

Although other horizontal inclinometers are used to monitor the preconvergence, some related problems were highlighted (Chung et al., 2010). For instance, the manual measurements do not allow a high sample frequency, therefore impeding the evaluation of the relationship between the measured quantities and the application of a statistical approach. Moreover, as the displacements cannot be measured near to the excavation face during the drilling phase, fundamental data are lost. These data include the trend of deformations induced by the excavation on the tunnel face, or the preliminary displacements occurred, both useful to define and project the best support system applying the C.C method.

Among others, Volkmann and Schubert (Volkmann & Schubert, 2005) have proposed a system based on an in-place horizontal inclinometer. Like other traditional horizontal inclinometers, this system requires a dedicated borehole to install the tool, due to its dimension. Generally, the distance between each sensor is equal to 2 meters, so the measurement accuracy is low compared to the one in the Pre-Conv Array. Moreover, in-place horizontal inclinometers show other disadvantages, including electromagnetic interference, signal loss for long-distance transmission, gravity dependence, and poor durability. All these features result in poor monitoring of horizontal deformations (Dunnicliff, 1993). Finally, in-place horizontal inclinometers have a rigid connection, susceptible to water infiltration.

The instrument presented here allows overcoming most of these disadvantages. Indeed, the Pre-Conv Array allows to monitor continuously displacements occurring ahead of the tunnel face. Continuous monitoring with a near real-time elaboration permits to define the influence of each excavation step or other works realized during tunnel drilling and to define the influence of displacements on the designed support system. Due to its reduced dimension, Pre-Conv Array could be installed directly inside the preconfinement system, without the need for another dedicated excavation. Other preconvergence instruments are generally bigger than Pre-Conv Array and cannot be installed inside preconfinement intervention causing an increase of costs and a delay in terms of excavation planning. With respect to traditional instruments, Pre-Conv Array permits a simple and fast installation procedure that does not interfere with planned working operations. Furthermore, the connection between each sensor is not rigid so the instrument can precisely follow the displacement that occurred above the tunnel crown. For all these reasons, we think that this instrument represents a great improvement in the difficult tasks of monitoring the rock mass stability and project the best confinement and preconfinement systems to apply during the tunnel construction.

5. Introduction to the case studies

In order to test whether the proposed monitoring tool is capable of detecting displacements occurring ahead and behind the tunnel face, we installed the Pre-Conv Array system in two different pilot sites. The first site is located in the Principality of Monaco, and the second in a tunnel situated in the north of Italy. The two pilot sites present significant differences in terms of overburden, stress state, and involved material. Indeed, the first one is a shallow tunnel that connects the city centre to underground parking. Instead, the second is a deep tunnel built in a glacial deposit that connects two important valleys with an overburden of approximately 50 meters. Before going into the details of the monitoring results and the validation of the instrument, a series of considerations must be explained.

In Monaco, Pre-Conv Arrays was installed and cemented inside preconfinement intervention on the 23rd of October 2019, one month before the start of the tunnel excavation, while the cement mortar injection started the 25th of October. In this stable configuration, an unexpected behaviour was observed. Indeed, the received data showed a strong correlation with the temperature change, probably due to the concrete mortar maturation phase. Figure 5.1 shows the displacements and the temperature recorded by the calculation point 9 of the installed Pre-Conv Array.

Point A shows a steep increase of displacement, approximately 5 mm, which occurred during the injection phase, presumably caused by the 5 bar injection pressure. Then, after few hours, the calculation point detected a 1.2 mm increase of displacement. Interestingly, the recorder displacement followed the trend of the temperature measured (Point B). Indeed, the temperature reached 45°C during the night between the 25th and the 26th of October, due to the endothermic reaction of the concrete maturation, and finally, the temperature rapidly decreased. The same behaviour was observed few days later, the 28th of October, when another temperature variation followed by a displacement was detected (Point C). To evaluate if the displacement were caused by an algorithm error or by a thermal contribution, the raw acceleration data recorded along *x*-axis were analysed (Figure 5.2).

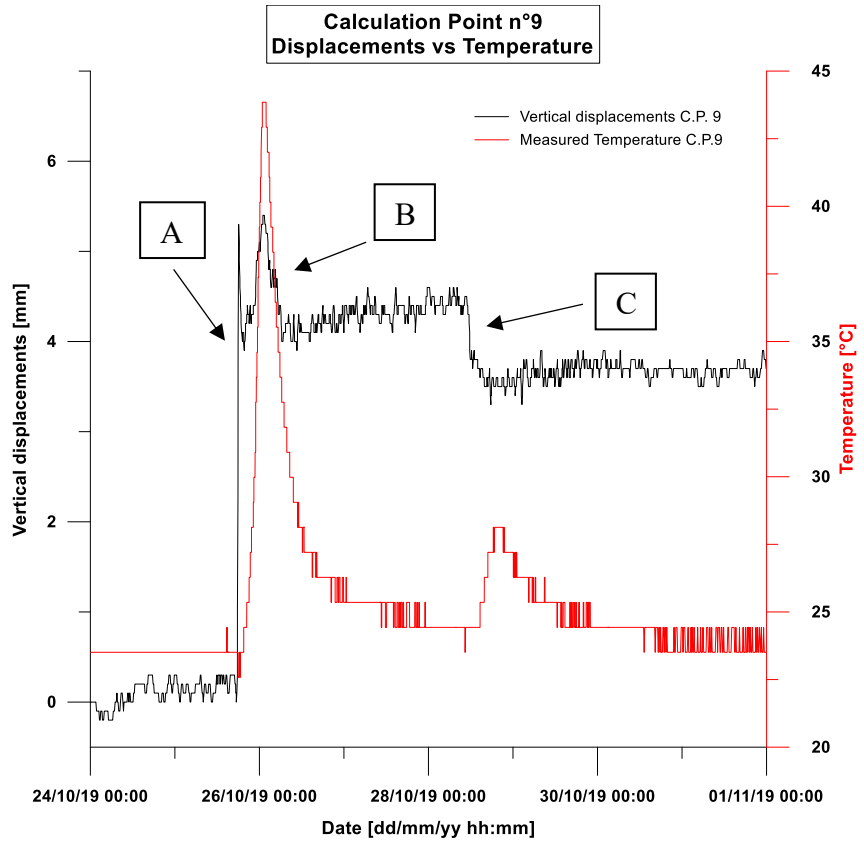

Figure 5.1 Displacement and temperature recorded by Calculation Point n°9

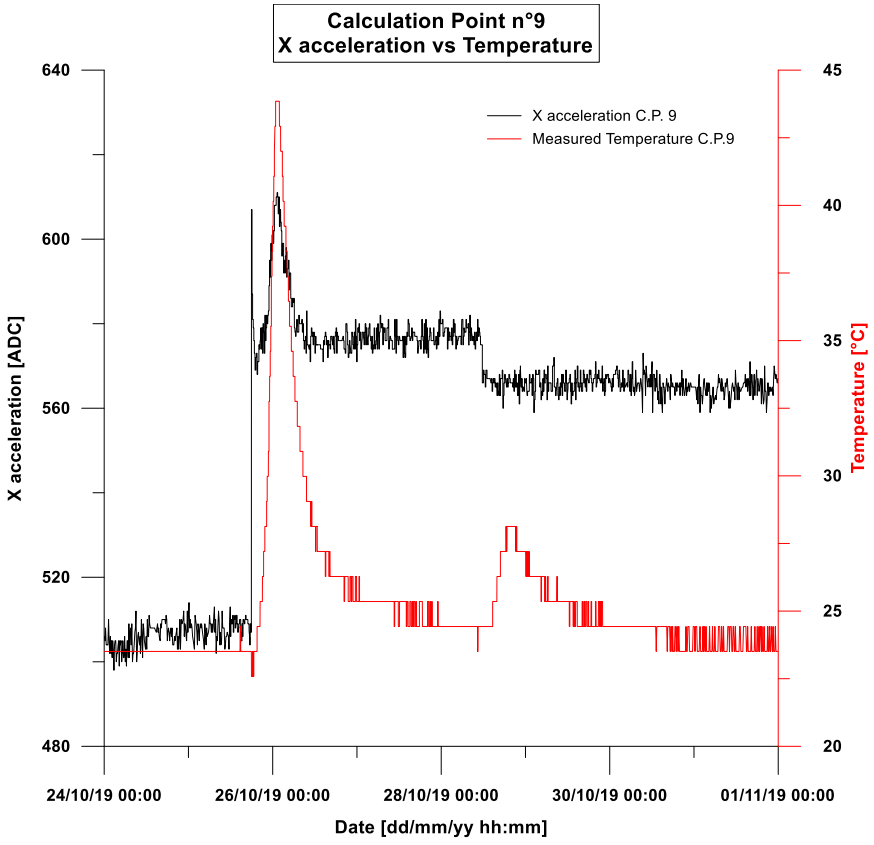

Figure 5.2 X raw acceleration and temperature recorded by Calculation Point n°9

As the *x*-axis acceleration displays the same trend as the one reported in Figure 5.1, these data can underline the presence of a thermal and mechanical influences on embedded MEMS sensors. With the aim of understanding whether the displacements recorded by Pre-Conv Array suffer the thermal and mechanical influences, a series of laboratory tests were conducted. We analysed the deformative response of a sensor subjected to high-pressure value, and to a concrete maturation in two different configurations.

5.1. Pressure test

A pressure test was initially designed to verify the mechanical influences on the on-board sensors. Since the mechanical stress suffered by the embedded sensor cannot be known *a priori*, we decided to initially explore possible relationships between pressure and displacements by taking advantage of a high-performance autoclave.

To this aim, the Pre-Conv Link was fixed on the circular bottom plate of the tank by applying a thick layer of hot glue. Different pressure stages were applied, ranging from 3 bar to 23 bar, with the latter being the maximum appliable pressure without causing water spilling around the cable entry. Pressure stages were applied by alternating loading and unloading phases, simulating a continuous variation of field stress.

The autoclave does not provide remote control of the applied pressure, therefore a manual variation was imposed. Table 5.1 summarizes the pressure stages carried out.

Table 5.1 Pressure stages applied on Pre-Conv Link

Day	Time	Pressure [bar]	Day	Time	Pressure [bar]
1	16:00	21.1	**2**	17:00	17
1	17:30	9	**3**	07:59	17.3
2	08:29	3	**3**	08:00	10.5
2	08:30	23	**3**	10:00	14.2
2	12:59	16	**3**	13:29	10.2
2	13:00	9.7	**3**	13:30	16.9
2	16:59	8.1	**3**	16:00	10.6

After 48 hours test, the acquired data were elaborated to define or exclude the existence of a relationship between pressure and the displacements recorded. Figure 5.3 and Figure 5.4 show the calculated displacement along the *x*-axis and *y*-axis, respectively, plotted together with the applied pressure.

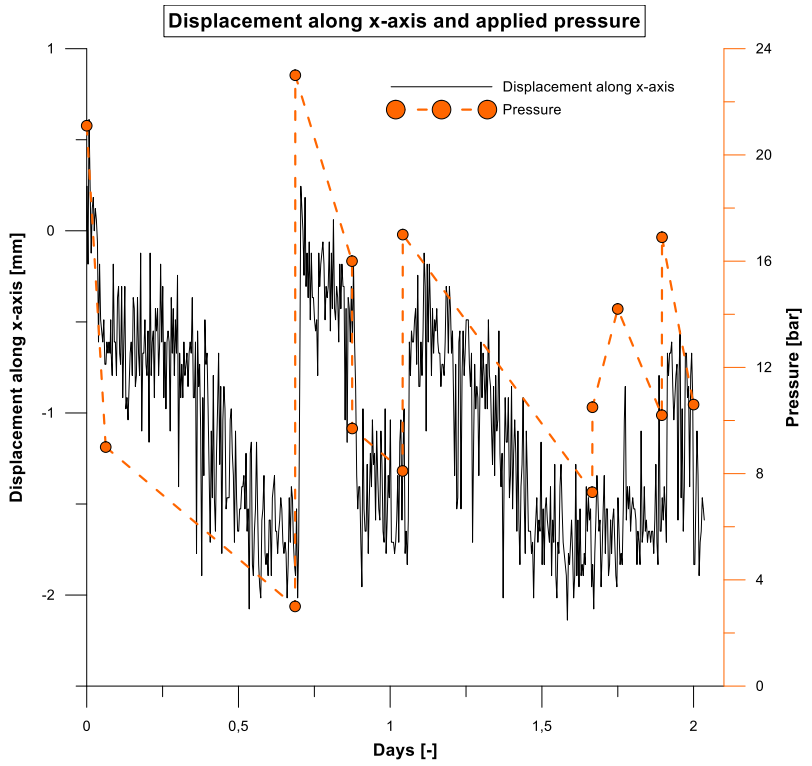

Figure 5.3 Displacements recorded along x-axis and applied pressure

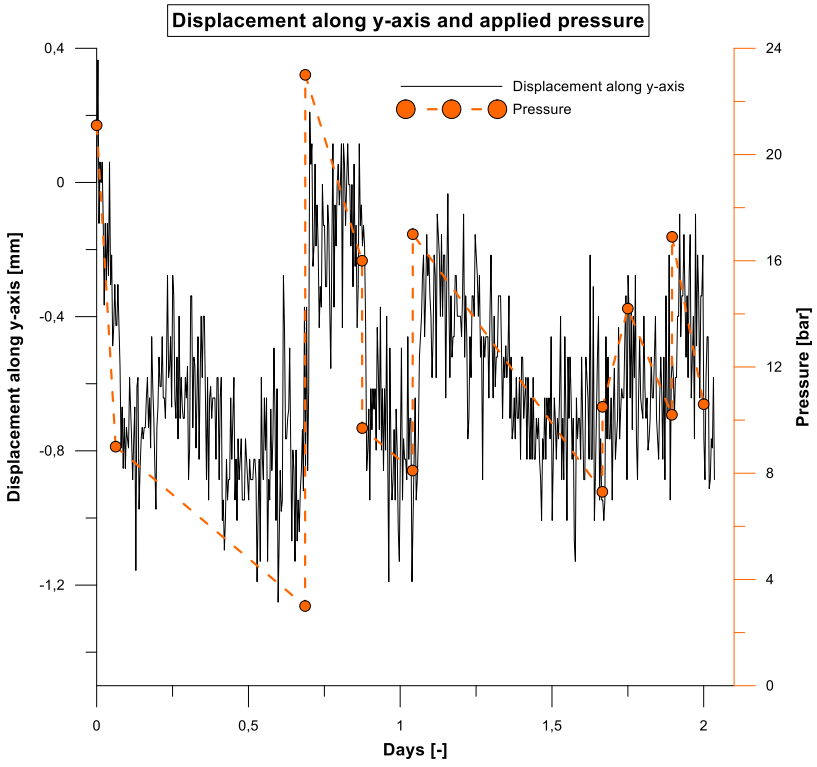

Figure 5.4 Displacements recorded along y-axis and applied pressure

Strikingly, we observed a clear relationship between the measured quantities. The highest displacement recorded along the *x*-axis is equal to approximately 2 mm, instead along the *y*-axis the

highest measured value is approximately 1 mm. To exclude the possibility that the recorded displacements were due to the deformation of the tank, its deformative state was studied.

The circular iron tank has the following characteristics:

- Young's modulus, $E = 210'000\ N/mm^2$;
- Radius, $r = 100\ mm$;
- Bottom plate thickness, $h = 45\ mm$;
- Poisson's coefficient, $\nu = 0.3$.

The deformative state of the iron tank was defined by applying the loading scheme presented in Figure 5.5. The loading scheme consists of a circular stuck plate subjected to a distributed loading, where the maximum longitudinal displacement can be evaluated by Equation [5.1].

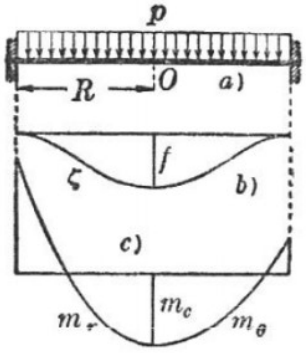

Figure 5.5 Autoclave loading scheme

$$f = \frac{3(1-\nu^2)}{16}\frac{p \cdot r^4}{E \cdot h^3} \qquad [5.1]$$

Where p is the maximum pressure applied during the performed test (Table 5.1).

Applying Equation [5.1], the highest deformation evaluated is equal to $2 \cdot 10^{-3}$ mm. The theoretical tank deformation is much lower than the evaluated displacement obtained from the Pre-Conv Link. This result indicates a pressure influence on the on-board accelerometer probably due to the mechanical deformations transfer from the resin shell to the 3D sensor, or to the sensor sensible components. In fact, higher deformations were observed along the *x*-axis, that is disposed along the sensor length (Figure 5.6), where the inertia momentum is lower than the same on the transversal direction. To explain these data, we can hypothesize that the pressure state acting on the resin shell is transferred to the sensor, causing longitudinal and transversal deformations. Figure 5.6 shows a possible configuration of the MEMS sensor subjected to a variable and high-pressure state.

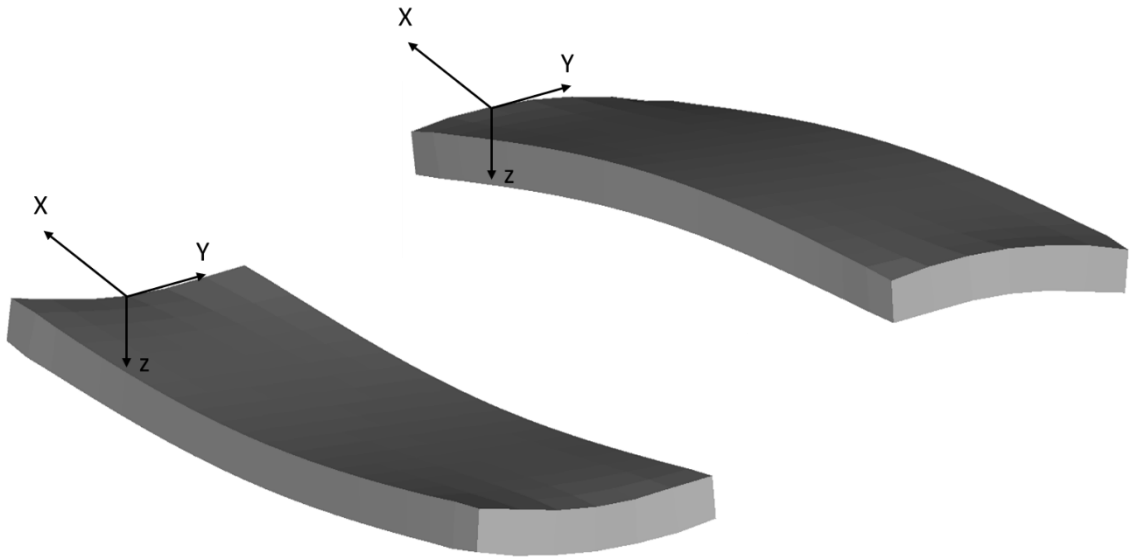

Figure 5.6 Possible deformations induced on MEMS sensor by pressure variations

5.2. Thermal test

Referring to Figure 5.1 and Figure 5.2, sensors show a temperature influence both during the mortar maturation and during the monitoring phase. However, as previously stated, every sensor is calibrated in temperature. The observed behaviour led us to hypothesize that the calibration is not optimized for rapid and intense temperature variations. To address this point, a study on the mortar maturation was conducted to define the influences in terms of displacement induced both by the mortar hardening and the related temperature increase. Then, the thermal effect was analysed to define a procedure for compensating thermal influence during the whole monitoring phase. The test was executed on two different Pre-Conv Links cemented with two types of mortar. Indeed, mortar can be compensated shrinkage or not. We started by two working hypotheses: we expect that the compensated shrinkage mortar has higher mechanical energy transfer on the sensor, while without shrinkage compensation, mortar reduces its volume without interacts with the sensor. The test was conducted by recording data from sensors cemented with the two types of mortar in a PVC casing (Figure5.7). Data were collected with a 5 minutes sampling frequency for 28 days, hence until the complete mortar maturation.

Figure 5.7 Sensor immersed in the concrete mortar inside a PVC casing

Finally, sensors were placed in a plastic box, surrounded by ground to simulate a real on-site application (Figure 5.8).

Figure 5.8 Sensor placed inside plastic box and surrounded by ground

After 28 days, recorded raw accelerations were elaborated to define the mortar maturation and the temperature influences on the measured data. Figure 5.9 and Figure 5.10 show the data obtained from the Pre-Conv Link cemented with compensated shrinkage mortar (Pre-Conv Link 1) and with no-shrinkage compensated mortar (Pre-Conv Link 2), respectively. Data are expressed for the *x*-axis, plotted together with temperature.

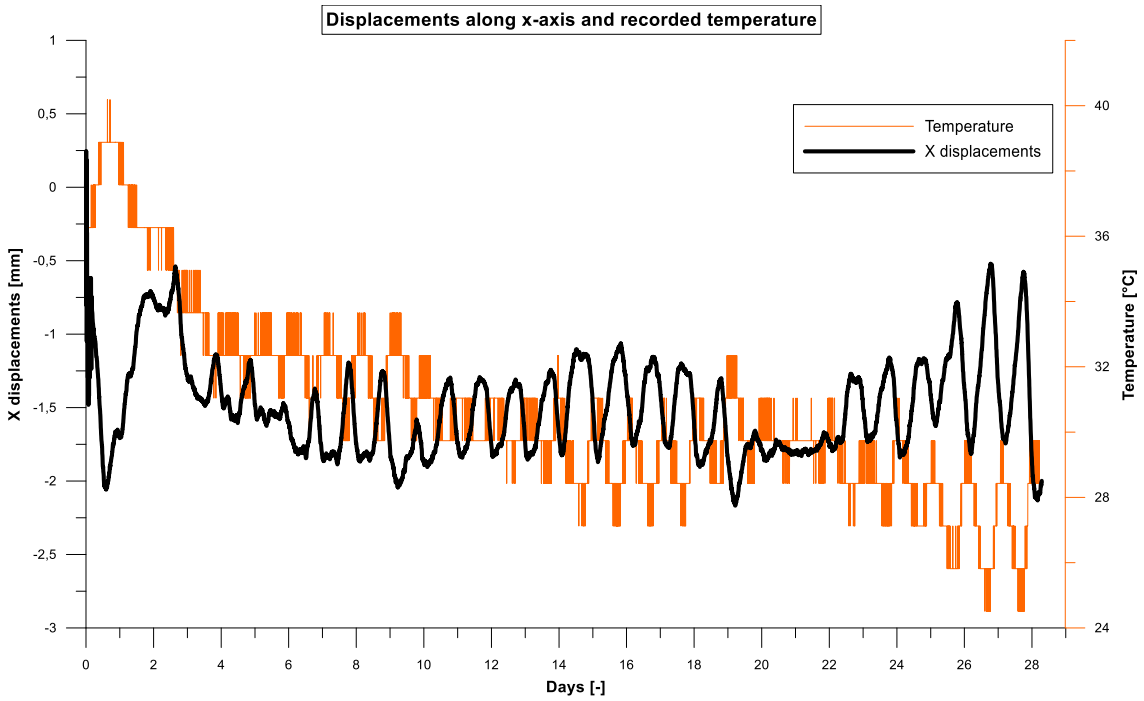

Figure 5.9 Pre-Conv Link 1 cemented with compensated shrinkage mortar. Displacements along x-axis and recorded temperature

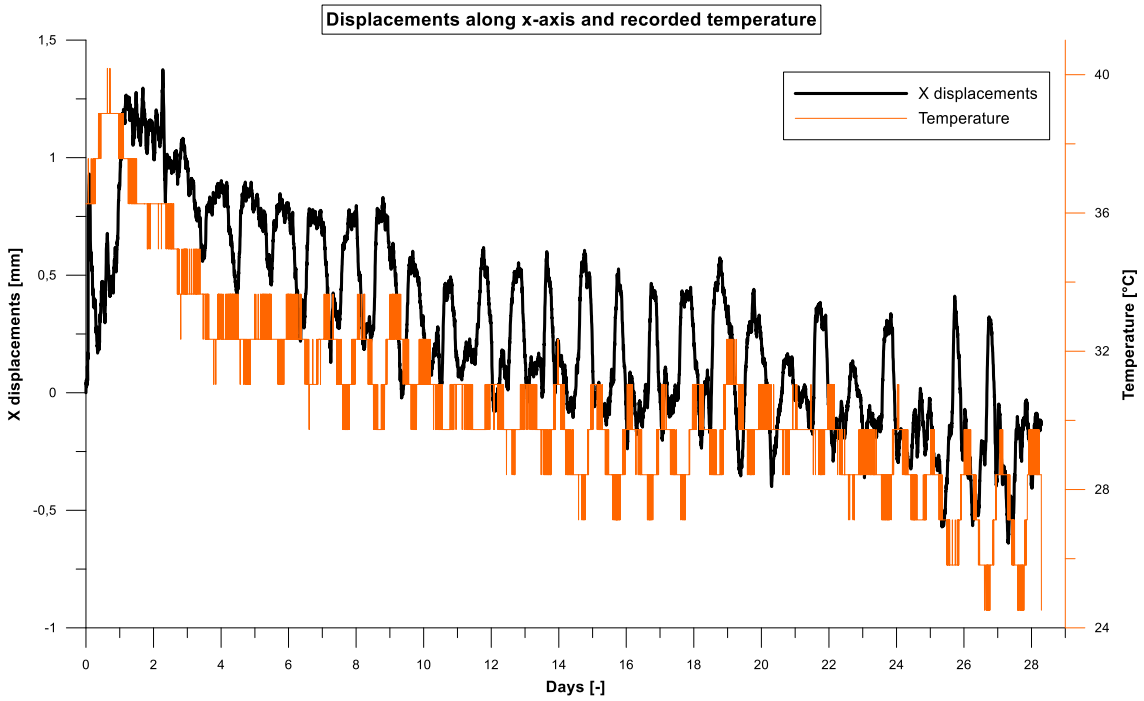

Figure 5.10 Pre-Conv Link 2 without compensated shrinkage mortar. Displacements along x-axis and recorded temperature

Represented graphs show a quick displacement occurred in the first monitoring days. Shrinkage compensated mortar induces approximately 2.5 mm displacement during the initial maturation, while the other Pre-Conv Link suffers a lower displacement, approximately 1.2 mm. These data indicate a thermal-mechanical influence of the mortar maturation on the sensors. This influence is higher

considering a shrinkage compensated mortar, which probably can generate stronger stress on the resin shell that is ultimately transferred to the accelerometer. The data recorded during this test showed displacements of minor entity compared to the data recorded in the on-site application of the Pre-Conv Links, which was 5 mm. These discrepancies can be due to the high injection pressure applied in the on-site application, approximately 5 bar.

Starting from day 3, the mortar contribution seems to disappear for both sensors. However, Pre-Conv Links highlighted a thermal influence on the recorded data. Indeed, Pre-Conv Link 2 was firm, but the trend indicates an apparent displacement downward directed. Instead, Pre-Conv Link 1 does not suffer from this thermal trend variation, but its data oscillation becomes higher for stronger temperature variations. Thermal influence generated data noise and an acceleration oscillation of ± 1 mm for Pre-Conv Link 1 and of ± 0.5 mm for Pre-Conv Link 2.

Starting from these experimental shreds of evidence, we implemented a thermal filtering algorithm in the ATD software to define, more accurately, displacement trends and removing all the external influences that affect the monitoring tool. The proposed filter was initially defined by a back-analysis procedure, based on the acquired monitoring data. In the next section, the filter will be presented and discussed.

5.3. Thermal filter

Thermometer calibration is obtained by Equation [4.6], where the temperature is defined by a linear equation that links the collected raw value in ADC to the physical value by the slope and the intercept. The displacement is defined by Equation [4.11], that can be schematized as:

$$a_{x_j} = A a'_{x_j} + b \qquad [5.2]$$

In which:

- a_{x_j} is the acceleration recorded along *x*-axis for the *j* node;
- a'_{x_j} is the raw acceleration recorded along *x*-axis for the *j* node;
- A is the slope determined by calibration procedure;
- b is a coefficient that represent the thermal contribution, defined by Equation [4.6], or simply:

$$b = cT + d \qquad [5.3]$$

Where c is the temperature slope and d is intercept of the temperature.

Thermal parameters are defined by linearizing raw temperature as a function of parameter b, obtaining thermal slope and intercept, and the determination coefficient R^2. Generally, during thermometer calibrations, sensors reach R^2 values higher than 0.65 ÷ 0.70.

The first attempt to define a more accurate thermal calibration process was carried out by considering a second-degree equation to describe the relationship between T and b. The graphs that follow show the temperature calibration process for two different installed sensors in one of the pilot sites, Pre-Conv Link 18 and Pre-Conv Link 12 (Figure 5.11).

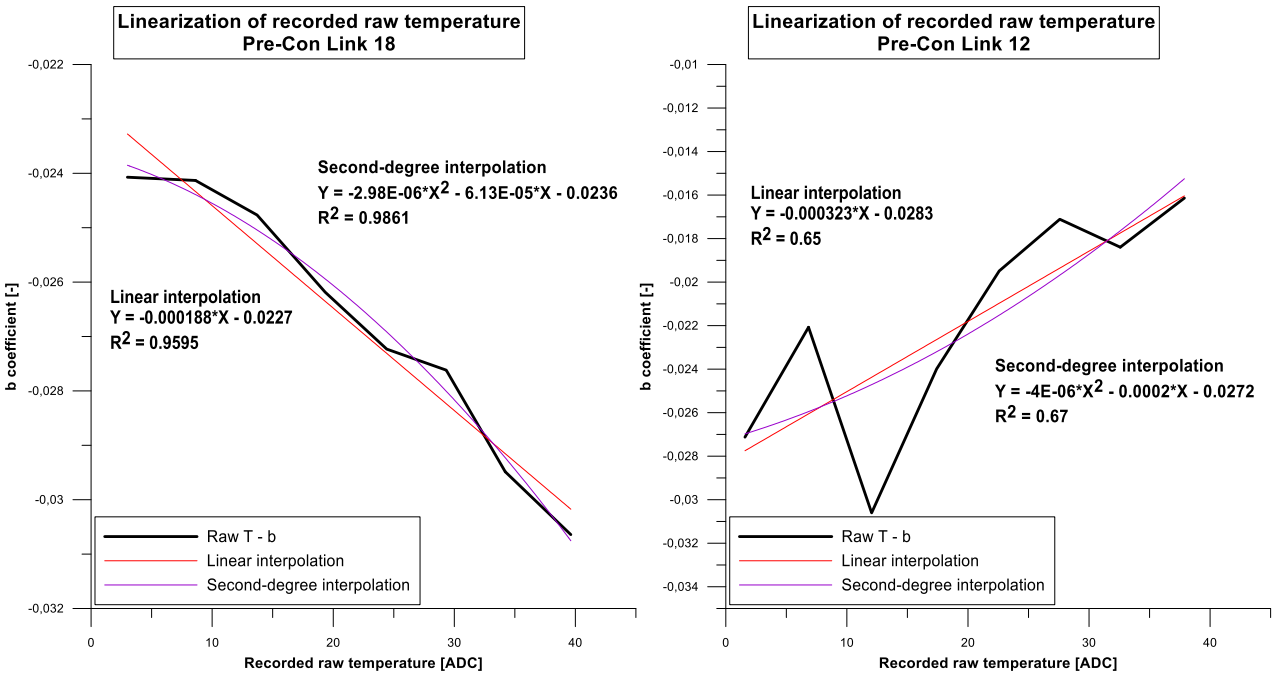

Figure 5.11 Example of linear and second-degree interpolation of Pre-Conv Links. Left: Pre-Conv Link 18, right: Pre-Conv Link 12

A second-degree interpolation increases the coefficient of determination for each sensor, from 0.960 to 0.986 for Pre-Conv Link 18, and from 0.65 to 0.67 for Pre-Conv Link 12. By replacing the second-degree equation in Equation [5.3], and then in Equation [4.11], displacements can be evaluated and compared with the linear relationship. Figure 5.12, and Figure 5.13 show two examples of evaluation of the displacements during the first week of monitoring. The graphs focus on the comparison of displacement data, elaborated by a linear or second-degree equation. The displacement values and trends will be presented and discussed in the Chapter 6 and 7.

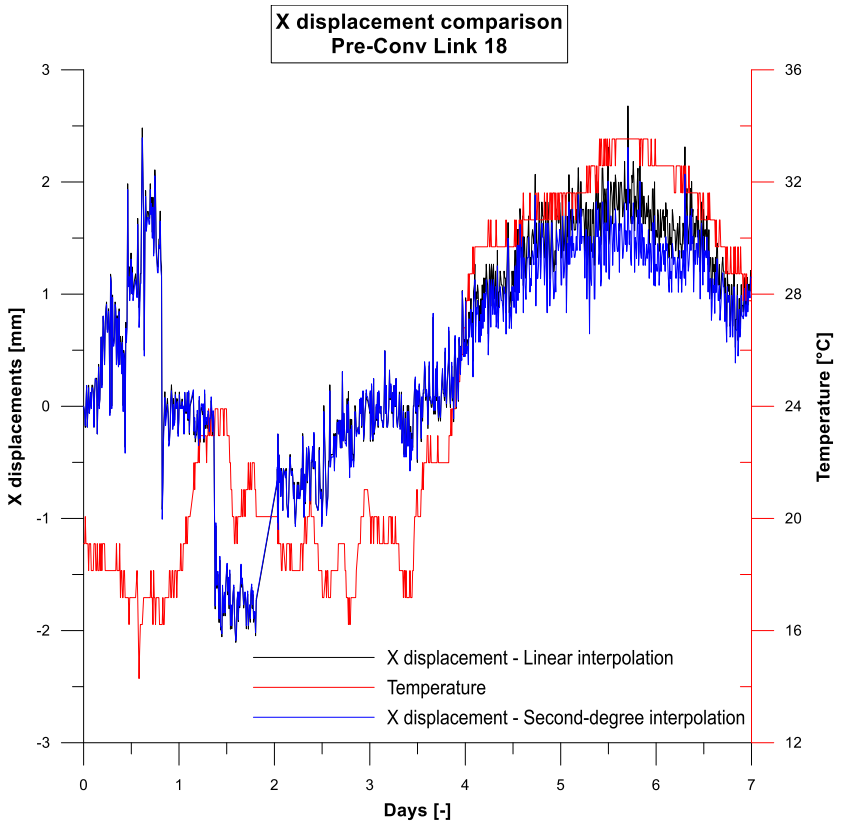

Figure 5.12 Comparison of displacement using a linear interpolation (black line) or a second-degree equation (blue line) for Pre-Conv Link 18. The red line represents the measured temperature

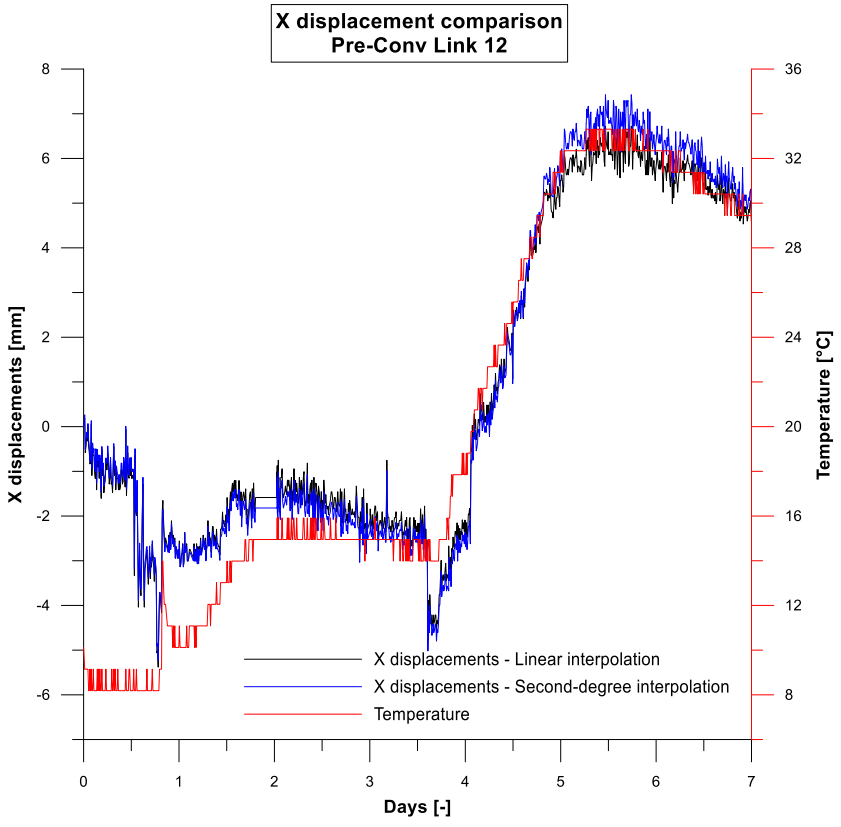

Figure 5.13 Comparison of displacement using a linear interpolation (black line) or a second-degree equation (blue line) for Pre-Conv Link 12. The red line represents the measured temperature

Figure 5.12 represents elaborated data obtained from Pre-Conv Link 18. The first monitoring days are characterized by displacement due to the contribution to the start of the excavation phases and the mortar concrete hardening. After four days, when the excavated face was several meters after the calculation point, a displacement of higher entity was recorded. This increase, overlapped with the recorded temperature, shows a direct relationship between the measured quantities. Figure 5.13 presents data acquired by Pre-Conv Link 12. As in the previous sensor, the first two days are characterized by the mortar influence, while during the 3rd monitoring day, a steep vertical settlement of approximately 2.5 mm could be highlighted, corresponding to the excavation advance of the tunnel face. From the 4th , displacements are affected by thermal variation alone.

The two calibration methods applied produce similar data, indeed the two evaluated curves are similar in terms of trends, and values, therefore demonstrating that a high order calibration method does not solve the thermal influence on the on-board sensors.

An additional attempt was tried by considering the slope and the intercept of each couple of points of the broken curve obtained from raw temperature value, and the relative intercept, b, as in Figure 5.11. In this case, displacements can be defined considering the measured raw temperature and the range in which they are included. For example, Pre-Conv Link 12 presents 7 different raw temperature and b ranges (Figure 5.11 on the right). The corresponding slope and intercept are reported in Table 5.2

Table 5.2 Calibration parameters of Pre-Conv Link 12 obtained from the broken curve method

Raw temp. range	***b* range**	**Slope**	**Intercept**
1.58 ÷ 6.83	-0.027 ÷ -0.022	0.00096	-0.02865
6.83 ÷ 12.04	-0.022 ÷ -0.031	-0.00164	-0.01088
12.04 ÷ 17.42	-0.031 ÷ -0.024	0.00123	-0.04543
17.42 ÷ 22.58	-0.024 ÷ -0.019	0.00087	-0.03915
22.58 ÷ 27.58	-0.019 ÷ -0.017	0.00048	-0.03022
27.58 ÷ 32.58	-0.017 ÷ -0.018	-0.00026	-0.01004
32.58 ÷ 37.88	-0.018 ÷ -0.016	0.00043	-0.03228

Raw acceleration data were evaluated considering the measured raw temperature values and the temperature range in which are included. The defined slope and intercept in Table 5.2 are inserted in Equation [5.3], calculating the displacements. Figure 5.14 and Figure 5.15 show the comparison between the displacement evaluated by a linear relationship and by parameters obtained throughout the defined broken curve. A particular behaviour was observed: by applying the broken curve

parameters, Pre-Conv Link 12 data display a worse in terms of thermal influences. The blue line relative to the broken curve method in Figure 5.14 shows a downward displacement of approximately -14 mm, which exactly follows the temperature trend. Instead, Pre-Conv Link 18 does not highlight this behaviour, and the two curves elaborated with the two different methods show a similar behaviour.

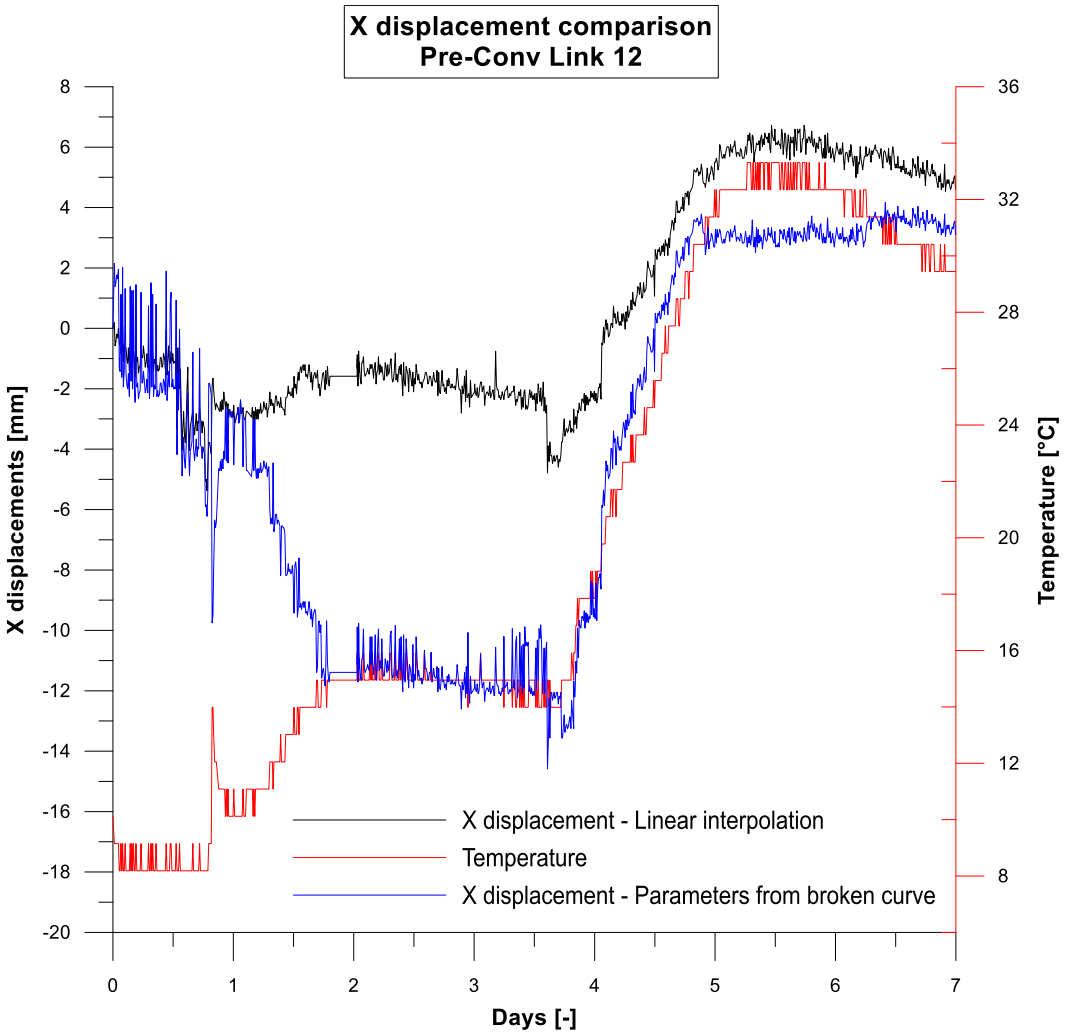

Figure 5.14 Displacements comparison using a linear interpolation (black line) or the broken curve parameters (blue line) for Pre-Conv Link 12. The red line indicates the recorded temperature

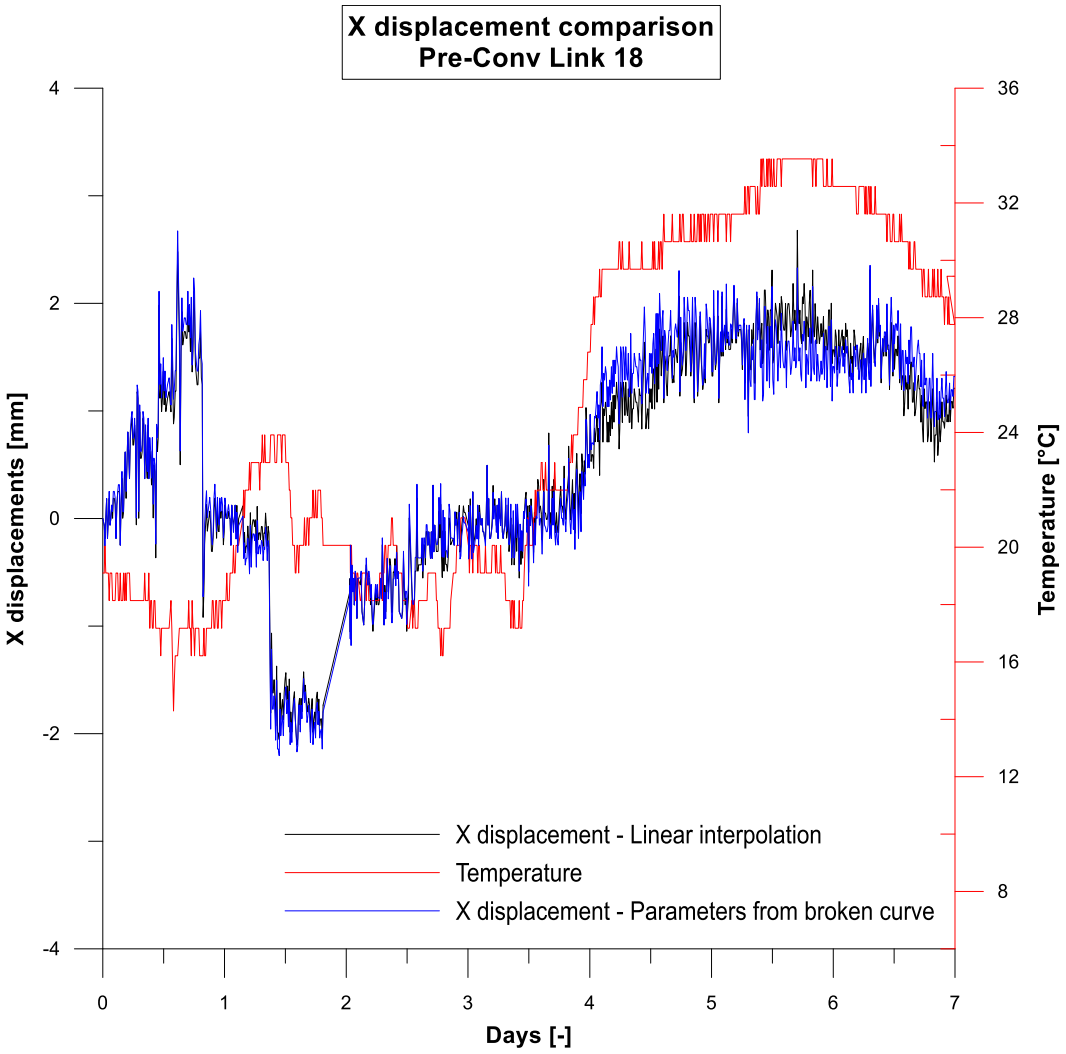

Figure 5.15 Displacement comparison using a linear interpolation (black line) or the broken curve parameters (blue line) for Pre-Conv Link 18. The red line indicates the recorded temperature

Pre-Conv Link 12 data highlight that the method of parameters from broken curves cannot recognize and correct measured data that occurred during steep temperature variation. This phenomena can be due to the mechanical influence of the resin shell on the MEMS sensor that reduces data accuracy for a wide temperature range. Moreover, the thermal dilation of the mortar concrete can affect the monitoring data as well. However, dilation is hard to define without an accurate thermal 3D model that can give an evaluation of the induced dilation displacements that occur during the whole monitoring.

The correlation between displacement data and the temperature is more evident far from excavation work, when the thermal contribution is probably higher than the displacement contribution. Indeed, in the first days of monitoring, during the face drilling works exactly under the calculation point, rapid and well-defined displacements can be highlighted, while after 4 days of monitoring the thermal influence is more evident (Figure 5.15).

This observation suggests a different approach to apply on elaborated data, based on the variation rate of temperature and vertical settlements in time.

In order to define, and finally delete, the thermal influence on each sensor, the daily variation rate of temperature and displacements were recorded. A procedure was implemented trying to define a unique parameter for every installed sensor or an equation that can compensate for thermal contribution. The method consists in applying a linear regression to both the measured vertical settlements and the measured temperature.

Firstly, temperature and vertical displacement are normalized by a feature scaling process. The feature scaling process is a method for data resizing that permits to compare different quantities with different measure units, analysing a possible existing correlation (Peshawa & Rezhna, 2014). The data normalization is defined by Equation [5.4] and Equation [5.5].

$$X_{norm} = \frac{X - \mu(X)}{\max(X) - \min(X)} \quad [5.4]$$

$$T_{norm} = \frac{T - \mu(T)}{\max(T) - \min(T)} \quad [5.5]$$

Where:

- X and T are the monitoring data acquired for a fixed sensor, representing the local vertical displacement and the temperature, respectively;
- $\mu(X)$ and $\mu(T)$ are the medium of the local displacement and the temperature for the entire monitoring dataset;
- $\max(X)$ and $\max(T)$ are the maximum data acquired;
- $\min(X)$ and $\min(T)$ are the minimum data acquired.

Figure 5.16 shows the normalized data obtained by applying Equation [5.4] and Equation [5.5] for Pre-Conv Link 18. The first two monitoring days define an inverse relationship between temperature and displacement, due both to the concrete hardening and the start of the excavation process. Monitoring day 3, corresponding to the tunnel face passage, shows a steep normalized increase in the displacement. Starting from day 4, a similar trend between temperature and displacements is shown, due both to the thermal contribution and the Link stabilisation after the support installation. Normalized temperature ranges between 0 and -0.2, instead normalized displacement show a similar trend, but with opposite values in a smaller range.

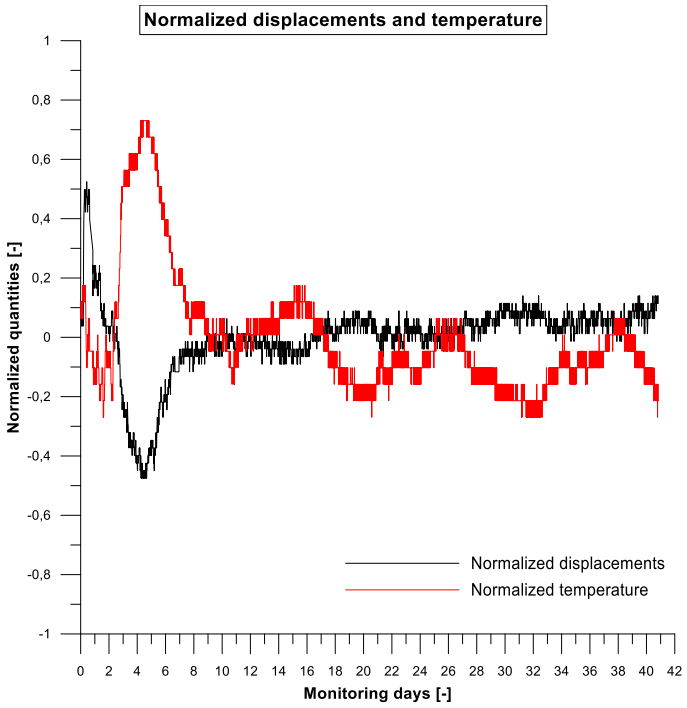

Figure 5.16 Example of data normalization for Pre-Conv Link 18

After data normalization, the daily slopes of temperature and displacements for each monitored day were calculated. Since displacements can be in phase or out of phase with temperature values, the absolute value for each parameter is considered. Finally, the daily delta slope is determined and plotted.

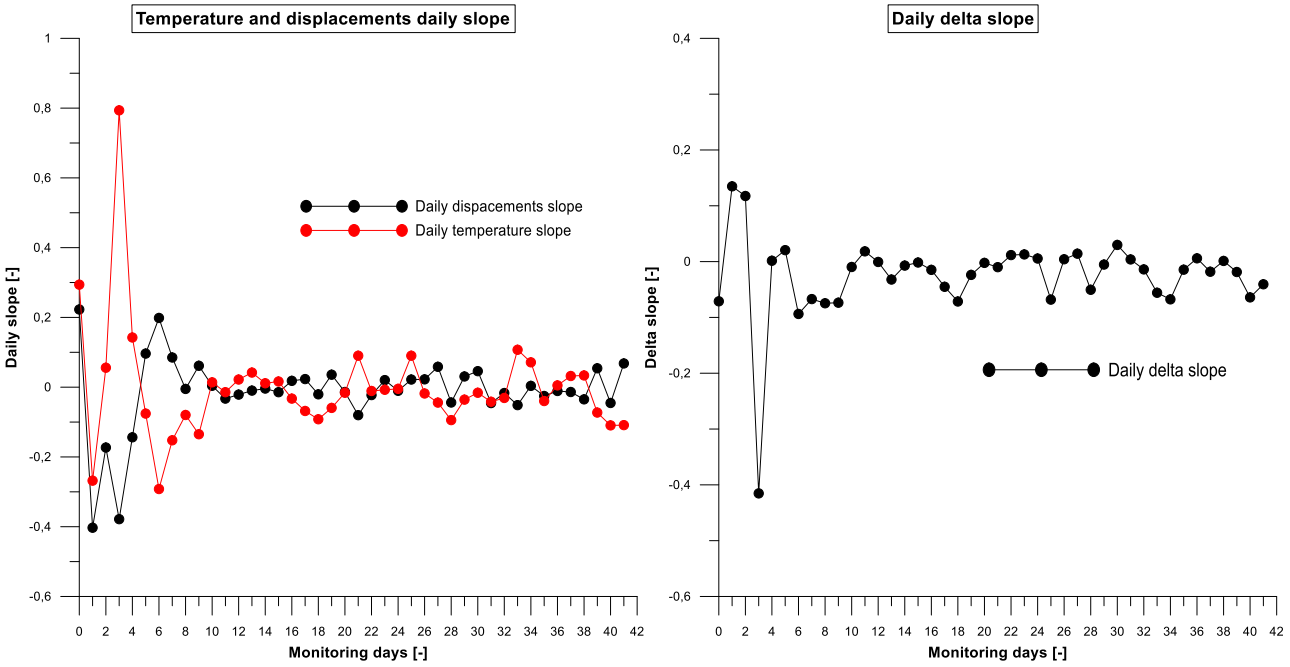

Figure 5.17 Daily temperature and displacements slope (on the left), and relates delta (on the right). Pre-Conv Link 18

Figure 5.17 represents the daily displacements and temperature slope for the Pre-Conv Link 18. The first three monitoring days show both high slope coefficient and delta values, due to the start of the excavation process, and, as evidenced by the thermal test, to the concrete mortar maturation as well. Delta values can recognize the different working stages, that are the tunnel drilling and the support installation, and when excavation is occurring far from the monitored section. Indeed, in the first days of monitoring, corresponding to the start of the excavation phase, high delta values were obtained. Afterwards, low delta value can be observed, oscillating from -0.05 to 0, which are caused by the tunnel face passage and the support installation on the monitored section. While higher delta values can underline a stronger displacement contribution, lower delta values indicate a similar normalised data trend. In this case, the thermal influence can be the major components, or, simply, temperature and displacements are not variating. Since delta values underline the working stages of the tunnel construction, the definition of a threshold is necessary to compensate for thermal influence. Hence, when delta values are higher than the defined threshold, displacements data are the principal contribution, instead, when delta values are lower than a threshold, temperature is the principal contribution that generates data noise or apparent displacement.

After a back-analysis process, studying all the calculation point and their thermal behaviour a threshold value equal to ±0.05 was defined. In the next chapters, the implemented approach for defining the thermal threshold will be discussed, together with two cas studies in which the method was applied.

After defining delta slope and threshold, a data filtering system is applied, to recalculate temperature values by imposing a linear relationship as in Equation [5.6]:

$$T' = a \cdot T + b \qquad [5.6]$$

Where:

- T' is the temperature recalculated;
- T is the temperature acquired;
- a and b are the slope and the intercept to apply on thermal data for compensating displacement values.

Then, a deviation between recalculated temperature and displacement is evaluated, Equation [5.7]:

$$\delta = (T' - X_{loc})^2 \qquad [5.7]$$

Where:

- δ is the deviation;

- X_{loc} is the local vertical displacement for each sensor.

Parameters a and b are estimated by a linear regression, searching the minimum value for the δ summation, $\sum \delta$, for each sensor and for the entire monitoring period composed by n data, by applying Equation [5.8]:

$$\sum_{1}^{n} \delta = min[(a \cdot T + b) - X_{loc}]^2 \quad [5.8]$$

Then, $X_{loc,elab}$ is calculated as:

$$X_{loc,elab} = X_{loc} - T' \quad [5.9]$$

The $X_{loc,elab}$ are determined only for days in which the delta between temperature and displacement slope are higher than ±0.05. When the delta slope lies within the defined threshold, displacements are defined null, due to a stronger thermal contribution.

Parameters a and b obtained by a linear regression for each node were firstly analysed, trying to define a valid relationship for each sensor. Since parameters a and b vary for all the monitoring instruments, indicating a different thermal influence on each on-board sensor, a limited dataset was taken. More specifically, we took monitoring data after the support installation and far from the tunnel face, where the surrounding ground was almost stable (Figure 5.18). Afterwards, a series of parameters a and b were defined by applying the linear regression for each Link and minimizing δ (Table 5.3).

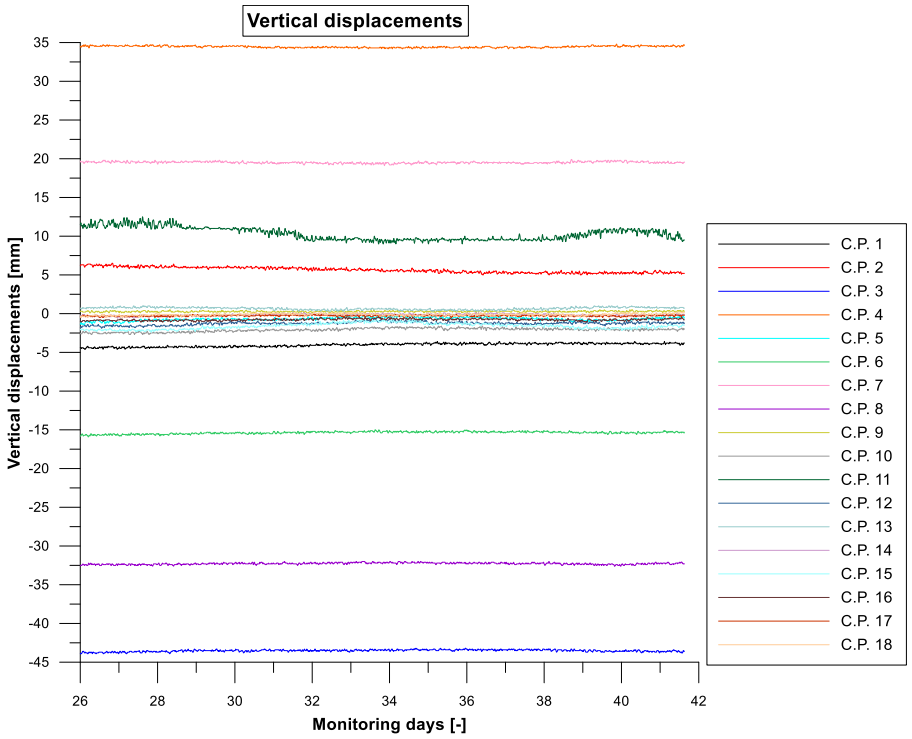

Figure 5.18 Example of range used to evaluate a and b parameters for the pilot site installation in the north of Italy

Table 5.3 Example of a and b parameters obtained for the pilot site installation in the north of Italy

Calculation Point	*a*	*b*	Calculation Point	*a*	*b*
1	-0.24	-0.15	**10**	-0.30	3.14
2	0.36	-0.39	**11**	1.22	-10.20
3	-0.08	-42.08	**12**	-0.25	3.08
4	0.08	33.12	**13**	0.20	-2.77
5	-0.21	3.06	**14**	-0.13	2.15
6	-0.14	-12.92	**15**	-0.54	7.78
7	0.11	17.62	**16**	-0.13	1.49
8	-0.11	-30.38	**17**	-0.03	0.34
9	0.00	0.20	**18**	-0.03	0.53

In the next chapters, two case studies where thermal filter was successfully applied will be presented together with monitoring data and their validation through topographic monitoring.

6. Case Study 1 – Tunnel in the North of Italy

6.1. Introduction: geological and geotechnical framework

The first Pre-Conv Array has been installed in a deep tunnel located in the north of Italy that connects two important valleys. The designed works include a modification of the pre-existing national road, the realization of a bridge, and the excavation by explosive of a tunnel for a length of 990 meters (Figure 6.1). The construction company did not accept to disclose sensitive information, therefore no references to the project name or to the real date of excavation are exposed.

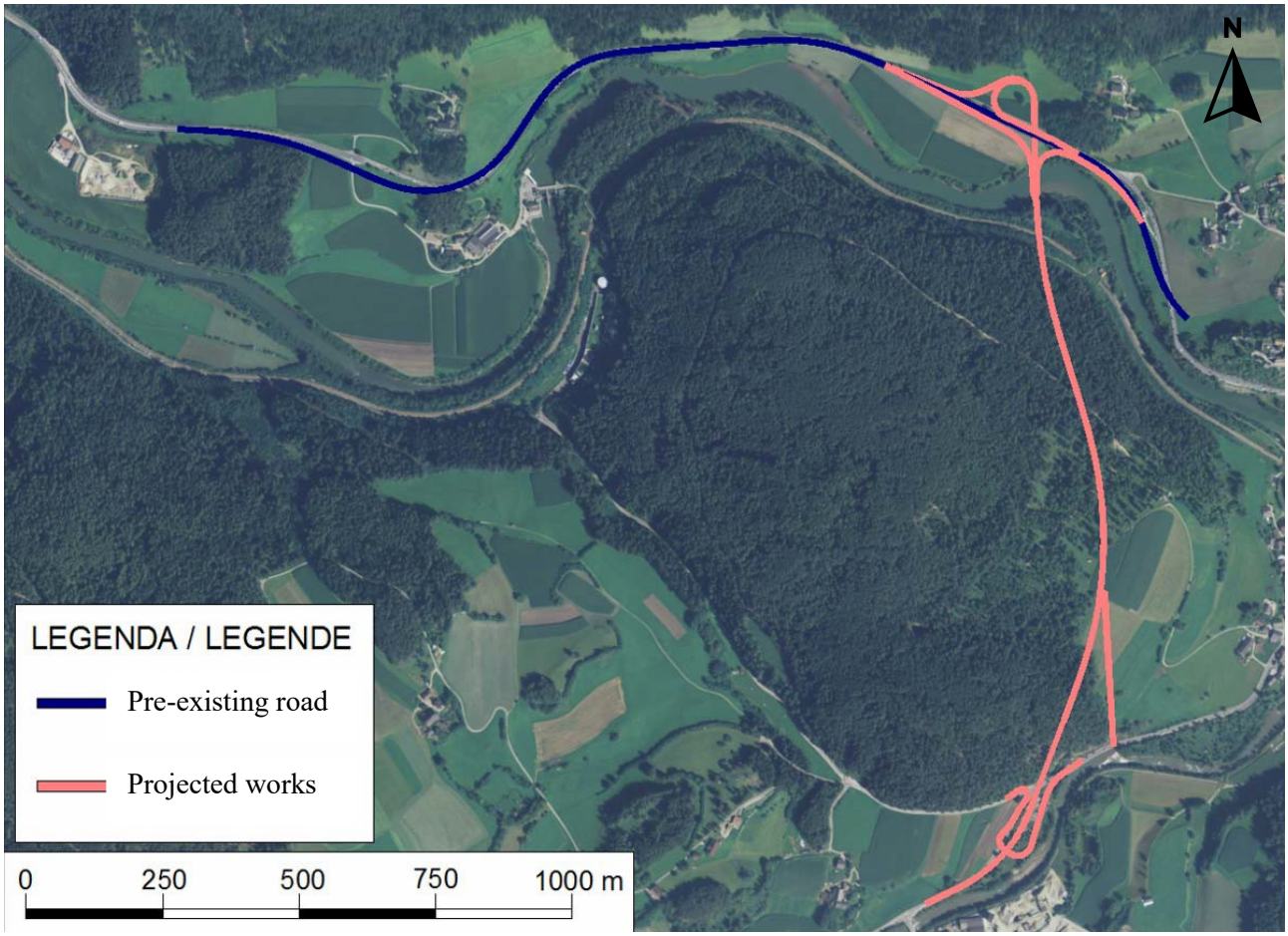

Figure 6.1 Aerial photography of the construction site

The roadway presents a medium altitude of 810 meters above the sea level (m.a.s.l.), while the mountain peak has a height of 970 m.a.s.l. The geological context of the construction area is characterized by a high risk of falling rocks or rock detachments in the upper portion of the mountain caused by the vibration induced by the excavation works.

The mountain is composed of a high presence of glacial deposit, while the bedrock mainly of quartz phyllite (Figure 6.2). The north entrance of the tunnel, on the right in Figure 6.2, is completely

excavated inside melted deposit, which has been intensively studied, and characterized by laboratory tests together with on-site surveys. The Pre-Conv Array was installed inside melted deposits to monitor and verify the pre-displacement induced by the excavation works ahead of the tunnel face, and to monitor the convergence displacement after the tunnel face passage. The tool has been installed at 180 m from the north entrance for a length of 18 meters, with 18 sensors spaced at one meter each other. The ground characterization defines the following geotechnical properties of the glacial deposit (Table 6.1).

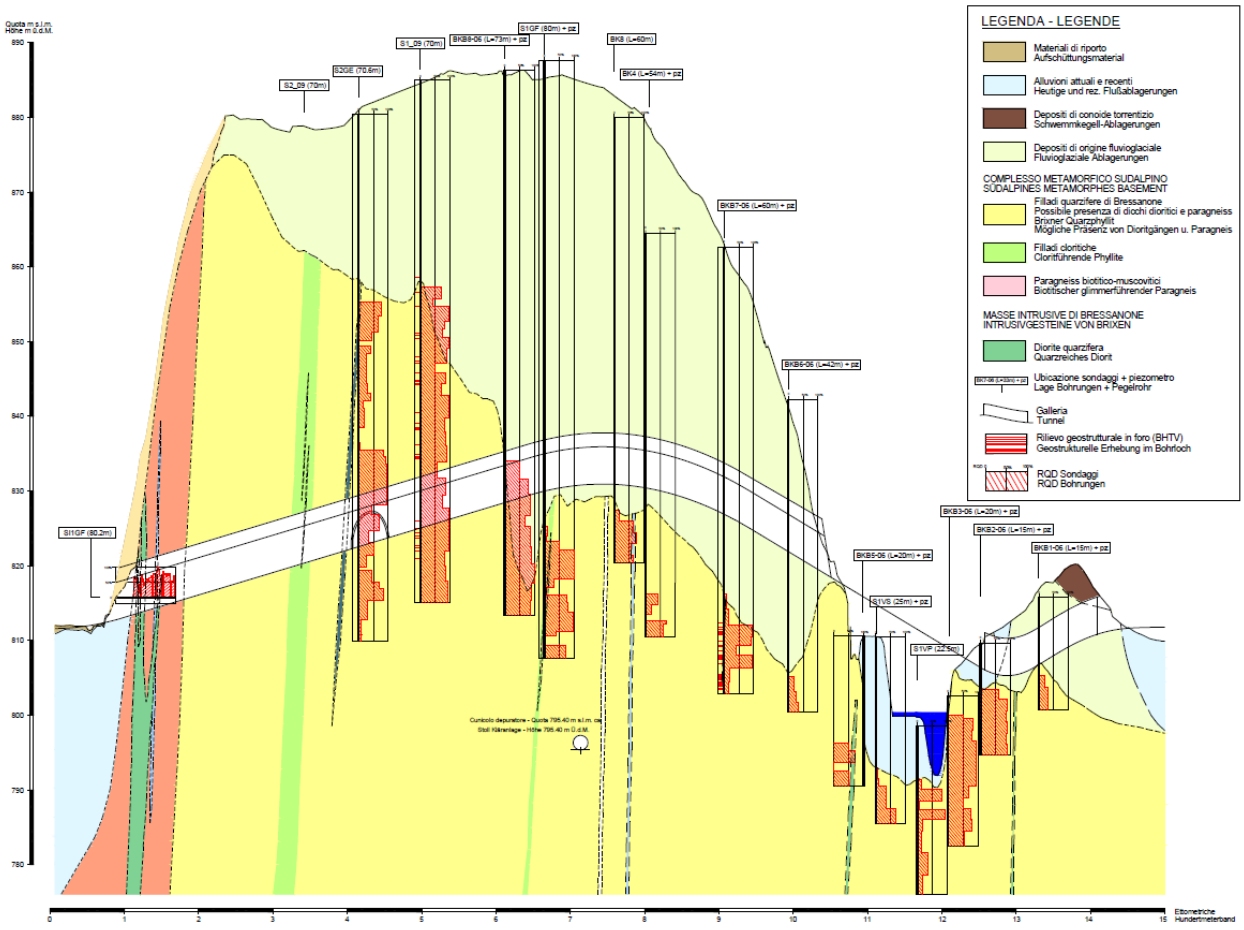

Figure 6.2 Geomechanical section of the tunnel

Table 6.1 Geotechnical parameters of glacial deposits

Glacial deposit				
Volume weight γ [kN/m^3]	**Friction angle φ [°]**	**Cohesion c [kPa]**	**Elastic modulus E [MPa]**	**Poisson coefficient υ [-]**
20	35-38	10-15	25-125	0.3

6.2. Tunnel excavation and evaluation of expected displacements

The tunnel has been excavated by a preliminary crown digging, with an equivalent radius of 4.28 m, followed by the inverted arch, according to NATM principles, with a total equivalent radius of 5.78 m (Figure 6.3). The temporary confinement support system is composed of shotcrete, and rock bolts, while the preconfinement interventions are realized by fore poles tilted at 5°, injected with concrete grout (Figure 6.4).

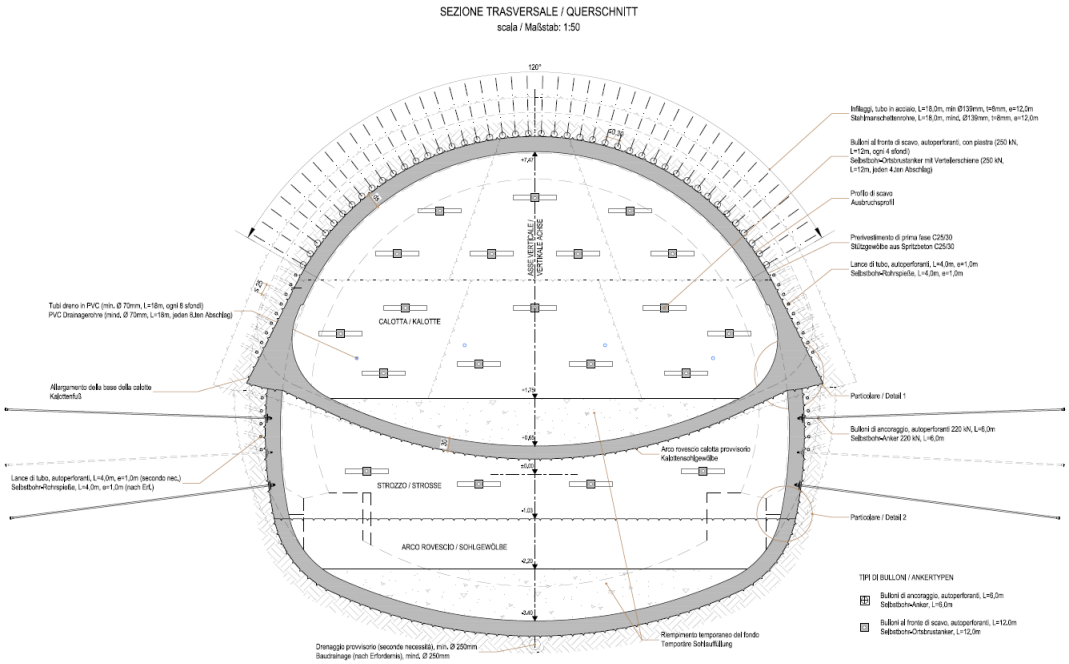

Figure 6.3 Typical excavation section

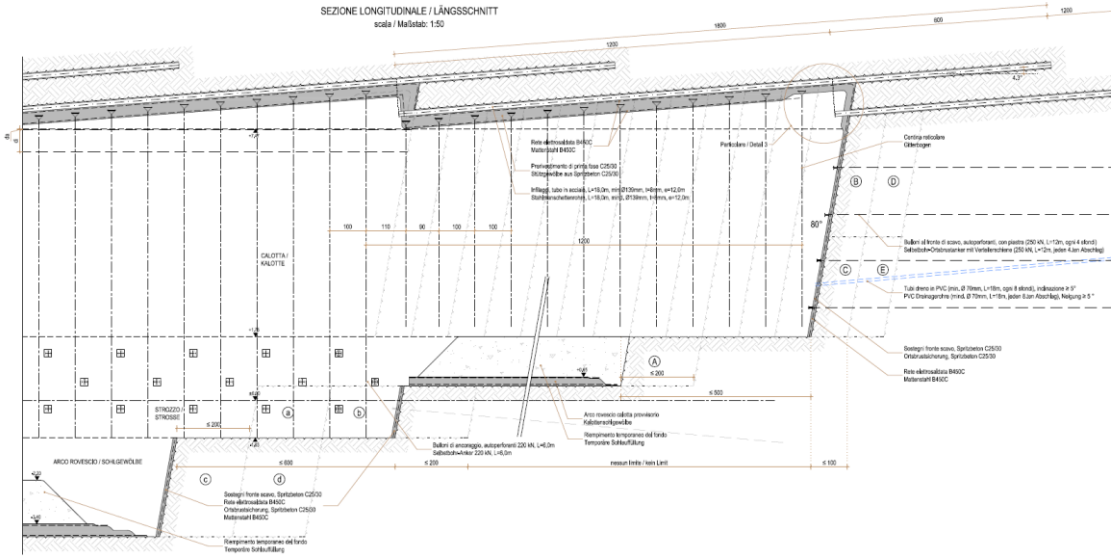

Figure 6.4 Advance method and confinement and preconfinement support systems

The project designer has defined four verification sections in which the expected displacements were evaluated by a plane numerical model realized by Plaxis 2D®. The Pre-Conv Array has been installed between BKB7-06+PZ and BQ 4 sections with a medium overburden of 50 meters (Figure 6.5).

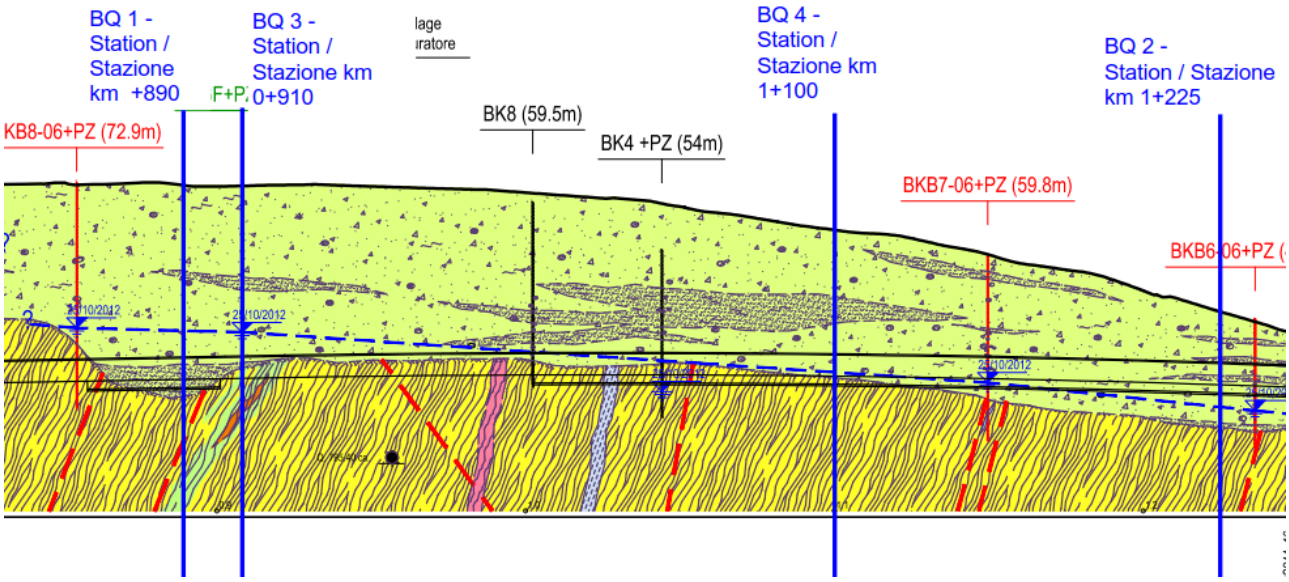

Figure 6.5 Verification sections (blue line)

The expected displacements were evaluated by the geotechnical parameters (Table 6.1). Two different scenarios were considered: the first considers the worst parameters, as defined in Table 6.1, while the second scenario considers also a null cohesion coupled with the highest friction angle. Elaboration results were evaluated also considering the confinement and preconfinement systems. Displacements were finally evaluated in five different points simulating the convergence star (Figure 6.6). Target n°1 was considered to compare the numerical model and the displacement obtained through Pre-Conv Array.

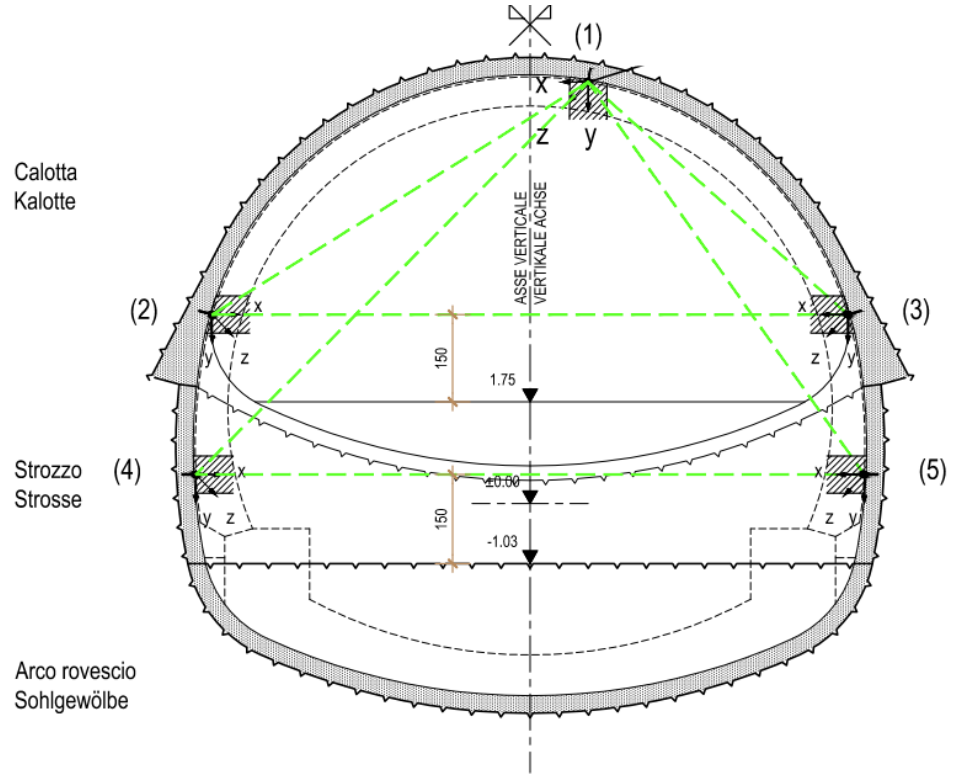

Figure 6.6 Geodetic monitoring during the tunnel construction

The numerical model defines the following displacements, divided for each scenario on the target n°1 (Table 6.2). Furthermore, no alarm or alert threshold were defined for the evaluated section.

Table 6.2 Expected displacements obtained by the numerical model

Scenario 1	***x*** **[mm]**	***y*** **[mm]**	**Scenario 2**	***x*** **[mm]**	***y*** **[mm]**
Crown excavation	-2	78	**Crown excavation**	-3	79
Inverted arch excavation	-3	85	**Inverted arch excavation**	-4	84

6.3. Pre-Conv Array installation and excavation works

As described before, the Pre-Conv Array has been installed at 180 meters from the north entrance inside the top centre pipe, tilted at 5° for a length of 18 meter (Figure 6.7).

Figure 6.7 Left: Pre-Conv Array installation. Right: Pre-Conv Array preparation

The tool was initially prepared, linking the fiberglass rods to each other by a fiberglass connector for a duration of approximately one hour. The tool assembly can be executed outside the tunnel or near the tunnel face without interfere with the working phases. The total mounting phase lasted one hour, while the installation phase lasted approximately of 10 minutes, excluding the forepoles digging and injection. Figure 6.8 represents the preconvergence monitoring section. The referring *x* and *y* absolute coordinates are defined in Table 6.3.

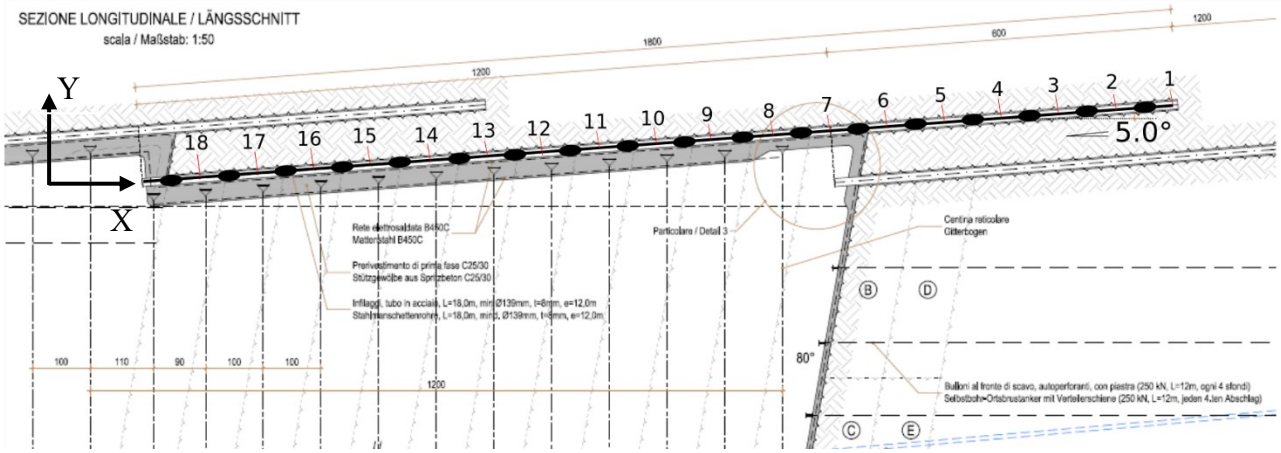

Figure 6.8 Example of the monitored section

Absolute coordinates were defined considering the forepole ledge of 20 cm in correspondence of the tunnel face, where the anchor starts with absolute coordinates *x* and *y* equal to 0 m. The calculation point 18, C.P. 18, is the most external, while the C.P. 1 is the farthest from the anchor.

Table 6.3 Absolute coordinates x and y for each calculation points

Calculation Point	x [m]	y [m]	Calculation Point	x [m]	y [m]
1	17.731	1.569	**10**	8.765	0.784
2	16.734	1.482	**11**	7.769	0.697
3	15.738	1.395	**12**	6.773	0.610
4	14.742	1.307	**13**	5.776	0.523
5	13.746	1.220	**14**	4.780	0.436
6	12.750	1.133	**15**	3.784	0.349
7	11.754	1.046	**16**	2.788	0.262
8	10.757	0.959	**17**	1.792	0.174
9	9.761	0.872	**18**	0.795	0.087

The excavation advance has a medium value of 2.86 m/day, excluding one week when the following excavation field was prepared by installing the preconfinement system, which overlapped with the previous one of 6 meters. Table 6.4 summarizes the excavation works and the related advance in meters per monitoring day, starting from monitoring day 0, namely, when the concrete mortar was injected inside forepole preconfinement support. The considered excavation range comprises the excavation and the mucking process. All data reported are based on the daily report obtained from the construction company.

Table 6.4 Excavation advance

Excavation advance [m]	Starting day [-]	Starting time [hh:mm]	Finishing day [-]	Finishing time [hh:mm]
1.25	1	22:30	2	03:30
2.50	2	13:30	3	00:00
3.75	3	04:00	3	19:00
5.00	4	00:30	4	05:00
8.75	4	06:00	4	22:00
10.00	5	11:00	5	16:00
11.25	5	23:00	6	03:00
12.50	6	04:00	6	09:00
13.75	6	12:00	6	19:00
15.00	6	21:00	7	02:00
16.25	12	12:00	12	19:00
17.50	12	22:00	13	03:00

6.4. Monitoring results

The zero-reference, imposed as a starting point for the displacement evaluation, was defined during the first day of monitoring, starting from 19:00, namely three hours earlier than the start of the excavation activity. The zero references was chosen considering the injection influence and the induced vibration that provides displacements. Indeed, the sensors provide displacements induced by the high injection pressure, approximately 5 bar, and by the vibrations occurred during the finishing work on the previous excavation field. The Pre-Conv Array collects data with a 10 minutes sampling frequency and it automatically sends data every hour to the elaboration centre. Such a high sample frequency permits to apply a statistical approach to the collected data and to define accidental errors provided by vibrations or electronic error during the sensors' queries, and finally delete them.

As outlined in section 5.2.3., data were compensated by applying a thermal filter, which is capable to reduce the thermal influence. In order to apply the thermal filter, the delta slope must be defined first. The delta slope is the difference between the daily temperature and the displacement slope. After a procedure of back-analysis, the delta slope to consider was defined. The procedure considers the excavation phases in correspondence of each calculation point and the thermal filter response: in fact, a higher threshold involves a stronger thermal influence detection, while a smaller threshold cannot detect the thermal contribution. The calibration of the delta slope parameter was also obtained through the comparison between the monitoring results defined by the Pre-Conv Array and the displacement defined by the topographic surveys. The next figures show the applied procedure to obtain the delta value threshold for C.P. 1 and C.P. 11, as shown in Figure 6.9 and Figure 6.10, respectively.

Figure 6.9 shows the elaborated local vertical displacements for the C.P.1, that is the farthest point from the anchor of the Pre-Conv Array. The red line represents the temperature, while the black line represents the evaluated displacement without applying the thermal filter. Interestingly, C.P. 1 did not highlight a pick in the recorded temperature, particularly during the first days of monitoring. Indeed, mortar maturation should create a thermal response with a high pick value of approximately 30÷40°C, that is not appreciated in this sensor. Moreover, in this period, when the tunnel face was far from C.P. 1, lower delta slope values cannot recognize and precisely compensate the thermal contribution. Indeed, delta slope values equal to 0.01 or 0.03 gave instrumental noise and apparent displacement induced by temperature variation. Moreover, higher delta values cannot recognize the real thermal response. Indeed, delta value equal to 0.1 involves no displacement for C.P. 1. This behaviour results from the consideration of a higher range, in which every daily delta slope was included. Finally, a delta value equal to 0.07 show a trend for the displacements similar to a delta value of 0.05. The trend is similar until monitoring day 14, although the two final displacement values

present a difference of about 1 mm. Between monitoring days 14 and 16, the excavation face was 1 meter over the C.P. 1, therefore, the convergence phenomenon could be shown till the support installation, that occurred on day 16. For these reasons, it is reasonable to consider data until day 16 with a delta slope equal to 0.05.

Between day 12 and day 14, when the tunnel face was drilled exactly under this considered point, elaborated data show an initial local displacement of 1 mm upward-directed. Afterwards, displacements starts to highlight a downward trend until a final value of -2.7 mm. This behaviour is due to the initial preconvergence response where the sensor tends to tilt counterclockwise, attracted by the tunnel excavation. After the tunnel face passage, a clockwise tilt can be observed due to the convergence displacement induced by the work proceeding till day 16.

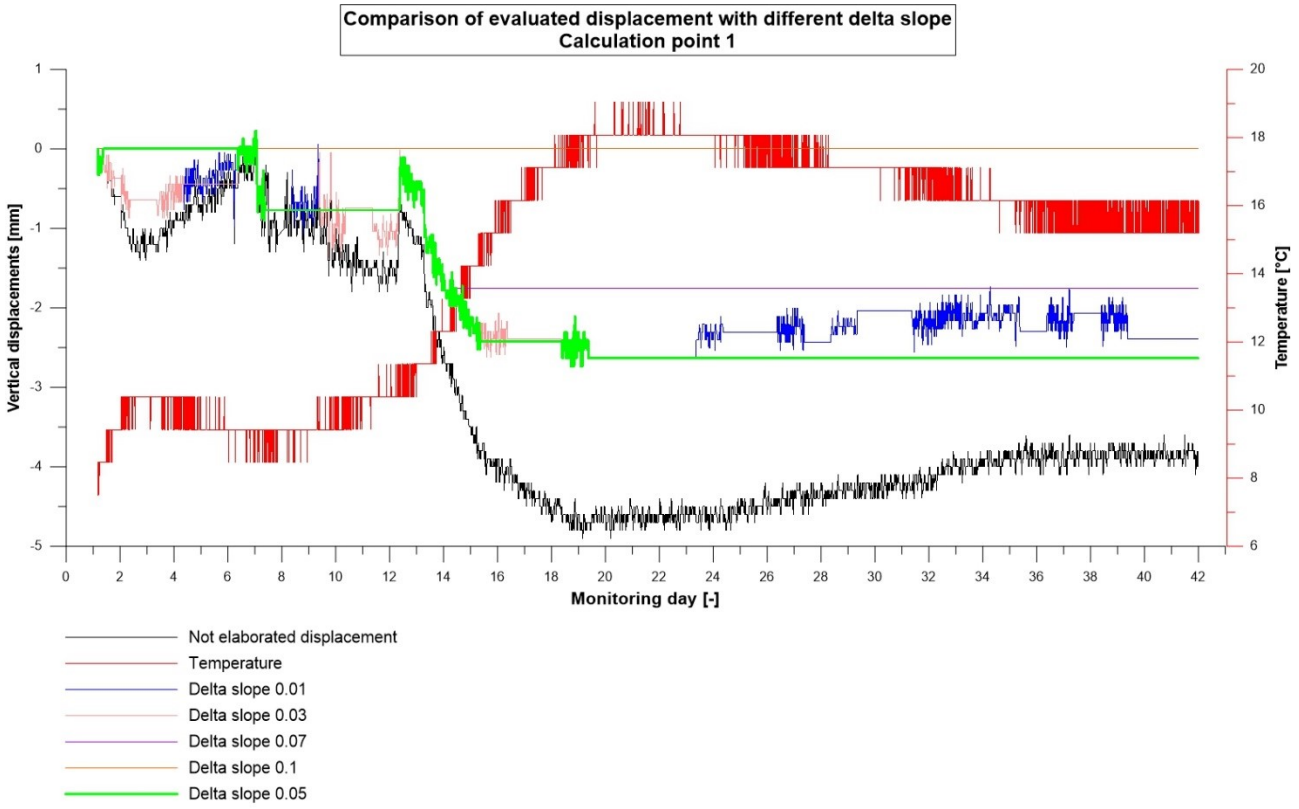

Figure 6.9 Local displacement calculated for C.P. 1 by applying different delta slope

Figure 6.10 represents the thermal response and the calculated local vertical displacements for the C.P.11, which is the sensor that indicated the highest thermal influence. Higher delta values, such as 0.07 or 0.1, involve no displacement detection. In fact, these two overlapped curves cannot distinguish deformations from thermal contribution. Lower delta values, such as 0.01 or 0.03 results in two overlapped curve and define a final local displacement of 8 mm. A delta value of 0.05 defines a local displacement of 4 mm. Between monitoring day 3 and 4, the tunnel face was excavated under C.P.

11. The resulting preconvergence deformation is highlighted with every delta value lower than 0.05. However, starting from day 4, a topographic station was installed in proximity of C.P. 11, which detected a -1 mm of displacement during the entire geodetic monitoring. A back-analysis based on the topographic monitoring was useful in defining the delta value to consider, which is equal to 0.05. The comparison between evaluated displacement and monitoring data will be shown in section 6.5.

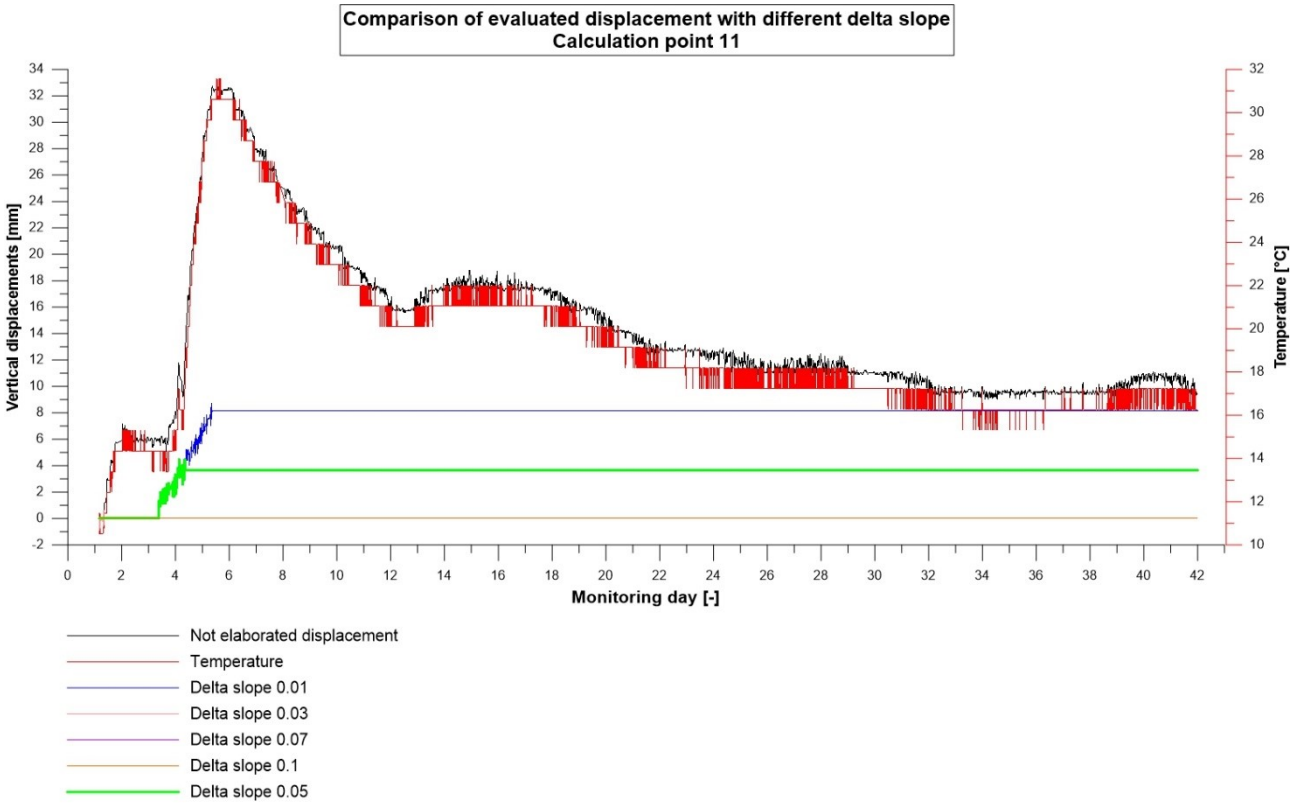

Figure 6.10 Local displacement calculated for C.P. 11 by applying different delta slope

Once defined the delta slope to compensate the thermal influence, monitoring data can be elaborated starting from the zero reference and analysed as a function of the excavation phases indicates in Table 6.4.

The following graphs show the local displacement at each excavation step, where monitoring data were initialized at the start of the drilling work, to verify the influence of each advance step. Finally, the total local and cumulated displacements referred to the zero reference are shown for every advance step.

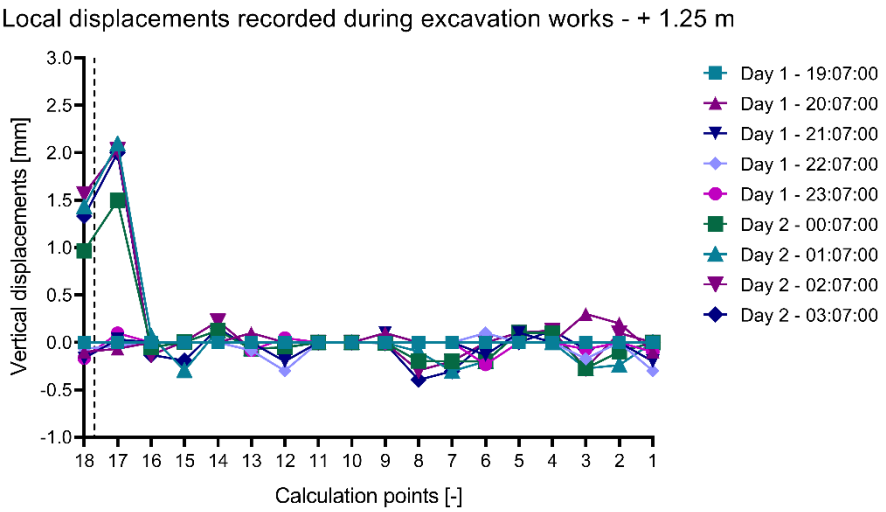

Figure 6.11 Local displacements occurred during the first excavation stage. The black dotted line indicates the tunnel face position referred to the Pre-Conv Array Calculation Points.

Figure 6.11 shows the local vertical displacements that occurred during the first excavation advance of +1.25 m. The calculation points mostly affected by the tunnel drilling were C.P. 18 and C.P. 17. These sensors showed an expected result: during the tunnel advance, sensors were initially downward attracted. Considering the calculation direction explained in section 4.3.1., these results indicate a vertical displacement upward directed. In this case, the excavation caused a local displacement of 2 mm starting from Day 2 – 00:07 on C.P. 17. Figure 6.12 shows the local displacement starting from the zero references (equal to the previous graph, only for the first excavation stage) and the resulting cumulative displacements.

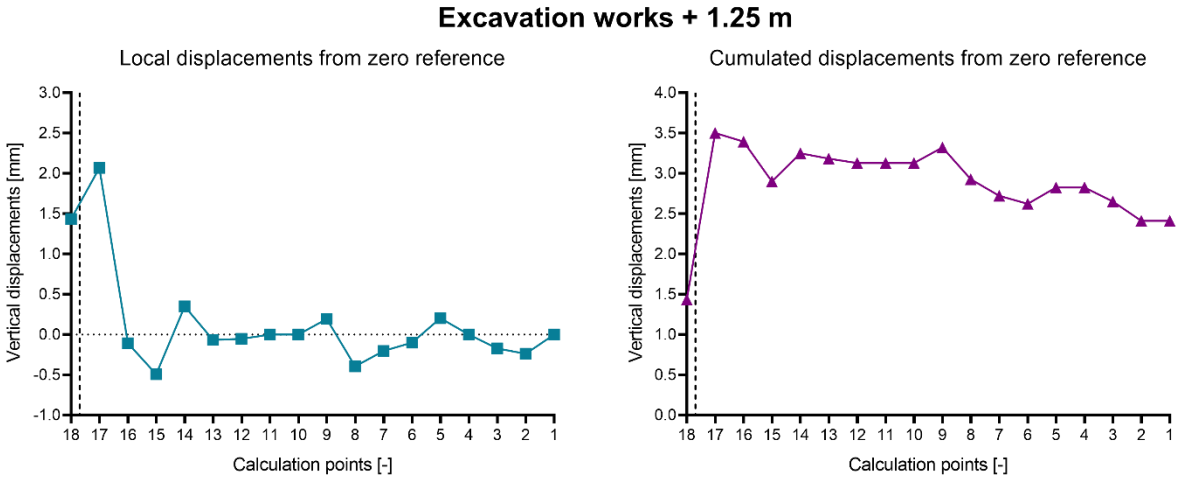

Figure 6.12 Left: Vertical local displacements evaluated from zero reference. Right: cumulated displacements evaluated from the referring date. The black dotted line indicates the front position

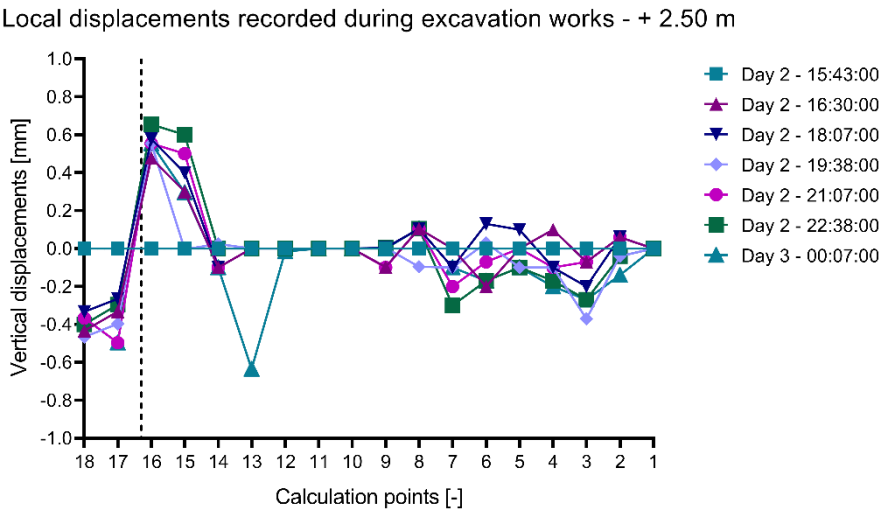

Figure 6.13 Local displacements occurred during the tunnel face advance of 2.50 m. The black dotted line indicates the tunnel face position referred to the Pre-Conv Array calculation Points.

Figure 6.13 refers to the excavation advance of +2.50 m, and it shows the same behaviour observed for the advance of +1.25 m. Calculation points 16 and 15 were attracted to the tunnel face highlighting a vertical local displacement of approximately 0.7 mm. The previous calculation points, such as C.P. 18 and C.P. 17, showed the start of the convergence phenomena indicating a local displacement of -0.5 mm.

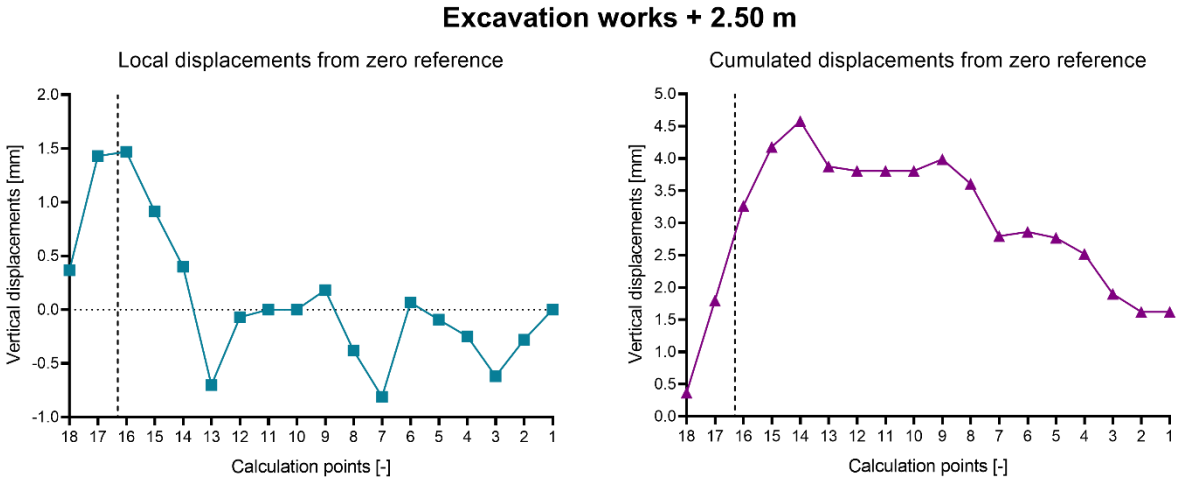

Figure 6.14 Left: Vertical local displacements evaluated from zero reference. Right: cumulated displacements evaluated from the referring date. The black dotted line indicates the front position

Cumulated displacements seem to indicate that the melted deposit surrounding the tunnel face is moving upward. This curve is affected by the calculation direction and the referring system of the Pre-Conv Array, so cumulated displacements need to be observed with the local displacement, to correctly understand the acting deformative state. A particularity can be pointed out: local and

cumulated displacements showed an inflection point near the tunnel face. This inflection indicates that the calculation points behind the tunnel face started to converge radially, while the calculation points ahead of the tunnel face showed the expected preconvergence deformation.

Figure 6.15 shows the local displacements that occurred during the tunnel advance of + 3.75 m. The maximum evaluated local displacements were -2.5 mm and 2.1 mm for C.P. 16 and C.P. 14, respectively.

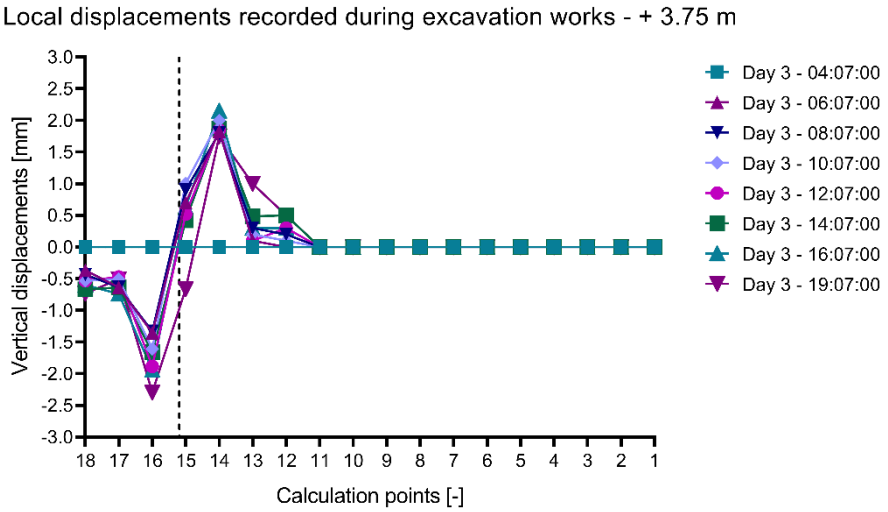

Figure 6.15 Local displacements occurred during the tunnel face advance of 3.75 m. The black dotted line indicates the tunnel face position referred to the Pre-Conv Array calculation Points.

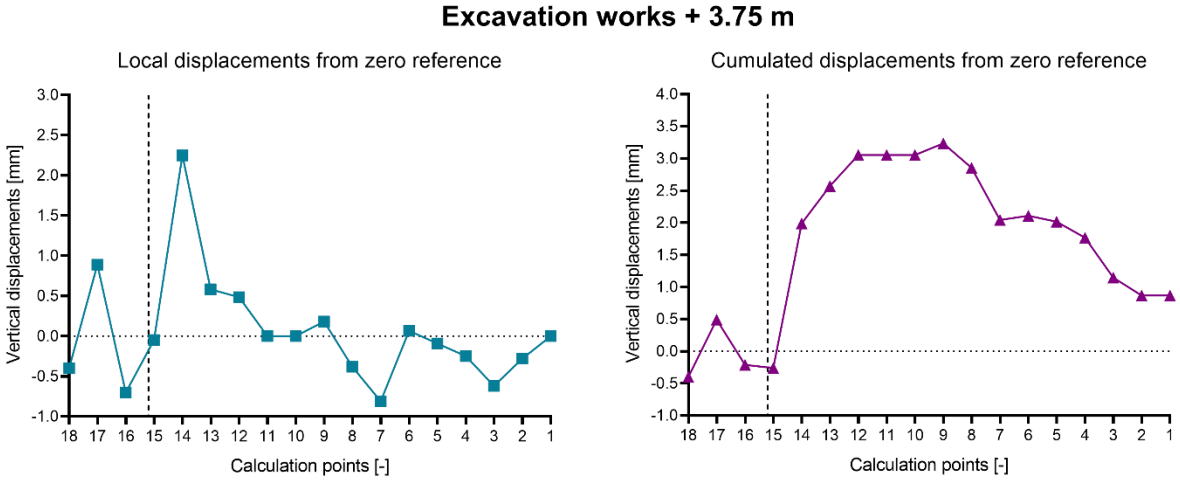

Figure 6.16 Left: Vertical local displacements evaluated from zero reference. Right: cumulated displacements evaluated from the referring date. The black dotted line indicates the front position

Recorded displacements during the tunnel advance of + 5.00 m were lower than 1 mm, and a data oscillation was shown, due to the sensor's resolution (Figure 6.17).

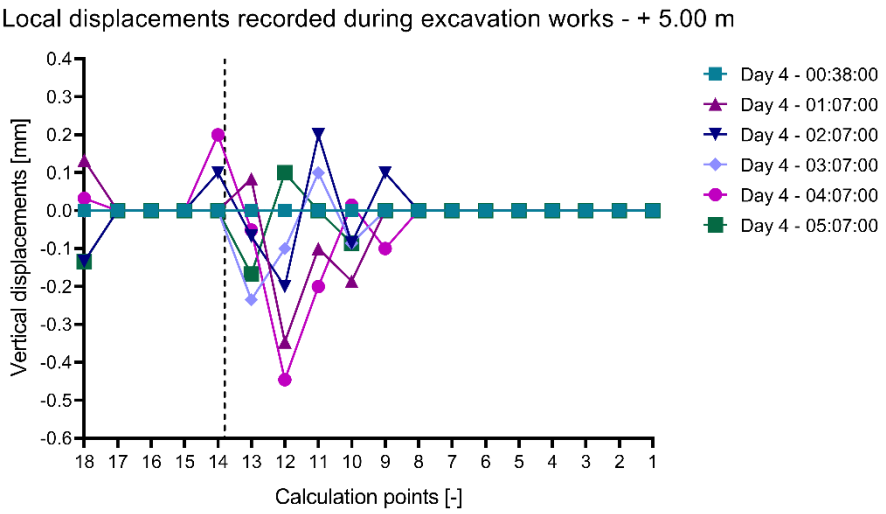

Figure 6.17 Local displacements occurred during the tunnel face advance of 5.00 m. The black dotted line indicates the tunnel face position referred to the Pre-Conv Array calculation Points.

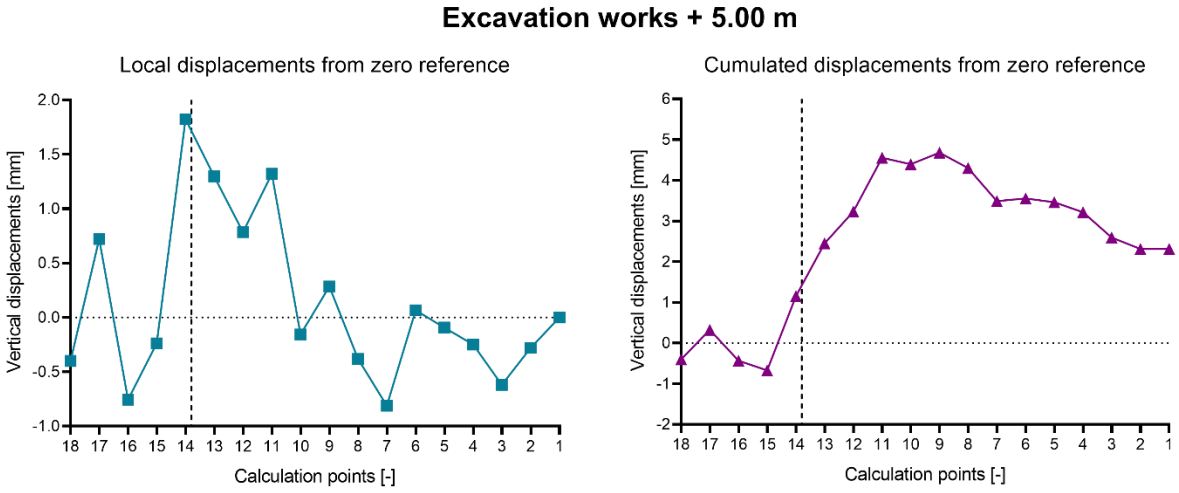

Figure 6.18 Left: Vertical local displacements evaluated from zero reference. Right: cumulated displacements evaluated from the referring date. The black dotted line indicates the front position

Figure 6.19 shows the local displacements that occurred during the tunnel advance of + 8.75 m. The maximum evaluated local displacements were of -2.5 mm and 2.1 mm for C.P. 12 and C.P. 11, respectively. C.P. 11 showed an upward local displacement, probably caused by a vertical settlement acting before the Pre-Conv Link 11, that determined a counterclockwise rotation. C.P. 10 evidenced a preconvergence deformation of +1.5 mm.

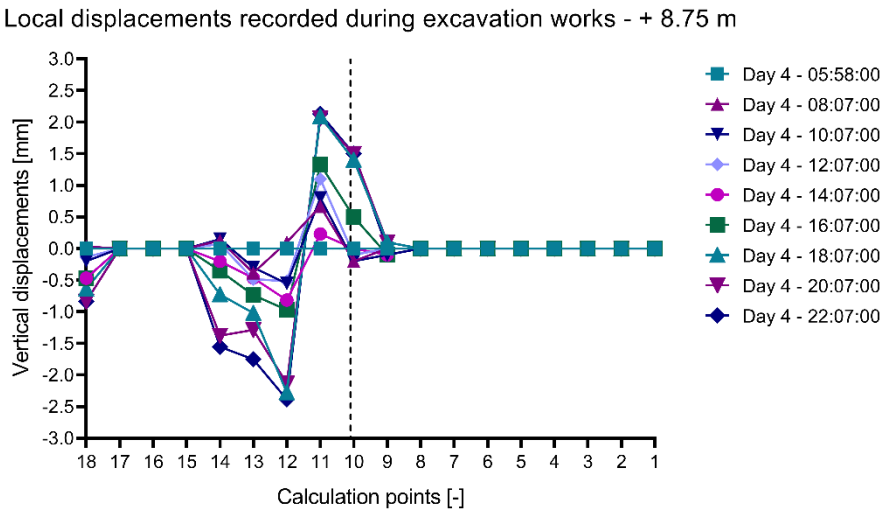

Figure 6.19 Local displacements occurred during the tunnel face advance of 8.75 m. The black dotted line indicates the tunnel face position referred to the Pre-Conv Array calculation Points.

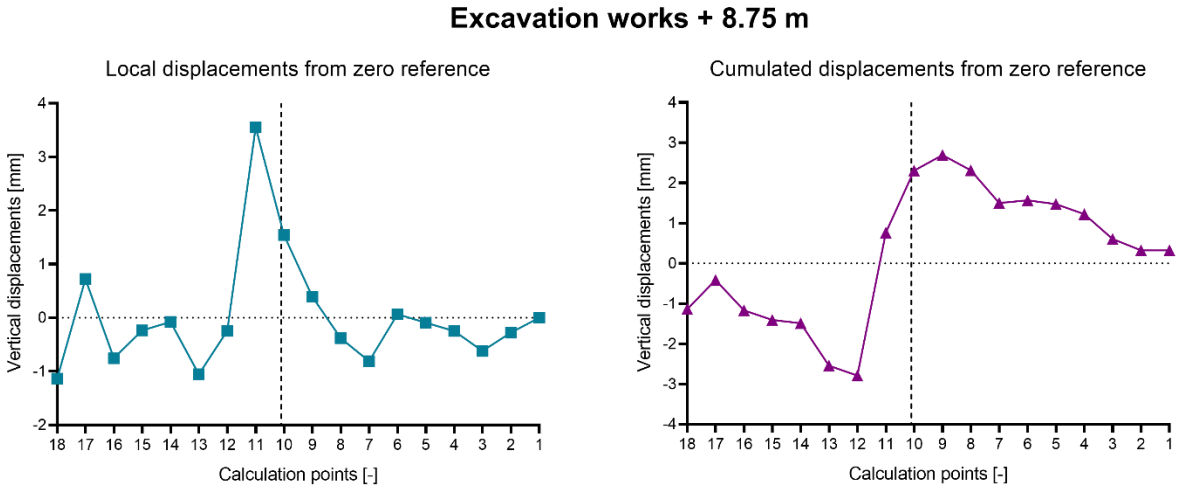

Figure 6.20 Left: Vertical local displacements evaluated from zero reference. Right: cumulated displacements evaluated from the referring date. The black dotted line indicates the front position

Figure 6.21 shows the local displacements that occurred during the tunnel advance of + 10.00 m. The maximum evaluated local displacement was -28.8 mm for C.P. 8. The excavation started on day 5 – 11:00, however, in the previous hours, C.P. 8 defined a steep increase of the preconvergence deformation.

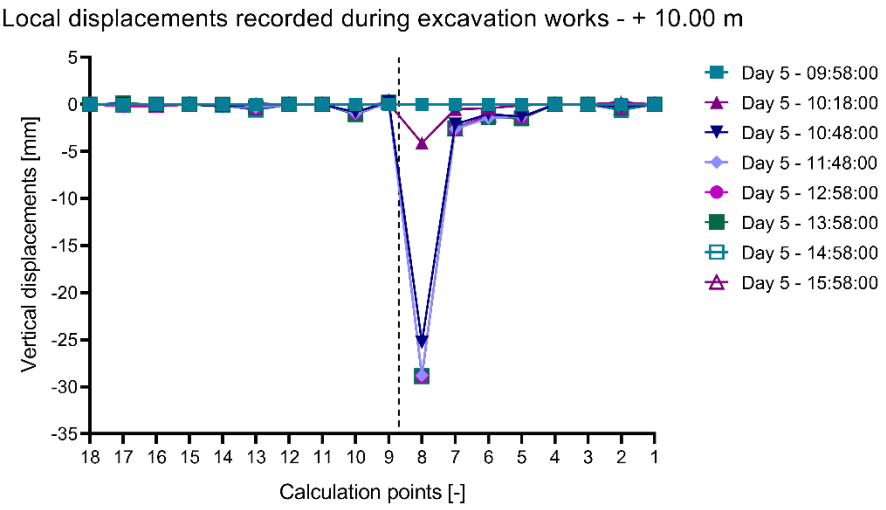

Figure 6.21 Local displacements occurred during the tunnel face advance of 10.00 m. The black dotted line indicates the tunnel face position referred to the Pre-Conv Array calculation Points

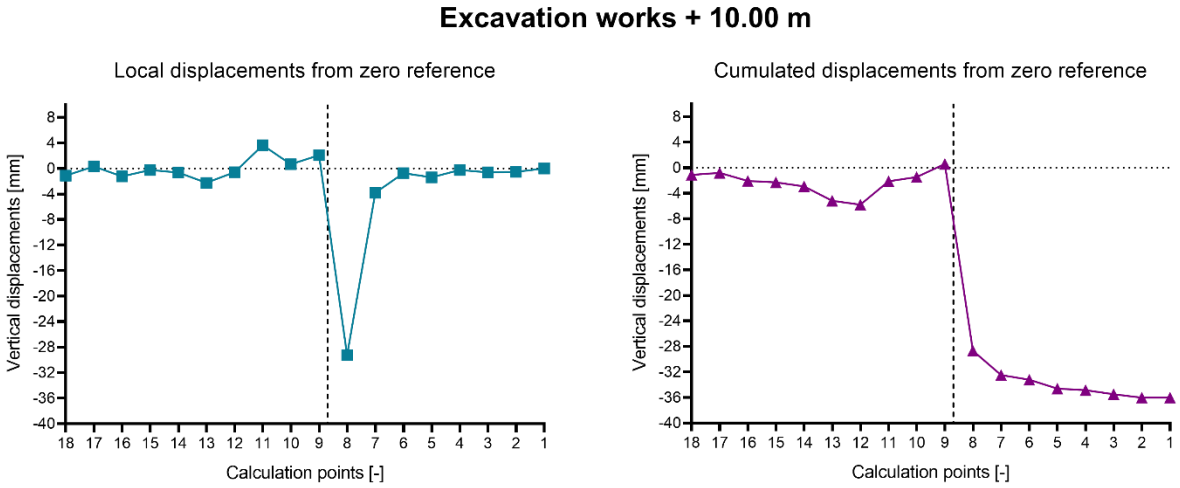

Figure 6.22 Left: Vertical local displacements evaluated from zero reference. Right: cumulated displacements evaluated from the referring date. The black dotted line indicates the front position

Figure 6.20 and Figure 6.22 indicate an increase of the convergence phenomena acting on the calculation points behind the tunnel face, much lower than the displacements defined by the numerical model. We can hypothesize that the first calculation points are in a ground structure where the geotechnical parameters are greater than expected. Instead, an increase of the preconvergence deformations can be underlined starting from +10.00 m of advance.

Starting from +11.25 m of advance, preconvergence deformations on C.P. 7 indicated a local vertical displacement of 22 mm, followed by an increase of preconvergence movement of -14 mm on C.P. 6 (Figure 6.23). Cumulated displacements reached -32 mm of displacements (Figure 6.24).

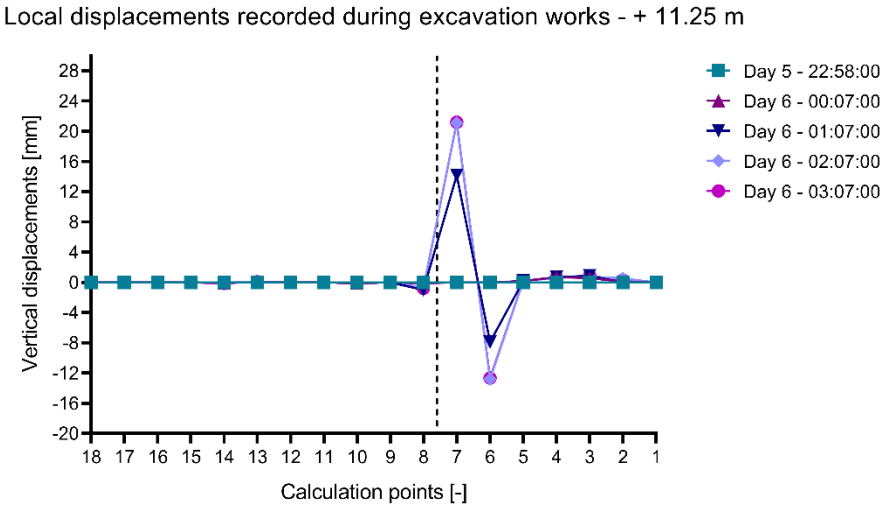

Figure 6.23 Local displacements occurred during the tunnel face advance of 11.25 m. The black dotted line indicates the tunnel face position referred to the Pre-Conv Array calculation Points

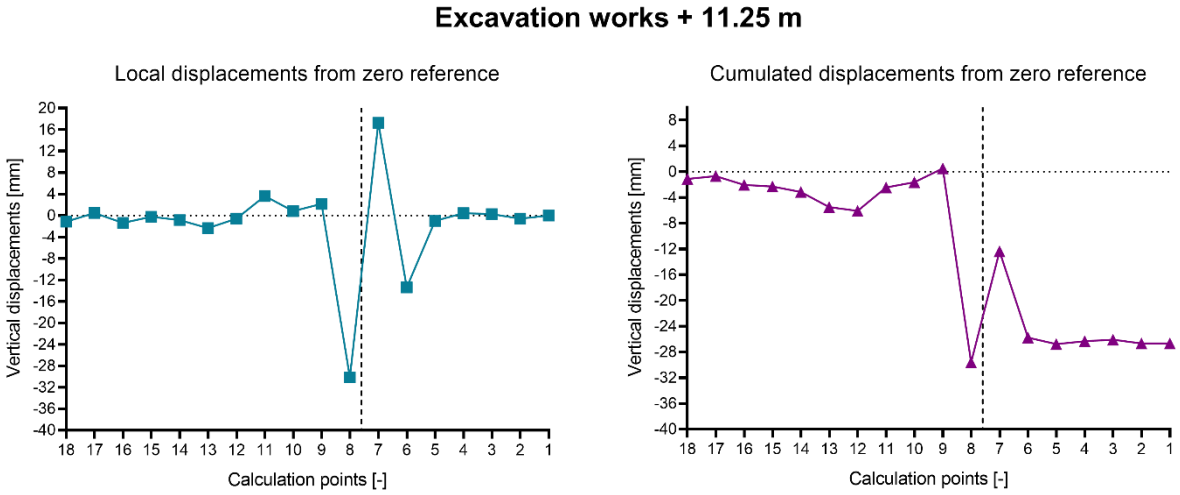

Figure 6.24 Left: Vertical local displacements evaluated from zero reference. Right: cumulated displacements evaluated from the referring date. The black dotted line indicates the front position

The tunnel advance of +12.50 m did not highlight a significant change in the deformative stress, showing a preconvergence displacement equal to 1.3 mm in C.P. 6 (Figure 6.25).

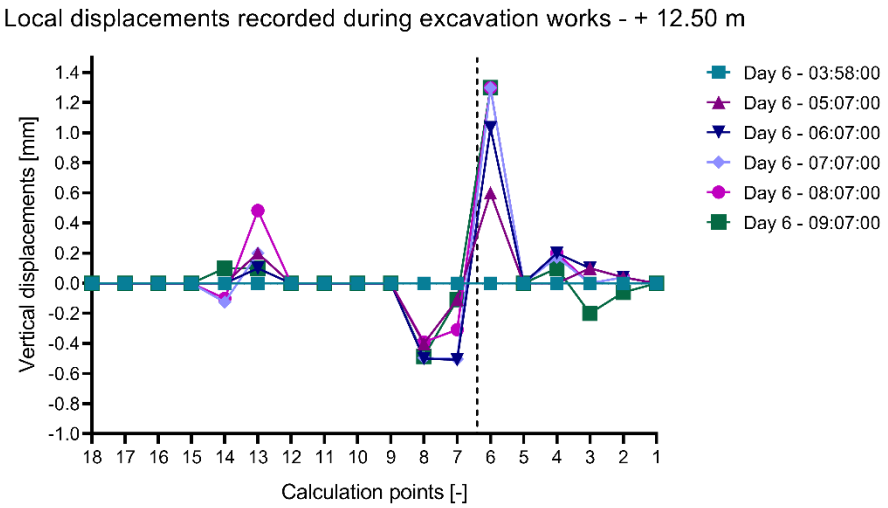

Figure 6.25 Local displacements occurred during the tunnel face advance of 12.50 m. The black dotted line indicates the tunnel face position referred to the Pre-Conv Array calculation Points

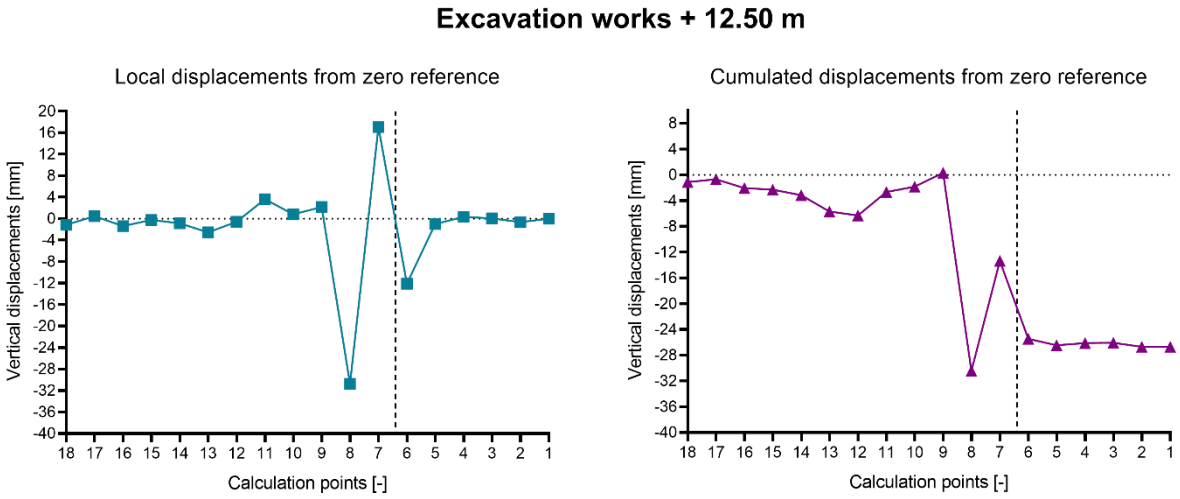

Figure 6.26 Left: Vertical local displacements evaluated from zero reference. Right: cumulated displacements evaluated from the referring date. The black dotted line indicates the front position

Local displacements recorded during the advance works of +13.50 m defined a slight increase of the preconvergence deformations on the C.P. 4, approximately 2.6 mm. C.P. 6, behind the tunnel face, indicates a convergence deformation of -1.6 mm (Figure 6.27 and Figure 6.28).

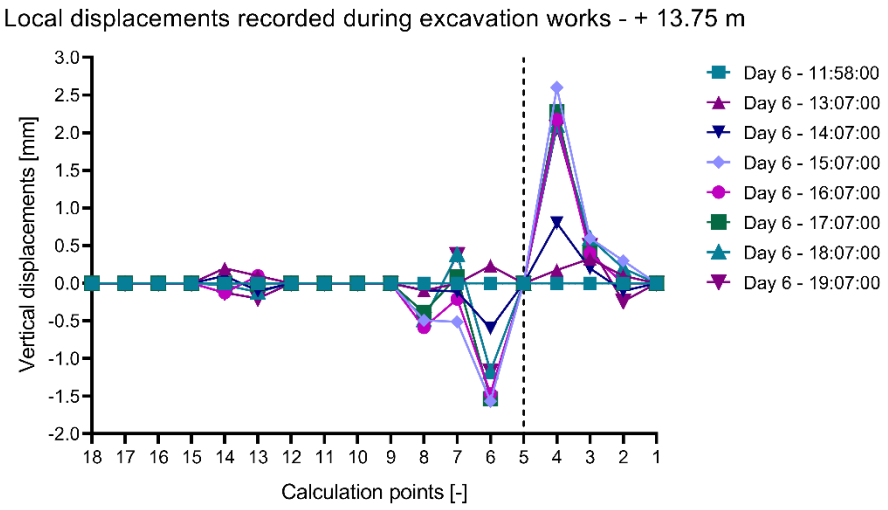

Figure 6.27 Local displacements occurred during the tunnel face advance of 13.75 m. The black dotted line indicates the tunnel face position referred to the Pre-Conv Array calculation Points

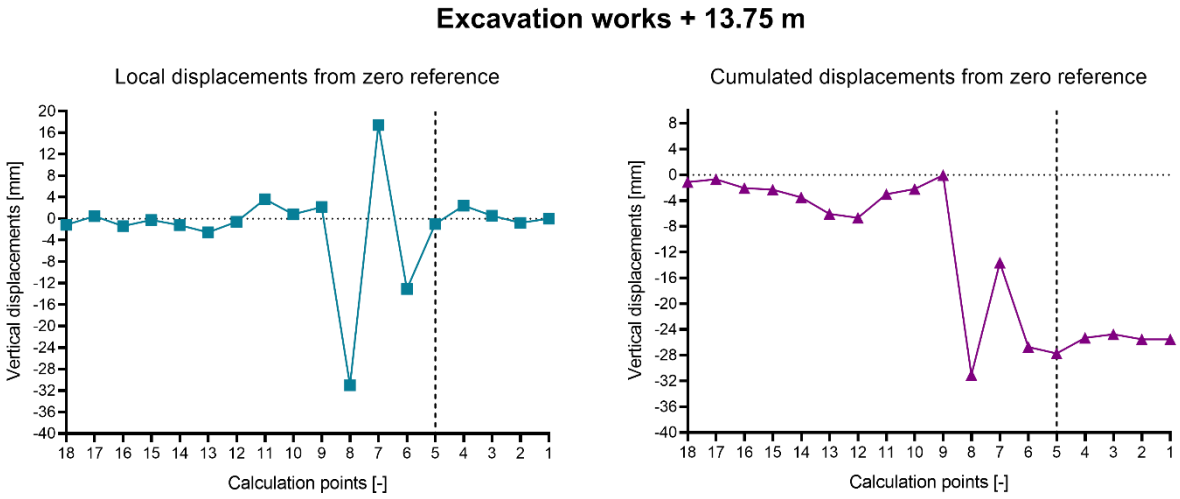

Figure 6.28 Left: Vertical local displacements evaluated from zero reference. Right: cumulated displacements evaluated from the referring date. The black dotted line indicates the front position

Local displacement recorded during tunnel advance of +15.00 m indicated an increase of convergence and preconvergence phenomena, reaching a maximum value of -37 mm on C.P. 3. Figure 6.29 indicates a starting preconvergence effect on C.P. 4 that occurred during the start of the excavation. Between C.P. 5 and C.P. 4, a vertical settlement can be highlighted during the excavation stage, causing a counterclockwise tilt of C.P. 4. Finally, another important settlement can be defined between C.P. 3 and C.P. 2 causing a clockwise rotation of Pre-Conv Link 3, therefore indicating two important deformations acting between day 6 and day 7 during the advance works.

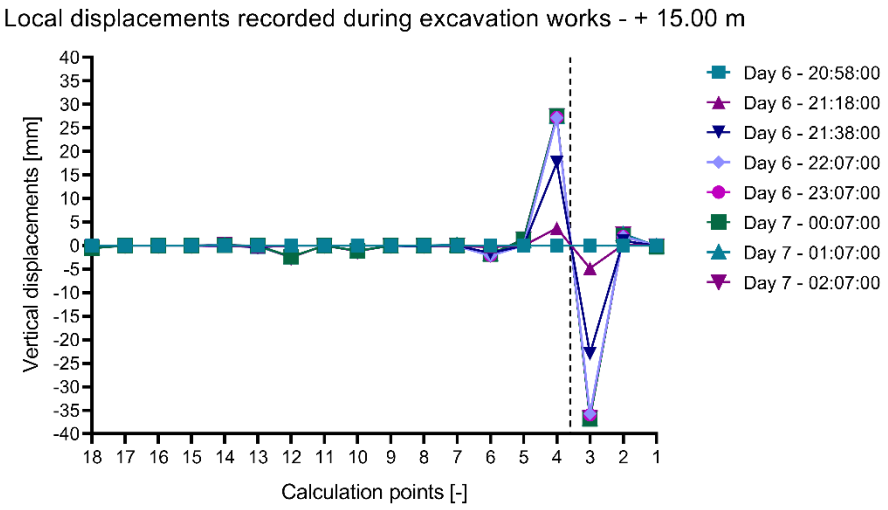

Figure 6.29 Local displacements occurred during the tunnel face advance of 15.00 m. The black dotted line indicates the tunnel face position referred to the Pre-Conv Array calculation Points

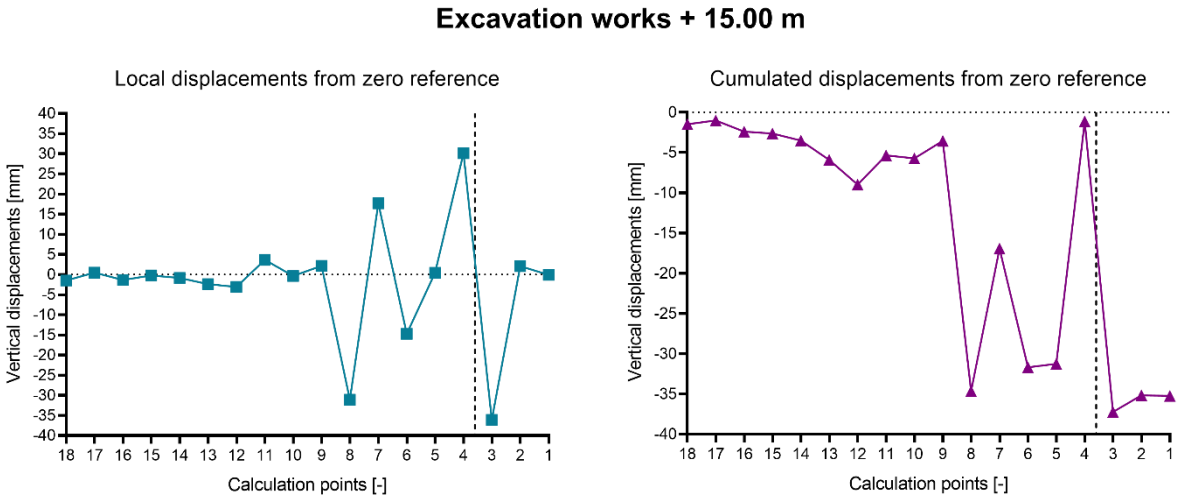

Figure 6.30 Left: Vertical local displacements evaluated from zero reference. Right: cumulated displacements evaluated from the referring date. The black dotted line indicates the front position

After reaching progressive +15.00 m of advance, excavation works were stopped to prepare the next excavation field. Forepoles were installed and cemented from this section for 18 meters length. The forepoles installation generated an increase of preconvergence displacement on C.P. 3 of -6.2 mm. The concrete mortar injection did not affect the deformative state of the surrounding ground, generating an increase of induced vibrations and data oscillation (Figure 6.31).

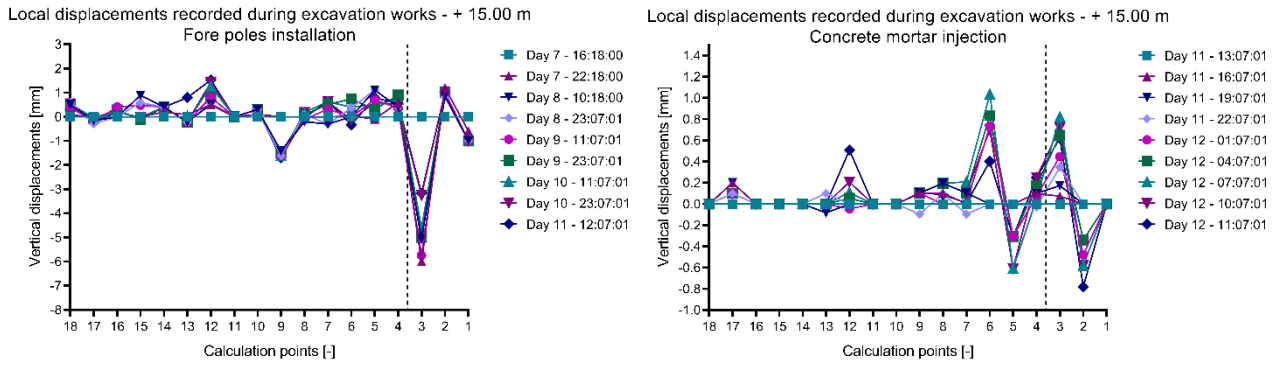

Figure 6.31 Left: Vertical local displacements during fore poles installation. Right: Vertical local displacements during fore poles injection

The penultimate excavation step considered, +16.25 m, indicated a preconvergence deformation of 1.1 mm acting on C.P. 2. Moreover, cumulated displacements reached a maximum value of -35 mm (Figure 6.32 and Figure 6.33).

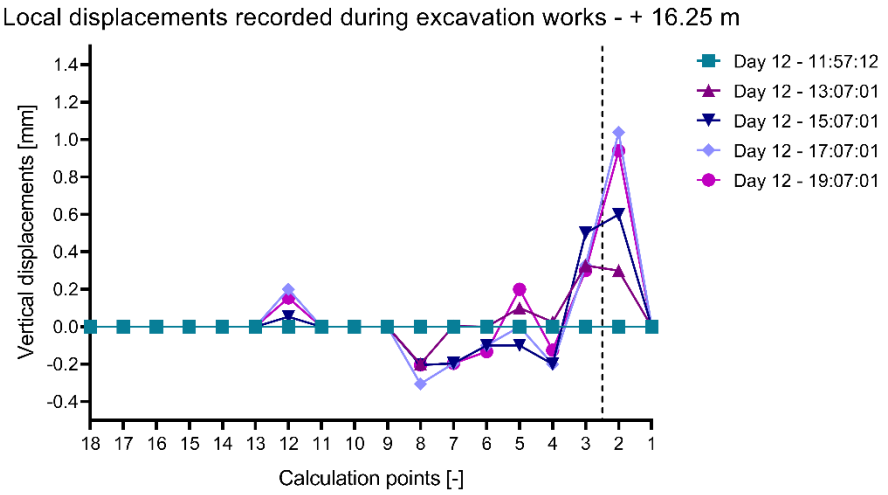

Figure 6.32 Local displacements occurred during the tunnel face advance of 16.25 m. The black dotted line indicates the tunnel face position referred to the Pre-Conv Array calculation Points

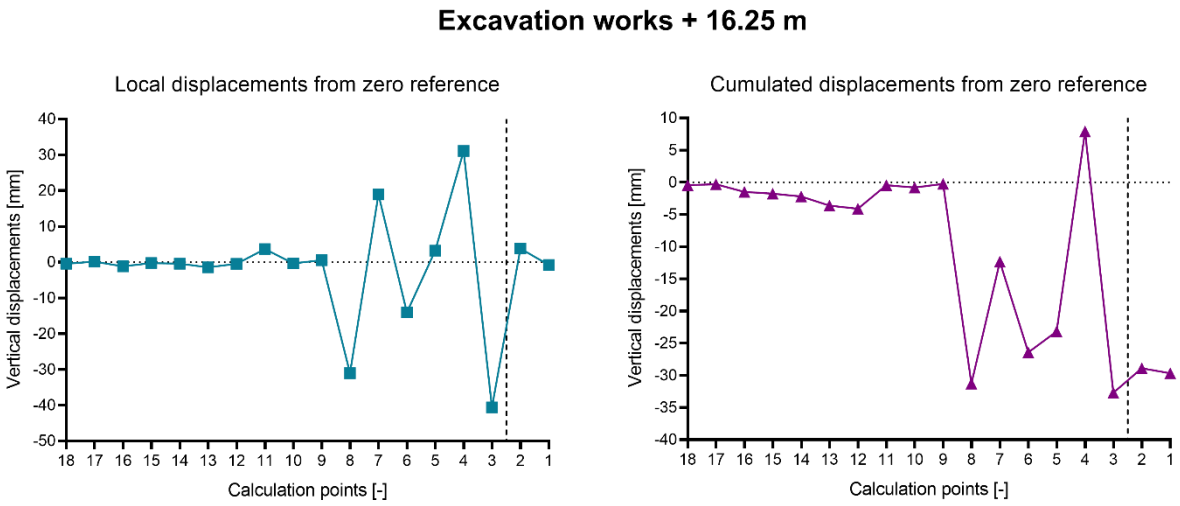

Figure 6.33 Left: Vertical local displacements evaluated from zero reference. Right: cumulated displacements evaluated from the referring date. Black dotted line indicates the front position

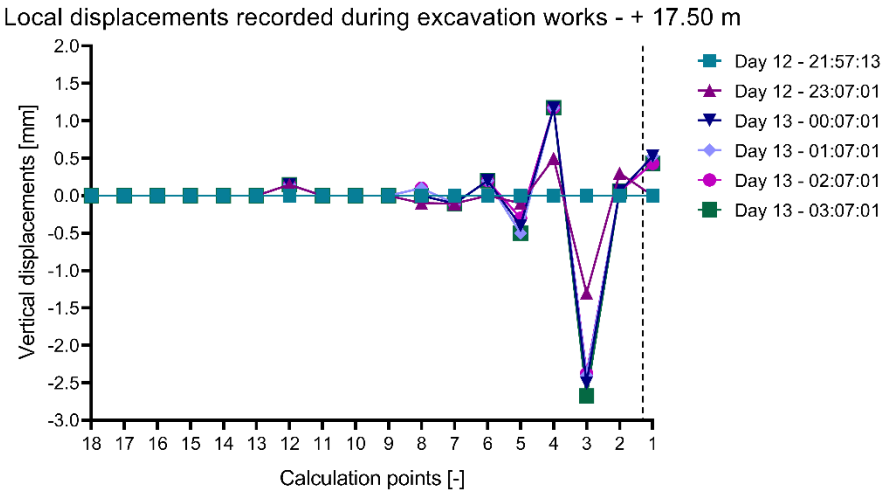

Figure 6.34 Local displacements occurred during the tunnel face advance of 17.50 m. The black dotted line indicates the tunnel face position referred to the Pre-Conv Array calculation Points

The last considered excavation step was at +17.50 m, where the tunnel face was exactly under the C.P. 1, that is the end of the Pre-Conv Array. Recorded displacements showed an increase of convergence settlement on C.P. 3 of -2.7 mm (Figure 6.34). The cumulated displacements from the referring date are shown in Figure 6.35, which indicates a total cumulated displacement of -35 mm. Moreover, a displacement ratio much higher moving from C.P. 9 to C.P. 1 in respect to the previous calculation points is shown. These data indicate changes in the mechanical behaviour and response of the surrounding ground between C.P. 9 to C.P. 1.

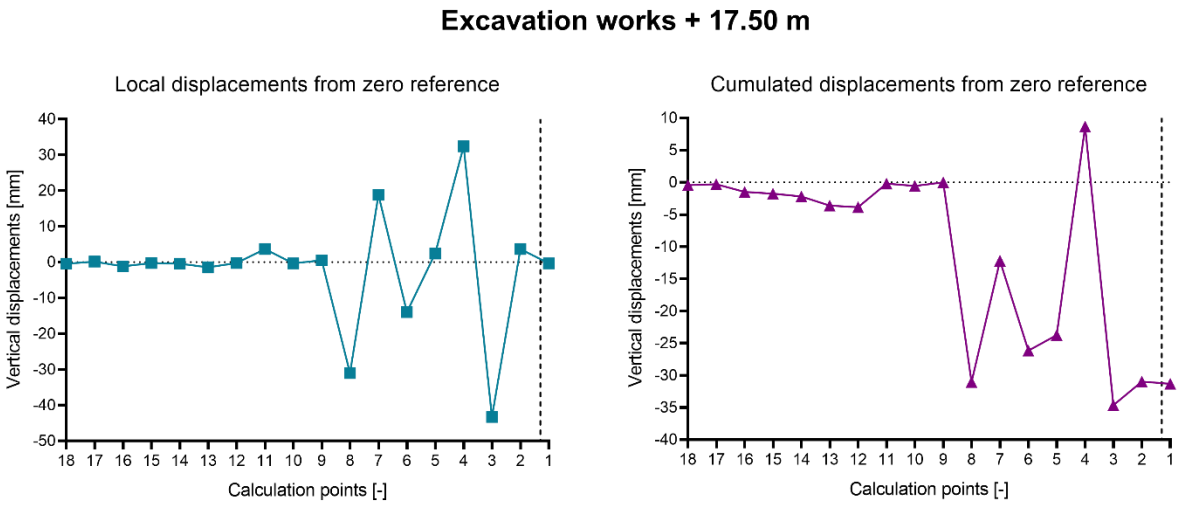

Figure 6.35 Left: Vertical local displacements evaluated from zero reference. Right: cumulated displacements evaluated from the referring date. The black dotted line indicates the front position

6.5. Monitoring data validation

The Pre-Conv Array data can be validated by comparison with topographic surveys or by comparing deformative responses obtained with numerical models. Topographic data can only give information about the tunnel convergence and the numerical model realized by the construction company was not available. Therefore, to verify the preconvergence data highlighted by Pre-Conv Array, a comparison with theoretical curves was carried out, considering the theoretical LDP proposed by Hoek (Carranza-Torres & Fairhurst, 2000) and Panet (Panet, 1995).

Hoek obtained an LDP curve based on monitoring data measured by Chern (Chern et al., 1998) that present convergence data from a tunnel in the Mingtam Power Cavern project (Carranza-Torres & Fairhurst, 2000). The Hoek empirical best-fit relationship between radial displacements of the tunnel and distance to the face is:

$$\frac{u_r}{u_{r,max}} = \left[1 + exp\left(\frac{-x/r}{1.10}\right)^{-1.7}\right] \quad [6.1]$$

Where:

- u_r is the radial displacement at a certain distance from the face;
- $u_{r,max}$ is the maximum radial displacement occurred;
- $-x/r$ is the ratio between the distance of the calculation point to the tunnel face, x, and the equivalent radius of the tunnel, r, considering a perfectly cylindrical shape.

Panet, from elastic models, suggested the following relationship between radial displacement and distance to the face:

$$\frac{u_r}{u_{r,max}} = 0.25 + 0.75 \cdot \left[1 - \left(\frac{0.75}{0.75 + {}^{x}/_{r}}\right)^2\right] \qquad [6.2]$$

Equation [6.2] can be applied only for positive values of x, hence only for convergence deformations. Figure 6.36 shows the presented curves obtained by Equation [6.1] and [6.2]. Theoretical curves indicates that the maximum displacement occurs at approximately 8 tunnel radius behind the tunnel face, and that the radial deformation is zero at approximately 4 tunnels radius ahead the tunnel face (Carranza-Torres & Fairhurst, 2000). In correspondence of the tunnel face, the radial displacement is around 30 ÷ 35 % of the maximum value. This relationship and the presented curves are valid for an unsupported cylindrical excavation.

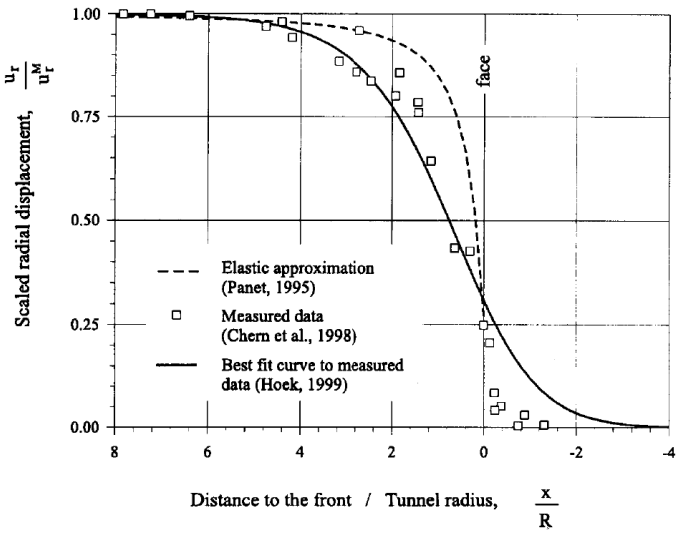

Figure 6.36 Deformation profiles derived from: elastic models (Panet, 1995)*; measurements in a tunnel* (Chern et al., 1998) *and best fit to the measurements from Hoek. Source:* (Carranza-Torres & Fairhurst, 2000)

Before comparing Pre-Conv data with the theoretical curves, some considerations must be done. Monitoring data from Pre-Conv Array can be positive or negative as a function of the displacement location (before or after a calculation point). For this comparison, displacements obtained through the Pre-Conv Array are considered in their absolute value, based on the assumption that every displacement is a vertical settlement independent from the calculation principle applied. Finally, each calculation point was considered fixed, evaluating and cumulating its recorded displacements at a different distance from the tunnel face, depending on the excavation phases. The comparison between instrumental data and theoretical curves are represented in the figures that follow.

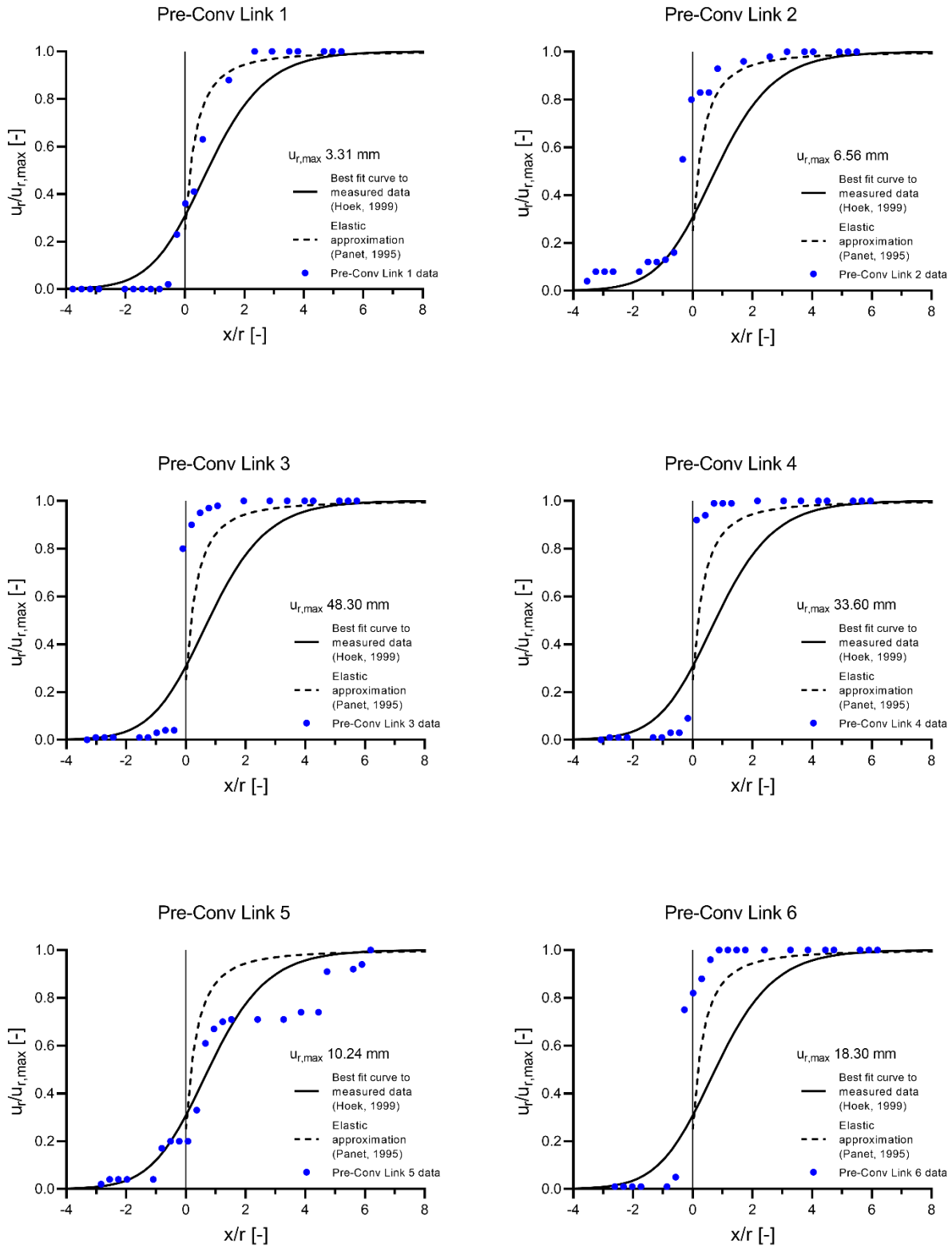

Figure 6.37 Comparison between instrumental data and theoretical curves. Pre-Conv Link from 1 to 6

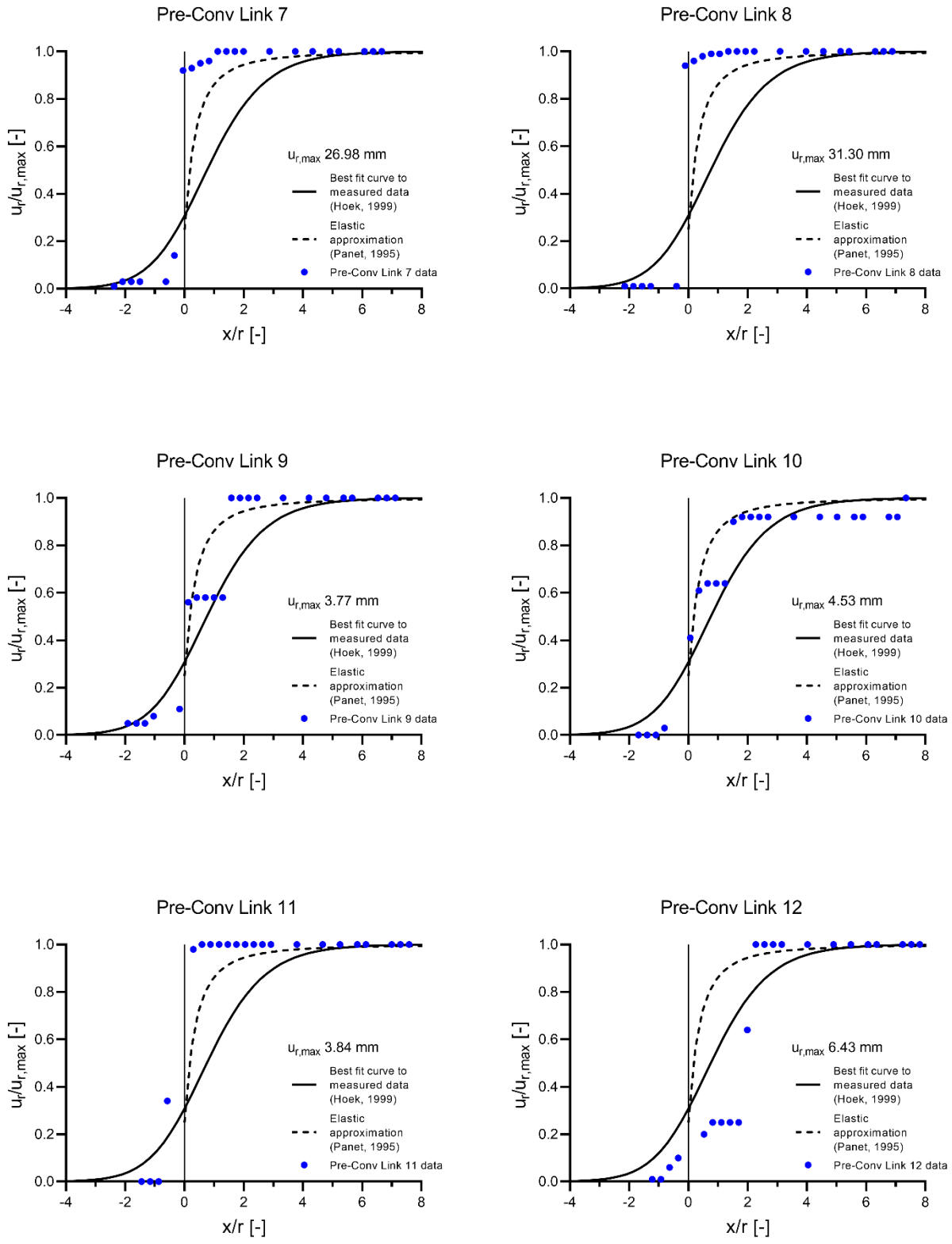

Figure 6.38 Comparison between instrumental data and theoretical curves. Pre-Conv Link from 7 to 12

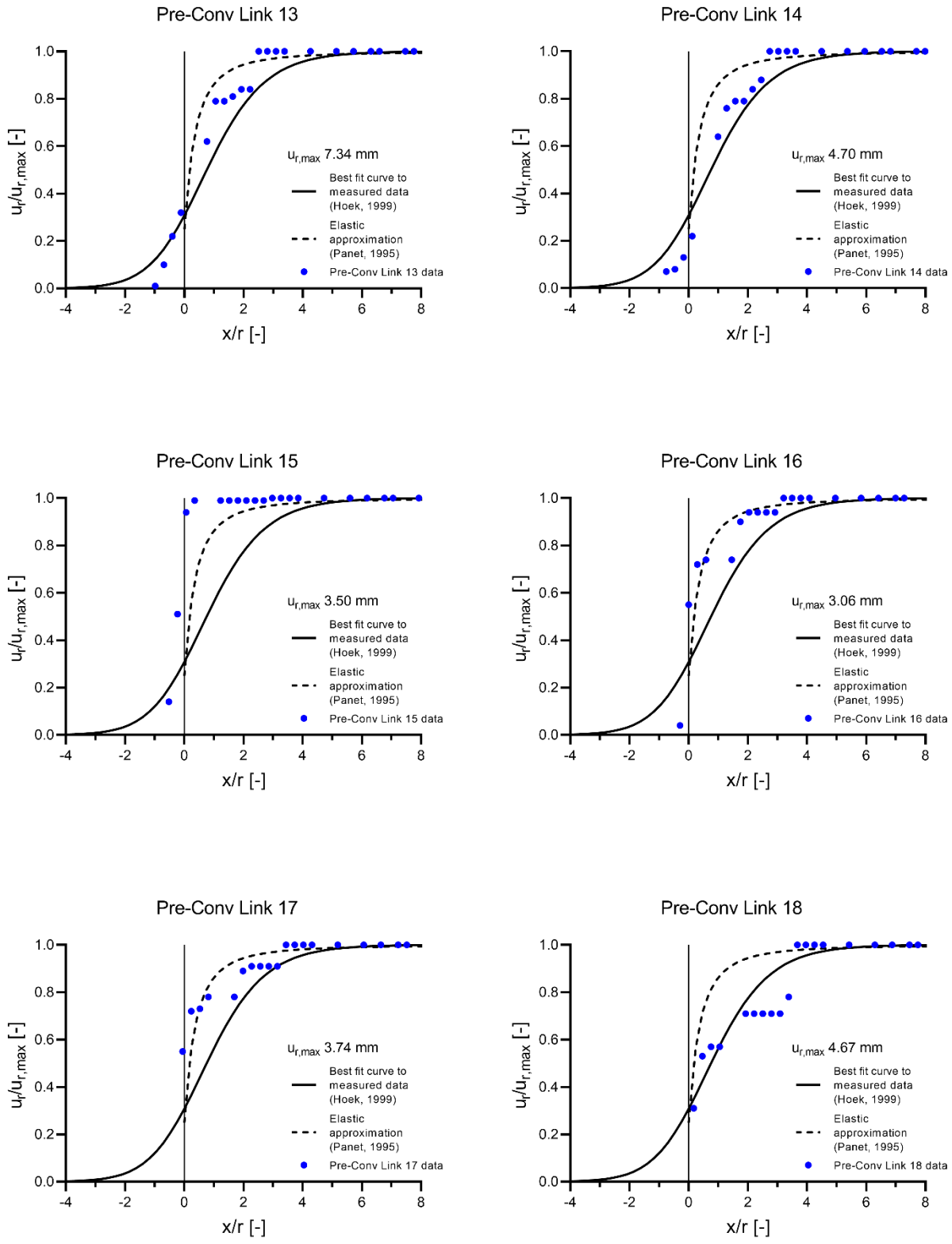

Figure 6.39 Comparison between instrumental data and theoretical curves. Pre-Conv Link from 13 to 18

Figure 6.37, 6.38, and 6.39 show the comparison between the evaluated longitudinal displacement profile for each calculation point, compared with the presented theoretical curves. Generally, curves

are well described through monitoring data. Some calculation points, for example C.P. 3, C.P. 4, C.P. 6, and C.P. 7 show a strong displacement increase in the proximity of the tunnel face, that immediately reach the maximum value on the *y*-axis, without any further displacement.

Hoek and Panet curves are defined for an unlined tunnel, but the presented monitoring data are referred to a supported cavity. However, these representations could be useful to verify the support efficiency: when a supported section reach the maximum value exactly under the tunnel face, the support system is well designed, and no more settlements could be defined.

Finally, every presented calculation point does not present further displacements after the tunnel passage, so the surrounding ground are well-consolidated, as well as the support and preconfinement systems.

A last validation must be analysed, which compares monitoring data obtained through topographic survey and Pre-Conv Array. A topographic monitoring station was installed at progressive +188.00 m, near to calculation point 11 ($x = 7.769\ m, y = 0.697\ m$) between monitoring day 4 and 5. The C.P. 11 is 23 cm far and 70 cm above the monitoring station. Topographic monitoring presents an uncertainty of ± 1.5 mm (declared by the topographic survey company). Figure 6.40 shows the comparison between the Pre-Conv Link 11 and the topographic survey. Pre-Conv Link 11 data were elaborated taking the same zero reference of the geodetic survey.

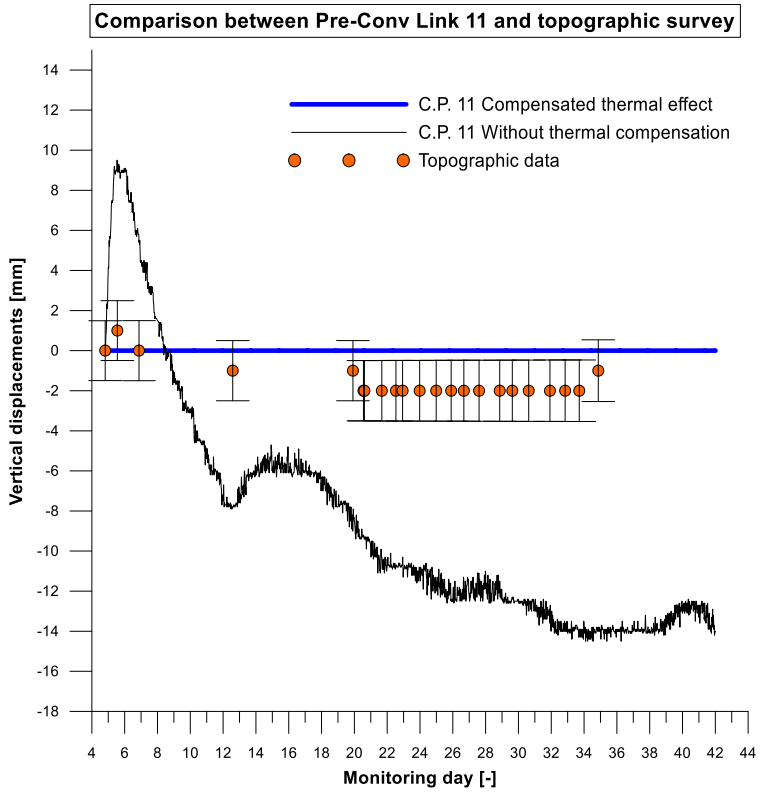

Figure 6.40 Comparison between Pre-Conv Link 11 and topographic survey

Figure 6.40 shows both the C.P. 11 local displacements, thermal compensated and not. Topographic data are reported considering the provided uncertainty. Pre-Conv Link 11 is probably the sensor most affected by thermal effects: without thermal compensation, it provided high displacement contribution, approximately 26 mm in total. Instead, applying the thermal compensation, the displacements evaluated are null, indicating a high thermal influence. Topographic data indicated a final vertical displacement of -1 mm. As previous explained, delta slope value applied in the thermal filter were calibrated by a back-analysis procedure that considered the topographic readings. Compensated data are finally comparable to the monitoring data obtained by the geodetic survey.

6.6. Conclusion

The Pre-Conv Array has been installed to monitor the preconvergence displacements occurred during the excavation phases. After a preliminary data elaboration to compensate the thermal influence, the data were analysed as a function of the working stages, verifying whether the Pre-Conv Link detected preconvergence and convergence displacements. Finally, data were compared with the geodetic survey.

Unfortunately, the numerical model realized during the tunnel design was not available, but some observation and further analysis can be underlined.

Pre-Conv Array has been developed with the purpose to help the project designer in defining the best advance ratio and method, and the most efficient support system to apply during the drilling phase. A continuous exchange of observations on data elaboration between the project designer and the monitoring responsible should be the key aspect to consider during the tunnel construction. Indeed, knowing the numerical model and its preliminary hypothesis, can help in defining the GRC of the surrounding rock mass or ground. Furthermore, monitoring data permits to define the LDP, that coupled with GRC, permits to evaluate the displacement that occurred on a determined section until the tunnel face passage. Finally, the support system can be precisely defined and projected with the suitable safety factor to consider (Carranza-Torres & Fairhurst, 2000).

The next figures show an example of the starting point to project the most efficient support system. First, a GRC was reconstructed using the defined ground geotechnical parameter (Table 6.1), and applying the Ribacchi & Riccioni method (Ribacchi & Riccioni, 1977). Then, through Pre-Conv Array, LDP is finally evaluated and plotted with GRC.

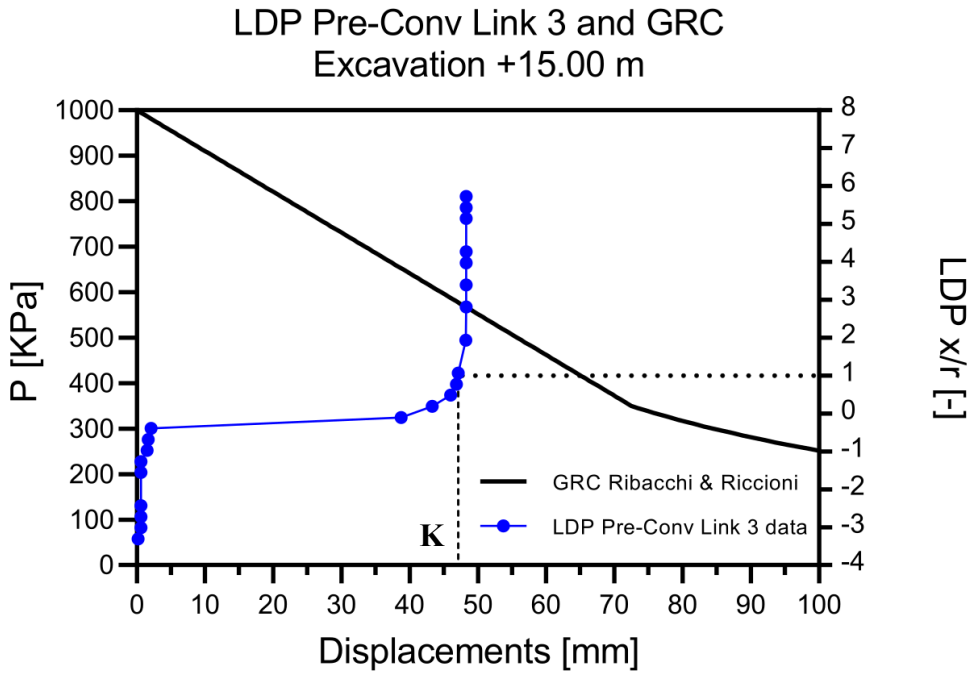

Figure 6.41 Example of GRC and evaluated LDP during the excavation advance of +15.00 m

Figure 6.41 shows the defined LDP and GRC. Once defined the distance of the support installation from the tunnel face, equal to 1 meter in the example reported in Figure 6.41, the pre-deformations acted on the section can be exactly evaluated thanks to Pre-Conv Array monitoring data (point K). Finally, the support can be projected by inserting its SCC into the previous graph, as in Figure 6.42.

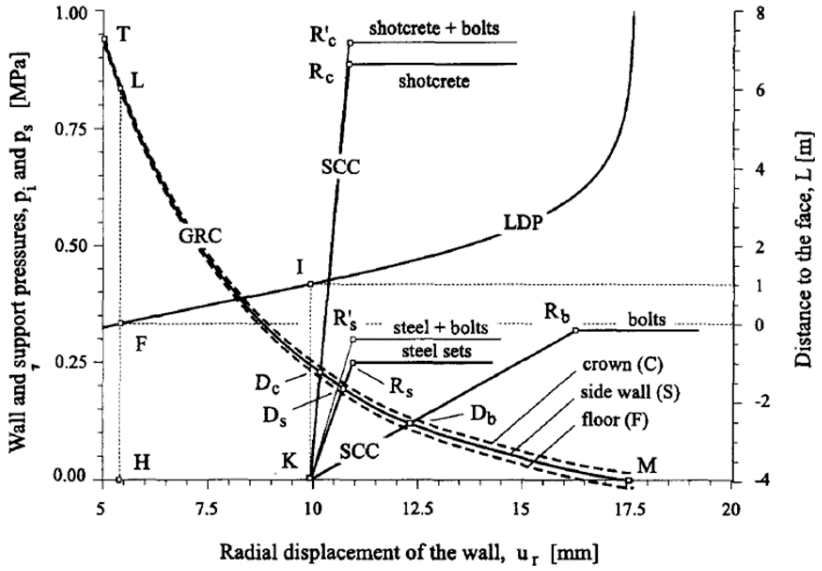

Figure 6.42 GRC, LDP and SCC

In conclusion, all together, the presented graphs can help the project designer to find the best solution and compromise in terms of support system, installation distance from the tunnel face, construction site safety, and money and time saving.

7. Case Study 2 – Tunnel SS30 in the Principality of Monaco

7.1. Introduction: geological and geotechnical framework

The second Pre-Conv Array has been installed in the Principality of Monaco, during the realization of a pedestrian shallow tunnel, called Tunnel SS30. Tunnel SS30 has been realized to connect an underground parking to the city centre, near the hospital. Tunnel will also connect a housing complex realized in the summit area of Monaco, near to the border with France in correspondence of the "Entrée de Ville Ouest Supérieure (EVOS)", towards Nizza (Figure 7.1).

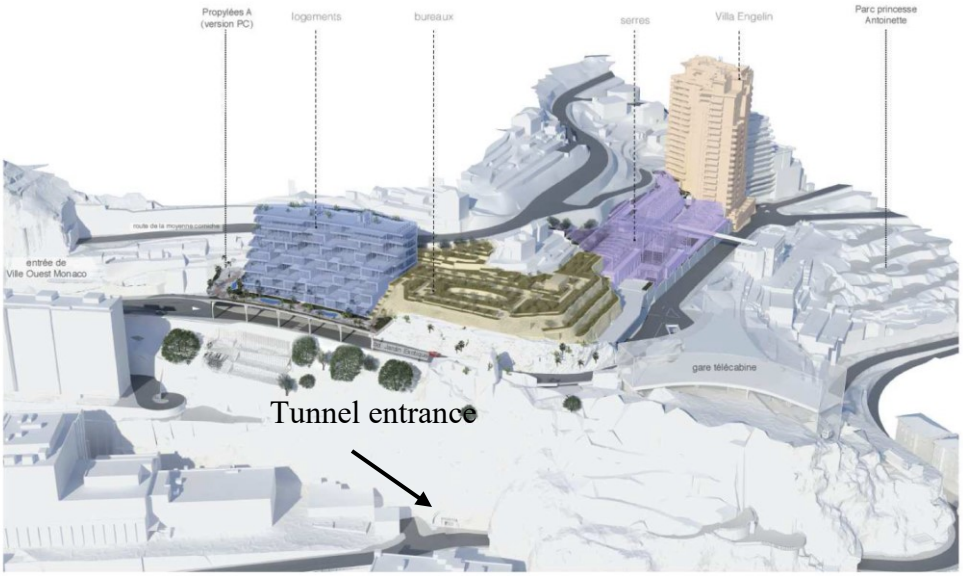

Figure 7.1 EVOS project

Figure 7.2 Tunnel SS30 floor plan

Pre-Conv Array has been installed at the tunnel entrance (Figure 7.2) for a monitored length of 15 m, with a medium overburden of approximately 7 meters. An extensive geological and geotechnical investigation was conducted to define the ground lithostratigraphy and the mechanical and deformative parameters of the involved ground (Figure 7.3).

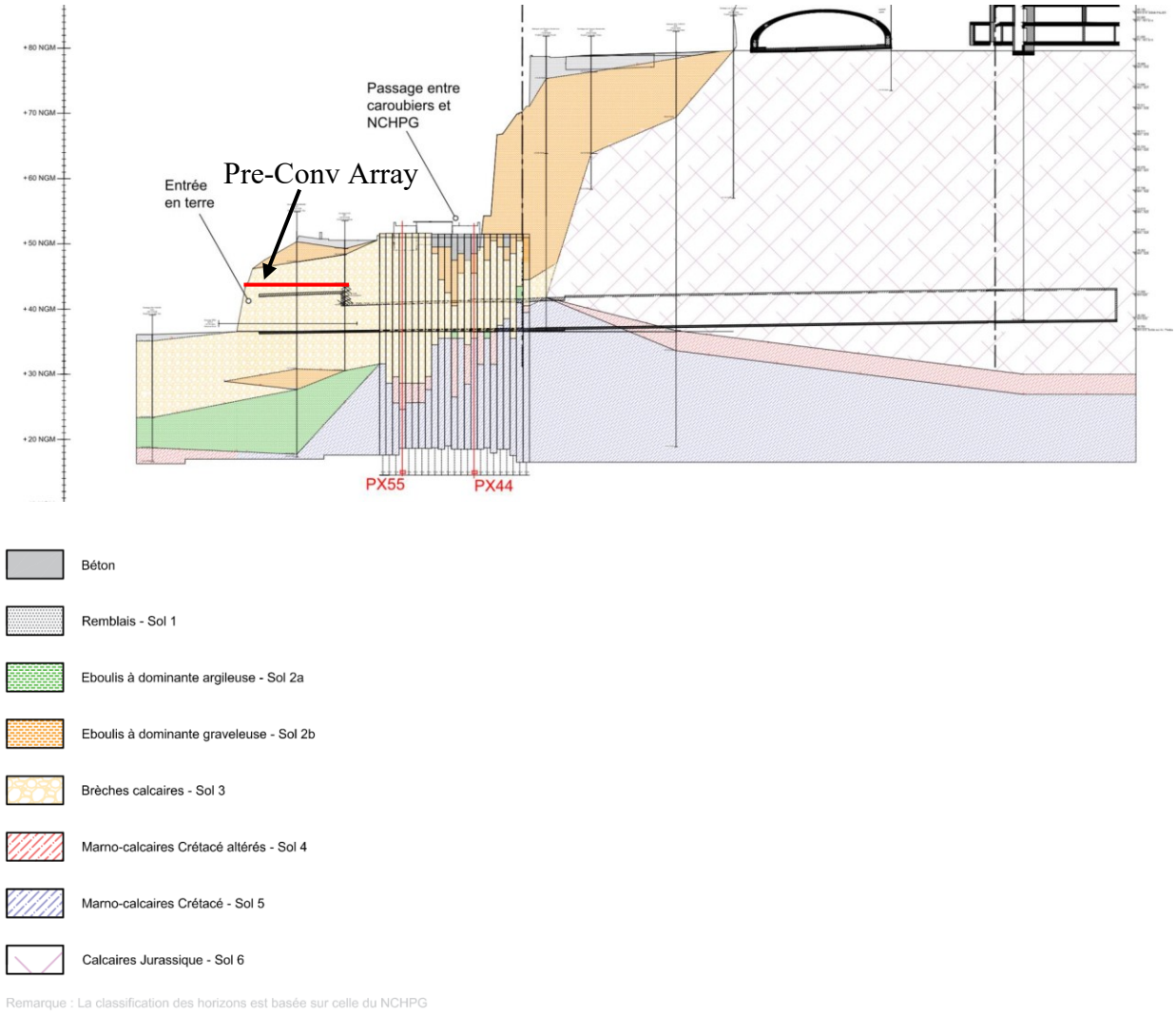

Figure 7.3 Geomechanical section of the tunnel SS30

The involved material consists of calcareous breccias with the following geotechnical parameters (Table 7.1).

Table 7.1 Geotechnical parameters of the involved ground

Calcareous breccia				
Volume weight γ [kN/m³]	**Friction angle φ [°]**	**Cohesion c [kPa]**	**Elastic modulus E [MPa]**	**Poisson coefficient υ [-]**
21	35	20	695	0.3

7.2. Tunnel excavation and evaluation of expected displacements

Tunnel SS30 has been full-face excavated by a drilling jumbo with an advance ratio of approximately 1 m/week. The advance velocity must be limited to reduce noise and vibrations on the nearby buildings. The upper area of the shallow tunnel was reinforced by a series of micropiles arranged as quincunx. The Pre-Conv Array was installed in the top centre of the tunnel entrance inside a dedicated PVC casing, 40 cm above the tunnel crown (Figure 7.4).

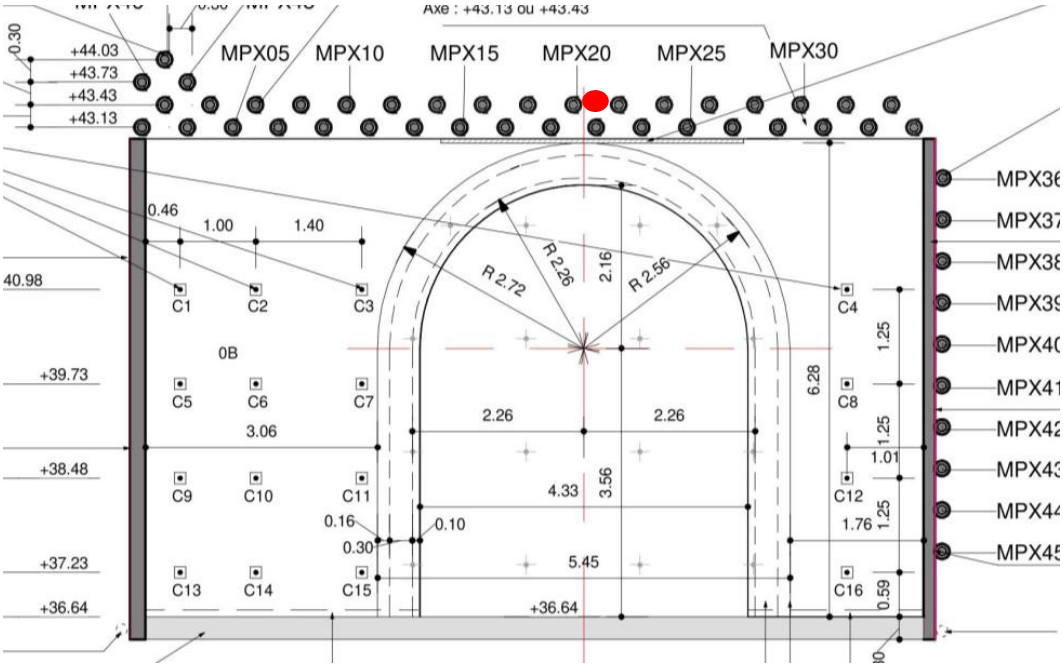

Figure 7.4 Tunnel entrance section and Pre-Conv array position (red dot)

At each excavation step, confinement supports consisting in steel ribs HEB100, were installed. Moreover, a preconfinement system on the tunnel face was applied by a thick layer of shotcrete and by fiberglass reinforcement.

The construction company realized a numerical model of the tunnel entrance to verify the displacements on the surface. The maximum allowed surface displacement is equal to 7.00 mm. The numerical model was realized through Plaxis® code, in which the vertical settlement on surface was defined as -2.194 mm by applying a deconfinement value of 0.7 (Figure 7.5).

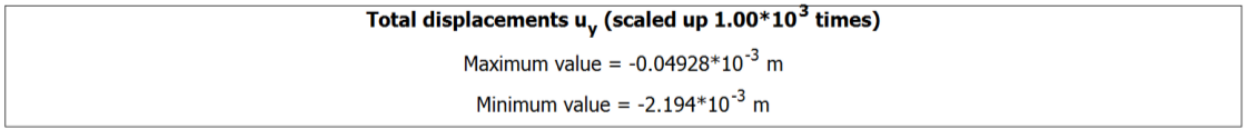

Figure 7.5 Vertical settlement defined in the numerical model

Furthermore, an extensive geodetic monitoring was conducted both on the tunnel entrance and on the excavated ground. In particular, a topographic marker has been installed near to the Pre-Conv Array anchor, I14 (Figure 7.6), and also other 4 monitored section has been installed at different excavation progressive, +0.4 m, +4.4 m, +9.40 m, and +14.40 m. The monitored section consists of 5 topographic targets to create the typical convergence star. Two different thresholds were defined for the geodetic monitoring: an alert value of ±2.00 mm and an intervention value of ±4.00 mm.

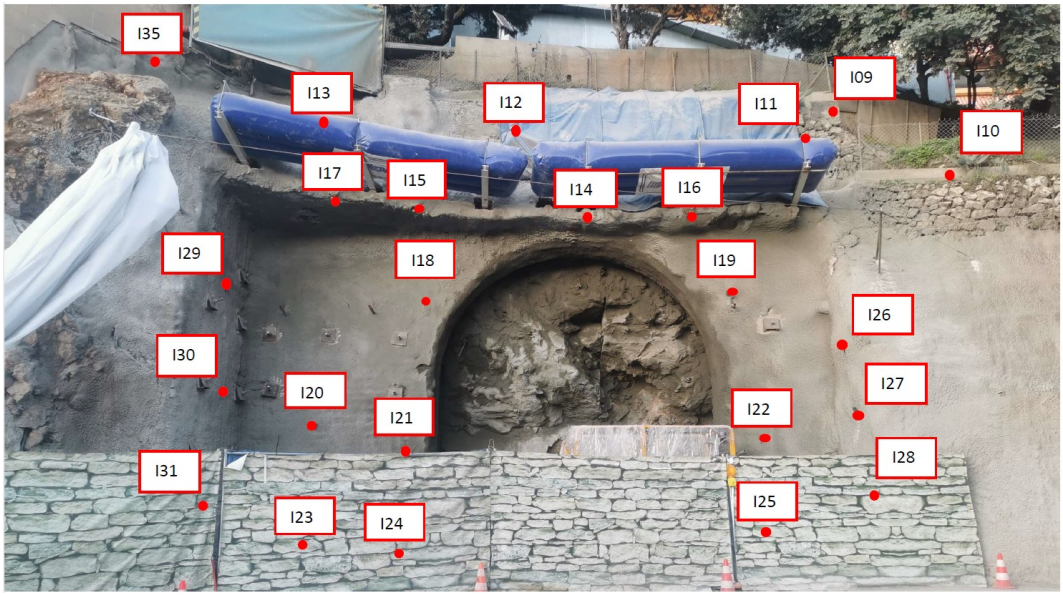

Figure 7.6 Geodetic survey on the tunnel entrance

7.3. Pre-Conv Array installation and excavation works

The Pre-Conv Array was installed at the top centre of the tunnel SS30, inside a PVC casing, for a monitored length of 15 m. Figure 7.8 schematize the Pre-Conv Links position and the referred *x* and *y* starting position are defined in Table 7.2.

Figure 7.7 Pre-Conv Array installation procedure

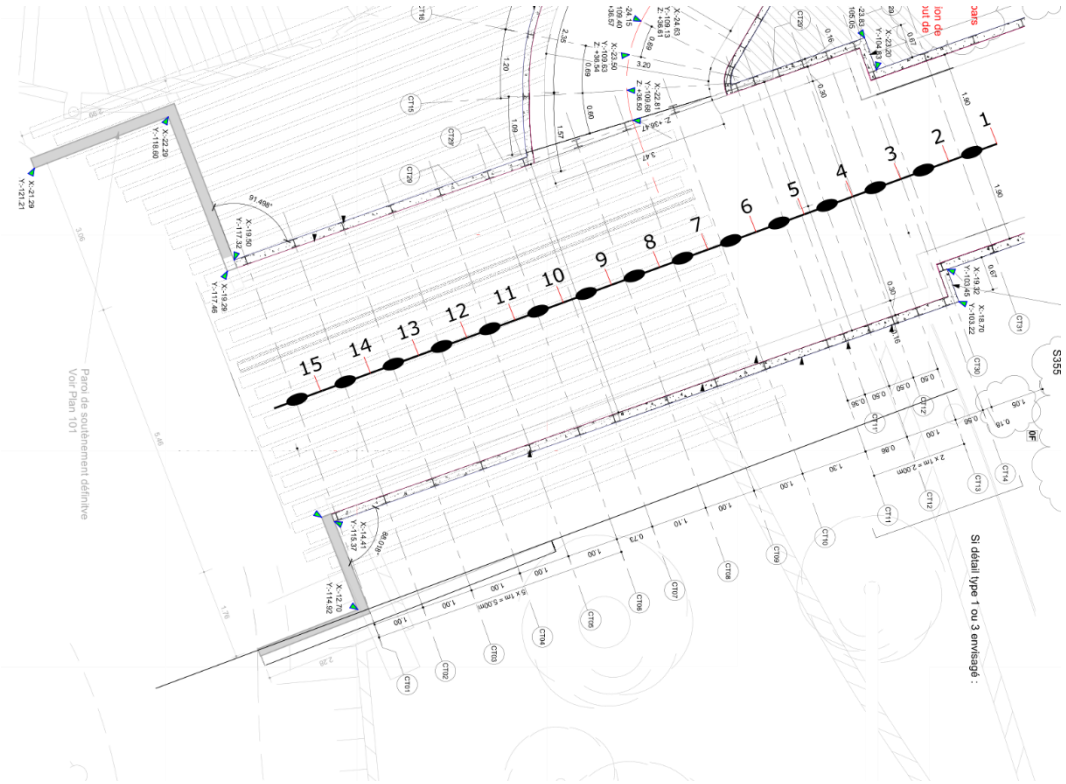

Figure 7.8 Pre-Conv Links position on the monitored section

Absolute coordinates were defined considering the PVC ledge of 50 cm in correspondence of the tunnel face, where the anchor has absolute coordinates *x* and *y* equal to 0 m.

Table 7.2 Calculation points absolute coordinates x and y

Calculation Point	x [m]	y [m]	Calculation Point	x [m]	y [m]
1	15.00	0.00	**9**	7.00	0.00
2	14.00	0.00	**10**	6.00	0.00
3	13.00	0.00	**11**	5.00	0.00
4	12.00	0.00	**12**	4.00	0.00
5	11.00	0.00	**13**	3.00	0.00
6	10.00	0.00	**14**	2.00	0.00
7	9.00	0.00	**15**	1.00	0.00
8	8.00	0.00			

As previously described, the excavation works proceeded with an advance ratio of 1 m/week, reducing the induced vibrations and noise on the nearby buildings. The excavation works are schematized in Table 7.3, considering the time period from the start of the drilling and the start of the next excavation advance. The excavation advance is referred to the tunnel reference system, hence it is necessary to consider that the Pre-Conv Array anchor is installed with a ledge of 50 cm.

Table 7.3 Excavation advance as declared by the construction company

Excavation advance [m]	Starting day [-]	Starting time [hh:mm]	Finishing day [-]	Finishing time [hh:mm]
0.35	25/11/19	08:00	10/12/19	07:00
1.35	10/12/19	08:00	16/12/19	07:00
2.35	16/12/19	08:00	06/01/20	07:00
3.35	06/01/20	08:00	13/01/20	07:00
5.35	13/01/20	08:00	20/01/20	07:00
7.35	20/01/20	08:00	03/02/20	07:00
9.35	03/02/20	08:00	10/02/20	07:00
11.35	10/02/20	08:00	18/02/20	07:00
13.35	18/02/20	08:00	02/03/20	07:00
14.35	04/03/20	08:00	09/03/20	07:00

7.4. Monitoring results

The Pre-Conv Array has been installed in October 2019, during the installation of the micropiles above the tunnel entrance. On the 25th of November the I14 topographic target was installed before the start of the excavation works, that were planned for the same day. The zero reference for the evaluation of the vertical displacements was taken according to the topographic mark installation, approximately one month after the real installation procedure. Unfortunately, monitoring data from 27/11/19 to 04/12/19 were lost. The SIM for data transmission was installed only on 04/12/19 causing an increase in data storage, that compromised the transmission operations.

This delayed zero reference allowed to completely delete the thermal influence of the concrete mortar maturation. However, a thermal compensation was applied anyway, in order to completely delete all the thermal influence, that can affect measurements during the day and night temperature cycles, as evinced by the laboratory tests previously described (see section 5.2).

To reduce the defined thermal influence, firstly, a and b parameters were obtained considering a limited dataset. The dataset was taken between March and April 2020, when the construction site was closed because of the COVID-19 global pandemic. We chose this period of time because the sensors were almost stable (Figure 7.9).

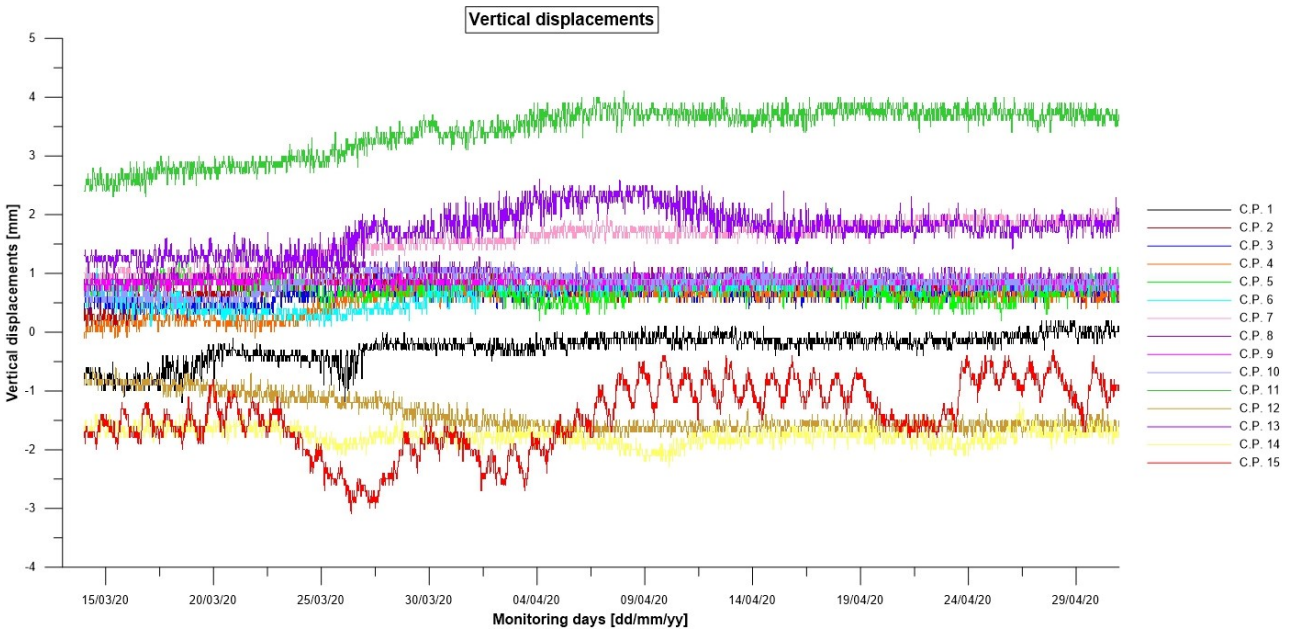

Figure 7.9 Range used for evaluating a and b parameters for the second pilot site installation

The data presented in Figure 7.9 show limited displacements for the considered period except for the C.P. 15, which is the most external sensor, hence the one most subjected to thermal influence. Indeed, monitoring data from C.P. 15 clearly show a continuous data oscillation, coincident with day and

night temperature variations. By applying the linear regression presented in section 5.3, a and b parameters were defined (Table 7.4).

Table 7.4 a and b parameters obtained for the second pilot site installation

Calculation Point	a	b	Calculation Point	a	b
1	-0.18	3.10	**9**	-0.002	0.89
2	-0.10	2.57	**10**	-0.16	3.59
3	-0.08	2.02	**11**	-0.48	11.66
4	-0.24	4.71	**12**	0.37	-7.55
5	0.07	-0.48	**13**	-0.49	9.60
6	-0.14	3.18	**14**	0.05	-2.58
7	-0.01	1.14	**15**	0.32	-6.36
8	-0.28	6.64			

Then, we carried out the calibration of the threshold to consider. The calibration procedure considers the excavation phases in correspondence of each calculation point and the thermal filter response: in fact, as previously stated, higher threshold involves a stronger thermal influence detection, instead a smaller threshold could not detect the thermal contribution.

Figure 7.10 shows the evaluated displacements for the C.P. 14 applying several delta slopes. The black line indicates the evaluated vertical displacements without thermal compensation, while the red line indicates the temperature recorded. The evaluated displacements suffer a slight thermal influence due to the lower deformative state observed in this construction site. Thermal compensation considering delta slope lower than 0.05 can delete the temperature contribution. Higher delta slope, such as 0.07, cannot detect the displacements induced by the excavation work from 11/12/19 to 24/12/19, when the tunnel face was exactly under the C.P. 14. Instead, lower delta slope causes an increment of data noise and oscillation without difference in terms of evaluated displacements. The same results can be appreciated in Figure 7.11, in which the C.P. 5 displacements are shown. A delta slope equal to 0.07, cannot recognize the deformative state of the C.P. 5. Indeed, between 30/01/20 and 14/02/20 the tunnel face was approximately one meter far from the considered point but no displacements were detected. Finally, lower delta slope can recognize the displacement occurred during each excavation step.

In conclusion, as in the previous case study, a delta slope of 0.05 was applied as threshold for the thermal data compensation.

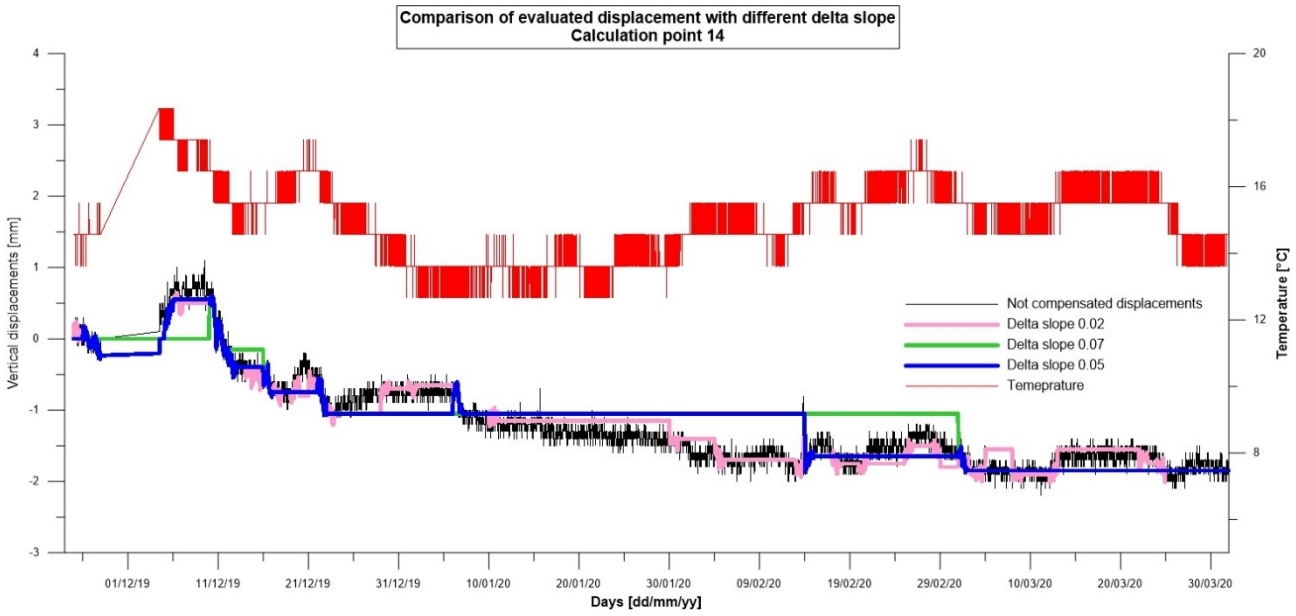

Figure 7.10 Evaluated local displacement for calculation point n°14 with different delta slope

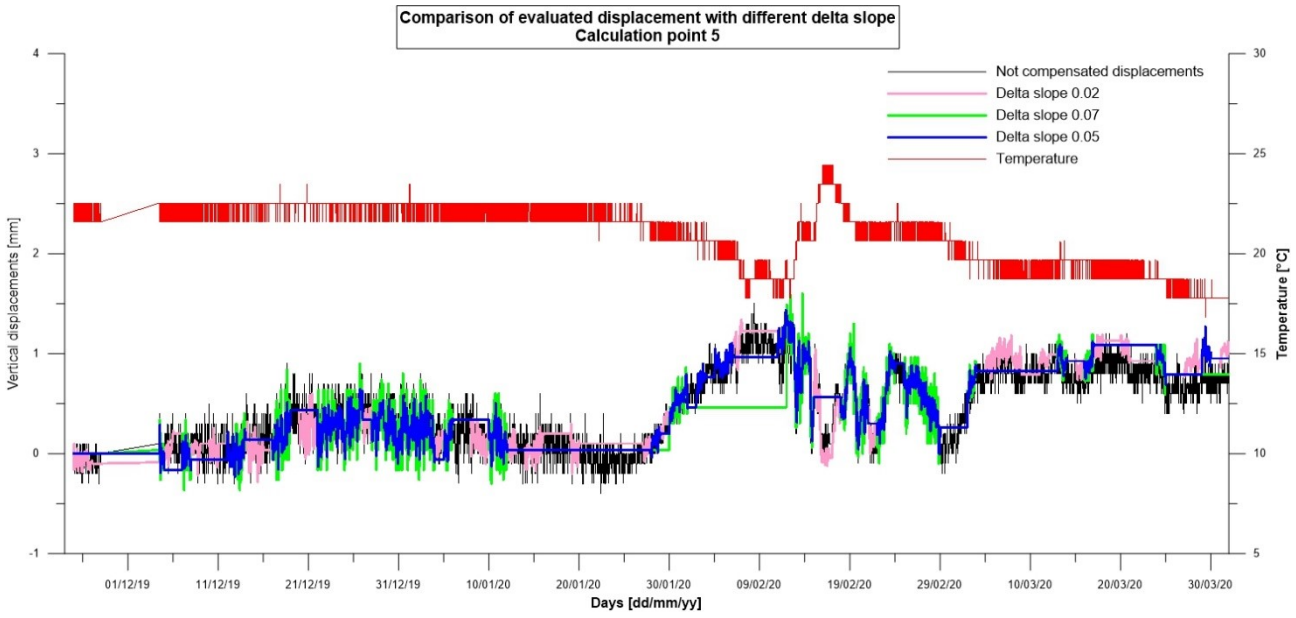

Figure 7.11 Evaluated local displacement for calculation point n°5 with different delta slope

After the delta slope calibration, monitoring data were elaborated starting from the zero reference and analysed as a function of the excavation phases (Table 7.3).

The graphs that follow show the local displacement calculated for each excavation advance, in which data are initialized at the start of the considered drilling step, to verify the influence of the working stage. Finally, the total local and cumulated displacements referred to the zero reference are shown for every drilling advance.

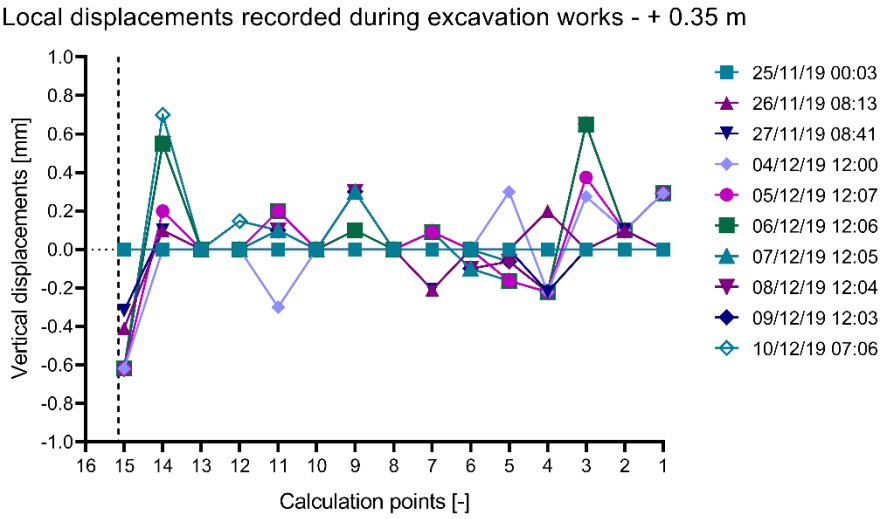

Figure 7.12 Local displacements occurred during the tunnel face advance of 0.35 m. The black dotted line indicates the tunnel face position referred to the Pre-Conv Array calculation Points

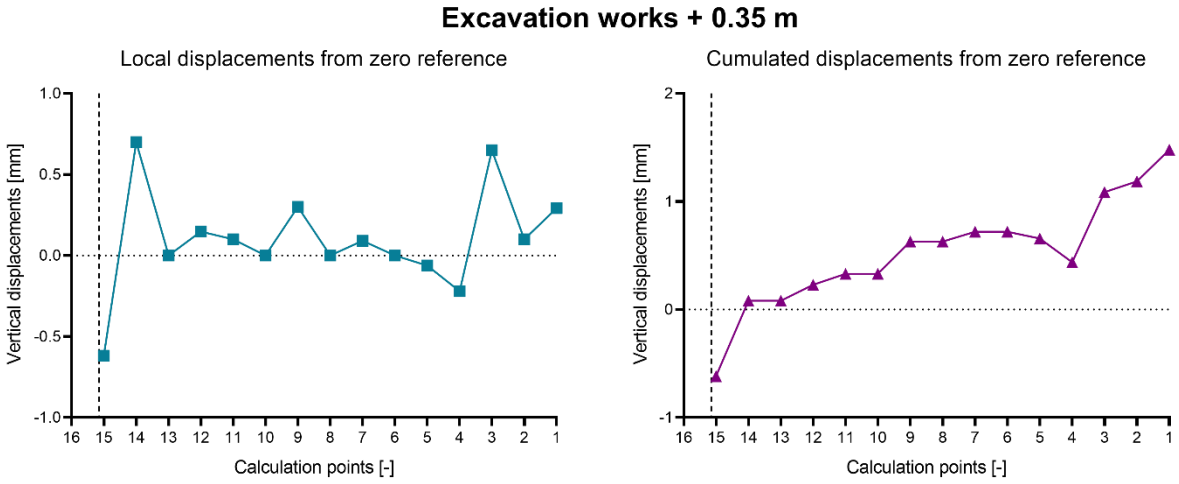

Figure 7.13 Left: Vertical local displacements evaluated from zero reference. Right: cumulated displacements evaluated from the referring date. The black dotted line indicates the front position

Figure 7.12 and Figure 7.13 indicate the C.P. 16. This calculation point coincides with the anchor, and it was inserted to represent the excavation face position referred to the Pre-Conv Array reference system.

Figure 7.12 shows the local vertical displacements that occurred during the first excavation advance of + 0.35 m. The calculation points mostly affected by tunnel drilling were C.P. 15 and C.P. 14. C.P.15 indicates a preconvergence deformation of -0.6 mm, instead C.P. 14 shows an opposite preconvergence deformation of 0.7 mm.

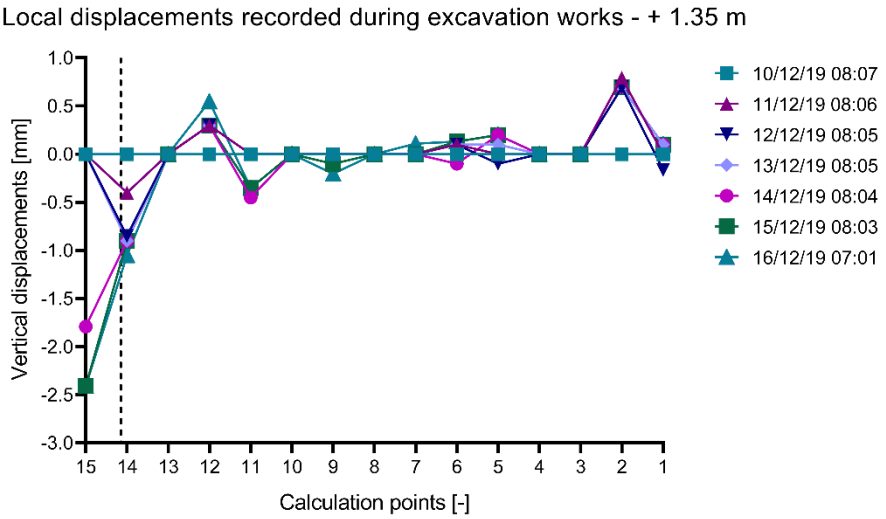

Figure 7.14 Local displacements occurred during the tunnel face advance of 1.35 m. The black dotted line indicates the tunnel face position referred to the Pre-Conv Array calculation Points

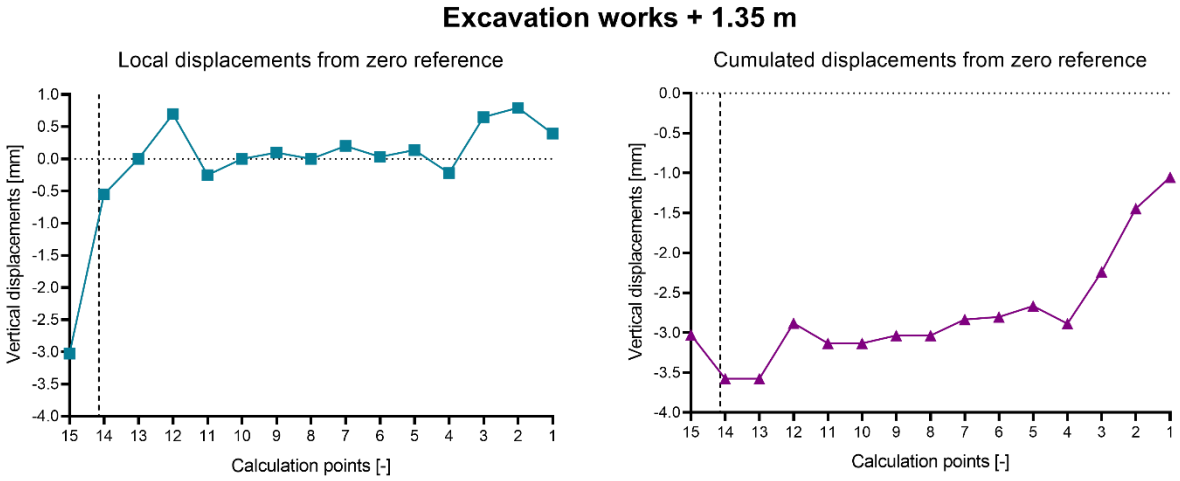

Figure 7.15 Left: Vertical local displacements evaluated from zero reference. Right: cumulated displacements evaluated from the referring date. The black dotted line indicates the front position

The second advance step of + 1.35 m caused an increase of the convergence deformations on the C.P. 15 and C.P. 14. The C.P. 15 reached a convergence deformation of -3.0 mm, instead C.P. 14 defined a convergence displacement of -1.0 mm. Figure 7.14 shows that the preconvergence deformations on the C.P. 12 increased over time, reaching a total local displacement of 0.6 mm.

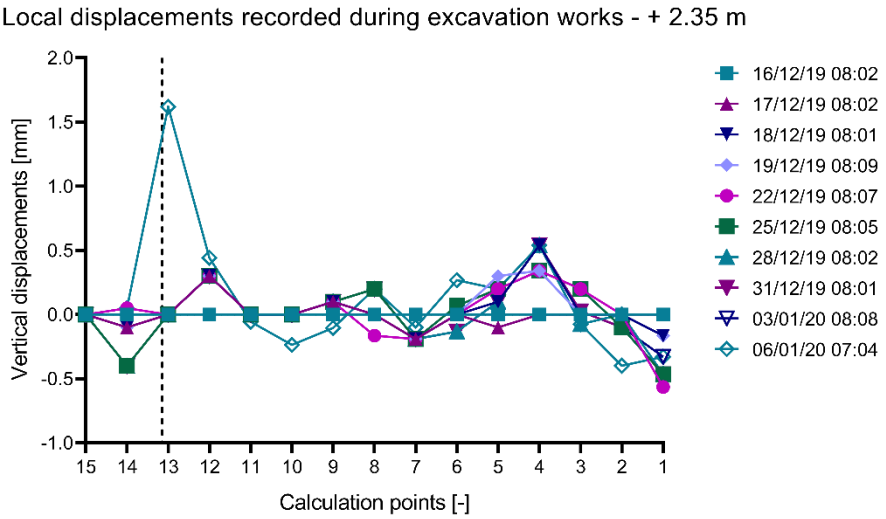

Figure 7.16 Local displacements occurred during the tunnel face advance of 2.35 m. The black dotted line indicates the tunnel face position referred to the Pre-Conv Array calculation Points

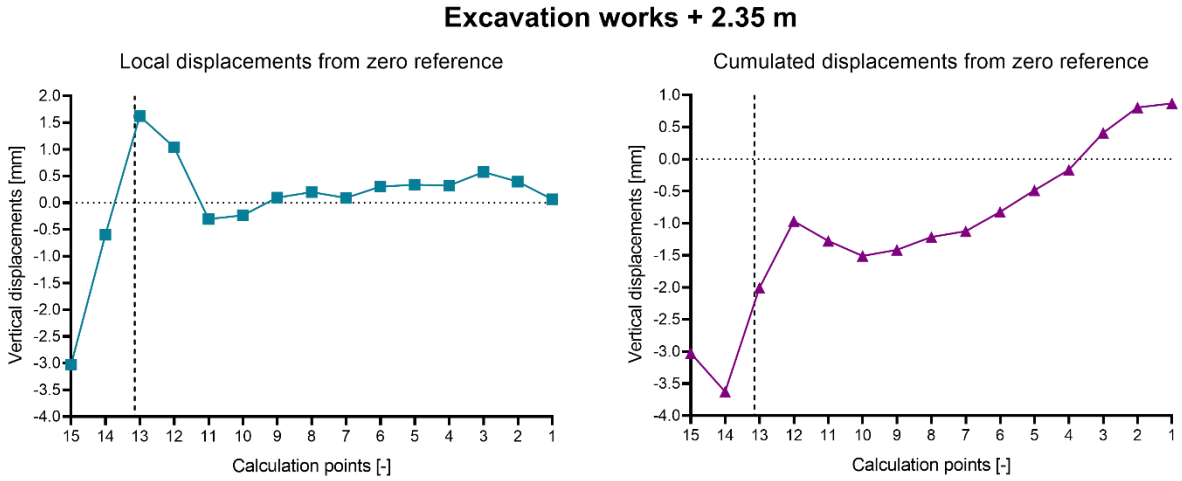

Figure 7.17 Left: Vertical local displacements evaluated from zero reference. Right: cumulated displacements evaluated from the referring date. The black dotted line indicates the front position

Figure 7.16 shows the local displacement that occurred during the excavation advance of +2.35 m. C.P. 13 showed an increase of preconvergence displacements between 03/01/20 and 06/01/20 of 1.6 mm. Cumulated displacements show exactly the preconvergence theoretical trend: a slight vertical deformation ahead of the tunnel face followed by a steep increase of the convergence deformation behind the tunnel front (Tonon, 2010) (Figure 7.17).

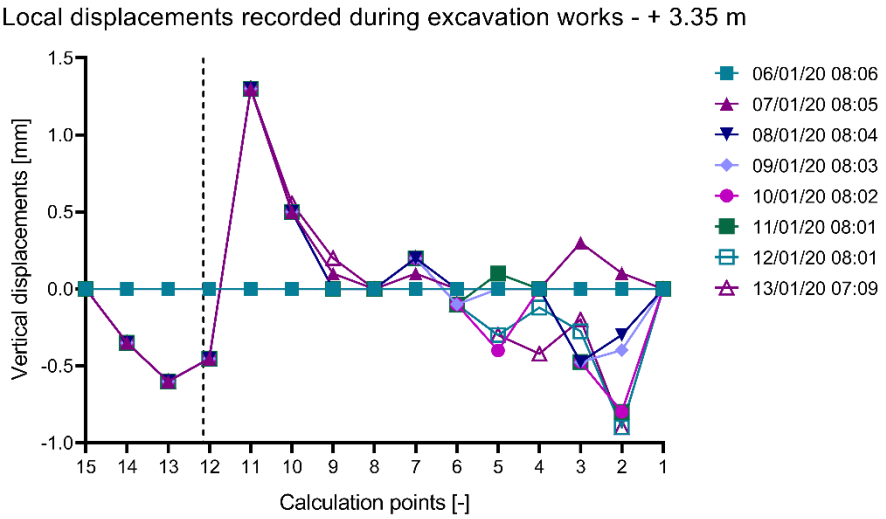

Figure 7.18 Local displacements occurred during the tunnel face advance of 3.35 m. The black dotted line indicates the tunnel face position referred to the Pre-Conv Array calculation Points

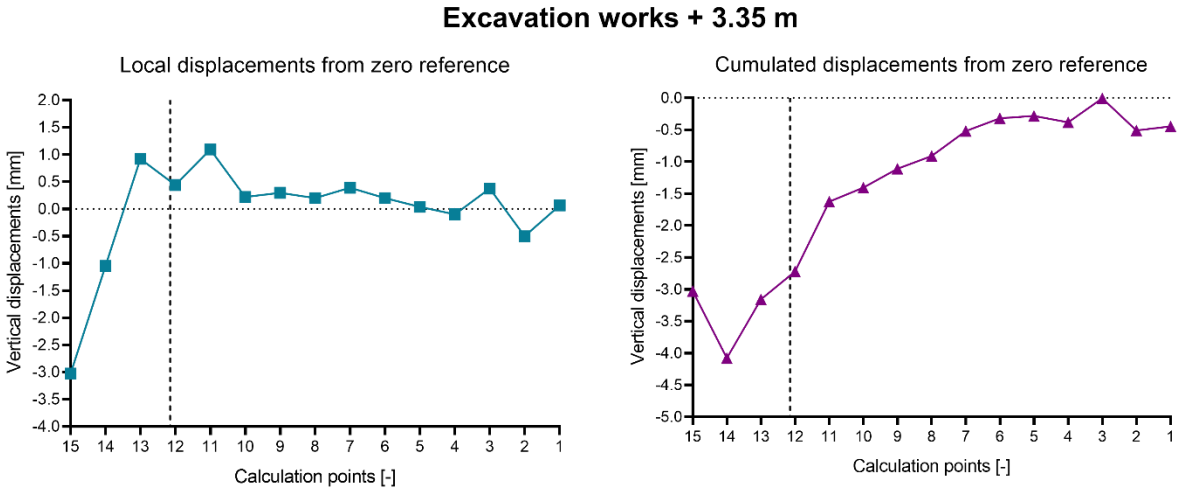

Figure 7.19 Left: Vertical local displacements evaluated from zero reference. Right: cumulated displacements evaluated from the referring date. The black dotted line indicates the front position

The tunnel advance of + 3.35 m caused an increase of the preconvergence deformations acting on the C.P. 11, for a total local displacement of 1.3 mm. C.P. 2, which is 10 meters far from the tunnel face, showed a downward vertical displacement of -0.90 mm (Figure 7.18).

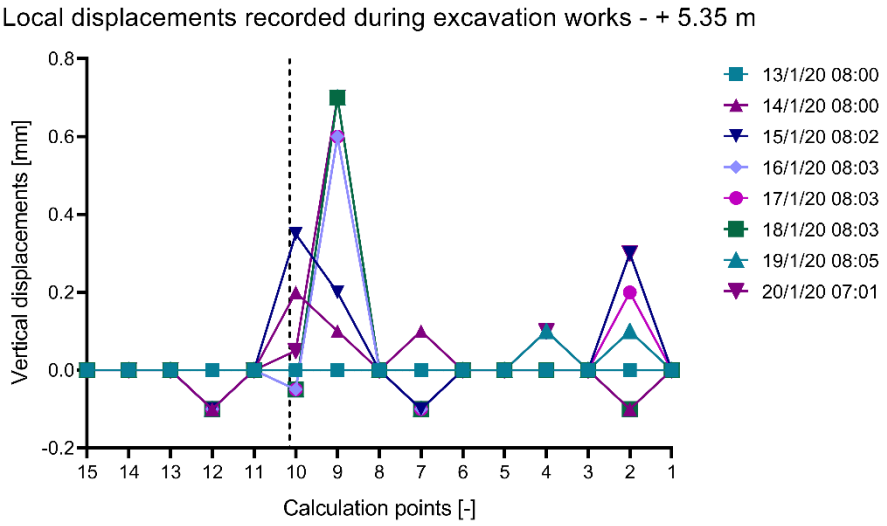

Figure 7.20 Local displacements occurred during the tunnel face advance of 5.35 m. The black dotted line indicates the tunnel face position referred to the Pre-Conv Array calculation Points

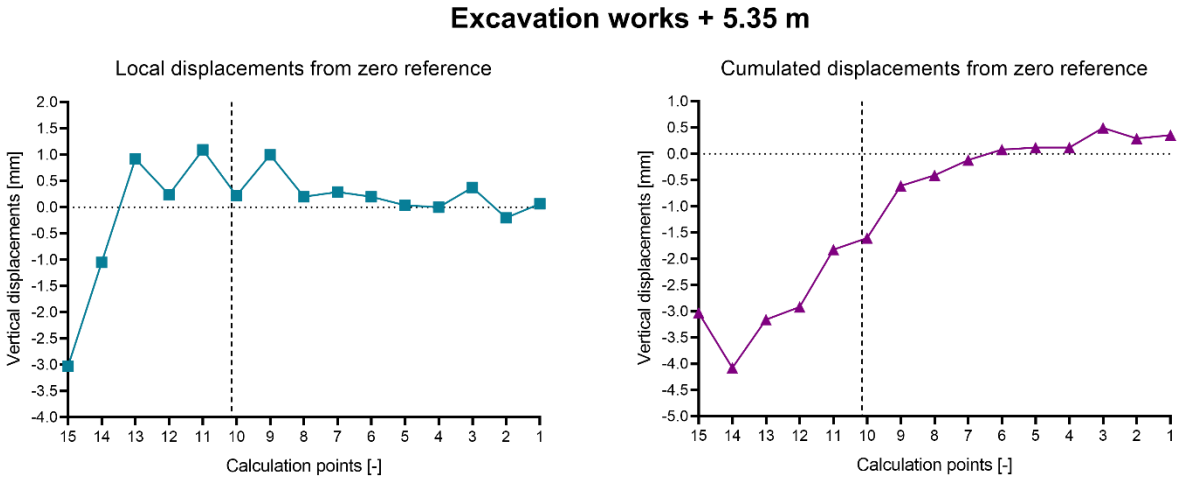

Figure 7.21 Left: Vertical local displacements evaluated from zero reference. Right: cumulated displacements evaluated from the referring date. The black dotted line indicates the front position

Figure 7.20 shows the local displacement that occurred during the excavation advance of +5.35 m. During the considered period of monitoring, C.P. 10 showed an initial preconvergence displacement of 0.4 mm on 15/01/20, when Pre-Conv Link 10 was ahead of the tunnel face. Afterward, when Pre-Conv Link 10 was behind the tunnel face, C.P. 10 started to move downward till reaching the starting position, according to a convergence deformation. Finally, C.P. 9 showed a preconvergence deformation of 0.7 mm. Local and cumulated displacement did not evidence considerable changes, indeed the deformations recorded by Pre-Conv Array were of the order of approximately 1 mm (Figure 7.21).

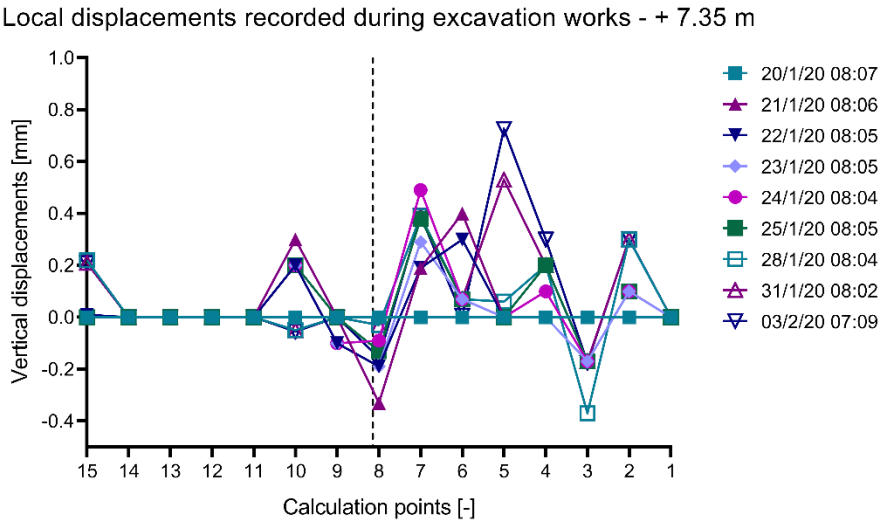

Figure 7.22 Local displacements occurred during the tunnel face advance of 7.35 m. The black dotted line indicates the tunnel face position referred to the Pre-Conv Array calculation Points

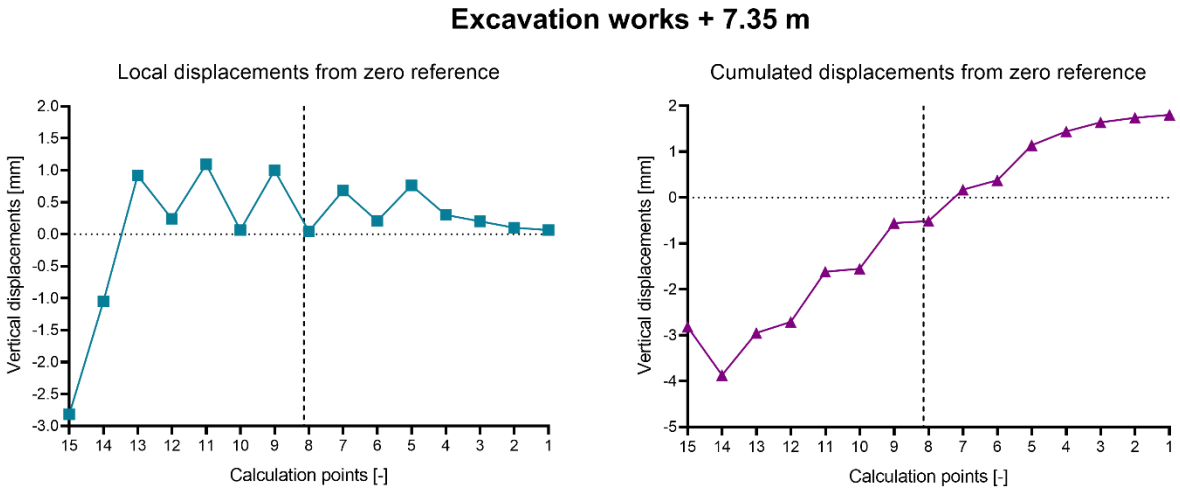

Figure 7.23 Left: Vertical local displacements evaluated from zero reference. Right: cumulated displacements evaluated from the referring date. The black dotted line indicates the front position

Figure 7.22 shows the local displacement that occurred during the excavation advance of +7.35 m. Calculation points ahead of the tunnel face indicated a preconvergence deformation acting on all the sensors, with local displacements between the range of 0.6 ÷ 0.8 mm.

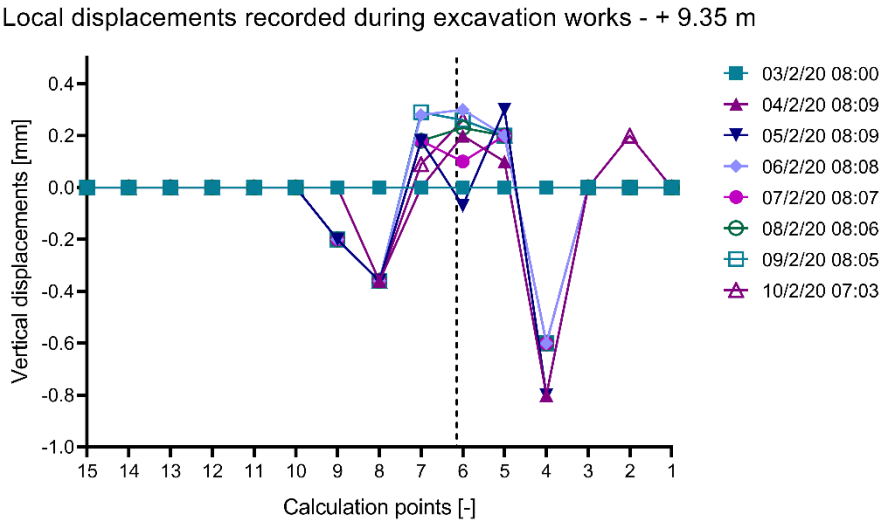

Figure 7.24 Local displacements occurred during the tunnel face advance of 9.35 m. The black dotted line indicates the tunnel face position referred to the Pre-Conv Array calculation Points

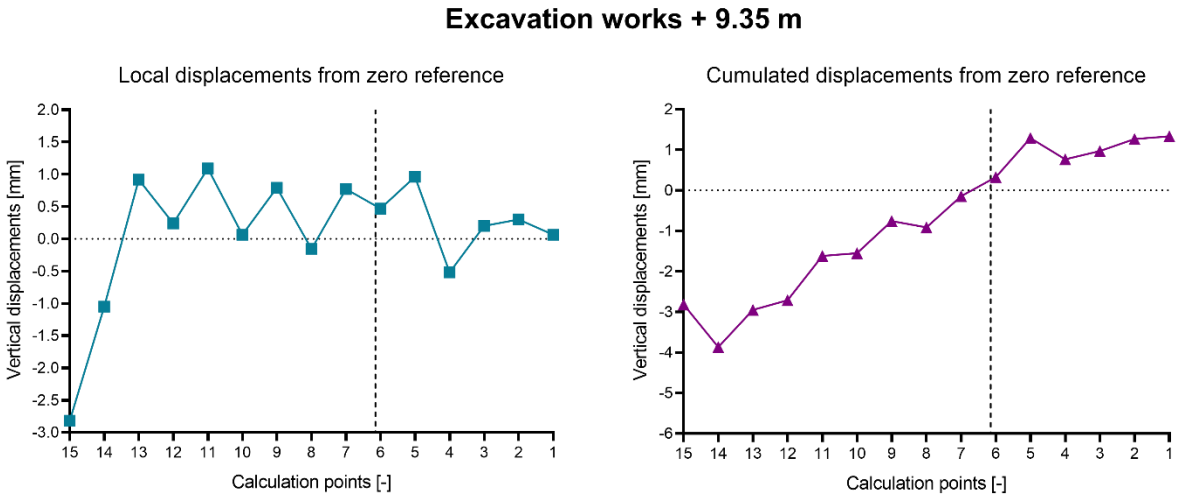

Figure 7.25 Left: Vertical local displacements evaluated from zero reference. Right: cumulated displacements evaluated from the referring date. The black dotted line indicates the front position

Figure 7.24 shows the local displacement that occurred during the excavation advance of + 9.35 m. C.P. 4 indicated a preconvergence displacement of -0.8 mm, while C.P. 5 and C.P. 6 showed a preconvergence displacement of 0.3 mm.

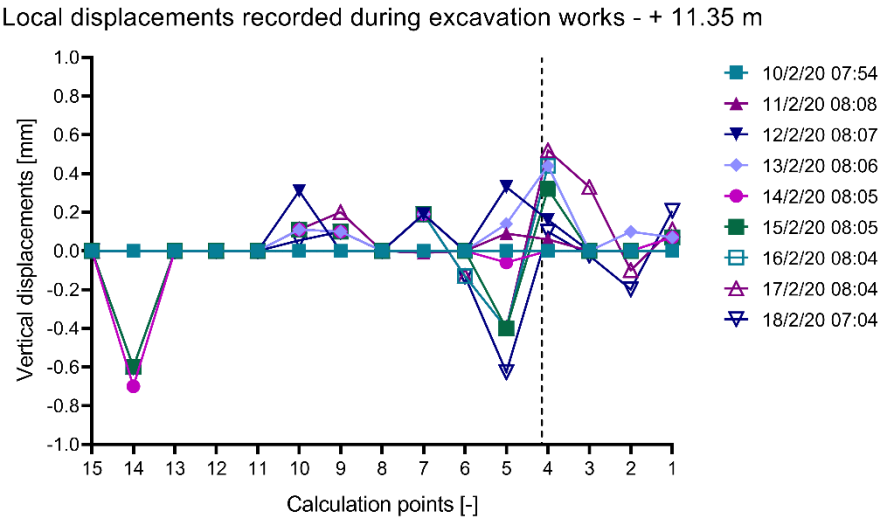

Figure 7.26 Local displacements occurred during the tunnel face advance of 11.35 m. The black dotted line indicates the tunnel face position referred to the Pre-Conv Array calculation Points

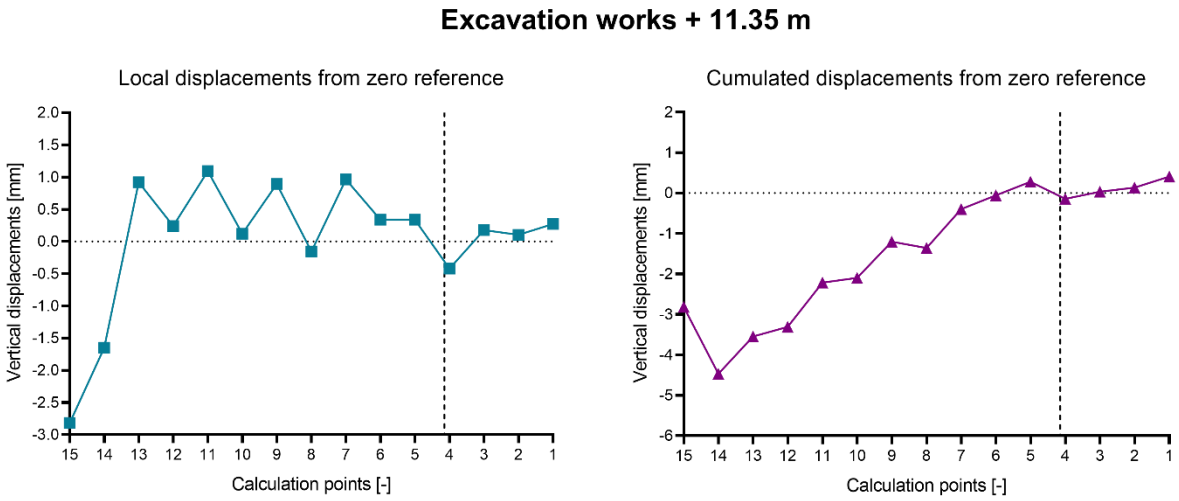

Figure 7.27 Left: Vertical local displacements evaluated from zero reference. Right: cumulated displacements evaluated from the referring date. The black dotted line indicates the front position

Figure 7.26 shows the local displacement that occurred during the excavation advance of +11.35 m. Recorded displacement are lower than 0.6 mm on all the installed sensors, therefore local and cumulated displacement did not evidence considerable changes.

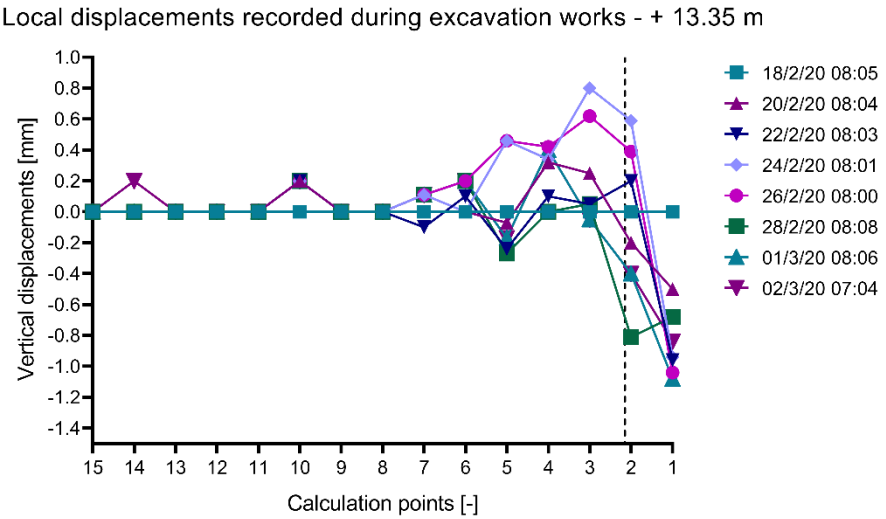

Figure 7.28 Local displacements occurred during the tunnel face advance of 13.35 m. The black dotted line indicates the tunnel face position referred to the Pre-Conv Array calculation Points

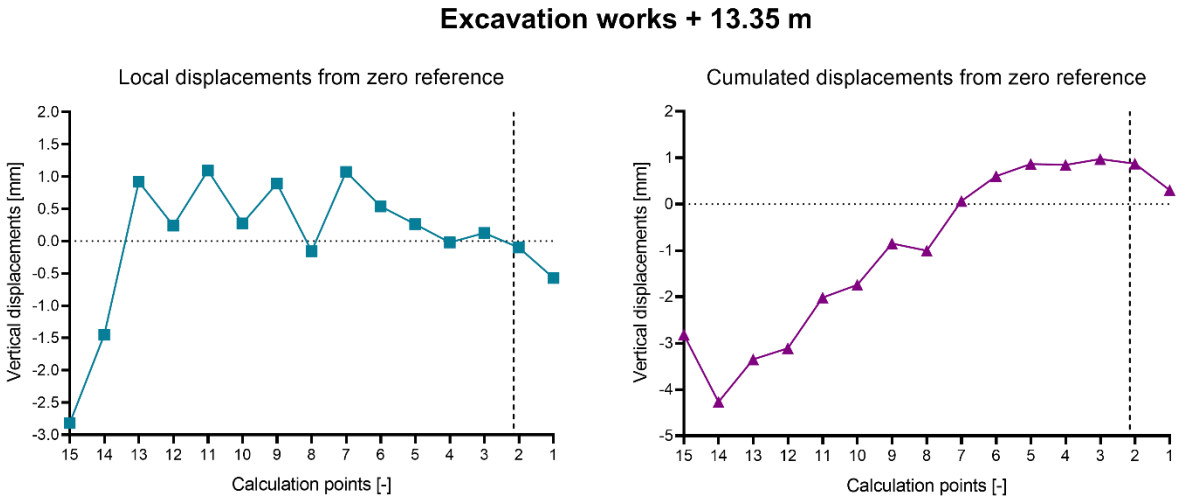

Figure 7.29 Left: Vertical local displacements evaluated from zero reference. Right: cumulated displacements evaluated from the referring date. The black dotted line indicates the front position

Figure 7.28 shows the local displacement that occurred during the excavation advance of +13.35 m. Preconvergence deformations acting on C.P. 1 reached a final value of -1.2 mm. C.P. 2 indicated an initial preconvergence deformation of approximately 0.6 mm. After 24/02/20, when Pre-Conv Link 2 was behind the tunnel face, it started to move downward according to a convergence phenomenon.

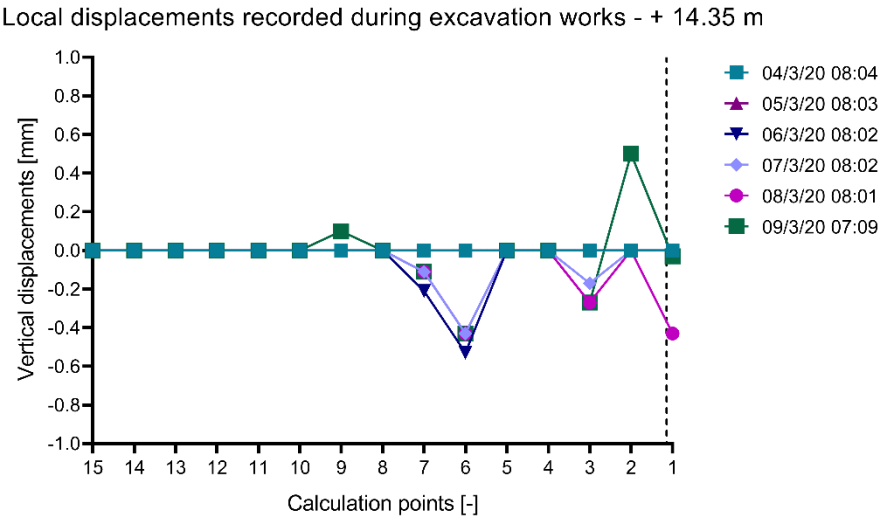

Figure 7.30 Local displacements occurred during the tunnel face advance of 14.35 m. The black dotted line indicates the tunnel face position referred to the Pre-Conv Array calculation Points

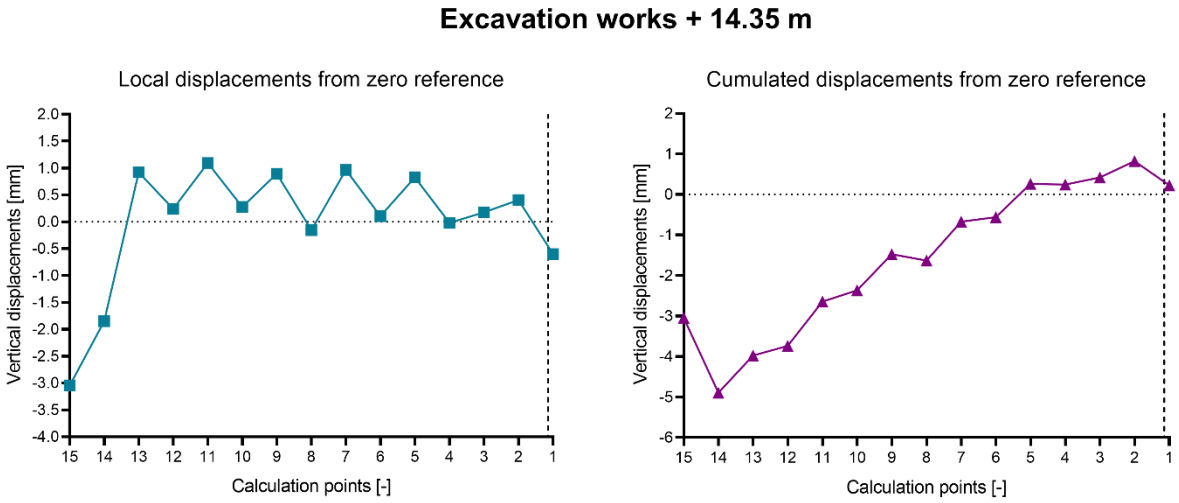

Figure 7.31 Left: Vertical local displacements evaluated from zero reference. Right: cumulated displacements evaluated from the referring date. The black dotted line indicates the front position

Figure 7.30 shows the local displacement that occurred during the excavation advance of + 14.35 m. This final stage did not evidence considerable changes on the deformative stress acting on the monitored section. Cumulated displacements highlighted a maximum vertical settlement of -5 mm on the C.P. 14.

7.5. Monitoring data validation

The Pre-Conv Array validation was carried out by comparing monitoring data and the geodetic survey installed during the tunnel advance. In particular, four monitored stations were defined (Figure 7.32). According to the tunnel reference system, the first topographic station is at + 0.40 m, while the others topographic stations are at +4.40 m, +9.40, and +14.40.

Figure 7.32 Topographic stations installed

Convergence data acquired through Pre-Conv Array are calculated by imposing the same zero reference defined from the topographic survey. For the comparison, only data from topographic marker on the tunnel crown are considered.

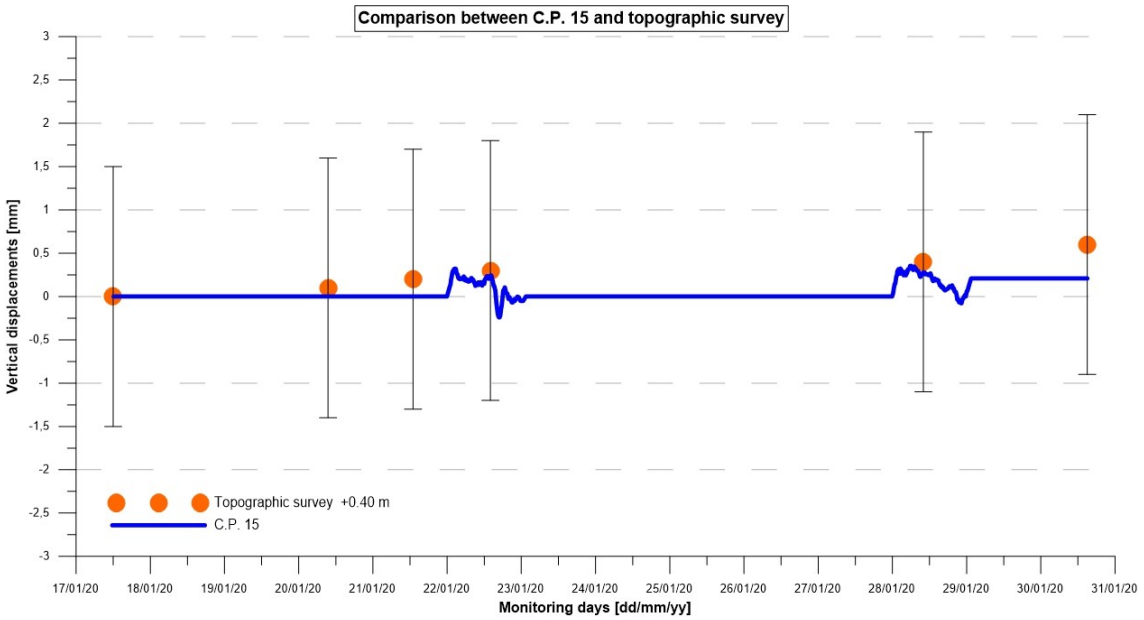

Figure 7.33 Comparison between C.P. 15 and topographic survey at +0.40 m

Figure 7.33 shows the comparison between C.P. 15 and topographic target on tunnel crown at +0.40 m. Topographic data present an uncertainties of ± 1.5 mm, as declared by the topographic monitoring company. The data uncertainties are plotted together with topographic data. C.P. 15 is 40 cm above the tunnel crown. The monitoring station +0.40 was investigated from 17/01/20 to 31/01/20. A maximum vertical displacement of +0.6 mm was highlighted, while the C.P. 15 defined a maximum vertical displacement of +0.21 mm. Monitoring data acquired with the two different technologies are comparable in terms of directions of displacement and values.

Figure 7.34 indicates the comparison between the C.P. 11 and the topographic survey on the tunnel crown at +4.40 m. Monitoring station +4.40 was investigated from 17/01/20 to 27/07/20, and highlighted a maximum vertical displacement of +0.9 mm. The C.P. 11, 40 cm above the tunnel crown presents the same data trend with a final vertical displacement of +0.15 mm. Topographic data showed an oscillation, probably due to the defined uncertainties.

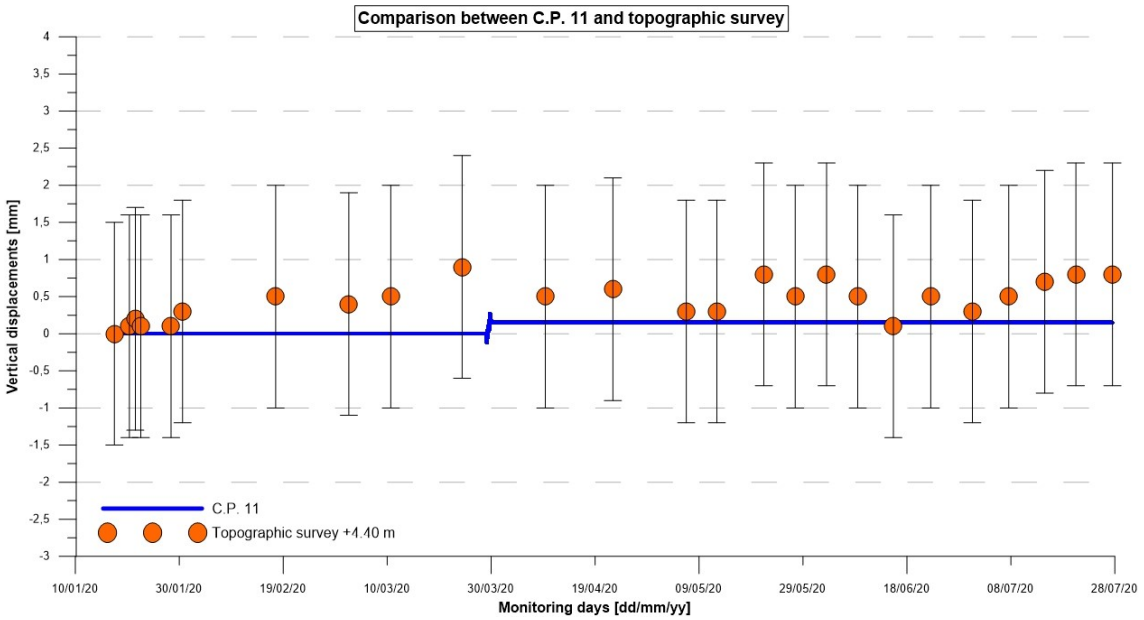

Figure 7.34 Comparison between C.P. 11 and topographic survey at +4.40 m

Figure 7.35 indicates the comparison between the C.P. 6 and the topographic survey on the tunnel crown at +9.40 m. Monitoring station +9.40 was investigated from 11/02/20 to 27/07/20, highlighting a final vertical displacement of -0.7 mm. C.P. 6. However, from 13/06/20, topographic survey defined an increase of convergence deformations with data oscillation until a final value of -0.7 mm, while C.P. 6 defined a final vertical displacement of +0.4 mm.

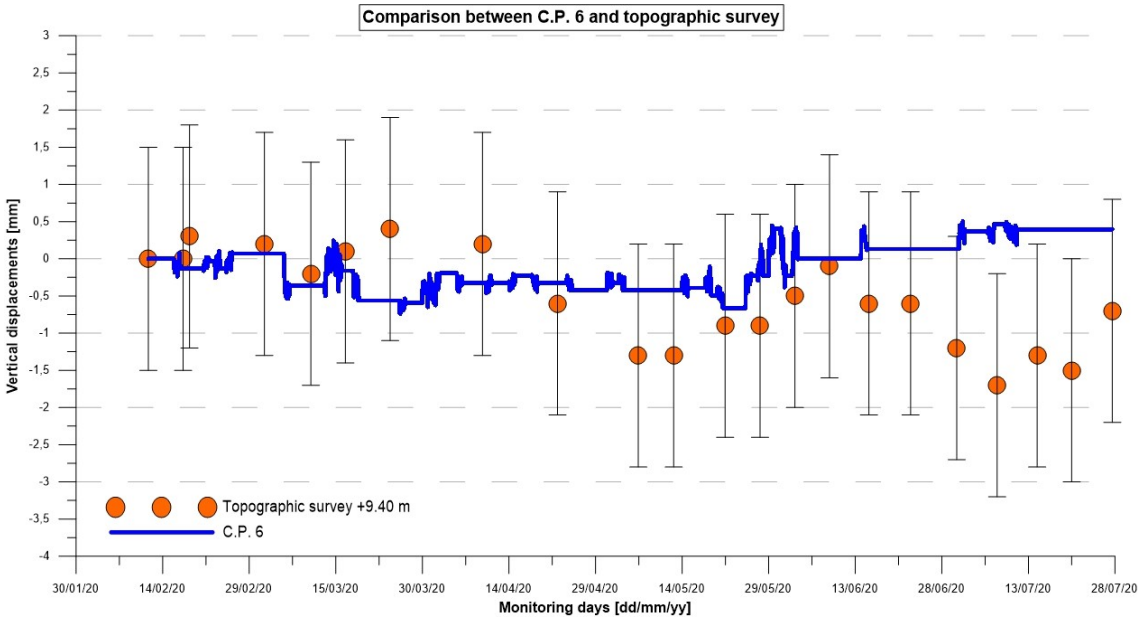

Figure 7.35 Comparison between C.P. 6 and topographic survey at +9.40 m

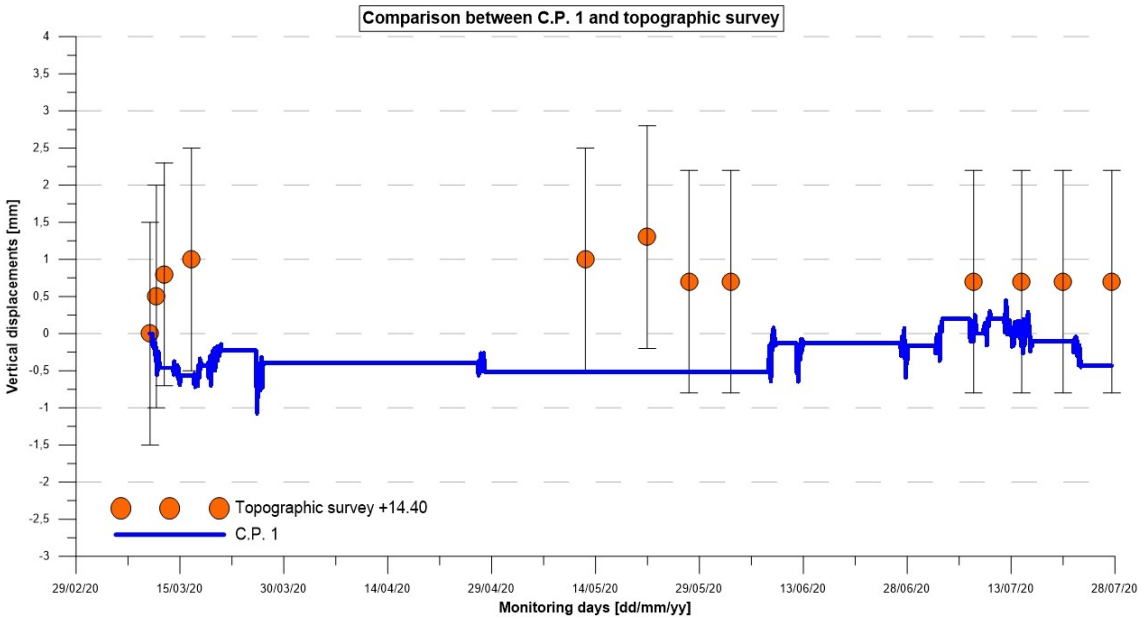

Figure 7.36 Comparison between C.P. 1 and topographic survey at +14.40 m

Figure 7.36 indicates the comparison between the C.P. 1 and the topographic survey on the tunnel crown at +14.40 m. Monitoring station +14.40 was indagated from 10/03/20 to 27/07/20, highlighting a final vertical displacement of +0.7 mm. C.P. 1 defined vertical displacements ranging from -0.5 to +0.5 mm, with a final vertical displacement of -0.44 mm.

Taken together, the comparison between topographic survey and the Pre-Conv Array data indicates a good correspondence in terms of displacements and trends. Finally, monitoring data did not highlight a high range values, and all the acquired data were included in the topographic uncertainties range.

Moreover, also the preconvergence deformative state was analysed. To validate the preconvergence deformations defined by the Pre-Conv Array, as in the previous case study, only numerical analysis can be considered. The construction company has realized a numerical model of the tunnel entrance with Plaxis®, creating several stages that simulate the excavation works. The numerical model was divided in 6 stages:

1. Geostatic condition;
2. Application of a 10 kPa loading on the surface to simulate the slope of the ground above the tunnel;
3. Tunnel excavation: steel rib installation and shotcrete projection;
4. Shotcrete maturation;
5. Seismic analysis;
6. Long-term analysis.

However, the construction company did not provide the numerical model. Only the forecasted displacement defined for the third stage were provided, with a maximum vertical settlement on surface equal to -2.194 mm (Figure 7.4).

To define the LDP of the presented shallow tunnel, we realized a numerical model by applying the RS2® code. Firstly, an axisymmetric analysis was conducted to define the relaxation factor to assign on the elastic modulus of the ground to simulate the excavation advance (E. Hoek, 2004) (Figure 7.37). Tunnel section was schematized as a circular opening with an equivalent radius of 3.26 m. To avoid significant errors the increment of each modelled stage was lower than 0.4D, where D represents the tunnel diameter (Vlachopoulos & Diederichs, 2009). The numerical model has the same geometrical size of the Tunnel SS30, with an overburden of 6.3 m, for a total height of 9.56 m. The ground above is divided in two different geotechnical units: calcareous breccia, extended for 4.3 m above the tunnel crown, and cover soil for the remaining 2 meters. Cover soil presents the geotechnical parameters highlighted in Table 7.5.

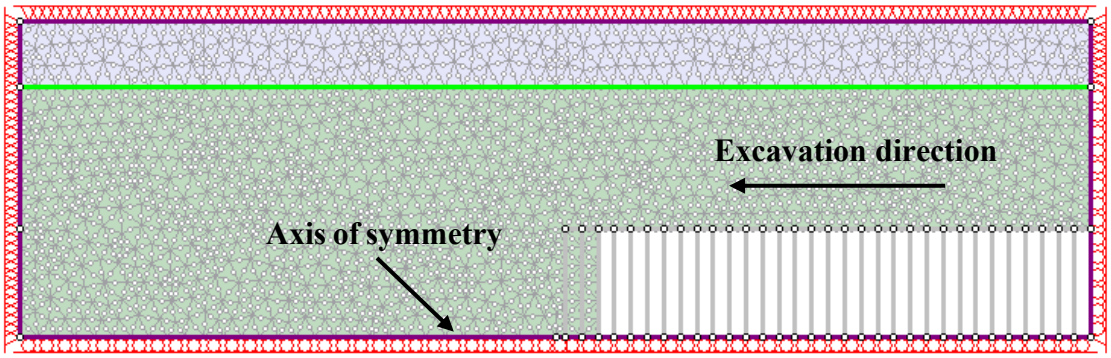

Figure 7.37 Axisymmetric model in RS2®

Table 7.5 Mechanical and deformative parameters of the cover soil

Cover soil				
Volume weight γ [kN/m³]	**Friction angle φ [°]**	**Cohesion c [kPa]**	**Elastic modulus E [MPa]**	**Poisson coefficient υ [-]**
18	30	5	67.5	0.3

The axisymmetric model permits to define the LDP of the unsupported tunnel, and finally, to obtain the relaxation factor to apply at the elastic modulus of the ground as a function of the distance from

the tunnel face. The relaxation factor permits to simulate the ground deformative response in a 2D plane stress model (M. Kavvadas, 2005).

The analysis was conducted for 15 m of advance, equal to the length of the monitored tunnel entrance. The LDP was obtained considering a constant field stress in two different configurations: σ_v and σ_h, that represent the vertical and horizontal field stress, respectively. Field stresses were calculated considering the tunnel depth and the surrounding ground unit weight. The coefficients of lateral earth pressure, K_0, were provided by the construction company. Calcareous breccia presents a K_0 equal to 0.426, instead the cover soil presents a value equal to 0.5. Each axisymmetric model configuration was analysed for a fixed position at 15 m inside the tunnel. The mean of the evaluated displacements defined by the numerical models were then used to reconstruct the longitudinal displacement profile on the tunnel crown for the unsupported tunnel.

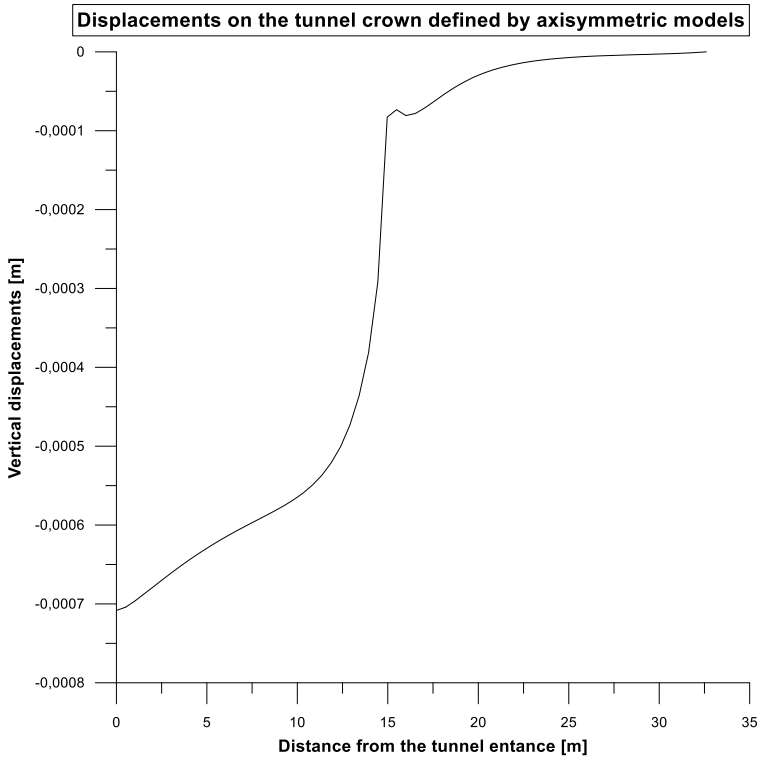

Figure 7.38 Longitudinal displacement profile on the tunnel crown for the unsupported tunnel

From displacements data in Figure 7.38, we defined a relaxation factor to assign to the elastic modulus of the tunnel face. The relaxation factor was obtained by dividing the displacement at each distance from the tunnel entrance for the maximum vertical settlement.

The axisymmetric model represents the input for the 2D plane stress model, in which also the support system and the shotcrete maturation are modelled. RS2® permits to simulate the support system as a

composite liner (Hoek, 1998), in which an homogeneous thickness and elastic modulus must be defined. The homogeneous thickness and elastic modulus are defined by the following equations:

$$E_{hom} = \frac{\left[E_{sc} \cdot s + \left({}^{E_{sr}}/_{E_{sc}} - 1\right) E_{sc} \cdot {}^{A_{sr}}/_{d}\right]^{3/2}}{\sqrt{E_{sb} \cdot s^3 + 12 \cdot \left({}^{E_{sr}}/_{E_{sc}} - 1\right) \cdot E_{sc} \cdot {}^{I_{sr}}/_{d}}} \quad [7.1]$$

$$s_{hom} = \sqrt{\frac{E_{sb} \cdot s + 12 \cdot \left({}^{E_{sr}}/_{E_{sc}} - 1\right) \cdot E_{sc} \cdot {}^{I_{sr}}/_{d}}{E_{sc} \cdot s + \left({}^{E_{sr}}/_{E_{sc}} - 1\right) E_{sc} \cdot {}^{A_{sr}}/_{d}}} \quad [7.2]$$

Where:

- E_{hom} is the homogeneous elastic modulus;
- s_{hom} is the homogeneous thickness;
- E_{sc} is the shotcrete elastic modulus;
- E_{sb} is the steel rib (HEB100) elastic modulus;
- s is the shotcrete thickness;
- A_{sr} is the steel rib area;
- d is the distance of installation of each steel rib;
- I_{sr} is the Inertia modulus of the steel rib.

Furthermore, shotcrete maturation was modelled applying different elastic modulus as a function of the maturation time (Bryne, 2014), as schematized in equation [7.3]:

$$E_{sc,t} = E_{28} \cdot (1 - e^{-0.42t}) \quad [7.3]$$

Where:

- $E_{sc,t}$ is the shotcrete elastic modulus in time;
- E_{28} is the final shotcrete elastic modulus;
- t is the modelled time, expressed in days.

Table 7.6 and Table 7.7 show the mechanical parameters of the shotcrete and of the steel ribs, respectively.

Table 7.6 Shotcrete mechanical properties

Shotcrete

Type	Unit weight γ [kN/m^3]	Elastic modulus E_{sc} [MPa]	Poisson coefficient υ [-]
$f_{ck} = 25\ MPa$	25	10000	0.2

Table 7.7 HEB 100 Steel ribs mechanical properties

Steel ribs

Type	Unit weight γ [kN/m^3]	Elastic modulus E_{sc} [MPa]	Poisson coefficient υ [-]
S355	78.5	210000	0.2

The shotcrete maturation was modelled by inserting three different stages that simulate the support installation and the excavation advance in two different time-points. The shotcrete elastic modulus in each stage is defined by equation [7.3] imposing three different installation time, t: 0.5, 2, and 28 days, simulating the support installation, the advance of 1.5 m, and the advance of 5.5 m, respectively.

The mechanical and deformative parameters obtained are inserted in the plane stress model to simulate a composite liner (Rocscience manual), together with the relaxation factor assigned to each stage.

The plane stress was divided in 16 different stages to simulate and define the LDP:

1. Geostatic conditions;
2. Application of a 10 kPa loading on surface, to simulate the slope of the ground above the tunnel;
3. Tunnel face 13 m ahead of the considered section;
4. Tunnel face 10 m ahead of the considered section;
5. Tunnel face 5 m ahead of the considered section;
6. Tunnel face 1 m ahead of the considered section;
7. Excavation of the considered section;
8. Installation of the composite liner, +0.5 m advance ($t = 0.5$ day);
9. Shotcrete maturation, +1.5 m advance ($t = 2$ days);
10. Shotcrete final maturation, +5.5 m advance ($t = 28$ days);
11. Tunnel face 7 m far from the considered section;
12. Tunnel face 9 m far from the considered section;
13. Tunnel face 10 m far from the considered section;

14. Tunnel face 11 m far from the considered section;
15. Tunnel face 12 m far from the considered section;
16. Tunnel face 13 m far from the considered section;

Table 7.8 indicates the Elastic modulus obtained from the relaxation factor in the axisymmetric model.

Table 7.8 Elastic modulus for each modelled stage obtained from the axisymmetric models

Stage	Elastic modulus [MPa]	Stage	Elastic modulus [MPa]
1	695	**9**	210.31
2	695	**10**	127.51
3	691.14	**11**	111.36
4	686.69	**12**	93.52
5	680.09	**13**	79.85
6	631.61	**14**	64.57
7	327.64	**15**	47.77
8	273.83	**16**	29.88

The composite liner was installed in stage 8. From equation [7.1] and equation [7.2] the homogeneous thickness and elastic modulus were defined (Table 7.9).

Table 7.9 Homogeneous elastic modulus and thickness

Stage	Homogeneous Elastic modulus [MPa]	Homogeneous thickness [mm]
8	5638.15	149.89
9	9343.38	154.26
10	13577	156.21

To avoid boundary effects, the 2D plane model is 100 m width and 60 m height (Figure 7.39).

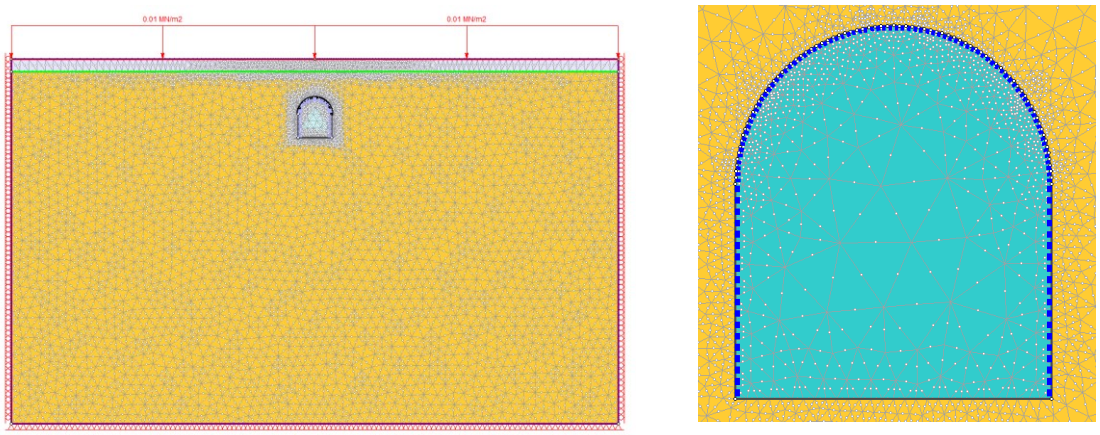

Figure 7.39 Left: 2D plane stress model. Right: zoom of the supported excavation face

For each defined stage, displacements on the surface and on the tunnel crown were considered. As previously stated, the vertical displacement defined by Plaxis® model is -2.194 mm (Figure 7.5). The vertical settlement defined by the RS2® model in stage 8 is -1.9 mm, with a difference of 0.294 mm. The displacement on the tunnel crown for each stage were finally collected to define the LDP of the supported tunnel, with a maximum vertical displacement of -5.49 mm in the last considered stage (Figure 7.40).

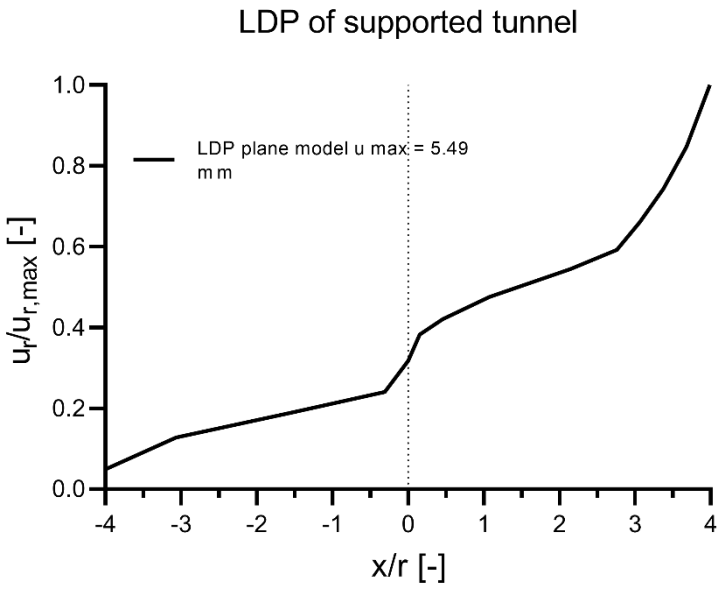

Figure 7.40 LDP of the supported tunnel obtained from the plane stress model

Finally, each calculation point was considered fixed, cumulating its recorded local displacements at different distances from the tunnel face, which dependent on the excavation phases. The comparison between instrumental data and the modelled curve are represented in the figures that follow.

Figure 7.41, 7.42, and 7.43 presents the cumulated displacement defined at each excavation step, indicating the maximum radial displacement, $u_{r,max}$, obtained from every Pre-Conv Link.

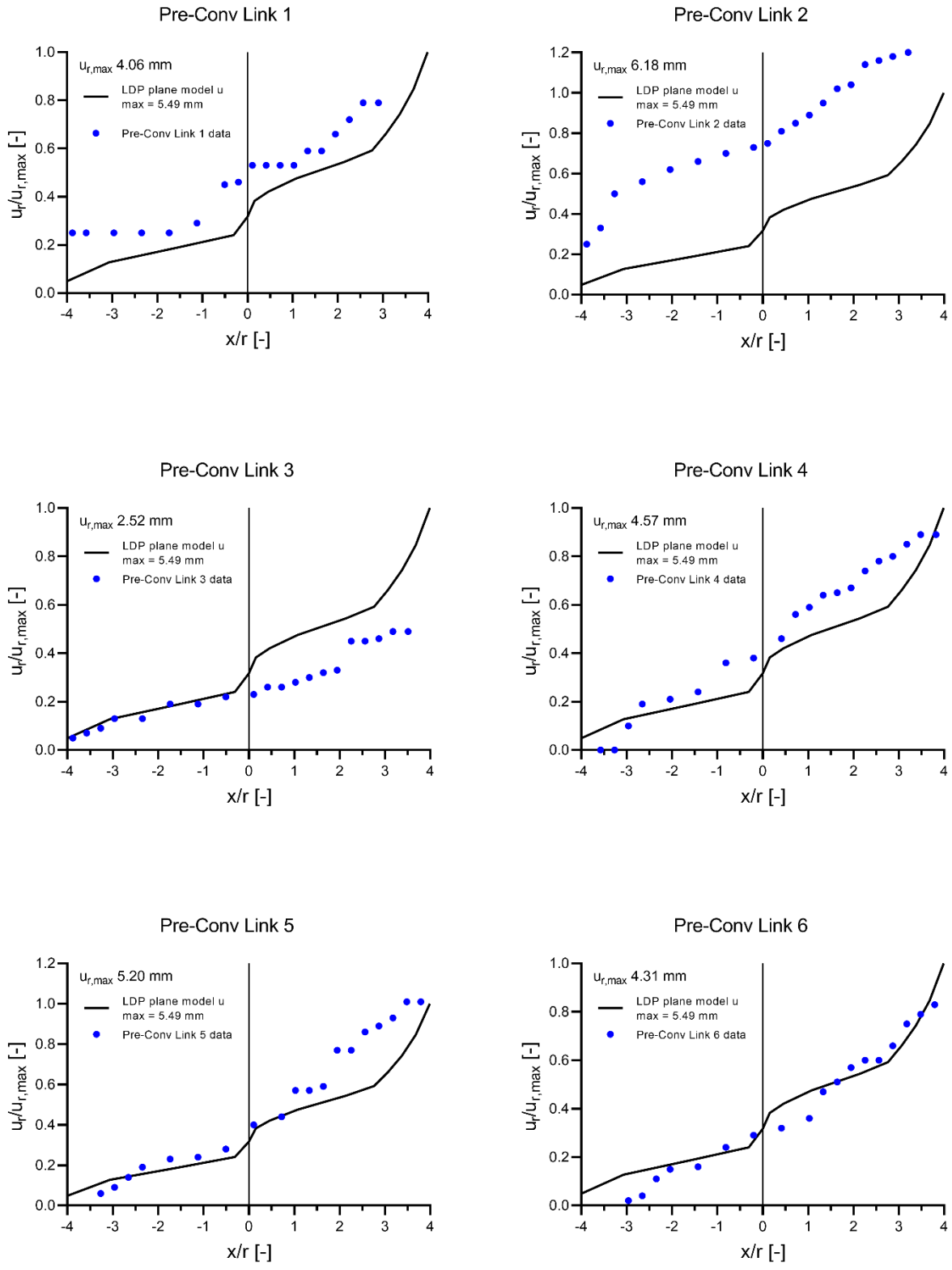

Figure 7.41 Comparison between instrumental data and LDP obtained through the numerical model. Pre-Conv Link from 1 to 6

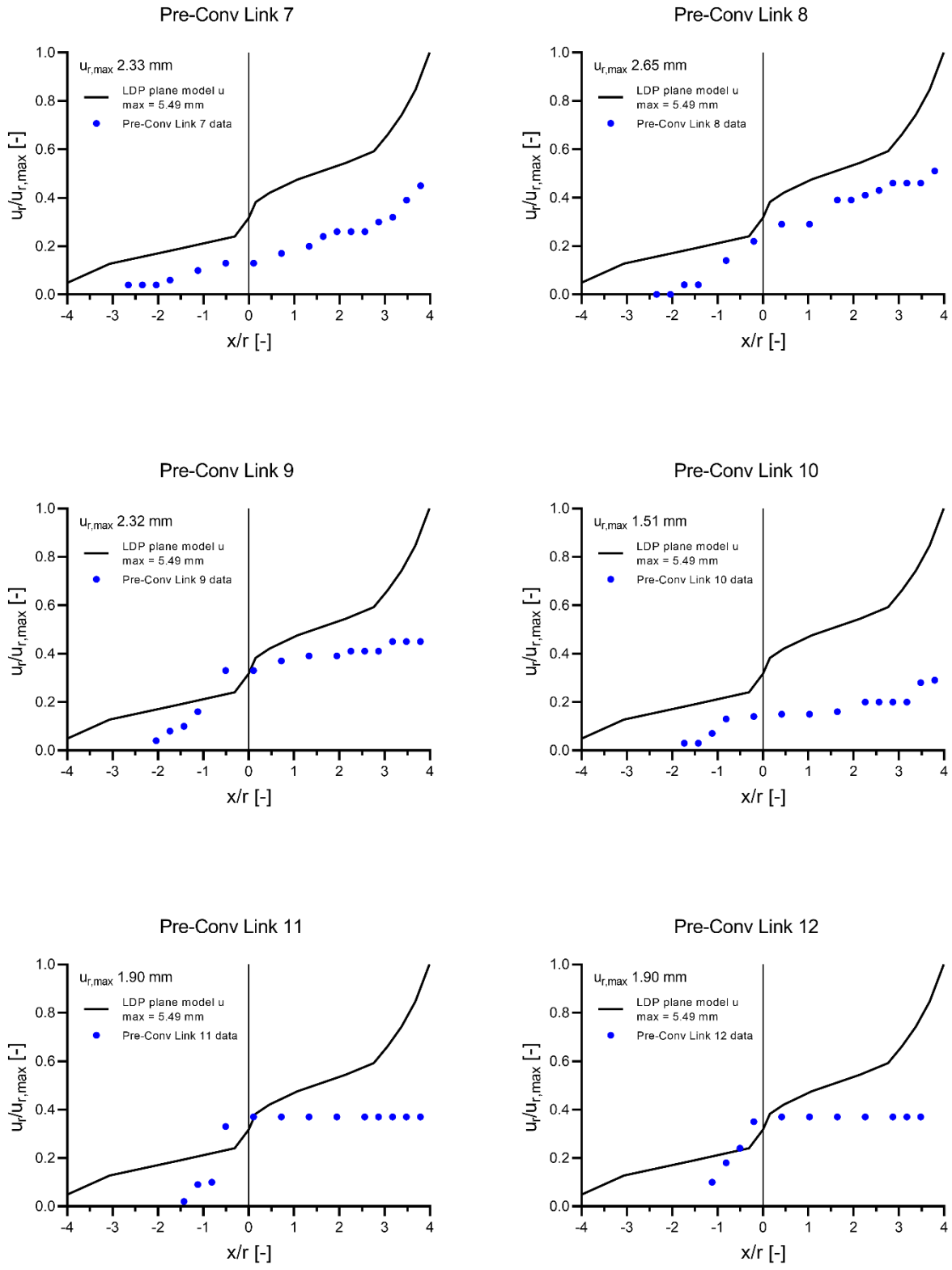

Figure 7.42 Comparison between instrumental data and LDP obtained through the numerical model. Pre-Conv Link from 7 to 12

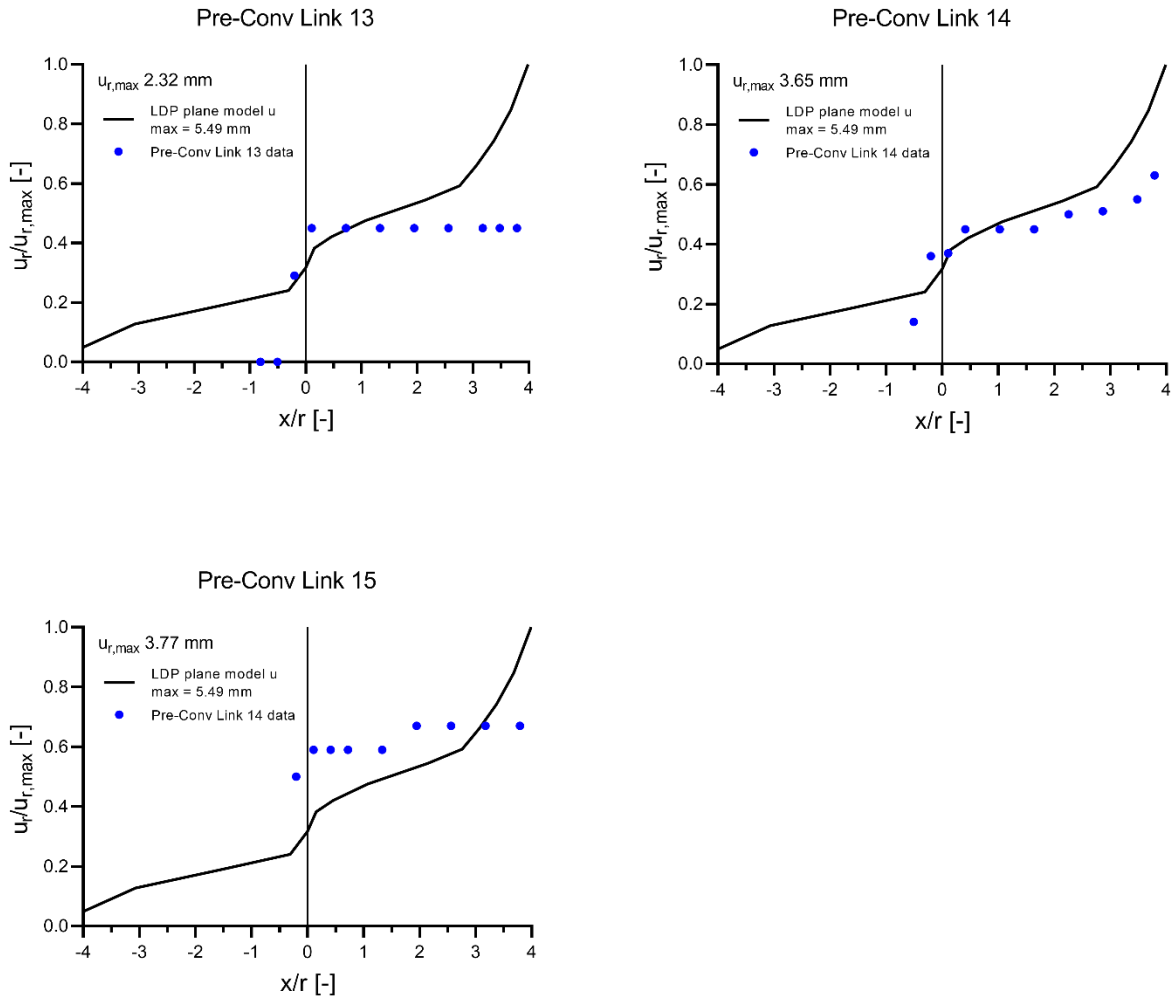

Figure 7.43 Comparison between instrumental data and LDP obtained through the numerical model. Pre-Conv Link from 13 to 15

The comparison between instrumental and modelled LDP shows a good correspondence for Pre-Conv Links from 1 to 8, with the exception of the Pre-Conv Link 2, which defined a vertical settlement higher than the one reported by the modelled LDP, equal to 6.18 mm. Starting from Pre-Conv Link 9, which corresponds to the initial instrumented portion of the tunnel entrance, monitoring data highlighted a similar trend for the preconvergence deformations. Instead, after the tunnel face passage and after the support installation, only Pre-Conv Link 14 defined an increase of convergence deformations, while the other Links were almost stable. This behaviour could indicate that in the first 6 meter of advance the mechanical and deformative parameters of the ground are higher than expected.

7.6. Conclusion

Pre-Conv Array has been installed to monitor the pre-deformations that occurred during the excavation of a shallow tunnel in the Principality of Monaco. The proposed monitoring system highlighted a limited range of displacements. These displacements were validated through a geodetic survey. A numerical model was realized in order to define the LDP of the supported cavity, and, finally, compare the data to the ones measured by the Pre-Conv Array. The comparison shows a good agreement between the Pre-Conv Array data and the modelled LDP.

For what concerns the geodetic survey, it analysed also the vertical displacements on the tunnel entrance, near to the Pre-Conv Array anchor, which is the starting point for the displacement evaluation. The definition of displacements with Pre-Conv Array system is based on the hypothesis that the anchor is a fixed point, with constant coordinates. In reality, some deformations during the monitoring phase can be evidenced on the tunnel entrance. Figure 7.44 shows the vertical displacement of the topographic target I14, from the zero reading on 25/11/19 to 09/03/20, the end of the excavation works under the monitored length of the Pre-Conv Array. During this period, the target I14 defines -2.8 mm of vertical displacement.

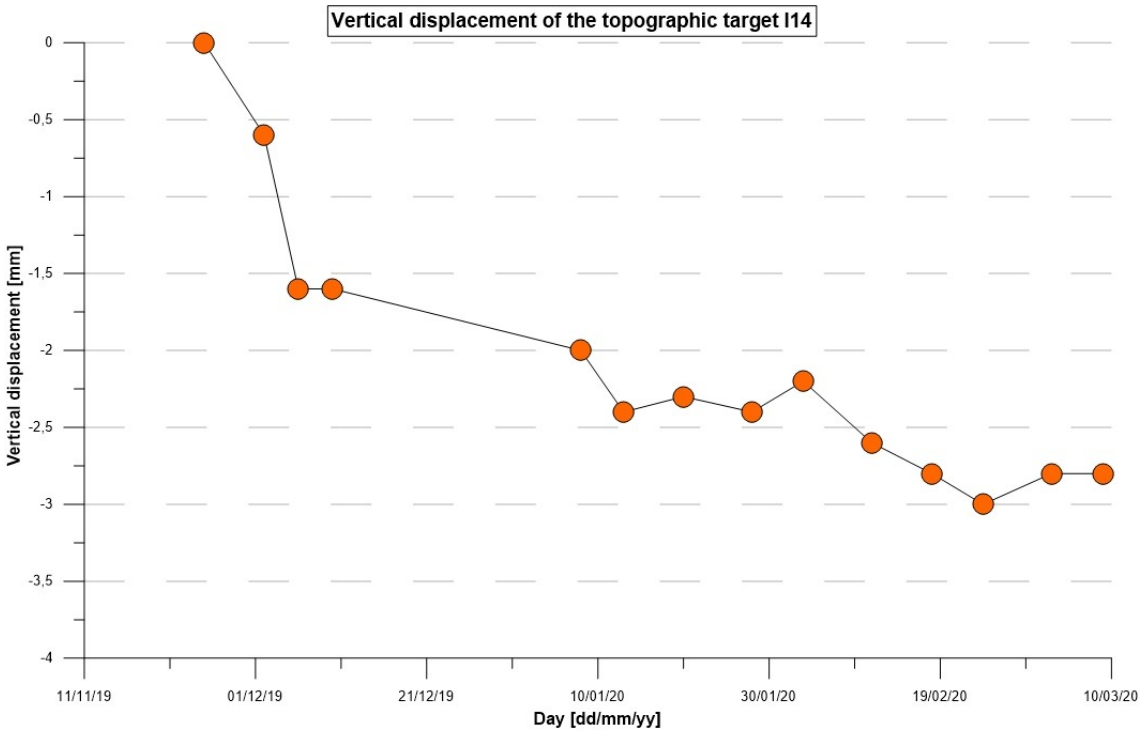

Figure 7.44 Vertical displacement of the topographic target I14

The installation of a topographic target near the Pre-Conv anchor permits to exactly evaluate the deformations acting on the reference point, finally defining a correct evaluation of the cumulated displacement. Referring to Figure 7.31, local and cumulated displacement can be evaluated

considering the displacement of the anchor. Figure 7.45 shows the corrected local and cumulated displacement, starting from the vertical settlement of the external anchor.

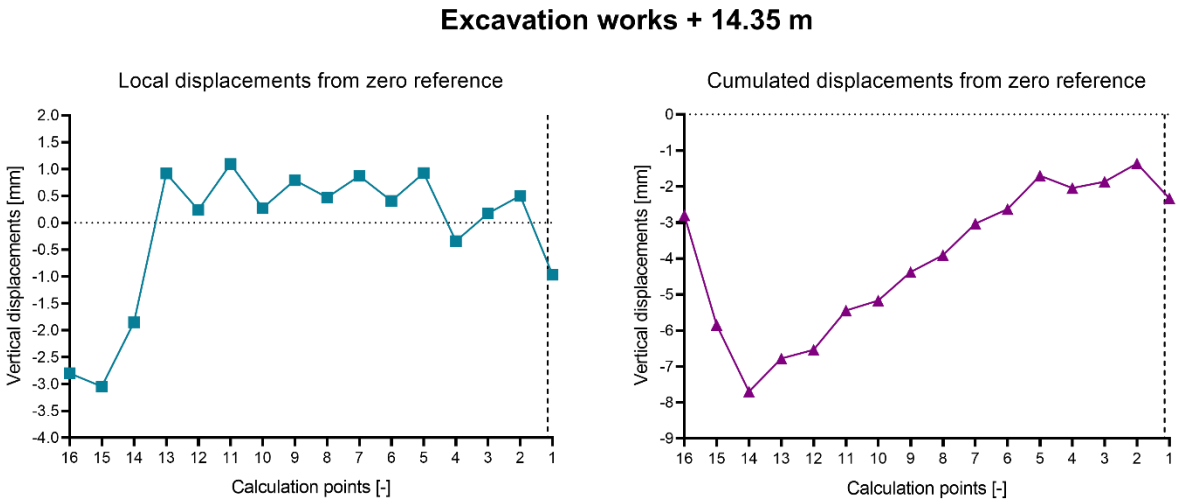

Figure 7.45 Left: Vertical local displacements evaluated from zero reference. Right: cumulated displacements evaluated from the referring date considering the vertical settlement of the anchor. Black dotted line indicates the front position

8. Conclusion

Pre-Conv Array has been developed with the aim to measure the preconvergence deformation acting on the rock mass within the tunnel excavation. The pre-deformations acting on the advance core represents a key aspect to consider during tunnel excavation. Indeed, an extensive three-dimensional monitoring ahead and behind the tunnel face can help the project designer to define the best solution and compromise in terms of support system, installation distance from the tunnel face, construction site safety, and money and time saving. Furthermore, Pre-Conv Array installation is simple and fast, and does not interfere with the working phases.

Pre-Conv Array permits to acquire data with a high sampling frequency both during the tunnel drilling and within the tunnel operativity, giving additional information about the convergence deformations that could affect the preliminary or definitive tunnel lining. Furthermore, a high sampling frequency allows to implement a statistical approach, to apply self-check data control to individuate spike noises, wrong measurements, malfunctions, and generally every external factor that can affect data elaboration.

The main aim of this research was to study the Pre-Conv Links performance to define whether the proposed monitoring sensors were capable to detect displacements. With this purpose, a series of laboratory test were carried out, simulating preconvergence deformations derived from extrusion measurements. The imposed displacements were finally compared with a total station. The Pre-Conv Array data compared to the geodetic data, presented a maximum error of 9% in the horizontal configuration, while in the tilted installation defined a maximum error of 5%.

Pre-Conv Array has been installed in two pilot sites. During the first installation, a strong thermal influence was underlined. After several laboratory tests, sensors highlighted a pressure influence, correlated to the compression strength generated by the mortar maturation, and a thermal influence caused by rapid temperature variations. The experimental results lead us to develop a filter able to compensate monitoring data from the external disturbances. The filtering process is based on the difference between the daily slope of temperature and displacements. When delta values are higher than a defined threshold, displacements data represent the principal contribution, instead, when delta values are lower than a threshold, temperature is the principal contribution that generates data noise or apparent displacement. After testing different delta slopes, the one that best compensated the temperature influence was equal to 0.05. The proposed thermal filter was finally validated in two different case studies.

The first case study was a deep tunnel in the North of Italy. Monitoring data were validated by two different approaches: first, data were compared with the geodetic survey. Secondly, Pre-Conv Array LDP of each calculation point were compared with the Hoek and Panet theoretical LDP. In this case, we obtained a good correspondence between Pre-Conv Array data and the theoretical curve.

The second case study was a shallow tunnel realized in the Principality of Monaco. The pre-deformations defined by the Pre-Conv Array showed a lower deformative state than the previous case study. Also in this case, the Pre-Conv Array data were validated through two different approaches: first, through comparison of monitoring data with the ones obtained by four topographic monitoring stations. Secondly, through comparison of monitoring data with a 2D model of the tunnel entrance, which permitted to define the LDP of the tunnel.

In both case studies, we were able to highlight displacements in correspondence of each step of advance of the excavation works. More specifically, the instrument recorded displacements relative to both the preconvergence and convergence of the tunnel crown. Taken together, the Pre-Conv link sensors turned out to be fundamental instruments to monitor the stability of the advance core and to project the best support system.

Future investigations will focus on delete the thermal influence highlighted by the pilot site installations. With this aim, we will develop a semi-automatic calibration procedure that allows to define different delta values for every installation site. In parallel, we will test a new sensor that implements a self-calibration procedure that deletes the thermal influence. In particular, we will study the sensor response to thermal and pressure influences by conducing the same tests described in this thesis.

Furthermore, to ameliorate the isolation of the sensors from the external influences, we foresee two possible solutions: on the one hand, we will study other kinds of resin shell, in order to find the one that shows less deformation induced by temperature variations. On the other hand, we will project a shell that mechanically isolate the sensors from the external factor, such as the surrounding resin subjected to temperature dilation, although minimized.

To finely reconstruct the local and cumulated displacements, our instrument will be implemented with a topographic target on the anchor.

Moreover, in the future installations, the Pre-Conv Array will be installed without the cement grout injection. In this way, the instrument can be reusable and installed in several excavation advance,

depending on the different geological and geotechnical contexts. To recover the tool and install it in a different site or progressive, the Pre-Conv Array will be placed in an inclinometer casing together with a wheels system, similar to the one of the inclinometer probe. This structure allows the instrument to slide and easily recover it if the deformations caused by the tunnel excavations let to extract it.

Another innovation that we will carry out is in the Web platform. In order to facilitate the design phase, we will implement the platform to show the GRC and LDP of the rock mass and the SCC of the confinement support, uploaded directly on the platform by the project designer. These graphs, coupled with the near real-time monitoring data of each calculation point, will help the project designer to constantly verify the acting deformative state and, eventually, to change the project decision according to the “learn as you go” approach.

References

AFTES. (1978). Analysis of tunnel stability by the Convergence-Confinement Method. *Underground Space*, *4*, 221–223.

Aydemir, G. A., & Saranli, A. (2012). Characterization and calibration of MEMS inertial sensors for state and parameter estimation applications. *Measurement: Journal of the International Measurement Confederation*, *45*(5), 1210–1225. https://doi.org/10.1016/j.measurement.2012.01.015

Bieniawski, Z. T. (1993). *Classification of Rock Masses for Engineering: The RMR System and Future Trends*. Elsevier Ltd. https://doi.org/https://doi.org/10.1016/B978-0-08-042066-0.50028-8

Bryne, L. E. (2014). *TIME DEPENDENT MATERIAL PROPERTIES OF SHOTCRETE FOR HARD ROCK TUNNELLING*. KTH.

Cai, M. (2011). Rock mass characterization and rock property variability. Considerations for tunnel and cavern design. In *Rock Mechanics and Rock Engineering, n.44* (pp. 379–399). https://doi.org/10.1007/s00603-011-0138-5

Carranza-Torres, C., & Fairhurst, C. (2000). Application of the Convergence-Confinement Method of tunnel design to rock masses that satisfy the Hoek-Brown failure criterion. *Tunnelling and Underground Space Technology*, *15*(2), 187–213. https://doi.org/10.1016/S0886-7798(00)00046-8

Carri, A. (2019). *Innovative monitoring instrumentations and methods for landslide risk management and mitigation*. University of Parma.

Carter, T. G. (1992). PREDICTION AND UNCERTAINTIES IN GEOLOGICAL ENGINEERING AND ROCK MASS CHARACTERIZATION ASSESSMENTS. *4th Italian Rock Mechanics Conference*, 1.1-1.22.

Cavalca, E., Carri, A., & Savi, R. (2018). Validazione per mezzo di analisi numeriche di una strumentazione innovative per il monitoraggio delle misure di convergenza in scavi in sotterraneo. *VIII IAGIG*.

References

Chern, J. C., Shiao, F. Y., & Yu, C. W. (1998). An empirical safety criterion for tunnel construction. *Regional Symposium on Sedimetary Rock Engineering*, 222–227.

Chung, S. K., Ryu, D. W., Jang, W. Il, & Yang, H. S. (2010). Characterization of complete radial displacement of tunnel using a horizontal inclinometer. *Geosystem Engineering*, *13*(2), 77–82. https://doi.org/10.1080/12269328.2010.10541312

Daemen, J. J. K. (1975). *Tunnel support loading caused by rock failure*. University of Minnesota.

Dodds, R. K. (1982). *Preliminary investigations* (J. . and K. T. R. Bickel (ed.)). Van Nostrand, Reinhold Company, Inc., New York.

Dunnicliff, J. (1993). *Geotechnical Instrumentation for Monitoring Field Performance | Wiley*.

Fenner, R. (1938). *Untersuchungen zur Erkenntnis des Gebirgsdrucks*. Glückauf.

Glaisher, J. W. L. (1871). XXXII. On a class of definite integrals . *The London, Edinburgh, and Dublin Philosophical Magazine and Journal of Science*, *42*(280), 294–302. https://doi.org/10.1080/14786447108640568

Hoaglin, D. C., Mosteller, F., & Tukey, J. W. (1983). *Understanding Robust and Exploratory Data Analysis | Wiley*.

Hoek, E. (2004). *Numerical modelling for shallow tunnels in weak rock*. www.rocscience.com.

Hoek, E., Carranza-Torres, C., Diederichs, M., & Corkum, B. (2008). The 2008 Kersten Lecture Integration of geotechnical and structural design in tunneling The 2008 Kersten Lecture Integration of geotechnical and structural design in tunneling. *56th Annual Geotechnical Engineering Conference*, *February*.

Hoek, Evert. (1998, November). Tunnel support in weak rock. *Keynote Address, Symposium of Sedimentary Rock Engineering*.

Jeon, J. S., Martin, C. D., Chan, D. H., & Kim, J. S. (2005). Predicting ground conditions ahead of the tunnel face by vector orientation analysis. *Tunnelling and Underground Space Technology*, *20*(4), 344–355. https://doi.org/10.1016/j.tust.2005.01.002

Kavvadas, M. (2005). Numerical Analysis in the Design of Urban Tunnels. In *11th International conference of IACMAG*.

References

Kavvadas, M. J. (2003). Monitoring and Modelling Ground Deformations During Tunnelling. *FIG Symposium on Deformation Measurements, Santorini, Greece, 2003.*

Kim, C.-H., Chae, Y.-S., & Park, Y.-J. (2008). Prediction of Preceding Displacement of a Soil-Tunnel by Displacement Monitoring using Horizontal Inclinometer -Tunnel and Underground Space | Korea Science. In *Tunnel and Underground Space* (Vol. 18, pp. 355–365). https://www.koreascience.or.kr/article/JAKO200800557077579.page

Kim, C. (2013). Measurement of Tunnel Arch Settlements Ahead of and Behind the Tunnel Face Using a Horizontal Inclinometer and Settlement Pins. *Journal of Korean Society For Rock Mechanics*, *23*(2), 120–129. https://doi.org/10.7474/tus.2013.23.2.120

Kontogianni, V. A., & Stiros, S. C. (2005). Induced deformation during tunnel excavation: Evidence from geodetic monitoring. *Engineering Geology*, *79*(1–2), 115–126. https://doi.org/10.1016/j.enggeo.2004.10.012

Labasse, H. (1949). Les pressions de terrains dans les mines de huiles. In *Revue Universelle des Mines, Series 9, Vol. 5, No.3* (pp. 78–88).

Lollino, G. (1992). Automated inclinometric system. *Proceedings of the Sixth International Symposium on Landslides*.

Lunardi, P. (1991). Aspetti progettuali e costruttivi nella realizzazione di gallerie in situazioni difficili: interventi di precontenimento del cavo. In *Proc. Il Consolidamento del Suolo e delle Rocce nelle Realizzazioni in Sotterraneo* (pp. 567–580).

Lunardi, P. (1994). Progetto e costruzione di gallerie – Analisi delle deformazioni controllate nelle Rocce e nei suoli. *Quarry and Contruction*.

Lunardi, P. (1999). L'influenza della rigidezza del nucleo d'avanzamento sulla stabilità degli scavi in galleria. In *Gallerie e grandi opere sotterranee n. 59*.

Lunardi, P. (2000). The design and construction of tunnels using the approach based on the analysis of controlled deformation in rocks and soils. *T&T International ADECO-RS*, *May*, 3–30.

References

Lunardi, P. (2001). The ADECO-RS approach in the design and construction of the underground works of Rome to Naples high speed railway line: a comparison between final design specifications, construction design and "as built." In *AITES-ITA World Tunnel Congress "Progress in tunnelling after 2000"* (pp. 329–340).

Lunardi, P. (2008). *Design and Construction of Tunnels*. Springer, Berlin, Heidelberg. https://doi.org/10.1007/978-3-540-73875-6

Lunardi, P., & Bindi, R. (2004). The evolution of reinforcement of the advance core using fibre-glass elements. *Felsbau*, *22*(4), 8–19.

Lunardi, P., Bindi, R., & Cassani, G. (2007). From the ADECO-RS approach to the tunnelling industrialisation. *Proceedings of the International Conference on "Tunnels, Drivers of Change."*

Lunardi, P., & Cassani, G. (2006). *Prime evidenze e risultati dell'impiego dell'approccio ADECO - RS per la realizzazione di oltre 73 km di galleria di linea*. 178–184.

Lunardi, P., Cassani, G., & Bellocchio, A. (2014). Construction of the T8 and T8A tunnels in the "Dubler Kurortnogo prospekta" in Sochi (Russia). First implementation of the ADECO-RS approach in the Russian Federation. In *Gallerie e grandi opere sotterranee n.110*.

Lunardi, P., Focaracci, A., Giorgi, P., & Papacella, A. (1992). Tunnel face reinforcement in soft ground design and controls during excavation. In *Proceedings of the International Conference Towards New Worlds in Tunnelling* (Vol. 2, pp. 897–908).

NTC, I. M. of I. and. (2018). Norme Tecniche per le Costruzioni. DM 17/1/2018. *Gazzetta Ufficiale Della Repubblica Italiana*.

Panet, M. (1995). *Caractéristiques techniques du livre "Le calcul des tunnels par la méthode convergence-confinement"* (P. de l'école nationale des P. et Chaussées (ed.)).

Panet, M., & Guenot, A. (1982). Analysis of convergence behind the face of a tunnel. *International Symposium "Tunneling 82."*

Pantelidis, L. (2009). Rock slope stability assessment through rock mass classification systems. *International Journall of Rock Mechanics and Mining Sciences*, *46*(2), 315–325. https://doi.org/10.1016/j.ijrmms.2008.06.003

References

Peck, R. B. (1969). Advantages and limitations of the observational method in applied soil mechanics. *Geotechnique*. https://doi.org/10.1680/geot.1969.19.2.171

Peila, D. (1994). A theoretical study of reinforcement influence on the stability of a tunnel face. *Geotechnical and Geological Engineering*, *12*(3), 145–168. https://doi.org/10.1007/BF00426984

Peshawa, J. M. ., & Rezhna, H. F. (2014). *Data Normalization and Standardization: a technical report*. https://docs.google.com/document/d/1x0A1nUz1WWtMCZb5oVzF0SVMY7a_58KQulqQVT8LaVA/edit

Riaz, A. (2015). *Tunnel Convergence Monitoring - From Concept to Implementation*. *August 2015*, 0–28. https://doi.org/10.13140/RG.2.1.3015.8569

Ribacchi, R., & Riccioni, R. (1977). Stato di sforzo e deformazione intorno ad una galleria circolare. *Gallerie e Grandi Opere Sotterranee*, *4*, 7–18.

Rocscience. (n.d.). *RS2: Axisymmetric Analysis*. Retrieved November 11, 2020, from https://www.rocscience.com/help/rs2/tutorials/rs2__axisymmetric_analysis.htm

Sakurai, S., Akutagawa, S., Takeuchi, K., Shinji, M., & Shimizu, N. (2003). Back analysis for tunnel engineering as a modern observational method. *Tunnelling and Underground Space Technology*, *18*(2–3), 185–196. https://doi.org/10.1016/S0886-7798(03)00026-9

Savi, R., Carri, A., Cavalca, E., & Valletta, A. (2019). Applicazione di un sistema di monitoraggio innovativo in una galleria stradale danneggiata da un terremoto. *IAGIG - Incontro Annuale Dei Giovani Ingegneri Geotecnici 2019*.

Savi, R., Cavalca, E., Carri, A., Segalini, A., & Valletta, A. (2019). Preliminary test of an innovative pre-convergence monitoring tool for traditional tunnels. *Tunnels and Underground Cities: Engineering and Innovation Meet Archaeology, Architecture and Art- Proceedings of the WTC 2019 ITA-AITES World Tunnel Congress*, 3040–3049. https://doi.org/10.1201/9780429424441-322

References

Savi, R., Valletta, A., Carri, A., Cavalca, E., & Segalini, A. (2019). Application of innovative monitoring tools for safety and alert procedures in road tunnels Monitoring of Landslide View project ScienceDirect ScienceDirect Application of innovative monitoring tools for safety and alert procedures in road tunnels ScienceD. *Transportation Research Procedia*, *40*, 0–000. https://doi.org/10.1016/j.trpro.2019.07.213

Segalini, A., Carini, C., & Cristalli, L. (2011). Monitoring Underground Landslide Displacement : A New MUMS Based Device. *Slope Stability 2011: International Symposium on Rock Slope Stability in Open Pit Mining and Civil Engineering*.

Segalini, A., Carri, A., & Savi, R. (2017). *ROLE OF GEOTECHNICAL MONITORING: STATE OF THE ART AND NEW PERSPECTIVES*. 19–26. https://doi.org/10.35123/geo-expo_2017_3

Segalini, A., Carri, A., Savi, R., Cavalca, E., Alessio, C., & Kalamaras, G. (2018a). Tunnel restoration in unstable rock masses: Numerical analysis and validation of monitoring data from innovative instrumentation. *Geomechanics and Geodynamics of Rock Masses*, *1*, 747–754.

Segalini, A., Carri, A., Savi, R., Cavalca, E., Alessio, C., & Kalamaras, G. (2018b). Tunnel restoration in unstable rock masses: Numerical analysis and validation of monitoring data from innovative instrumentation. *Geomechanics and Geodynamics of Rock Masses*, *1*.

Segalini, A., Carri, A., Valletta, A., & Cavalca, E. (2019). Internet-of-Things principles applied to geotechnical monitoring activities: The Internet of Natural Hazards (IoNH) approach. *3rd ICITG - International Conference on Information Technology in Geo-Engineering*.

Segalini, A., Chiapponi, L., Pastarini, B., & Carini, C. (2014). Automated inclinometer monitoring based on micro electro-mechanical system technology: Applications and verification. In *Landslide Science for a Safer Geoenvironment: Volume 2: Methods of Landslide Studies* (pp. 595–600). Springer International Publishing. https://doi.org/10.1007/978-3-319-05050-8_92

Skog, I., & Händel, P. (2006). XVII IMEKO WORLD CONGRESS Metrology for a Sustainable Development CALIBRATION OF A MEMS INERTIAL MEASUREMENT UNIT. *CALIBRATION OF A MEMS INERTIAL MEASUREMENT UNIT*.

References

Subcommittee on Geotechnical Site Investigations, U.S. National Committee on Tunneling Technology, Commission on Engineering and Technical Systems, & National Research Council. (1984). *Geotechnical Site Investigations for Underground Projects* (Vol. 2). National academy press.

Tanzini, M. (2015). *Gallerie. Aspetti geotecnici nella progettazione e costruzione* (D. Flaccovio (ed.); 2. ed. agg).

Tonon, F. (2010). Sequential excavation, NATM and ADECO: What they have in common and how they differ. *Tunnelling and Underground Space Technology*, *25*(3), 245–265. https://doi.org/10.1016/j.tust.2009.12.004

Tonon, F. (2011). ADECO full-face tunnel excavation of two 260m2 tubes in clays with sub-horizontal jet-grouting under minimal urban cover. *Tunnelling and Underground Space Technology*, *26*(2), 253–266. https://doi.org/10.1016/j.tust.2010.09.006

Topcon Manual. (n.d.). *Topcon DS series Specifications*. Retrieved November 12, 2020, from https://www.topconcare.com/en/hardware/optical/ds-200-i/speci/

Vlachopoulos, N., & Diederichs, M. S. (2009). Improved longitudinal displacement profiles for convergence confinement analysis of deep tunnels. *Rock Mechanics and Rock Engineering*, *42*(2), 131–146. https://doi.org/10.1007/s00603-009-0176-4

Volkmann, G., & Schubert, W. (2005). The Use of Horizontal Inclinometers for the Optimization of the Rock Mass – Support Interaction. *31st ITA-AITES World Tunnel Congress*

Ringraziamenti

Eccoci qua, alla fine di un lungo percorso, partito tanti anni fa dalla passione per l'ingegneria e per l'ambiente. Durante questo lungo, a volte faticoso, spesso stimolante percorso ho avuto modo di conoscere persone che hanno alimentato la mia voglia di imparare. Desidero per questo ringraziare il Prof. Andrea Segalini, che fin dall'ultimo anno di laurea magistrale mi ha guidato nel mondo della geotecnica e del monitoraggio, permettendomi di lavorare nel suo gruppo e partecipare allo sviluppo del progetto di tesi.

Vorrei ringraziare l'Ing. Luca Chiapponi, per il suo fondamentale contributo ed i suoi ottimi ed apprezzati consigli durante questi anni, oltre che per la sua disponibilità nonostante i suoi mille impegni. Ringrazio l'Ing. Marco Puccinelli, per il contributo tecnico e le proficue collaborazioni.

Una speciale menzione per il collega Ing. Roberto Savi, compagno di percorso, di fantastiche trasferte e momenti di difficoltà condivisi insieme.

Ringrazio i miei colleghi Ing. Andrea Carri e Ing. Alessandro Valletta, per gli impegnativi momenti di lavoro, condivisione e collaborazione trascorsi insieme, oltre che per le agguerrite e spensierate pause pranzo.

Desidero ringraziare profondamente Ambra, in realtà per innumerevoli motivi, ma particolarmente per il fondamentale ed apprezzatissimo contributo, per la sua continua vicinanza e per tutti i momenti condivisi insieme.

Dedico infine questo lavoro di tesi ai miei genitori, Elisabetta e Marino, per il supporto durante tutti questi anni e la continua fiducia nei miei confronti e nelle mie scelte.